

Bioinorganic Vanadium Chemistry

Dieter Rehder

Department Chemie, Universität Hamburg, Germany



John Wiley & Sons, Ltd

This page intentionally left blank

Bioinorganic Vanadium Chemistry

Inorganic Chemistry

A Wiley Series of Advanced Textbooks
ISSN: 1939-5175

Editorial Board

Derek Woollins, University of St. Andrews, UK
Bob Crabtree, Yale University, USA
David Atwood, University of Kentucky, USA
Gerd Meyer, University of Hannover, Germany

Previously Published Books in this Series

Inorganic Structural Chemistry, Second Edition
Ulrich Müller
ISBN: 978-0-470-01865-1

Lanthanide and Actinide Chemistry
Simon Cotton
ISBN: 978-0-470-01006-8

Mass Spectrometry of Inorganic and Organometallic Compounds: Tools – Techniques – Tips
William Henderson & J. Scott McIndoe
ISBN: 978-0-470-85016-9

Main Group Chemistry, Second Edition
A. G. Massey
ISBN: 978-0-471-49039-5

Synthesis of Organometallic Compounds: A Practical Guide
Sanshiro Komiya
ISBN: 978-0-471-97195-5

Chemical Bonds: A Dialog
Jeremy Burdett
ISBN: 978-0-471-97130-6

Molecular Chemistry of the Transition Elements: An Introductory Course
François Mathey & Alain Sevin
ISBN: 978-0-471-95687-7

Stereochemistry of Coordination Chemistry
Alexander Von Zelewsky
ISBN: 978-0-471-95599-3

Bioinorganic Chemistry: Inorganic Elements in the Chemistry of Life – An Introduction and Guide
Wolfgang Kaim
ISBN: 978-0-471-94369-3

For more information on this series see: <http://eu.wiley.com/WileyCDA/Section/id-302900.html>

Bioinorganic Vanadium Chemistry

Dieter Rehder

Department Chemie, Universität Hamburg, Germany



John Wiley & Sons, Ltd

Copyright © 2008

John Wiley & Sons Ltd, The Atrium, Southern Gate, Chichester,
West Sussex PO19 8SQ, England
Telephone (+44) 1243 779777

Email (for orders and customer service enquiries): cs-books@wiley.co.uk
Visit our Home Page on www.wiley.com

All Rights Reserved. No part of this publication may be reproduced, stored in a retrieval system or transmitted in any form or by any means, electronic, mechanical, photocopying, recording, scanning or otherwise, except under the terms of the Copyright, Designs and Patents Act 1988 or under the terms of a licence issued by the Copyright Licensing Agency Ltd, 90 Tottenham Court Road, London W1T 4LP, UK, without the permission in writing of the Publisher. Requests to the Publisher should be addressed to the Permissions Department, John Wiley & Sons Ltd, The Atrium, Southern Gate, Chichester, West Sussex PO19 8SQ, England, or emailed to permreq@wiley.co.uk, or faxed to (+44) 1243 770620.

Designations used by companies to distinguish their products are often claimed as trademarks. All brand names and product names used in this book are trade names, service marks, trademarks or registered trademarks of their respective owners. The Publisher is not associated with any product or vendor mentioned in this book.

This publication is designed to provide accurate and authoritative information in regard to the subject matter covered. It is sold on the understanding that the Publisher is not engaged in rendering professional services. If professional advice or other expert assistance is required, the services of a competent professional should be sought.

Other Wiley Editorial Offices

John Wiley & Sons Inc., 111 River Street, Hoboken, NJ 07030, USA

Jossey-Bass, 989 Market Street, San Francisco, CA 94103-1741, USA

Wiley-VCH Verlag GmbH, Boschstr. 12, D-69469 Weinheim, Germany

John Wiley & Sons Australia Ltd, 42 McDougall Street, Milton, Queensland 4064, Australia

John Wiley & Sons (Asia) Pte Ltd, 2 Clementi Loop #02-01, Jin Xing Distripark, Singapore 129809

John Wiley & Sons Canada Ltd, 22 Worcester Road, Etobicoke, Ontario, Canada, MPW 1LI

Wiley also publishes its books in a variety of electronic formats. Some content that appears in print may not be available in electronic books.

Library of Congress Cataloging in Publication Data

Rehder, Dieter.

Bioinorganic vanadium chemistry / Dieter Rehder.

p. ; cm. — (Inorganic chemistry, ISSN 1939-5175)

Includes bibliographical references and index.

ISBN 978-0-470-06509-9 (cloth : alk. paper) — ISBN 978-0-470-06516-7 (pbk. : alk. paper)

1. Vanadium. 2. Vanadium—Physiological effect. I. Title. II. Series: Inorganic chemistry (John Wiley & Sons) [DNLM: 1. Vanadium—pharmacology. 2. Vanadium. 3. Vanadium—diagnostic use. 4. Vanadium Compounds.]

QV 290 R345b 2007]

QD181.V2R34 2007

546'.522—dc22

2007044559

British Library Cataloguing in Publication Data

A catalogue record for this book is available from the British Library

ISBN 978-0-470-06509-9

Typeset in 10/12pt Times by Integra Software Services Pvt. Ltd, Pondicherry, India

Printed and bound in Great Britain by Antony Rowe Ltd, Chippenham, Wiltshire

This book is printed on acid-free paper responsibly manufactured from sustainable forestry
in which at least two trees are planted for each one used for paper production.

*This book is dedicated to my children
Miriam, Nadja, Matthias and Gunnar,
who helped me to comprehend life;
and to Renate,
in whom I found refuge and encouragement.*

This page intentionally left blank

Contents

Preface	ix
1 Introduction and Background	1
1.1 History	1
1.2 Occurrence, Distribution and Impact	5
Further Reading	10
References	11
2 Inorganic and Coordination Compounds of Vanadium	13
2.1 Inorganic Aspects of the Function of Vanadium in Biological Systems	13
2.1.1 The Aqueous Vanadium(III, IV and V) Systems	13
2.1.2 Binary and Ternary Systems Containing Vanadium(IV and V)	20
2.1.3 Halides and Esters Derived from Orthovanadic Acid	24
2.2 Interaction of Aqueous Vanadate and Vanadyl with Biogenic Ligands	26
2.2.1 Speciation in the Vanadate System	26
2.2.2 Speciation in the Vanadyl System	31
2.3 Vanadium Coordination Compounds	34
2.3.1 Structural Features	34
2.3.2 Coordination Compounds with (Potential) Model Character for Biogenic Vanadium Systems	40
2.4 The Vanadium–Carbon Bond	47
References	49
3 Physico-chemical Methods for the Characterisation of Native and Model Vanadium Compounds	53
3.1 ^{51}V NMR Spectroscopy	53
3.1.1 General	53
3.1.2 Shielding in Isotropic Media	54
3.1.3 Other ^{51}V NMR Parameters	61
3.1.4 NMR Parameters Under ‘Confined’ Conditions	64
3.2 NMR of Other Nuclei	66
3.3 EPR Spectroscopy	67
3.3.1 General	67
3.3.2 Applications	69
3.3.3 Other Paramagnetic Centres	74
3.4 ESEEM and ENDOR Spectroscopies	75
3.5 Optical Spectroscopies	77
3.5.1 UV-Vis	77
3.5.2 Circular Dichroism	79

3.6 X-ray Absorption Spectroscopy	80
3.6.1 Background and General	80
3.6.2 Biological Applications	83
References	84
4 Naturally Occurring Vanadium Compounds	87
4.1 Vanadium in Ascidians and Polychaete Worms	87
4.1.1 Ascidians: History, Speculations and Facts; An Introduction and Overview	87
4.1.2 Ascidians: The Present Stand	90
4.1.3 Polychaeta Fan Worms	96
4.1.4 Model Chemistry	97
4.2 Amavadin	100
4.3 Vanadate-dependent Haloperoxidases	105
4.3.1 History, Background and General Aspects	105
4.3.2 Structural and Catalytic Features	110
4.3.3 Model Chemistry	116
4.4 Vanadium and the Nitrogen Cycle	128
4.4.1 Vanadium Nitrogenases	128
4.4.2 Vanadium-dependent Nitrate Reductases?	144
4.5 Vanadate as Energiser for Bacteria, and Vanadophores	145
References	150
5 Influence of Vanadium Compounds on Cellular Functions	157
5.1 Medicinal Aspects of Vanadium	158
5.1.1 The Anti-diabetic Potential of Vanadium Compounds	158
5.1.2 Other Potential Medicinal Applications	175
5.2 Interaction of Vanadium with Proteins and Protein Substrates	182
5.2.1 Vanadium- and Phosphate-metabolising Enzymes	183
5.2.2 Inhibition of Lactamases	189
5.2.3 Structural Vanadium Analogues of Phosphate Esters and Anhydrides	189
5.2.4 Nonfunctional Binding of Vanadate and Vanadyl to Proteins	190
5.2.5 Modification of Proteins by Vanadate	195
References	198
6 Epilogue	203
References	205
Index	207

Preface

In the mid-1980s, shortly after I was appointed to a professorship at Hamburg University, I was asked to offer graduate courses in Bioinorganic Chemistry, a discipline which only slowly gained ground in Europe, despite the fact that its importance and oncoming impact were well acknowledged. My knowledge of this new subject was close to zero, and therefore I decided to attend the 2nd International Conference on Bioinorganic Chemistry, which took place in summer 1985 at a very beautiful location, the Algarve on the Atlantic coast in southern Portugal. Among the many people I met was Hans Vilter (now in Trier), who had discovered the first vanadium enzyme, a vanadate-dependent bromoperoxidase isolated from a marine brown alga a few years before. Since vanadium has always been in the centre of my scientific life (my original research activities were directed towards organovanadium chemistry and vanadium-51 NMR), I became particularly interested, all the more as many of the attendees at the conference were not ready to take it that vanadium was actually an essential constituent of an enzyme. A couple of fruitful years of cooperation followed, and my research focus increasingly turned towards the biological aspects of vanadium, and finally became anchored in these grounds when I participated in a symposium on Marine Bioinorganic Chemistry ('MICBIC') in summer 1989. The symposium site was Heron Island, a tiny coral island in the Barrier Reef, off the shores of the Gold Coast in Australia. We walked across shallow waters, and I became acquainted with animals that I only vaguely remembered from biology lessons at school: the sea squirts, or ascidians. Kenneth Kustin (Brandeis University, Waltham, MA) spent some time introducing me to the unique ability of sea squirts to accumulate vanadate from sea water. I haven't done any research in this area, but remained pretty much interested in these vanadium-sequestering creatures. Consequently, one of the chapters in this book deals with ascidians, and I am greatful to Ken for having proof-read this specific issue. A year later, Achim Müller (University of Bielefeld) encouraged me to write a review article on 'The Bioinorganic Chemistry of Vanadium' for *Angewandte Chemie*. I did so (the article appeared in 1991 and had quite some impact) – and swore never to try to accomplish such a tedious task again. With the present book, *Bioinorganic Vanadium Chemistry*, I broke my oath.

Vanadium does still not (yet) cover the broad bio-spectrum pertinent to most of the other biologically relevant transition metals. One of the reasons arises from the fact that, so far, only two vanadium-dependent enzyme families are known, the vanadate-dependent haloperoxidases and vanadium nitrogenases (a third enzyme, a nitrate reductase depending on vanadium, still awaits confirmation). Additional biological implications of vanadium are scarce: apart from vanadium's presence in sea squirts (and fan worms), a naturally occurring vanadium compound, amavadin, has been found only in one additional genus of living organisms, the *Amanita* mushrooms, the most prominent representative of which is the fly agaric. In addition to these 'classical' bio-vanadium areas, there are interesting and highly promising novel developments when it comes to biological functions, and beneficial (i.e. medicinal) applications of vanadium. These new areas include bacterial energy recovery from vanadate, modification of proteins by vanadium and, of course, the potential of vanadium compounds in the treatment of diabetes mellitus. Both the 'classical' and the 'futuristic' themes are covered in detail in the present book. Vanadium compounds as insulin mimetics have been one of the focal areas within the European COST programme, and I am indebted to 'my' COST group

(D21-0009-01, 2001–2006) for the long, close and fruitful cooperation in a humanly and scientifically ambitious atmosphere, the results of which have been incorporated here.

A second reason for the sometimes hesitant examination and analysis of vanadium-related chemistry lies in the fact that the chemistry of vanadium is more ‘touchy’, or at least considered more touchy, than that of its neighbours (titanium, chromium and molybdenum). With a chapter directed towards the basics and the impact (for biological systems) of inorganic and coordination compounds of vanadium, I hope to have provided an overview of the biologically relevant crucial points, and to convince the prospective and the active researcher of the beauty of vanadium chemistry. This includes the main physical methods of characterisation of vanadium compounds in its biologically relevant forms. I have certainly been in close scientific contact with many colleagues committed to bioinorganic (vanadium) chemistry, contacts which have an enduring bearing on my own work in this field. I mention only two of them at this point, David Garner (School of Chemistry, Nottingham) and Vincent Pecoraro (University of Michigan, Ann Arbor), with whom I had critical discussions on a basis of fairness and equity, which has become pretty rare in the scientific community.

All of the findings in the biological chemistry of vanadium have their history. In order to appreciate and to value the impact of early perceptions and their protagonists, I have analysed a couple of early and original documents on, e.g., vanadium nitrogenase, vanadium in the blood of ascidians and vanadium compounds as a ‘remedy’ for a plethora of diseases. Snapshots of these historical events have been included. Included, in the first chapter, is also a detailed account on the discovery of vanadium.

The present book thus covers all of the main areas of the bioinorganic and related chemistry of vanadium. Not all of the relevant aspects could be accounted for in the same detail. In particular, this applies to areas which are – according to my subjective judgement – less intimately connected to the theme. In any case, I have tried to provide the reader with key references for most of these more peripheral areas.

It is hoped that this book will contribute to overcoming the barriers of comprehension between biochemists, inorganic chemists and chemists dedicated to environmental and health aspects of vanadium. The establishment of bi- to triannual symposia on the ‘Chemistry and Biological Chemistry of Vanadium’ a decade ago (the first one, held in Cancun, Mexico, in 1997, was organised by Debbie Crans, Colorado State University in Fort Collins, Co, and Alan Tracey, Simon Fraser University in Burnaby, BC) has provided considerable momentum in this respect.

A final remark concerning units: I have used SI units throughout, except in two cases, where other units have not become generally accepted in the subject-related literature: (1) for the molecular ‘weight’ (of proteins), the unit dalton (Da) is commonly used in biochemistry – and in the present book; (2) for bond distances, the ångström (\AA) is favored by crystallographers and also employed here. All electrochemical potentials, if not provided relative to the normal hydrogen electrode (NHE) in the original literature, have been recalculated and refer to NHE = 0.

1 Introduction and Background

1.1 History

The discovery of the element vanadin, or vanadium as it is internationally known in its Latinised form, is as colourful as its chemistry.^[1] On 22 January 1831, J. J. Berzelius wrote a letter to cheer up F. Wöhler,^[2] who had missed discovering the new element by a hair's breadth, in which he told the following charming story to describe Wöhler's misfortune:¹

'As to the sample you sent me, I want to tell you the following anecdote: In olden times the beautiful and charming goddess Vanadis lived up in the far north. One day, someone knocked on her door. The goddess remained comfortably seated and thought: Let whoever it is knock again; but there was no more knocking, and whoever had knocked went back down the steps. The goddess was curious to see who was so indifferent to being admitted, sprang to the window and looked at who was going away. Alas! she said to herself, that's that rascal [Schalk] Wöhler. Well, he surely deserves it; if he had been a little more concerned about it, he would have been admitted. The fella does not even look up to the window in passing by. After a few days, someone knocked on the door again, and this time, the knocking continued. The goddess finally came herself and opened the door. Sefström entered, and from this encounter Vanadin was born.'

The sample mentioned at the beginning of the anecdote was a specimen (a white powder) obtained by treatment of brown lead ore from the district Zimapán in central Mexico. The ore had originally been given to Baron von Humboldt by the Spanish mineralogist del Rio in Mexico on the occasion of Humboldt's visit there in 1803–04, and brought to the Museum für Naturkunde in Berlin by Humboldt in 1805.^[3] A second sample of del Rio's brown lead ore was sent to the laboratory of Collet-Descotil in Paris. Collet-Descotil, who analysed the sample in 1805, came to the conclusion that the mineral contained chromium (which had been discovered in 1797). Wöhler began to investigate the brown lead ore in 1828 and noted that, in contrast to what had been established by Collet-Descotil, its properties did not match those of chromium. Wöhler became ill and stopped providing support for his findings. Later, he commented in a letter to Berzelius: 'I was an ass [*Ich war ein Esel*] not to have discovered [vanadin] two years before in the brown lead ore from Zimapán.'^[1] Wöhler

¹ Translation of the original letter (ref. [1]) adapted from ref. [2]; modified to match the original.

was not the only one to fall short of discovering vanadium: during the winter of 1830–31, J. F. W. Johnston in England analysed a lead mineral from Wanlockhead, Scotland, and discovered a new substance resembling chromium. He became aware of its true identity while reading the letter of Berzelius to P. L. Dulong, presented at the Académie Royale in Paris on 7 February 1831.^[4]

Meanwhile, Nils Gabriel Sefström, a physician and chemist, who taught chemistry at the School of Mines in Falun, Sweden, started, in the mid-1920s, to investigate a black powder obtained by treating bar iron from the Taberg with hydrochloric acid. The Taberg, rich in iron ore and the highest elevation in the province of Småland in South Sweden, rises up to 343 m (about 1000 ft). Sefström resumed his studies of the black powder in April 1830, discovering a substance which had certain properties in common with chromium and others with uranium. He soon found out that the substance contained neither chromium nor uranium,^[5] but was something entirely new. The experiments were continued in Berzelius' laboratory, where the blue colouring of the lower oxidation states² of the new element was established as one of its peculiarities (*Eigenthümlichkeiten*).

In the course of this work, Sefström originally proposed the name *Odinium* for the new metal. Odin is the god of the winds in the Northern Germanic mythology (Wotan for the Southern Germanic tribes). But then, Sefström asked Berzelius to choose a better name than odinium because 'it fits so badly in French and English' ['*det passer så illa in franskan och engelskan*']. The new metal was thus provisionally re-named *Erian*, after Erianae³, a by-name of Athena (= Minerva; see, e.g., Berzelius' letter to Wöhler of 27 December 1830^[2]). Wöhler, in his answer to Berzelius (4 January 1831), used the name *Sefströmium*. Sefström finally chose the name vanadin ('*på latin Vanadium*'⁴) for the new metal, after *Vanadis*, an epithet of the Nordic⁵ goddess Freya – Odin's wife,^[5] the most aristocratic goddess in the Gothic mythology ['*den förmästa gudinnam uti göthiska Mythologien*'],^[5a] who symbolises beauty and fertility – essential features of vanadium chemistry. Vanadis (Figure 1.1) is usually illustrated, in a somewhat martial attitude, spear in hand on a chariot drawn by cats, animals which were sacred to the Northern Germanic tribes. An additional motivation for Sefström when choosing vanadin (or vanadium) arose from the fact that none of the elements known so far started with the letter V ['... *hvars begynnelse-bokstaf ej förekommer ... enkla kroppars namn*'.]^[5a]

In a second letter to Berzelius (9 January 1831), Wöhler enclosed the white powder sample mentioned above, suggesting that it might be Erianoxyde. Wöhler was eventually able to show that his sample (from the Zimapán ore) was identical with Sefström's new metal vanadin (from bar iron and slag thereof), which prompted G. Rose to add *Vanadinbleierz* (vanadium lead ore; actually vanadinite, $Pb_5[VO_4]_3Cl$, Figure 1.2, which is isomorphous with hydroxyapatite) to Humboldt's original label describing the Zimapán ore exhibited in the Berlin museum.^[3]

² Acidic solutions containing the hydrated vanadyl ion (VO^{2+}) are light blue.

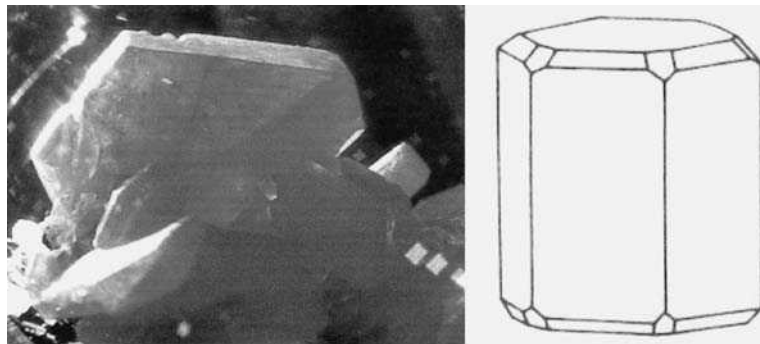
³ Actually *Eργανη* (Ergane), the patron of craftsmen and artisans. The Greek *ergón* (= energy, work), related to Ergane, is the root for the English 'work' (German and Dutch: Werk; Swedish: Verk).

⁴ The title of the Swedish version of Sefström's new discovery actually reads *Om Vanadium, en ny metall, funnen uti stångjern, som är tillverkad af malm ifrån Taberget i Småland* (On Vanadium, a new metal, found in bar iron which is manufactured from ore of the Taberg in Småland).^[5a] The German pendant^[5b] is entitled *Ueber das Vanadin ...* (On Vanadin ...).

⁵ Old-Icelandic *Vana-dis*, meaning woman from the *Vanir*, one of the two lineages of Gods in Norse mythology.

**Figure 1.1**

The Nordic goddess Vanadis, alias Freya.

**Figure 1.2**

Crystals and crystal habit of (hexagonal) vanadinite, $\text{Pb}_5[\text{VO}_4]_3\text{Cl}$. The crystals are deep orange-red.

Poggendorf (Editor of *Ann. Phys. Chem.*) added a note to Sefström's key article on the discovery of vanadium^[5b] in which he forestalls any allegations regarding the priority of Sefström's discovery, in particular with respect to del Rio's claim (which he later withdrew) to have discovered, in 1801–03, a new element in the brown lead ore from Zimapán.

Andres Manuel del Rio y Fernandez actually discovered vanadium when experimenting with the *plomo pardo de Zimapán* from the Cordonal Mine in Hidalgo. Fascinated by the

differently coloured salts of the new element obtained in varying preparations, he called it *Panchromo*. A brief note on this discovery is contained in *An. Cienc. Nat.* (Madrid) **1803**, 6, 46: ‘Panchromium. Novel metallic matter announced by Sñ. Manuel del Rio in a report from Mexico directed to Don Antonio Cavanillas, dated 26th September 1802.’ Later, del Rio renamed the new element *Eritrono* (erythronium)^[1] with reference to the red colour obtained when alkaline and alkaline earth metal salts of the new metal were heated or treated with acids. Since the properties of erythronium to some extent resembled those of chromium, del Rio lost confidence in his discovery, additionally discouraged by the slapdash analysis carried out by Collet-Descotils. He consequently noted that the supposed new element was nothing but chromium, factually renouncing his discovery. Del Rio later accused Humboldt of not having given his discovery its due attention and publicity, an essentially unjustified reproach, since papers documenting del Rio’s experiments were lost at sea when, unknown to del Rio, the vessel carrying them to France was shipwrecked.^[3]

From today’s point of view, it appears strange that the obvious differences between the chemical behaviour of chromium and erythronium were overlooked in the experiments carried out by del Rio himself and by Collet-Descotil, a renowned chemist of his time: as ammonia is added to digested vanadinite, white ammonium vanadate is obtained (ammonium chromate is yellow). When heated, bright red V_2O_5 forms; when treated with acids, a red solution of decavanadate (essentially $[H_2V_{10}O_{28}]^{4-}$) is formed. The respective reactions with chromate yield greenish Cr_2O_3 and orange dichromate.

Berzelius, Johnston and others tried in vain to isolate the metal itself. The substances they thought were metallic vanadium, obtained by reduction of vanadium oxide with carbon or potassium, or of vanadium chlorides (VCl_3 , $VOCl_3$) with potassium or ammonia, all turned out to be carbides, silicides, nitrides (VN) or low-valent oxides (VO).^[4] The first apparently successful generation of metallic vanadium was accomplished by Sir Henry Enfield Roscoe in 1869 by reduction of VCl_2 with hydrogen in a lengthy experiment:^[1]

‘When he [Roscoe] heated the tube [containing VCl_2 in a platinum boat inside a porcelain tube], hydrochloric acid gas came off in torrents, and continued to be evolved in decreasing quantity for from forty to eighty hours. When it finally ceased to come off, the tube was cooled and the boat was found to contain a light whitish grey-coloured powder, perfectly free from chlorine.’

Roscoe himself described the grey-coloured powder in the following way:^[6]

‘Metallic vanadium thus prepared examined under the microscope reflects light powerfully, and is seen to consist of a brilliant shining crystalline metallic mass possessing a bright silver-white lustre. Vanadium does not oxidise or even tarnish in the air. ... The metal is not fusible or volatile at a bright red heat in nitrogen; the powdered metal thrown into a flame burns with the most brilliant scintillations. Heated quickly in oxygen, it burns vividly, forming the pentoxide. ... The specific gravity of metallic vanadium at 15 °C is 5.5 [actually, the density of vanadium is 6.11 g cm⁻³]. It is not soluble in either hot or cold hydrochloric acid; strong sulphuric acid dissolves it on heating, giving a yellow solution. ... Fused with sodium hydroxide, the metal dissolves with evolution of hydrogen, a vanadate being formed.’

The first large-scale synthesis of 99.9% pure vanadium was carried out in 1927 by the Westinghouse Lamp Co. by heating a mixture of vanadic oxide, metallic Ca and $CaCl_2$ in

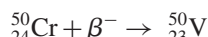
an electric furnace to 760 °C. Nowadays, pure vanadium metal is obtained by reduction of V₂O₅ with calcium, or following the van Arkel/de Boer process (thermolysis of VI₃).

1.2 Occurrence, Distribution and Impact

Vanadium (element No. 23) is comparatively abundant in the universe. At 0.0001%, its cosmic abundance is comparable to that of copper and zinc. The cosmic abundance is, e.g., reflected in chondritic meteorites, which contain 220 atoms of the isotope ⁵¹V in relation to 10⁶ silicon atoms. Cosmic formation of vanadium is based on the α, γ cascade up to ⁵²Cr, followed by the reaction sequence^[4]



The isotope ⁵¹V accounts for 99.75% of the naturally occurring isotopes. The remaining 0.25% is supplied by the isotope ⁵⁰V, whose cosmic formation is due to an electron-capture process by ⁵⁰Cr:



⁵⁰V is very mildly radioactive, decaying with a half life of 1.4 × 10¹⁷ years either by electron capture/positron emission (to generate ⁵⁰Ti; 83%) or via β⁻ decay (to form ⁵⁰Cr; 17%):



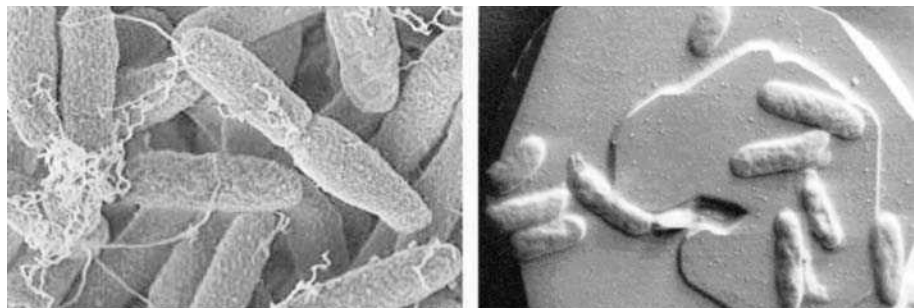
In the Earth's crust, vanadium is 22nd in abundance (0.013% w/w) and thus more abundant than copper and zinc. In sea water, commonly considered the cradle of life on our planet, the average concentration of vanadium, which is present mainly in the form of ion pairs Na⁺H₂VO₄⁻, is around 30 nm. Vanadium is thus the second most abundant transition element in marine environments, outmatched only by molybdenum [ca 100 nm molybdate(VI)]. Vanadium is supplied by riverine input; scavenging by vent-derived iron oxides helps to control the concentration and cycling of vanadium in the oceans.^[7] The vanadium content of human blood plasma is around 200 nm; this ca 10-fold increase with respect to sea water points to its possible biological function. The vanadium level in tissue is even higher, averaging 0.3 mg kg⁻¹ (ca 6 μM). Vanadium accumulates in bones, liver and kidneys.

Vanadium is a ubiquitous trace element. The average content in shales, which are particularly rich in vanadium, is 0.012% w/w. In sandstone and carbonate-based and magmatic rock, the vanadium content is lower by one order of magnitude. More than 120 vanadium-based minerals are known, containing the element in cationic and anionic form, and in the oxidation states III, IV and V. A cross-section representing these characteristics and the general inorganic chemistry of vanadium – which will be dealt with in Chapter 2 – is provided in Table 1.1. The most common minerals are vanadinite (Figure 1.2), patronite, roscoelite (vanadium mica), carnotite and descloizite.

Vanadium minerals are essentially formed in the course of geological processes. An epigenetic formation of specific minerals is, however, conceivable: certain bacteria, such as *Pseudomonas vanadiumreductans*^[8] and *Shewanella oneidensis*^[9] (Figure 1.3), can use vanadate(V) as an external electron acceptor, reducing vanadate(V) to vanadium(IV) [and perhaps even further to vanadium(III)], and thus producing sherwoodite-like inorganic

Table 1.1 Selection of vanadium minerals with information on the nature of vanadium.

Mineral name	Formula	Oxidation state of vanadium	Type of compound
Karelianite	V_2O_3	III	Oxide
Roscoelite (vanadium mica)	$\text{K}(\text{Al}, \text{V})_2(\text{OH}, \text{F})_2[\text{AlSi}_3\text{O}_{10}]$	III	V^{3+} aluminosilicate
Häggite	$\text{VO}(\text{OH}) \cdot \text{VO}(\text{OH})_2$	III and IV	Metahydroxide
Minasragrite	$\text{VOSO}_4 \cdot 5\text{H}_2\text{O}$	IV	Vanadyl salt
Simplotite	$\text{Ca}[\text{V}_4\text{O}_9]$	IV	Tetravanadate(IV)
Patronite	$\text{VS}_4 \equiv \text{V}(\text{S}_2)_2$	IV	Disulfide
Vanoxite	$2\text{V}_2\text{O}_4 \cdot \text{V}_2\text{O}_5 \cdot 8\text{H}_2\text{O}$	IV, V	Oxide
Sherwoodite	$\text{Ca}_9\text{Al}_2\text{V}_4^{\text{IV}}\text{V}_2^{\text{V}}\text{O}_{80} \cdot 56\text{H}_2\text{O}$	IV, V	Polyoxovanadate
Navajoitite	$\text{V}_2\text{O}_5 \cdot 3\text{H}_2\text{O}$	V	Oxide
Munirite	$\text{Na}[\text{VO}_3]$	V	Metavanadate
Steigerite	$\text{Al}[\text{VO}_4] \cdot 3\text{H}_2\text{O}$	V	Orthovanadate
Carnotite	$\text{K}(\text{UO}_2)[\text{VO}_4]$	V	Orthovanadate
Vanadinite	$\text{Pb}_5[\text{VO}_4]_3\text{Cl}$	V	Orthovanadate
Descloizite	$\text{Pb}(\text{Zn}, \text{Cu})\text{OH}[\text{VO}_4]$	V	Orthovanadate
Chervetite	$\text{Pb}_2[\text{V}_2\text{O}_7]$	V	Divanadate
Barnesite	$\text{Na}_2[\text{V}_6\text{O}_{16}]$	V	Hexavanadate
Hummerite	$\text{K}_2\text{Mg}_2[\text{V}_{10}\text{O}_{28}]$	V	Decavanadate
Sulanite	$\text{Cu}_3[\text{VS}_4]$	V	Thiovanadate

**Figure 1.3**

Scanning electron microscopy images of the soil bacterium *Shewanella oneidensis* (strain MR-1). The picture on the right shows the bacterium on haematite (Fe_2O_3).

deposits. The composition of the mixed-valence ($\text{V}^{\text{V}}/\text{V}^{\text{IV}}$) mineral sherwoodite is given in Table 1.1. This issue will be resumed in more detail in Section 4.5.

Another source of vanadium, of interest in biological and environmental contexts, are fossil ‘fuels’ such as peat, coal, bitumen, oil-shales, asphalts and crude oil. The vanadium content of hard coal can vary from 0.007 to 0.34%. Crude oil from Albania (0.034%), the Volga–Ural region (0.061%) and Venezuela (0.12%) (upper limit in all three cases) is particularly rich in vanadium.^[4] A high vanadium content is often associated with high sulfur contents. The reasons for the notable enrichment of vanadium in fossils compared with bio-mass precursors such as bacteria, protozoans, algae, plants and animals are still under debate. Possible mechanisms for a secondary input of vanadium in decaying

material include accumulation by phenolic compounds formed by degradation of lignin, by humic substances, and absorption from ground water, in particular in areas where the ground water is enriched by weathering of vanadium containing minerals and rocks. Anoxic conditions appear to promote vanadium absorption, possibly because of the very low solubility of vanadyl (VO^{2+})⁶ hydroxides at a pH of around 7. In the case of crude oil, accumulation of vanadium may also be traced back to vanadium scavenging as oil passes through sediments rich in vanadium. Crude oil contains various porphinogens, derived from chlorophylls and haems of decayed marine organisms. Porphinogens are excellent complexing agents for the vanadyl cation. Most of the vanadium contained in carbonaceous sedimentary rock, asphaltene/kerogene^[10] and geologically young oil is in fact present in the form of vanadyl porphyrins;^[11a] see, e.g., the chlorophyll-derived complex in Figure 1.4. Old oils contain most of the vanadium in non-porphinogenic compounds,^[11b] examples of which are also shown in Figure 1.4.

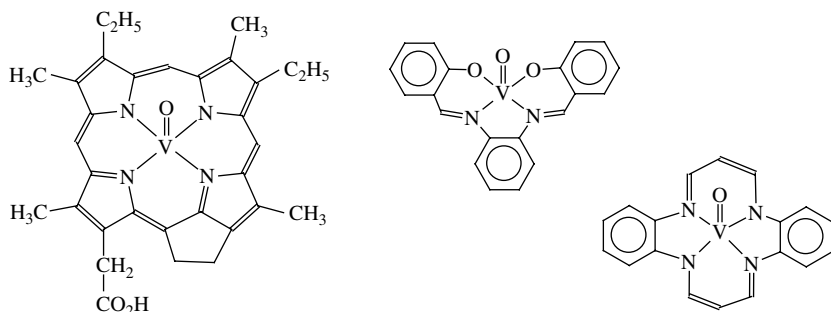


Figure 1.4

Examples of vanadyl compounds in crude oil. Left: porphinogenic (vanadyldesoxiphylerythrin); middle and right, non-porphinogenic.

In the course of refining crude oil, vanadium becomes enriched in the high molecular mass asphaltenes. Processing and combustion of fossil fuels convert the organic vanadium compounds into vanadium oxides (V_2O_4 and V_2O_5), which are, at least in part, emitted into the atmosphere, where they catalyse the conversion of sulfur dioxide to sulfur trioxide and thus promote the formation of sulfuric acid, one of the components of acid rain. Other industrial activities, such as the production of ferrovanadium (used in the fabrication of particularly strong and durable steels), ceramics containing vanadium oxide and vanadium oxide-based catalysts add to the anthropogenic emission, as do leachates and effluents from mining and milling. The overall loadings caused by human activities to land, oceans and the atmosphere is, however, considerably less than that resulting from other sources and events.^[12] Vanadium pollution is therefore not a global problem, but can have an impact in metropolitan and industrialised areas.

The vanadium content of normal food and drinking water is in the ppb to ppm region and thus well below any toxic level. Exposure to vanadium, e.g. by inhaling vanadium pentoxide, or from elevated vanadate levels in food and drinking water, does constitute a health risk. Inhaled particulate vanadium can induce oxidative stress and thus damage the

⁶ Throughout, the term ‘vanadyl’ will only be used for $\text{V}^{\text{IV}}\text{O}^{2+}$, i.e. *not* for the corresponding vanadium(V) fragment $\text{V}^{\text{V}}\text{O}^{3+}$.

respiratory epithelial cells and provoke inflammatory and fibrotic lung injuries. High-risk exposure includes mining and milling of vanadium-bearing ores, and particulate vanadium and vanadium oxide accompanied by, e.g., vanadium-based catalyst production. Fly ashes as a result of combustion processes may also contain high loadings of V_2O_5 . The established value for immediate danger to life or health is $70\text{ mg m}^{-3}\text{V}^{[13]}$ and the maximum allowable concentration (MAC) of V_2O_5 in the working environment is 0.05 mg m^{-3} (8-hour time-weighted average, 40-hour week). Table 1.2 summarises LD_{50} and LC_{50} values for oral and inhalatory administration of vanadium oxides (V_2O_5 , V_2O_3) and metavanadate ($K/NH_4[VO_3]$) to rats.^[14] The LD_{50} value indicates the level of a harmful substance (in mg per kg body weight) causing the death of 50% of the test animals within a defined period of time, commonly 14 days. The LC_{50} is the corresponding indicator for lethal concentration in air. There are therefore no substantial differences in the toxicity of the vanadium(V) compounds. V_2O_3 , on the other hand, is relatively nontoxic. *Dermal* (skin) contact with the vanadium oxides and metavanadates appears to be harmless. A more detailed account of the physiological effects of vanadium is included in Chapter 5.

Table 1.2 LD_{50} and LC_{50} values^a for vanadium oxides and metavanadates administered to rats^[14].^b

	$LD_{50}(\text{mg kg}^{-1} \text{ b.w.})$ (oral administration)	$LC_{50}(\text{mg l}^{-1})$ (inhalative administration)
V_2O_5	221–716	2.2–16.2
V_2O_3	>3000	>6.65
$K[VO_3]$	314–318	1.85–4.16
$NH_4[VO_3]$	141–218	2.43–2.16

^aSee text for definition.

^bRanges reflect differences in response due to sex and (V_2O_5) particle size.

The first applications of vanadium go back to Berzelius, who observed that an extract from gallnuts, when treated with small amounts of ammonium vanadate, yielded a deep-black liquid, which makes excellent ink.^[4] Wöhler noted, however, that the letters written with this ink faded and were barely legible after a couple of years (the recipe was later improved by Hélouis, who used tannin instead of gallnut preparations). The use of vanadium in oxidation catalysis, viz. the formation of aniline black from aniline, dates back to the mid-1870s. Aniline black is a black dye used to stain cotton and leather, and obtained by oxidation of aniline. The catalytic potential of vanadium pentoxide was discovered in 1895 in the context of the use of V_2O_5 in the oxidation of toluene and benzaldehyde.^[15] Nowadays, vanadium oxides are established oxidation catalysts in the production of sulfuric acid and maleic anhydride. Mixed ester–chlorides of the hypothetical orthovanadium acid (H_3VO_4) of the general composition $VOCl_n(\text{OR})_{3-n}$ (where R represents an alkyl residue) are sporadically applied in polymerisation reactions of alkenes, and low-valent vanadium compounds can act in reduction catalysis.^[16] About 80% of the world production of vanadium goes into ferrovanadium. Ferrovanadium contains ca 50% vanadium; it is manufactured by reduction of vanadium and iron oxides with coal and serves as an additive for specialised steels. Promising fields of future impact are catalytic applications of nanoscopic vanadium pentoxide materials (including nanowires/nanorods and nanoporous materials), vanadium redox batteries (employing the $\text{V}^{\text{V}}/\text{V}^{\text{IV}}$ and $\text{V}^{\text{III}}/\text{V}^{\text{II}}$ couples) and lithium/silver vanadium oxide batteries.

Objective evidence for the presence of vanadium in plants was provided by E. O. von Lippmann in 1888,^[17] and this period may be considered the entrée into the biological chemistry of vanadium:

'An even rarer element, which can accumulate in sometimes considerable amounts in charred slop, obtained in the course of manufacturing molasses [from sugar-beet], is vanadin, perceivable by its noticeable colourations, usually blue or blue-grey. The percentage of this matter present in charred slop cannot be minor, since I succeeded, already eight years ago, to separate from selected samples [of charred slop] ... ca 1.5 g of pure sodium vanadate (*vanadinsaures Natrium*).'

The first to start simple experiments on the influence of vanadium on the growth of bacteria, germinating seeds, fungi and infusorians and the response of animals (frogs, pigeons, rabbits, guinea pigs, dogs and cats) towards vanadate was John Priestley^[18]⁷ (not to be mistaken for Joseph Priestly, famous for his co-discovery (with Scheele) of the element oxygen, or with the writer John B. Priestley). 'The salt used in this research was tribasic sodium vanadate [Na_3VO_4], obtained by fusing a mixture of three molecules of sodium carbonate with one molecule of vanadium pentoxide.' While the germination of lettuce seeds was not affected by 0.1% solutions of sodium vanadate, it was totally prevented by 1% solutions. The elaborate descriptions of his animal experiments, which were injected lethal doses, read like horror stories. Excerpt from the protocol on a cat:

'3h.15m. [after injection]: Very feeble; may be handled with impunity. Respirations rapid, and heart extremely feeble. 3h.15m: Rolls over two or three times, as if in pain; breathing very rapid and shallow. Rises but cannot stand; lies on its side, stretches out its four paws, and seizes with them the bars of its cage. Slight opisthotonus. Right posterior extremity drawn forward. Great dispnoea apparently. Moans. 3h.20m: On touching the cornea, the eye was not closed. Dead.'

The amount of vanadate applied to the cat, which 'was small and adult', corresponded to 250 mg V_2O_5 (!), i.e. two to three orders of magnitude more than used nowadays in the treatment of diabetic animals.

Vanadium preparations containing substantially lower and thus subtoxic levels of vanadium were applied as early as 1899 for the treatment of anaemia, tuberculosis, chronic rheumatism and diabetes mellitus. A blend of vanadium salts and sodium chlorate, named *Vanadin*, was traded as a prescription against syphilis.^[4] The tradition of using vanadium compounds as a restorative goes back to the beginning of the last century. Commercially available preparations containing vanadyl sulfate, such as *Vanadyl Fuel*, are nowadays popular among body builders because they purport to increase muscle mass. Since vanadyl is precipitated in the form of insoluble hydroxides under the slightly alkaline conditions in the small intestine, it is barely absorbed. Absorption from the gastrointestinal tract averages 0.1–1%,^[13] rendering vanadyl sulfate preparations harmless – as long as these preparations do not contain chromium compounds as additives. In Japan, a mineral water from the Fuji region is on the market as *Vanadium Water* (Figure 1.5), which is supposed to act as a general tonic; it contains an innocent 54 µg of vanadium per litre.

The biological importance of vanadium was definitely established when in 1911 M. Henze reported on *Untersuchungen über das Blut der Ascidien* [Investigations on

⁷ J. Priestley, *Philos. Trans. R. Soc. London* **1876**, 166, 495–498



Figure 1.5

Vanadium water from the Fuji region contains ca 50 µg vanadium (in the form of hydrogenvanadate) in 1 litre. Inscriptions on the left-hand image: top line, ‘The natural water created by Fujisan gave [us] a marvel’; bottom left, ‘Super ions magic water (*hadosui*)’; bottom right, ‘Ground-water from the basalt bed/Fujisan vanadium water’.

the Blood of Ascidians], of the Mediterranean sea squirt *Phallusia mamillata*.^[19]⁸ Henze obtained a deep-blue precipitate from aqueous lysates of the ascidians’ blood cells which, upon evaporation with nitric acid, yielded vanadium pentoxide. Henze also noted the high acidity of the lysates, without establishing the identity of the acid (actually sulfuric acid), which he originally assumed to be of organic nature. Nor was he able to reveal the nature of the vanadium $\{[V^{IV}(H_2O)_5HSO_4]^{2+}$; see Section 4.1} present in the vanadoocytes, the vanadium-containing blood cells. Being aware of the potential of vanadium(V) compounds in oxidation catalysis, Henze proposed an analogous role for the vanadium containing ‘chromogen’ in oxygen activation. The function of vanadium in ascidians is still an enigma to date.

The next milestones in the biological chemistry of vanadium are listed chronologically below:

1933–36	H. Bortels: Discovery of the role of vanadium in nitrogen fixation.
1972	E. Bayer: Isolation of <i>amavadin</i> from the fly agaric.
1977	L. J. Cantley: Discovery of the role of vanadate as an efficient inhibitor of ATPases.
1983	H. Vilter: Isolation of the first vanadium enzyme, vanadate-dependent bromoperoxidase, in the marine alga <i>Ascophyllum nodosum</i> .
1986	Sussex Nitrogen Fixation Group: Isolation of a vanadium nitrogenase from <i>Azotobacter</i> .
Since ca 1980	Development of vanadium compounds for the treatment of diabetes mellitus.

Further Reading

- N. D. Chasteen (Ed.), *Vanadium in Biological Systems*, Kluwer, Dordrecht, **1990**.
- D. Rehder, Bioinorganic chemistry of vanadium, *Angew. Chem. Int. Ed. Engl.* **1991**, *30*, 148–167.
- H. Sigel and A. Sigel (Eds), *Vanadium and Its Role in Life*, Metal Ions in Biological Systems, Vol. 31, Marcel Dekker, New York, **1995**.

⁸ M. Henze, *Z. Physiol. Chem.* **1911**, *72*, 494–50.

- J. O. Nriagu (Ed.), *Vanadium in the Environment*, John Wiley Sons, Inc., New York, **1998**, Vol. 23.
A. S. Tracey and D. C. Crans (Eds), *Vanadium Compounds*, ACS Symposium Series, Vol. 711, American Chemical Society, Washington, DC, **1998**.
2nd Symposium on Biological Aspects of Vanadium, 1999, Berlin, *J. Inorg. Biochem.* **2000**, 80.
3rd International Symposium on the Chemistry and Biological Chemistry of Vanadium, 2001, Osaka, *Coord. Chem. Rev.* **2003**, 237.
D. C. Crans, J. J. Smee, E. Gaidamauskas and L. Yang, The chemistry and biochemistry of vanadium and the biological activities exerted by vanadium compounds, *Chem. Rev.* **2004**, 104, 849–902.
4th International Symposium on the Chemistry and Biological Chemistry of Vanadium, 2004, Szeged, *Pure Appl. Chem.* **2005**, 77.
A. S. Tracey, G. R. Willsky and E. S. Takeuchi, Vanadium – Chemistry, Biochemistry, Pharmacology and Practical Applications, CRC Press, Boca Raton, FL, **2007**.
K. Kustin, J. Costa Pessoa and D. C. Crans (Eds), *Vanadium: The Versatile Metal*, ACS Symposium Series, Vol. 974, American Chemical Society, Washington, **2007**.

References

- [1] M. E. Weeks and H. M. Leicester, *Discovery of the Elements*, 7th edn. Journal of Chemical Education, Easton, PA, **1968**, 351–382.
- [2] O. Wallach, *Briefwechsel zwischen J. Berzelius und F. Wöhler*, Vol. 1, Verlag von Wilhelm Engelmann, Leipzig, **1901**.
- [3] G. Hoppe, J. Siemroth and F. Damaschun, *Chem. Erde* **1990**, 50, 81–94.
- [4] *Gmelins Handbuch der Anorganischen Chemie*, Vanadium, Teil A, Lieferung 1 (System No. 48), Verlag Chemie, Weinheim, **1968**.
- [5] (a) N. G. Sefström, *Kgl. Vetenskapsacad. Handl.* **1830**, 255–261; (b) N. G. Sefström, *Ann. Phys. Chem.* **1831**, 21, 43–49.
- [6] H. E. Roscoe, *Philos. Mag.* **1870**, 39, 146–150.
- [7] J. H. Trefrey and S. Metz, *Nature* **1989**, 342, 531–533.
- [8] N. N. Lyalikova and N. A. Yukova, *Geomicrobiol. J.* **1992**, 10, 15–25.
- [9] W. Carpentier, K. Sandra, I. De Smet, A. Brige, L. De Smet and J. Van Beeumen, *Appl. Environ. Microbiol.* **2003**, 69, 3636–3639.
- [10] P. I. Premović, L. J. S. Jovanović and S. B. Zlatković, *J. Serb. Chem. Soc.* **1996**, 61, 149–157.
- [11] (a) A. Treibs, *Angew. Chem.* **1936**, 49, 682–686; (b) R. F. Fish and J. J. Komlenic, *Anal. Chem.* **1984**, 56, 510–517.
- [12] B. K. Hope, *Biochemistry* **1997**, 37, 1–13.
- [13] M. D. Cohen, *Toxicol. Ecotoxicol. News* **1996**, 3, 132–135.
- [14] J. Leuschner, H. Haschke and G. Sturm, *Monatsh. Chem.* **1994**, 125, 623–646.
- [15] J. Walter, *J. Prakt. Chem.* **1885**, 51, 107–111.
- [16] T. Hirao, *Chem. Rev.* **1997**, 97, 2707–2724.
- [17] E. O. von Lippmann, *Ber. Dtsch. Chem. Ges.* **1888**, 21, 3492–3493.
- [18] J. Priestley, *Philos Trans. R. Soc. London* **1876**, 166, 495–498.
- [19] M. Henze, *Z. Physiol. Chem.* **1917**, 72, 494–50.

This page intentionally left blank

2 Inorganic and Coordination Compounds of Vanadium

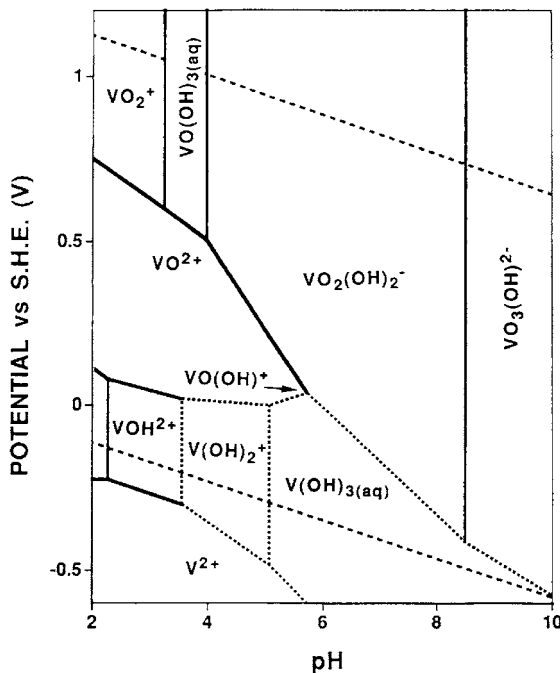
2.1 Inorganic Aspects of the Function of Vanadium in Biological Systems

2.1.1 The Aqueous Vanadium(III, IV and V) Systems

Acidification of vanadate(V) solutions yields yellow solutions of decavanadate $[H_nV_{10}O_{28}]^{(6-n)-}$ ($n = 0\text{--}3$, depending on the pH) or, for pH values <2 , the colourless hydrated dioxovanadium monocation, $[VO_2(H_2O)_4]^+$. If these V^V -containing solutions are reduced, gradual formation of vanadyl $V^{IV}O^{2+}$ (blue), V^{3+} (green) and V^{2+} (violet) occurs, again existing in the form of the aqua cations. This beautiful colour change has early fascinated chemists dealing with vanadium, and certainly is one of the justifications to name this element after Vanadis, the goddess of beauty. V^{2+} is not stable in aqueous media; it is rapidly reoxidised to V^{3+} by protons. The only vanadium oxidation states relevant for biological systems therefore are +III, +IV and +V. This situation is also reflected in the Baes–Mesmer diagram^[1] (Figure 2.1), describing the ranges of existence for vanadium in its different oxidation states and the speciation as a function of redox potential and pH.

The one-electron redox reactions for the three oxidation states of relevance are represented by Equations (2.1a)–(2.1c). Table 2.1 contains the standard potentials (E°) for the three redox pairs together with the respective potentials at pH 7, assuming equal equilibrium concentrations of the redox partners. Table 2.1 also summarises redox potentials (at pH 7) for biochemically relevant redox systems. All potentials in this chapter and throughout the book are quoted relative to the normal hydrogen electrode (NHE). Potentials referenced to other electrodes have been converted as depicted in Table 2.2.

The more positive the potential is, the stronger is the electron affinity of the oxidised form. Inspection of Table 2.1 thus reveals that, under aerobic conditions, V^V is stable whereas, in anoxic environments, which normally prevail in the cytoplasm, reducing agents such as ascorbate, glutathione and NADH readily reduce $V^V O_2^+$ to $V^{IV}O^{2+}$, provided that the inorganic species are available as such, i.e. not complexed to ligands present in the intra- and extracellular fluids. Vanadate ($[H_2VO_4]^-$) is less easily reduced, and the reduction of $V^{IV}O^{2+}$ to V^{3+} does not take place under common conditions. V^{III} is therefore of minor importance as it comes to physiological actions of vanadium, with

**Figure 2.1**

Baes–Messmer diagram for the aqueous vanadium system. Standard redox potentials (in V) vs the normal hydrogen electrode (NHE) are given. The two parallel dashed lines running from the upper left to the lower right indicate the range of stability of water. Reproduced from C. F. Baes and R. E. Messmer, *The Hydrolysis of Cations*, pp. 197–210. Copyright (1976), with permission from John Wiley & Sons, Ltd.

Table 2.1 Redox potentials [in V versus the normal hydrogen electrode (NHE)^a] for inorganic vanadium species (in bold) and selected physiological systems.

Species ^b	E°	$E^{\text{pH}=7}$
VO²⁺/V³⁺ (V^{IV}/V^{III})	+0.359	-0.462
H₂VO₄⁻/VO²⁺ (V^V/V^{IV})	+1.31	-0.34
NAD ⁺ /NADH ^c		-0.315
Pyruvate/lactate		-0.185
1/2(GS) ₂ /GSH ^d		-0.10
Ubiquinone/ubiquinol		+0.045
Dehydroascorbate/ascorbate		+0.06
VO₂⁺/VO²⁺ (V^V/V^{IV})	+1.016	+0.19
O ₂ /H ₂ O ₂	+0.695	+0.295
1/2O ₂ /H ₂ O	+1.23	+0.815

^aSee Table 2.2 for potentials of other reference electrodes vs NHE.

^bCationic vanadium species are present in the form of their aqua complexes.

^cNicotine adenine dinucleotide in its oxidised and reduced form.

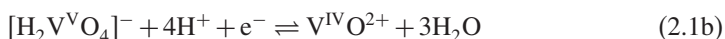
^dGlutathione in its oxidised and reduced form.

Table 2.2 Redox potentials of couples frequently used as references.

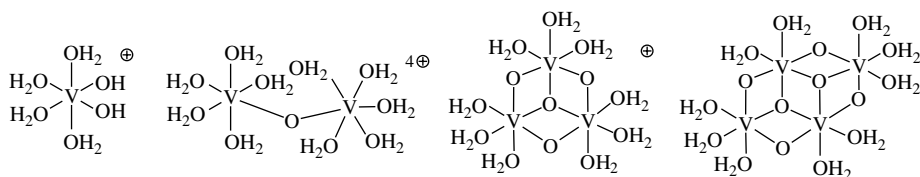
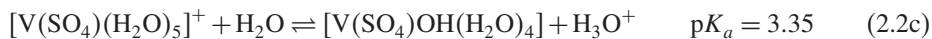
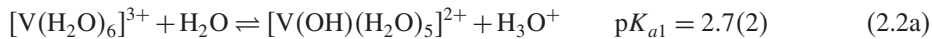
Couple	Potential vs NHE (V)
Ag/AgCl/saturated KCl	+0.197
SCE (saturated calomel electrode)	+0.244
Ferrocene/ferrocenium	ca +0.40 ^a

^aThis reference electrode is used in non-aqueous systems; the exact potential is subject to the conditions (such as the nature of the solvent).

the exception of ascidians and Polychaeta fan worms, where this oxidation state is the predominant one (cf. Section 4.1).



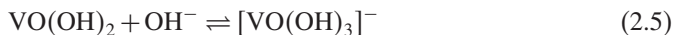
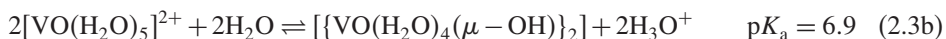
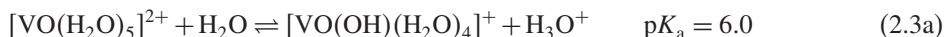
In aqueous solutions containing the V^{3+} cation, the following octahedral species, depending on pH (and concentration), can be present: $[\text{V}(\text{H}_2\text{O})_6]^{3+}$, $[\text{V}(\text{OH})(\text{H}_2\text{O})_5]^{2+}$, $[\text{V}(\text{OH})_2(\text{H}_2\text{O})_4]^+$ and $[\{\text{V}(\text{H}_2\text{O})_5\}_2(\mu-\text{O})]^{4+}$. At concentrations <1 mM, the oxo-bridged dinuclear complex can be neglected. For the acid – base equilibria involving the mononuclear species (including the pK_a values), see Equations (2.2a) and (2.2b).^[2] In addition, tri- and tetranuclear complexes have been suggested, on the basis of speciation studies, as a result of hydrolysis and condensation at $\text{pH} > 3.5$. Structural formulae are shown in Figure 2.2. The presence of sulfate in acidic solutions of V^{3+} leads to the formation of aqua-sulfato complexes such as $[\text{V}(\text{SO}_4)(\text{H}_2\text{O})_5]^+$, [Equation (2.2c)], which is of interest in the light of the conditions in the vanadium containing blood cells of ascidians.^[2]

**Figure 2.2**

Vanadium(III) species which can be present in aqueous solution around pH 3.^[2]

In contrast to V^{III}, V^{IV} forms monooxo complexes in aqueous media, based on the stable vanadyl ion, VO²⁺. Non-oxo vanadium(IV) complexes are known, including the naturally occurring amavadin, and the ‘bare’ V⁴⁺ ion likely plays a role in catalytic turnover in oxidation catalysis. The vanadyl ion, however, dominates V^{IV} chemistry.

The vanadyl ion remains in solution only under sufficiently acidic conditions [cf. Equations (2.3a) and (2.3b)]. Precipitation of insoluble hydroxide VO(OH)₂ (Equation (2.4)) and formation of oligonuclear hydroxo species such as {[(VO)₂(OH)₅]⁻}_n begins above pH 5. Concomitantly, vanadate(IV) [VO(OH)₃]⁻ starts to be present at nanomolar concentrations (Equation (2.5)), gaining importance beyond pH 10.



All vanadium(V) species present in water at ambient pH are anionic. The cationic VO³⁺ and VO₂⁺ exist only when stabilised by ligands. The speciation in the aqueous vanadate system has been thoroughly studied over the last two decades by Petterssons' group, employing a combination of H⁺ potentiometry and ⁵¹VNMR spectroscopy.^[3] Vanadium-51 NMR spectroscopy is a versatile tool for studying diamagnetic vanadium systems, and this method will be addressed in some detail in Section 3.1. Figure 2.3 is a demonstration of how the various vanadate species present at about pH 6 and a vanadium concentration [c(V)] of 5 mM can be differentiated by ⁵¹V NMR. The speciation is a function of pH, concentration and, to a lesser extent, the ionic strength of the aqueous medium.

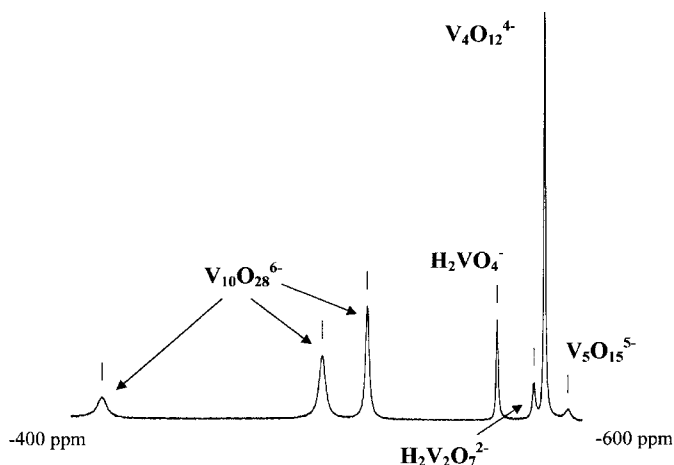


Figure 2.3
⁵¹V NMR spectrum of a 5 mM aqueous vanadate solution at pH 5.7 and an ionic strength of 0.6 M Na(Cl).

The influence of these parameters on the speciation is reflected in the distribution diagrams shown in Figure 2.4 and the predominance diagram in Figure 2.5. At physiological concentrations, i.e. $c(V) = 1 \mu\text{M}$ (Fig. 2.4, right) and less, only monovanadate exists.

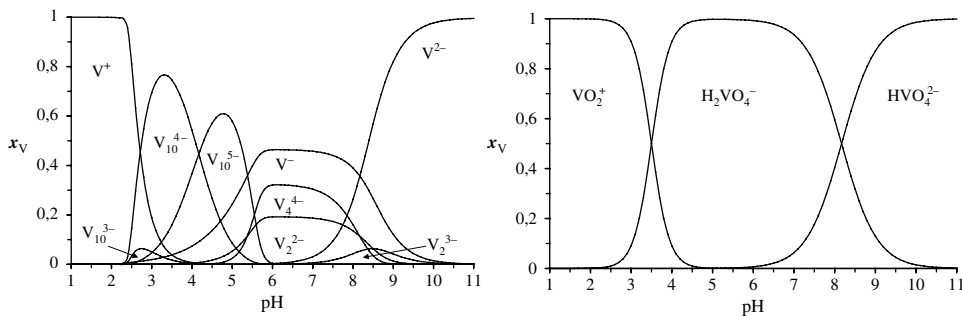


Figure 2.4

Speciation diagrams for aqueous vanadate solutions (mole fraction x_V vs pH) for $c(V) = 1 \text{ mM}$ (left) and $1 \mu\text{M}$ (right; calculated), $I_{\text{Na}(\text{Cl})} = 0.15 \text{ mM}$, 25°C . $\text{V}^+ = [\text{VO}_2(\text{H}_2\text{O})_4]^+$; for the notations of vanadates used in the diagram on the left, see Table 2.3. Species comprising less than 3% are not shown. Courtesy of L. Pettersson, Umeå University, Sweden.

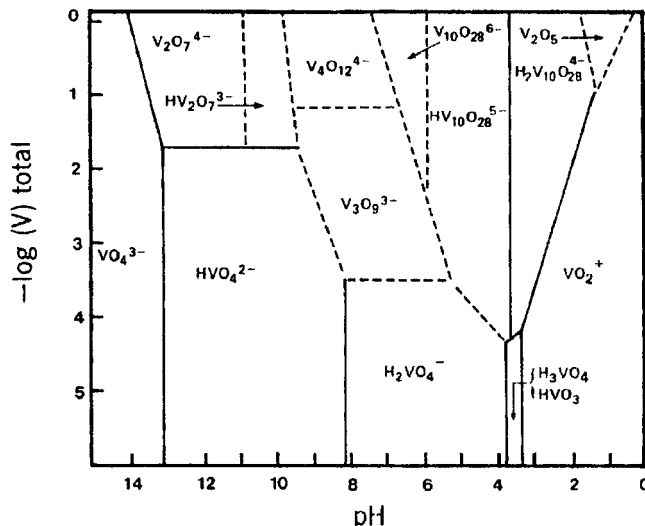


Figure 2.5

Predominance diagram, showing the regions in which the species indicated are those present in the highest concentration. Broken lines indicate less certain demarcations. Reproduced from C. F. Baes and R. E. Messner, *The Hydrolysis of Cations*, pp. 197–210. Copyright (1976) with permission from John Wiley & Sons, Ltd.

The structures of the more prominent vanadates are represented in Figures 2.6 and 2.7. Table 2.3 provides an overview of most of the vanadates which can be present, including the pK_a values [at ionic strengths of 0.6 and 0.15 M Na(Cl), respectively] for those species

which can be involved in protonation equilibria. An ionic strength of 0.15 M corresponds to the conditions in blood serum and an ionic strength of 0.6 M to the saline medium in the oceans.

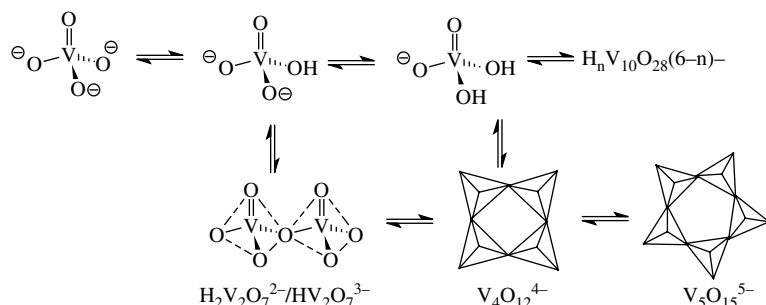


Figure 2.6

Structures of the most prominent tetrahedral vanadates present in aqueous solutions.

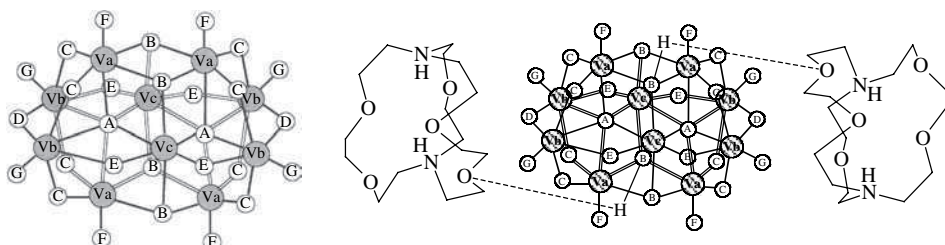


Figure 2.7

Left: schematic drawing of decavanadate, $V_{10}O_{28}^{6-}$, showing the different vanadium and oxygen sites. The oxygens B and C are potential sites for protonation. Right: dihydrogendifdecavanadate, $[H_2V_{10}O_{28}]^{4-}$, stabilised by two sandwiching cryptand cations, $[H_2C221]^{2+}$, through electrostatic and hydrogen bonding interaction.

Table 2.3 Selection of vanadate species present in aqueous solution at concentrations $c(V) > \text{ca } 1 \text{ mM}$. For protonated species, pK_a values are provided for two different ionic strengths, $I_{\text{Na(Cl)}}$ (cf. ref. 3). For the structures, see Figures 2.5 and 2.6.

Species	Notation ^a	pK_a at $I = 0.15 \text{ M}$	pK_a at $I = 0.6 \text{ M}$	δ (^{51}V)
HVO_4^{2-}	V^{2-}		13.36	-534
H_2VO_4^-	V^-	8.17	7.95	-560
$\text{HV}_2\text{O}_7^{3-}$	V_2^{3-}	10.34	9.79	-564
$\text{H}_2\text{V}_2\text{O}_7^{2-}$	V_2^{2-}	8.50	8.23	-573
$\text{HV}_4\text{O}_{13}^{5-b}$		9.35	8.73	-566 to -571
$\text{V}_4\text{O}_{12}^{4-}$	V_4^{4-}			-577

$V_5O_{15}^{5-}$				-585
$HV_{10}O_{28}^{5-}$	V_{10}^{5-}	6.62	6.07	-424, -499, -515 ^c
$H_2V_{10}O_{28}^{4-}$	V_{10}^{4-}	4.17	3.61	-422, -502, -519 ^c
$H_3V_{10}O_{28}^{3-}$	V_{10}^{3-}	1.86	1.21	-427, -515, -534 ^c
$H_{12}V_{13}O_{40}^{3-}$				-523, -538 ^d

^aSee Figure 2.4.^bLinear tetravanadate.^cThe signals correspond to sites Va (low-field), Vb and Vc (high field); cf. Figure 2.6, left.^dThe signal intensity ratio is 1:12, the low-field signal (-523) corresponding to the internal, tetrahedral vanadium site.^[5]

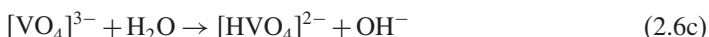
At pH 7, the most prominent species present in vanadate solutions of $c(V) > \sim 1\text{ mm}$ is cyclic tetravanadate $[V_4O_{12}]^{4-}$. Along with tetravanadate, di- and monovanadate can be detected, and also some cyclic pentavanadate, $[V_5O_{15}]^{5-}$ (Figure 2.3). The formation of condensed species is favoured at higher concentrations and higher ionic strengths. The vanadates of differing nuclearity are in equilibrium with each other, as indicated by the equilibrium arrows in Figure 2.6. Exchange rates are in the millisecond region. Mono- and divanadate are subject to rapid protonation/deprotonation. At pH 7, the diprotonated forms ($[H_2VO_4]^-$, $pK_a = 8.17$ for physiological ionic strength; $[H_2V_2O_7]^{2-}$, $pK_a = 8.50$) predominate. As far as monovanadate is concerned, this is of some interest in the context of its similarity with (and competitiveness to) phosphate which, at pH 7, is present mainly in its monoprotonated form, i.e. $[HPO_4]^{2-}$ (pK_a of $[H_2PO_4]^- = 6.7$), carrying two negative charges. In the medium to strong alkaline range, only mono- and divanadate exist.

On acidification, decavanadate forms, starting at a pH of ca 6. Whereas mono-, di-, tetra- and pentavanadate are built up of tetrahedral units, the vanadium centres in decavanadate (Figure 2.7) are in an octahedral environment. There are three different vanadium sites (represented by three different ^{51}V NMR signals; Figure 2.3), viz. V_A, V_B and V_C in a ratio of 2:2:1. The V_C sites correspond to two central, regular VO_6 octahedra and the V_A and V_B sites to peripheral tetragonal-pyramidal O=VO₄ units additionally linked, via a comparatively weak bond, to a sixth (bridging) oxo group. Of the seven distinct oxygen sites, labelled A–G in Figure 2.7, the doubly bridging B and the trebly bridging C sites can readily be protonated as the pH decreases. Below pH 3, decavanadate becomes unstable and $[VO_2(H_2O)_4]^+$ begins to form. This cationic species is the only one which exists below pH 2. Although thermodynamically also unstable above pH 6, decavanadate breaks down only slowly (within hours) in the mildly alkaline region to form lower nuclearity vanadates. Decavanadate solutions thus retain their yellow colour for some time even beyond pH 7. Large cations, such as the diprotonated cryptand $[H_2C221]^{2+}$ (Figure 2.7, right), can stabilise decavanates up to pH values of ca 9.^[4] This stabilisation, also against degradation at very low concentrations, may be achieved under physiological conditions by ionophores, peptides and related systems. Decavanadate has been shown to interact with biological systems, such as myosin and calcium ion channels.

Other condensed vanadates, e.g. trivanadate, hexavanadate, dodecavanadate and pentadecavanadate, are known, but play minor roles in the aqueous systems (tri- and hexavanadate) or are thermodynamically unstable with respect to decavanadate (polyoxovanadates with more than 10 vanadium centres). An interesting case from the structural point of view is the tridecavanadate $[H_{12}V_{13}O_{40}]^{3-}$, included in Table 2.3:^[5]

12 octahedrally coordinated vanadium atoms (four sets of three corner-sharing, distorted octahedra) are arranged around a tetrahedral central vanadium atom, a structural arrangement commonly known as Keggin structure (more information on the Keggin structure is given in Section 2.1.2).

In the solid state, metavanadates $M[VO_3]$ exist. These are hydrolysed to orthovanadate [Equation (2.6a)], and further condense to oligovanadates when dissolved in water; [Equation (2.6b)]. The term ‘solutions of metavanadate’ often encountered in the literature, particularly in biochemical and pharmaceutical contexts, refers to such a mixture, mainly containing $[H_2VO_4]^-$, $[H_2V_2O_7]^{2-}$ and $[V_4O_{12}]^{4-}$. The orthovanadate anion liberated as orthovanadates $M_3[VO_4]$ are dissolved in water reacts as a Brønsted base [Equation (2.6c)]; orthovanadate solutions thus are alkaline. Meta- and orthovanadates also occur naturally in the form of minerals, along with di-, hexa- and even decavanadates; cf. Table 1.1.



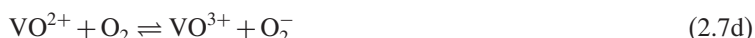
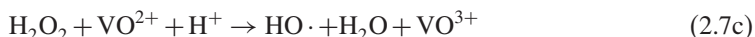
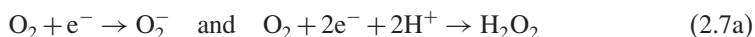
Thiovanadates such as $[VS_4]^{3-}$, $[VS_3(SH)]^{2-}$ and $[V_2S_7]^{4-}$ are known. Their range of existence (strongly alkaline solutions or non-aqueous media) is, however, beyond physiological relevance. In water, thiovanadates are readily hydrolysed via $[VS_{4-n}O_n]^{3-}$ intermediates. The only system comparatively stable in water is the lithium salt $Li_3[VS_4]$,^[6] apparently because intimate ion pairs are formed with the highly polarising counter cation Li^+ .

2.1.2 Binary and Ternary Systems Containing Vanadium(IV and V)

In this section, the existence and stability of species which form in aqueous vanadate solutions in the case where a second (and, eventually, third) inorganic component is present will be addressed. Here these systems are referred to as binary (and ternary), not necessarily in accordance with the literature, where H^+ , if included in the overall considerations, is treated as an additional reaction partner. In addition, oxovanadium(IV and V) ‘salts’ derived from phosphoric acids will be covered briefly.

Inorganic components of interest in the context of the physiological effects of vanadate are phosphate and peroxide. Hydrogenphosphate ($[H_2PO_4]^-/[HPO_4]^{2-}$), along with hydrogencarbonate ($[HCO_3]^-/CO_2$), is a physiological buffer; it is involved in rebuilding bone structures [the inorganic part of which is hydroxylapatite $Ca_5(PO_4)_3(OH)$], in the energy metabolism, and participates in the regulation of, *inter alia*, Ca^{2+} levels. The mean phosphate concentration in human blood plasma is 1.2(4) mm. As already pointed out, vanadate is an effective competitor for phosphate and may intervene with phosphate-metabolising enzymes (Section 5.2.1), with the activation of substrates by phosphorylation and the anaerobic energy production via ATP/ADP (adenosine triphosphate/diphosphate), and with cofactors in redox enzymes such as NADP (nicotinamide adenine dinucleotide phosphate). Peroxide can form in the course of the reduction of oxygen in the respiratory chain, through reduction or dismutation of superoxide or dimerisation of hydroxyl radicals which again are generated in a Fenton reaction from H_2O_2 and Fe^{2+} or VO^{2+} [cf. Equation (2.7)]. V^{IV} itself can be involved in the production of hyperoxide. In addition, the vanadate–peroxide interaction is of interest in the context of the insulin-mimetic (or

insulin-enhancing) properties of peroxovanadates and chemo-preventive carcinogenesis (Section 5.1). Further, peroxovanadate is the active cofactor species in vanadate-dependent haloperoxidases (Section 4.3).



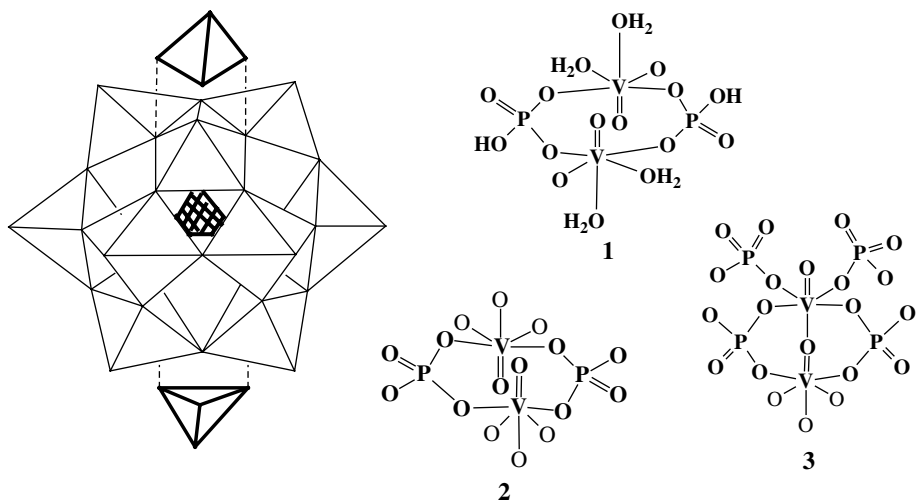
As a third inorganic component, hydroxylamine (NH_2OH) will be considered. Its physiological role is less obvious than that of phosphate and peroxide. There is, however, chemical comparability between the isoelectronic species H_2O_2 and NH_2OH when it comes to interaction with vanadium. In vanadate-dependent haloperoxidases, hydroxylamine acts as an antagonist to peroxide. An additional justification for addressing NH_2OH arises from the fact that an organic derivative of hydroxylamine constitutes the ligand system of amavadin, the V^{IV} complex present in mushrooms of the genus *Amanita*.

In the vanadate–phosphate system, the mixed species $[\text{H}_x\text{VPO}_7]^{(4-x)-}$ form, [Equation (2.8)], in all possible protonation states, i.e. $x = 1\text{--}4$.^[7] The formation is fast, and the mixed anhydrides are in rapid exchange with their hydrolysis products monovanadate and monophosphate. At physiological pH, $[\text{HVPO}_7]^{3-}$ and $[\text{H}_2\text{VPO}_7]^{2-}$ ($\text{pK}_a = 7.21$ at an ionic strength of 0.15 M) are present in about equimolar amounts. The formation constant of the mixed anhydride is 25 M^{-1} at pH 6.7 and 5.8 M^{-1} at pH 8.^[8] The phosphovanadate is thus by one to two orders of magnitude less stable than divanadate (the formation constant for the formation of divanadate from monovanadate is ca 350 M^{-1}), but 10^6 times more stable towards hydrolysis than diphosphate. An analogue to triphosphate, where one of the phosphorus atoms is replaced by vanadium, viz. $[\text{H}_2\text{VP}_2\text{O}_{10}]^{3-}$ ($\text{pK}_a = 6.31$), has also been detected.^[7] The question of whether the arrangement corresponds to VPP or PVP remains to be answered. At pH values <5.5 , the highly condensed species $[\text{H}_x\text{V}_{14}\text{PO}_{42}]^{(8-x)-}$ ($x = 3, 4$ and 5) gains importance. This polyoxophosphovanadate attains the bicapped α -Keggin structure (see Figure 2.8).



The cations VO^{3+} and VO^{2+} form ‘salts’ with phosphate, such as $\text{V}^{\text{V}}\text{O}(\text{PO}_4)$, $\text{V}^{\text{IV}}\text{O}(\text{HPO}_4)$ and $\text{V}^{\text{IV}}\text{O}(\text{H}_2\text{PO}_4)_2$, used as catalysts in, e.g., the conversion of butane to maleic anhydride and of propane to acrylic acid. Mixed salts with lithium, e.g. $\text{Li}_4\text{V}^{\text{IV}}\text{O}(\text{PO}_4)_2$, represent a promising new development in lithium- and vanadium (oxide)-based batteries. Structure information is available for several binary and ternary vanadylphosphates^[9] (Figure 2.8). In the coordination polymers containing the moieties VOPO_4 , $\text{VO}(\text{H}_2\text{O})_2(\text{HPO}_4)$ (**1** in Figure 2.8) and $(\text{VO})_2\text{P}_2\text{O}_7$, distorted VO_6 octahedra are bridged by PO_4 tetrahedra. The anionic matrix of $\text{Ba}[\text{VOPO}_4]_2 \cdot 4\text{H}_2\text{O}$ is built up of layered oxovanadium(IV)phosphate (**2**), whereas, in $\text{Na}_4[\text{VO}(\text{PO}_4)_2]$, isolated chains are formed by corner-sharing VO_6 octahedra, linked additionally through corners to PO_4 tetrahedra (**3**).

Evidence for the formation of vanadyl–phosphate complexes in aqueous solution relevant for physiological systems has been obtained from electron paramagnetic

**Figure 2.8**

Left: idealised polyhedral representation of the bicapped α -Keggin structure underlying the phosphovanadate core $H_x V_{14} PO_{42}^{(x)-}$, showing the 12 (4×3) corner-sharing VO_6 octahedra, the central tetrahedral phosphate (hatched) and the two capping tetrahedral vanadate subunits (bold; connected to the Keggin core by dashed lines), with the doubly bonded oxo group pointing towards the apices. Right: basic structural elements of $[VO(H_2O)_2][HPO_4] \cdot 2H_2O$ (**1**)^[9a], $Ba[VOPO_4]_2 \cdot 4H_2O$ (**2**)^[9b] and $\beta - Na_4[VO(PO_4)_2]$ (**3**)^[9c] counter-ions not shown.

resonance (EPR) and electron absorption spectroscopy.^[10] Examples of species detected in the slightly acidic to physiological range include $VO(H_2PO_4)_2$, $VO(HPO_4)$, $VO(H_2P_2O_7)$, $[VO(HP_2O_7)]^-$, cyclic $[(VO)_3(P_2O_7)_3]^{6-}$ and $[VO(P_3O_{10})_2]^{8-}$. The dominant species in the VO^{2+} – monophosphate system in the slightly acidic range is $VO(HPO_4)$. In the neutral to slightly alkaline range, it hydrolyses to form vanadium hydroxides; in the presence of a third component, such as maltol, hydrolysis is suppressed due to the formation of ternary complexes.^[10b] Maltolatovanadium(IV) complexes have attained an important role as insulin-enhancing agents, and will be covered in more detail in Section 5.1.1.

In all of these oxovanadium(IV and V) phosphates, the phosphate acts as a ligand for the oxovanadium unit, rather than as a counter-ion.

In the binary vanadate–peroxide system, mono-, di- and triperoxovanadates derived from mono- and divanadate in different protonation states are present.^[11] The ternary vanadate–phosphate–peroxide system contains additional mono- and diperoxo species derived from monophosphomonovanadate.^[7] The peroxy group coordinates exclusively in the symmetrical side-on fashion. In Figure 2.9, structures on selected peroxovanadates and peroxophosphovanadates are shown; Table 2.4 summarises data. Assignment of the various species is carried out on the basis of their ⁵¹V chemical shifts, which are sensitive to the amounts of peroxy groups present and, in particular, to the protonation state. The peroxovanadates rapidly form as peroxyde is added to vanadate solutions, suggesting that their generation is due to hydrolysis, by H₂O₂, of higher nuclearity species [Equation (2.9)], rather than by direct exchange of oxo anions in the parent vanadate by the peroxy anion of added H₂O₂. The stability of peroxovanadates in the acidic regime is restricted: vanadates tend to catalyse the disproportionation of hydrogen peroxide. The

composition of the peroxovanadates largely depends on the pH and the vanadate:H₂O₂ ratio. The main species present at pH 7 and with excess peroxide are [HV₂O₃(O₂)₄]³⁻ and [H₂V₂O₃(O₂)₄]²⁻. Figure 2.10 provides a speciation diagram for the peroxovanadate system.

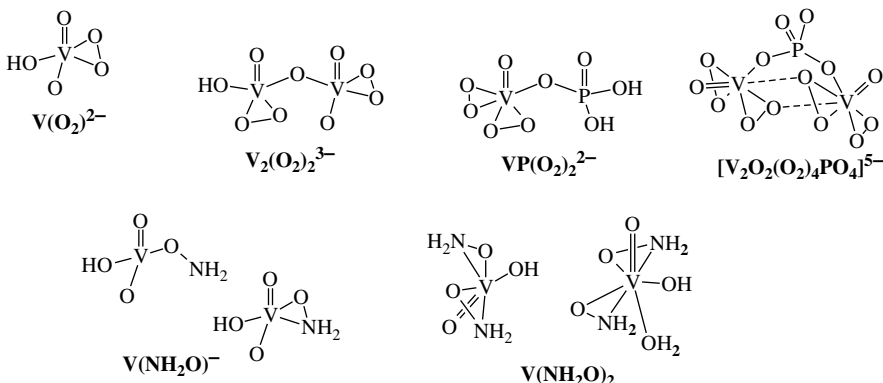
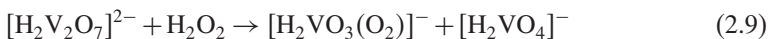


Figure 2.9

(Proposed) structures of peroxovanadates and -phosphovanadates and of hydroxamido derivatives of vanadate. For notations, see Table 2.3. For the species ‘ $\text{V}(\text{NH}_2\text{O})_2$ ’, only the major isomer (with the hydroxylamido oxygens in a *cis* position) is shown. The structures for $[\text{V}_2\text{O}_2(\text{O}_2)_4\text{PO}_4]^{5-}$ [12] is based on X-ray diffraction data.

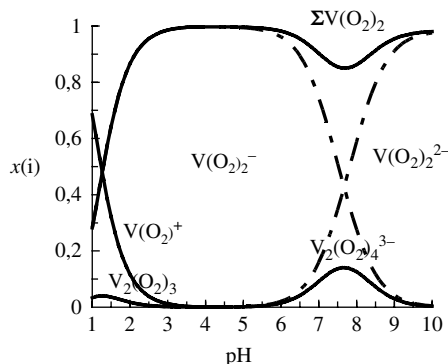


Figure 2.10

Speciation diagram for the vanadate–peroxide system. $c(\text{V}_{\text{total}}) = 10 \text{ mM}$, $c(\text{H}_2\text{O}_2)/c(\text{V}) = 2$, ionic strength 0.15 M NaCl, 25°C. Species containing less than 2% of V_{total} are not shown. Courtesy of L. Pettersson, Umeå University, Sweden.

The vanadate–hydroxylamine aqueous system does not show as extensive speciation as the corresponding peroxide system. All of the complexes identified in aqueous media derive from monovanadate $[\text{H}_2\text{VO}_4]^-$ by formally replacing one or two of the hydroxo or oxo groups by the hydroxamido (NH_2O^-) function (Figure 2.9 and Table 2.4).^[13] In the case of the formation of the monoligate species, two variants have been observed. In one of these,

Table 2.4 Peroxovanadates and –phosphovanadates, and hydroxylamido derivatives of vanadates.^a

Species	Notation	pK_a at $I_{\text{Na}(\text{Cl})} =$ 0.15 mM	$\delta(^{51}\text{V})$
$\text{HVO}_3(\text{O}_2)^{2-}$	$\text{V}(\text{O}_2)^{2-}$		-625
$\text{HVO}_2(\text{O}_2)_2^{2-}$	$\text{V}(\text{O}_2)_2^{2-}$		-765
$\text{H}_2\text{VO}_2(\text{O}_2)_2^-$	$\text{V}(\text{O}_2)_2^-$	7.67	-691
$\text{HVO}(\text{O}_2)_3^{2-}$	$\text{V}(\text{O}_2)_3^{2-}$		-732
$\text{HV}_2\text{O}_6(\text{O}_2)^{3-}$	$\text{V}_2(\text{O}_2)^{3-}$		-622, -563 ^b
$\text{HV}_2\text{O}_5(\text{O}_2)_2^{3-}$	$\text{V}_2(\text{O}_2)_2^{3-}$		-737, -555 ^b
$\text{HV}_2\text{O}_3(\text{O}_2)_4^{3-}$	$\text{V}_2(\text{O}_2)_4^{3-}$		-755
$\text{HVPO}_6(\text{O}_2)^{3-}$	$\text{VP}(\text{O}_2)^{3-}$		-617
$\text{HVPO}_5(\text{O}_2)_2^{3-}$	$\text{VP}(\text{O}_2)_2^{3-}$		-731
$\text{H}_2\text{VPO}_5(\text{O}_2)_2^{2-}$	$\text{VP}(\text{O}_2)_2^{2-}$	5.44	-711
$\text{HVO}_3(\text{ONH}_2)^-$	$\text{V}(\text{NH}_2\text{O})^-$		-569 ^c , -670 ^d
$\text{HVO}_2(\text{ONH}_2)_2$	$\text{V}(\text{NH}_2\text{O})_2$	5.9, 6.6 ^e	-819, -839 ^e
$\text{HVO}_2(\text{H}_2\text{O})(\text{ONH}_2)_2$	$\text{V}(\text{NH}_2\text{O})_2$	7.4	-852, -861 ^e

^aFor data, see refs. 7 and 11 (peroxovanadates) and 13 (hydroxylamido derivatives). For structures, see Figure 2.9.

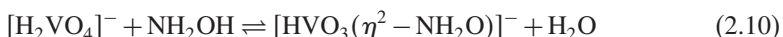
^bPeroxovanadate and vanadate moiety, respectively.

^cMonodentate coordination of NH_2O^- via O.

^dBidentate coordination.

^eThe low-field signal corresponds to the *trans*- and the high-field signal (major component) to the *cis*-isomer; cf. Figure 2.9.

hydroxylamide coordinates in a monodentate fashion through the oxo functionality. The second variant is an analogue of the respective monoperoxovanadate, i.e. side-on coordination is realised. The formation constant for the latter, [Equation (2.10)], is 540 M^{-1} . Two sets of two neutral species are observed for the bis(hydroxamido) species ‘ $\text{V}(\text{NH}_2\text{O})_2$ ’ in Figure 2.9. One of these sets derives from tetrahedral vanadate; the other set contains an additional water ligand and may thus be termed trigonal bipyramidal (if each hydroxylamide is considered to occupy one coordination site) or pentagonal bipyramidal (if the hydroxamides are taken as bidentate ligands). In either case, the two NH_2O^- ligands can be arranged so as to give rise to a *trans* or a *cis* arrangement of the hydroxylamide-O. The *cis* arrangement shown in Figure 2.9 is favoured. Corresponding complexes derived from vanadate have been noted for mono- and dimethylhydroxylamine. The side-on or η^2 coordination of hydroxylamides is of interest in the context of amavadin, which contains hydroxylamine-derived ligands. This topic will be discussed in Section 4.2.

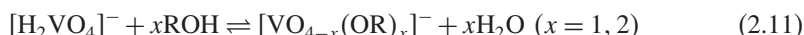


2.1.3 Halides and Esters Derived from Orthovanadic Acid

Formal substitution of three OH groups in hypothetical orthovanadic acid $\text{H}_3\text{VO}_4[\text{O}=\text{V}(\text{OH})_3]$ for halide leads to the trihalides VOX_3 ($\text{X} = \text{F}, \text{Cl}, \text{Br}$). The corresponding nitrate $\text{VO}(\text{NO}_3)_3$ is also known. The oxovanadium trihalides can add an additional

halide to form pentavalent, anionic $[\text{VOX}_4]^-$ ($\text{X} = \text{F}, \text{Cl}$) which, upon partial hydrolysis, are converted to the dioxovanadate anions, $[\text{VO}_2\text{X}_2]^-$. All of these compounds are of minor – if any – interest in the physiological context, because their formation and existence in aqueous media are obsolete.

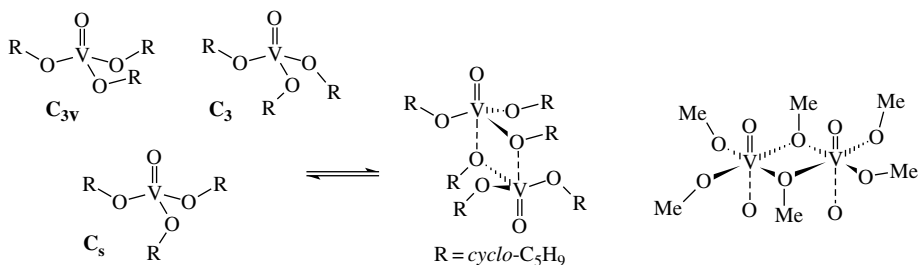
As pointed out in the previous section, phosphate derivatives related to ' H_3VO_4 ' are of interest when it comes to the phosphate–vanadate antagonism. Similarly, vanadate esters are analogues of phosphate esters; (Section 5.2.1). Esters of orthovanadic acid have been known since 1913.^[14] They are obtained by, e. g., condensation of vanadates and alcohols (ROH) in aqueous media [Equation (2.11)], alcoholysis of VOCl_3 [Equation (2.12)] or the reaction of vanadium pentoxide and alcohols in the presence of water scavengers [Equation (2.13)]. The triesters are sensitive to moisture. The primary product of hydrolysis is the hexavanadic acid derivative $\text{V}_6\text{O}_{13}(\text{OR})_4$, giving rise to a yellow colouration as the colourless triesters come into contact with moist air.



The formation constants for the monoesters [$x = 1$ in Equation (2.11)] are small, typically around 0.1 M^{-1} for alkyl alcohols, and an order of magnitude more for phenols.^[15] Esters derived from divanadate, such as $[\text{HV}_2\text{O}_6(\text{OR})]^3-$, have also been noted. In analogy with the vanadates, the esters are subject to protonation–deprotonation equilibria.

From a structural point of view, the triesters exhibit interesting features (Figure 2.11). For $\text{R} = \text{Me}$, the solid-state structure revealed a polymer,^[16] with the vanadium centres in a tetragonal pyramidal environment. The doubly bonded oxo group¹ is in the apex. A sixth, weak bond opposite the apical position is formed to the methoxy group of a neighbouring vanadium. In organic solvents, the esters are monomers with a trigonal pyramidal geometry, which can associate to give dimers (with a trigonal bipyramidal arrangement of each of the monomeric units) by weak interaction, mimicking the trigonal bipyramidal intermediate in enzymatic phosphoester hydrolysis. Monomers and dimers (and possibly species with a higher degree of association) are in equilibrium with each other, as shown in Figure 2.11. In the structurally characterised dimer $\{\text{VO}(\text{O}-\text{cycloC}_5\text{H}_9)_3\}_2$,^[17] the monomeric subunits contain the three alkoxo ligands in an all-*cis* arrangement, giving rise to idealised C_{3v} symmetry. In the structurally characterised monomeric ester $\text{VO}(\text{O}-\text{tertBu})_3$ the local symmetry is C_s .^[16] In solution, additional rotamers have been shown to exist, as evidenced by IR and Raman spectroscopy. Condensed (cluster-type) vanadate esters derived from tetra-, hexa- and decavanadate, containing diolates and triolates such as $\text{RC}(\text{CH}_2\text{O}^-)_3$ have been characterised in the solid state.^[18]

¹ The bonding situation in the VO moiety [and also as in the isoelectronic V(NR) moiety] is sometimes treated in terms of a triple bond ($\sigma + 2\pi$ donor bonds). Since the respective bonding orbitals are available, this view may be considered reasonable, and is supported by DFT calculations. In the frame of the valence bond description, the bond order between V and O^{2-} (or NR^-) is 2, or less, if the oxo group is involved in additional (weak) bonding interactions. Throughout this book, the VO bond will be referred to in terms of a *double* bond, and hence the descriptor $\text{V}=\text{O}$ will be used rather than $\text{V}\equiv\text{O}$.

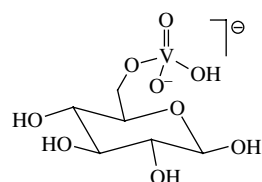
**Figure 2.11**

Structures of oxovanadium tris(alkoxides) (triesters of ' H_3VO_4 '). In solution, there are concentration-dependent equilibria between monomers and dimers. In the solid state, monomers (bulky R substituents), dimers (R = cyclopentyl) or polymers exist (R = Me).^[16,17]

2.2 Interaction of Aqueous Vanadate and Vanadyl with Biogenic Ligands

2.2.1 Speciation in the Vanadate System

The preceding section on vanadate esters links to the present, more general, section in so far as ester formation with biogenic ligands containing alcohol functions can occur under physiological conditions. The formation of glucose-6-vanadate (Figure 2.12) has thus been inferred from the observation that the catalysis, by glucose-6-phosphate dehydrogenase, of the oxidation of glucose by NADP⁺ is activated by vanadate. Given the fact that the formation constants for the formation of 1:1 esters with 'simple' alcohols are rather small – of the order of magnitude of 0.1–1 M⁻¹ – one might expect more efficient esterification of vanadate with biogenic 'alcohols' containing more than one OH function (such as sugars, nucleotides or ascorbic acid) or, in addition to OH, carboxylate (such as lactate and citrate), or peptide functions (as in the case where serine or threonine is a constituent of a peptide or protein building block).

**Figure 2.12**

Glucose-6-phosphate, a possible substrate in vanadate-activated oxidation of glucose by NADP, catalysed by glucose-6-vanadate dehydrogenase.

Table 2.5 provides an overview of the concentrations of important components of human blood, important in the sense that they constitute potential ligands for vanadium. The concentrations of lactate (1.5 mM) and citrate (0.1 mM) are comparatively high. Along with phosphate (1.2 mM), they are the major potential low molecular weight ligators for vanadate and vanadyl. The system containing vanadate(V) and lactate (lac) has been extensively studied,^[19,20] and the species identified on the basis of ⁵¹V NMR and H⁺ potentiometry include mono-, di-, tri- and tetranuclear forms, for which the structures

shown in Figure 2.13 have been proposed, in part on the basis of evidence obtained from X-ray diffraction studies.^[21] The closely related α -hydroxyisobutyric acid (Hhba; Figure 2.13) forms similar complexes,^[19] the formation constants of which, provided in Equations (2.14) for pH 7.06, indicate that the complex formation is indeed favoured, compared with monoalcohols, by these bidentate ligands. The predominant species in the vanadate–lactate system in the pH range 3–7 has the idealised composition $V_2(\text{lac})_2^{2-}$ (Figure 2.13). Complex formation with lactate is observed only in the acidic regime, competing with reduction of vanadate by lactate. Peroxide stabilises the system against redox interaction by the formation of ternary (peroxy–vanadate–lactate) complexes, such as $V(\text{O}_2)_2\text{lac}^{2-}$.^[20] Peroxide does not enhance complex formation, in contrast to ligand systems containing N-functions (see below), but extends the range of complex formation with lactate to the alkaline region. A dianionic, dinuclear lactate–oxo–peroxovanadium(V) complex, $[\{\text{VO}(\text{O}_2)\text{L-lac}\}]^{2-}$, has been structurally characterised (Figure 2.13).^[22] This complex represents one of the rare exceptions where the $\{\text{V}(\mu-\text{O})_2\}$ core is not planar.

Table 2.5 Mean concentrations of components in human blood plasma.

Component	mm	mg l ⁻¹	Component	mm	mg l ⁻¹
Phosphate	1.2	115	Glycine	2.3	173
Carbonate	25	$1.6 \cdot 10^3$	Histidine	0.08	12
Sulfate	0.3	29	Cysteine	0.03	4
Lactate	1.5	137	Glutamate	0.06	8
Citrate	0.1	18	Albumin ^a	0.6	44×10^3
Oxalate	0.015	1.3	Transferrin ^b	0.04	3.2×10^3

^a $M \approx 70 \text{ kDa}$.

^b $M \approx 80 \text{ kDa}$.

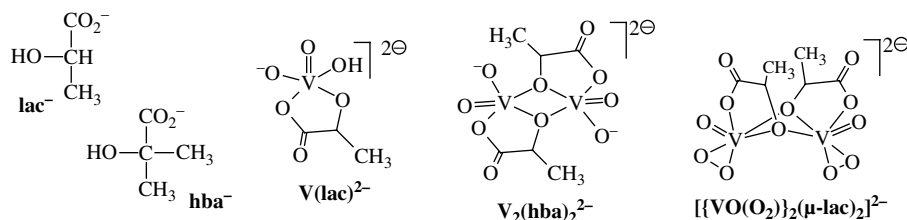
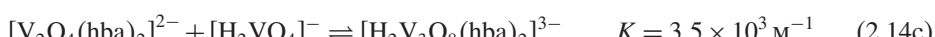
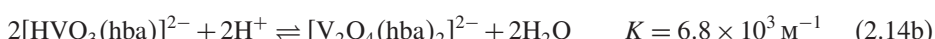


Figure 2.13

Hydroxycarboxylates and several of their complexes formed with vanadate in aqueous solution. Abbreviations: lac = L-lactate; hba = L- α -hydroxyisobutyric acid. The structures for the binary dinuclear complexes are based on X-ray structure determinations of mono-crystals isolated from the solutions.^[21,22] Note that the solid-state structure does not necessarily reflect the solution structure.



Unlike lactate, citrate (cit) forms complexes with vanadate also in the strongly acidic and in the alkaline regions.^[23] The main species present at pH 1–5, at a vanadate concentration $c(V) = 15 \text{ mM}$ and a threefold excess of citrate, is $V_2(\text{cit})_2^{2-}$ (Figure 2.14); the main species at pH 3–9 is $V_2(\text{cit})^{n-}$ ($n = 2–4$; increasing with increasing pH). At $c(V)$ as low as $1 \mu\text{M}$, and with a 10^4 -fold excess of citrate, complexes of composition $V(\text{cit})^{n-}$ ($n = 1, 2$), $V_2(\text{cit})_2^{2-}$ and $V_2(\text{cit})^{n-}$ ($n = 2–4$) dominate in the pH range 1–7. The dinuclear citrate complexes contain the very common planar $\{(\text{O}=\text{V})_2(\mu-\text{O})_2\}$ ‘diamond’ core (see Section 2.3). Various ternary peroxyo–vanadate–citrate complexes are generated on addition of H_2O_2 , including $V_2(\text{O}_2)_2(\text{cit})_2^{2-}$ (Figure 2.14), derived from $V_2(\text{cit})_2^{2-}$ by exchanging one oxo group per mononuclear subunit for the peroxy ligand. Interestingly, a mixed-ligand complex of composition $V_2(\text{cit})(\text{lac})^{2-/3-}$ forms in the ternary vanadate–citrate–lactate system. The proposed structure for this species is included in Figure 2.14.^[24]

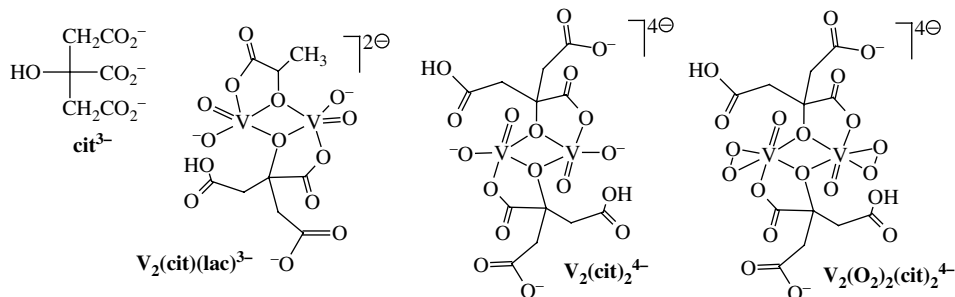
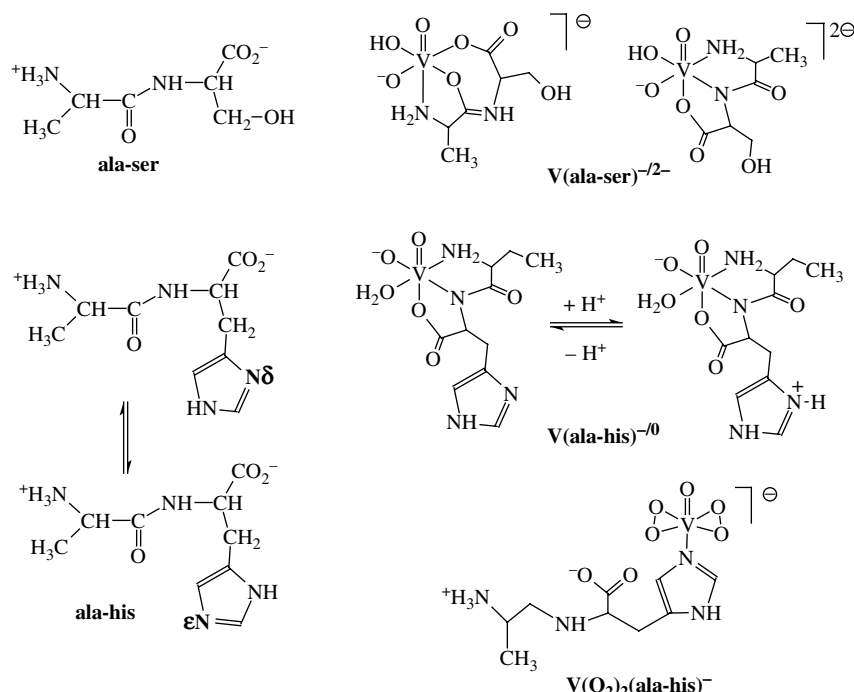


Figure 2.14

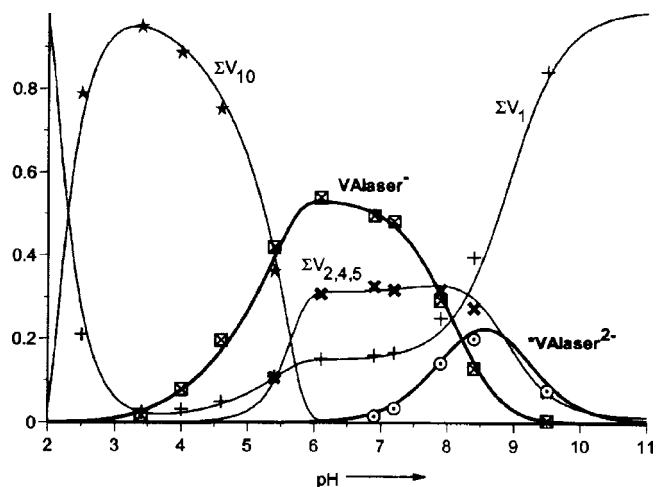
Citrate complexes. Abbreviations: cit = citrate; lac = lactate. For structurally characterised complexes, see ref. 24. The charges of the complexes vary with pH.

The hydroxyamino acid serine (ser) is found in the active centre of several phosphatases which are inhibited by vanadate. Vanadate further plays a role in the vanadate-dependent photo-oxidation of serine in certain protein (e.g. myosin) subfragments, and the photo-cleavage of sarcoplasmatic reticulum ATPase. In all of these instances, formation of a vanadate–serine ester $[\text{HVO}_3(\text{Oser})]^-$ or, as found for vanadate-inhibited *Escherichia coli* alkaline phosphatase, direct coordination of serinate to vanadate, may be the activating step. The model system vanadate–alanylserine (ala-ser; see Figure 2.15)² clearly demonstrates that complexes of composition $V(\text{ala-ser})^-$ (pH 3.5–9) and $V(\text{ala-ser})^{2-}$ (pH 7–10; $pK_a = 8.22$) form,^[25] as shown in more detail in the speciation diagram in Figure 2.16, along with proposed structures of the mono- and dianionic complexes in Figure 2.15. In the presence of peroxide, very slow formation (up to 10 days) of the ternary complexes $V(\text{O}_2)(\text{ala-ser})^-$ and, with excess peroxide, $V(\text{O}_2)_2(\text{ala-ser})^{2-}$ occurs in the pH range 6–10. Coordination of the alcoholate function in all of these complexes appears to be disfavoured with respect to the coordination via the terminal NH_2 and carboxylate, plus deprotonated amide, shown for $V(\text{ala-ser})^{1-/2-}$ in Figure 2.15. Similar observations apply to other multidentate ligand systems

² In the structural formulae of the dipeptides, the peptide bond is depicted in the common manner, i.e. with an sp^3 -hybridised nitrogen and the double bond between carbon and oxygen. Actually, this is just one of two mesomeric forms, the second resonance structure ($\text{sp}^2 - \text{N}$, double bond between N and C, positive charge on N and negative charge on O) being the more prominent one.

**Figure 2.15**

Structural formulae of L-alanyl-L-serine (ala-ser) and L-alanyl-L-histidine (ala-his) in their zwitterionic representation, and proposed structures of the predominant vanadate complexes. For the ala-ser complexes, see also the speciation diagram in Figure 2.16.

**Figure 2.16**

Distribution of vanadates and V(ala-ser) complexes as a function of pH.^[25] $c(V) = 4 \text{ mM}$, $c(\text{alanylserine}) = 16 \text{ mM}$, $I_{\text{Na}(\text{Cl})} = 0.15 \text{ M}$. Reproduced from A. Gorzsas *et al.*, *Dalton Trans.* **2004**, 2873–2882, by permission of The Royal Society of Chemistry.

containing serine moieties. DFT calculations carried out on the system $[\text{H}_2\text{VO}_4]^-$ -gly-ser indicate that both side-chain alcoholate and carboxylate coordination represent an energy minimum.

A similar situation is encountered with the dipeptide alanylhistidine (ala-his). The nitrogen atoms $\text{N}\delta$ and $\text{N}\varepsilon$ in the two tautomeric forms of the imidazolyl moiety of histidine (cf. Figure 2.15) are excellent donor functions for practically all of the bio-relevant metals, including vanadium, which is coordinated to $\text{N}\varepsilon$ in certain vanadate-inhibited phosphatases (Section 5.2.1) and in vanadate-dependent haloperoxidases, in the latter case both in its +V (vanadate) and +IV (vanadyl) states (Section 4.3). Despite these established bonding modes, the imidazolyl residue ‘appears to avoid’ coordination in the binary vanadate–alanylhistidine system.^[26] Complex formation is slow, amounting to several hours. The main components present are $\text{V}(\text{ala-his})$ (pH 3–8) and $\text{V}(\text{ala-his})^-$ (pH 5.5–9), in which – according to ^1H and ^{13}C NMR features (Section 3.2) – the ligand coordinates in the tridentate mode, again (as in the case of ala-ser) through the terminal amino and carboxylate functions and the deprotonated amide-N. The necessity to deprotonate the amide group might be responsible for the hesitant complex formation.

In contrast to the systems addressed above (i.e. those containing the ligands lactate, citrate or alanylserine), the coordination of alanylhistidine to vanadate is drastically enhanced by concomitant coordination of peroxide, a fact which also applies to the coordination of imidazole, which, in the absence of peroxide, forms only very weak complexes with vanadate. In the ternary system peroxide–vanadate–alanylhistidine, the predominant complex between pH 4 and 9 is $\text{V}(\text{O}_2)_2(\text{ala-his})^-$. In the peroxovanadates, alanylhistidine coordinates through $\text{N}\varepsilon$ (Figure 2.15).^[26]

In the presence of thiol (mercapto) groups, vanadate is usually redox labile, i.e. it is reduced to VO^{2+} , as has been demonstrated for the tripeptide glutathione ($\text{GSH} = \gamma\text{-glucys-gly}$; Figure 2.17), present in the intracellular medium in millimolar concentrations, which reduces vanadate to vanadyl and helps to keep vanadium in the oxidation state

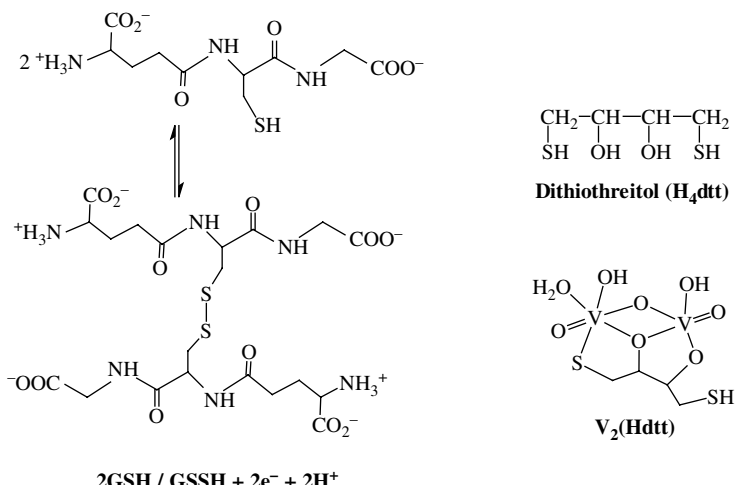
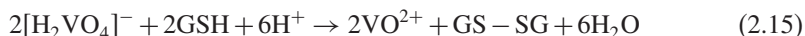


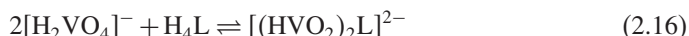
Figure 2.17

Thiofunctional ligands which redox-interact with vanadate(V) (glutathione, GSH), or form (comparatively) short-lived complexes with vanadate prior to redox (dithiothreitol). See refs 27 and 28.

IV by complexation.^[27] GSH is thereby oxidised to the disulfide GSSG, as shown in the idealised Equation (2.15).

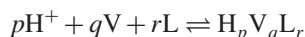


The reduction of vanadate can be slowed, as vanadium(V) is efficiently coordinated by multifunctional thiols such as dithiothreitol, (H₄dtt) (Figure 2.17). Reduction of vanadate by dithiothreitol occurs within ca 90 min, allowing for the identification of the intermediately formed vanadate complexes, such as V₂(Hdtt), with a formation constant [Equation (2.16)] of $K = 10^7 \text{ M}^{-2}$ at pH 7. Since this dinuclear complex gives rise to two resonance signals in the ⁵¹V NMR spectrum, there are two distinct vanadium sites. A possible structure is depicted in Figure 2.17.^[28]



2.2.2 Speciation in the Vanadyl System

In speciation analysis, it is common to refer to a system in terms of the so-called p,q,r notation, where p , q and r denote protons (H^+), metal centres (V) and ligands (L), respectively, i.e.



If deprotonation of the ligand and/or coordinated water occurs in the course of complex formation, the proton balance can be negative with respect to the composition of the product as related to the protons present in the educts, and this is then denoted H_{-x}V_qL_r (or V_qL_rH_{-x}), where x is the number of deficit protons. For an example, let us consider the formation of a complex between the vanadyl ion (VO²⁺) and lactic acid (H₂lac; one H refers to the carboxylic acid and the other to the alcoholic group) in aqueous solution:



For a coordination chemist used to conceiving a complex through its complete and/or structural formula, this notation does not necessarily allow for an unambiguous assessment of the species in question. Further, this notation is not necessarily used in a uniform manner. I have therefore refrained from employing this notation in discussing speciation, and tried to ‘translate’ the formula fragments used by the speciation analysts into more perceivable ones, including charges. These formulae may still be truncated, in the sense that not all of the information is implemented, e.g. the number of coordinated water molecules: [VO(Hlac)]⁺ instead of [VO(H₂O)₂Hlac]⁺.

Apart from being formed *in vivo* by reduction of vanadate, oxovanadium(IV) may also enter into the bloodstream when applied as a tonic or food additive or by oral treatment of diabetes mellitus (in animals).

The paramagnetic d¹ ion VO²⁺ is an excellent probe for electron paramagnetic resonance (EPR) spectroscopy. In combination with proton potentiometry and/or electron absorption spectrometry (UV-Vis), species distribution schemes for VO²⁺ in the presence of various ligands have been obtained, comparable to those discussed in Section 2.2.1 for vanadate(V) systems derived on the basis of ⁵¹V NMR plus potentiometry. EPR also allows, via the anisotropic hyperfine coupling constant in field direction (A_z or $A_{||}$,

coincident with the V=O axis) for a determination of the coordinating functions in the equatorial plane of an oxovanadium complex (Section 3.3), which considerably facilitates solution structure assignments.

Ligands containing the cysteine moiety, such as GSH or glycyl-L-cysteine (gly-cys), readily coordinate VO^{2+} without any further redox interaction. In the predominant species formed in aqueous solution around pH 7, $[\text{VO}\{\text{(gly-cys)}_2\text{H}\}]^-$, one of the dipeptides coordinates through carboxylate + thiolate and the other through the terminal NH_2 and the carbonyl-O of the peptide bond (Figure 2.18).^[29]

As in the vanadate – ala-his system (see above), the dipeptide glycyl-L-histidine (gly-his) prefers coordination through functions other than the imidazolyl-N, at least in the acidic to neutral pH range. The pK_a values for gly-his are 2.5 (terminal carboxylic acid group), 6.9 (protonated N δ of the imidazolyl moiety) and 8.3 (terminal ammonium group).³ Consequently, in acidic media (pH 1–5), the carboxylate function coordinates, along with the carbonyl oxygen of the peptide bond, to form the mono-ligand complex $[\text{VO}(\text{gly-his})\text{H}_2]^{3+}$ and the bis-ligand complex $[\text{VO}\{\text{(gly-his)}_2\text{H}_3\}]^{3+}$, where the protons indicate protonation of the N-termini and of N δ , as shown for $[\text{VO}\{\text{(gly-his)}_2\text{H}_3\}]^{3+}$ in Figure 2.18. With increasing pH, progressive deprotonation of the ligand occurs, and the terminal NH_2 begins to replace the carbonyl-O, cf. $[\text{VO}\{\text{(gly-his)}_2\text{H}_2\}]^{2+}$ in Figure 2.18. In the neutral to slightly alkaline pH range, coordination of the imidazole N δ occurs, and the deprotonated amide-N also participates in coordination, $\text{VO}(\text{gly-his})_2$ in Figure 2.18, forming robust bicyclic chelate structures.^[29]

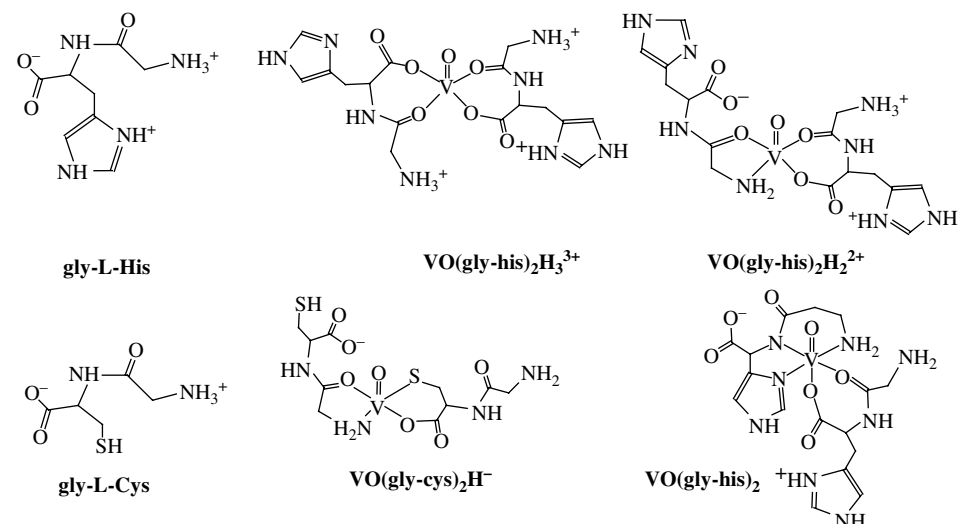


Figure 2.18

The dipeptides glycyl-L-histidine (gly-his) and glycyl-L-cysteine (gly-cys) and proposed structures for several of their complexes formed with the vanadyl ion, VO^{2+} . The coordination modes proposed are based on the EPR spectroscopic hyperfine coupling constant A_z .^[298]

³ $pK_a (= -\log K_a)$, where K_a is the acid constant) values vary with temperature and ionic strength I . The values reported here are valid for 25 °C and an ionic strength of $I_{\text{KCl}} = 0.2 \text{ M}$.

Most of the structurally characterised complexes formed between VO^{2+} and α -hydroxycarboxylic acids are dinuclear. In aqueous solution, however, mononuclear complexes are present. The underlying structure is a square pyramid (with the oxo group in the apex), somewhat distorted towards a trigonal bipyramidal. The degree of distortion, depending on the steric requirement of the substituent on $\text{C}\alpha$, can be extracted from the EPR parameters (Section 3.3).^[30a] Complexation with, e.g., lactic acid (H_2lac) starts at pH 3. The formation constant for the formation of the species $[\text{VO}(\text{Hlac})]^+$ [lactate, deprotonated at the carboxylic acid function: $pK_a = 3.4$], Equation (2.17)], is $K = 10^{-2.48}$. This is approximately one order of magnitude higher than for the complex formation with unfunctionalised carbonic acids, such as acetate ($K = 10^{-1.86}$), suggesting participation of the alcoholic group in coordination, as shown for $[\text{VO}(\text{Hlac})]^+$ in Figure 2.19.^[30b] As the pH increases, the OH function also becomes deprotonated ($[\text{VO}(\text{lac})]$), and bis-ligand complexes begin to form. At pH 7, the main species present is $[\text{VO}(\text{lac})_2]^{2-}$ (Figure 2.19). The two aldaric acids D-saccharic acid and D-mucic acid exhibit coordination modes similar to α -hydroxycarboxylic acids,^[31] i.e. with coordination through carboxylate and the neighbouring alcoholic function in the acidic region, as shown in Figure 2.19, and through carboxylate and alcoholate as the neutral pH is approached. Again in agreement with lactic acid, hydrolysis occurs above pH 8.

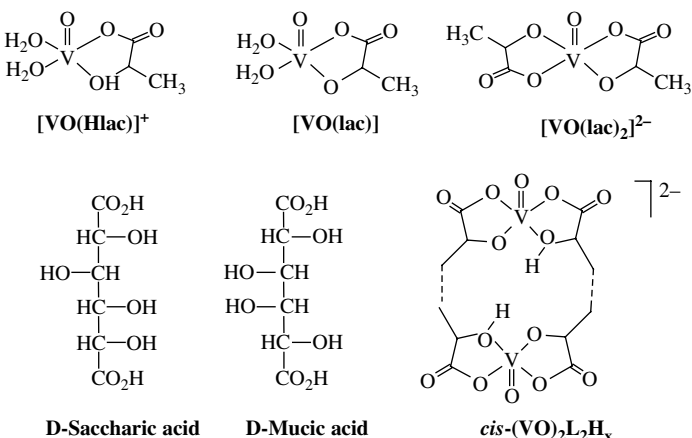
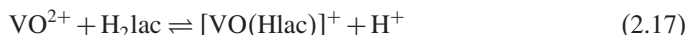


Figure 2.19

Proposed structures, based on complex formation constants and EPR evidence, for vanadyl complexes of lactic acid^[30b] and two aldaric acids, H_2L .^[31]

Citric acid (H_4cit), is a more efficient ligand for the vanadyl ion than lactic acid. Complex formation already starts at pH 1 and is still effective at pH 9, i.e. hydrolysis begins only at pH > 10. Mononuclear mono-ligand species play a secondary role below pH 5 and above pH 8. In the pH range 3.5–8.5, the main species are the anionic dinuclear bis-ligand complexes $[(\text{VO})_2(\text{Hcit})(\text{H}_2\text{cit})]^-$ (slightly acidic range) and $[(\text{VO})_2(\text{Hcit})_2]^{2-}$ (pH 4.5–9).^[32] Proposed structures for both complexes are provided in Figure 2.20. In either case, two citrato ligands bridge two vanadyl centres. The differing structures are based on EPR evidence. The structure proposed for $[(\text{VO})_2(\text{Hcit})_2]^{2-}$, with the doubly bonded oxo

groups in *anti* (*trans*) positions, corresponds to the solid-state structure determined for $[(\text{VO})_2(\text{cit})_2]^{4-}$, crystallised at pH 8.^[24b] At pH 5, crystals have been isolated containing the anion $[(\text{VO})_2(\text{cit})(\text{Hcit})]^{3-}$, also shown in Figure 2.20, in which the oxo groups are *syn* (*cis*). A more detailed discussion of the conformers observed for the $\{\text{VO}(\mu-\text{O})\}_2$ core is given in Section 2.3.1.

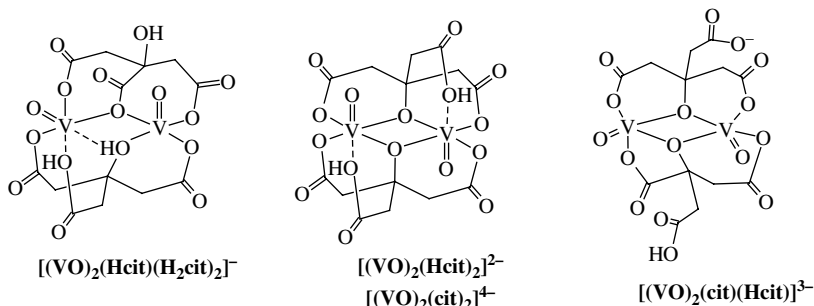


Figure 2.20

Structures for vanadyl complexes of citric acid.^[32] The formulae for the citrato complexes $[(\text{VO})_2(\text{Hcit})(\text{H}_2\text{cit})]^-$ and $[(\text{VO})_2(\text{Hcit})_2]^{2-}$ have been modified to account for the deprotonation grade of the coordinated citrate. Note, in the structurally characterised complex $[(\text{VO})_2(\text{cit})(\text{Hcit})]^{3-}$,^[24b] the differing coordination modes of the two Hcit^{3-} .

In Table 2.5 (Section 2.2.1), the high molecular mass blood constituents albumin and transferrin are listed along with the main low molecular mass constituents. Transferrin in particular is a very strong binder for the vanadyl ion [$\log K = 14.3(6)$] and more or less replaces other ligands. The coordination of vanadyl (and vanadate) to transferrin will be taken up in the more general context of vanadium–protein interaction (Section 5.2).

2.3 Vanadium Coordination Compounds

In Section 2.3.1, emphasis will be placed on general structural features of vanadium compounds, restricted – with a few exceptions – to mono- and dinuclear species. This restriction is justified in the light of the fact that vanadium compounds of higher nuclearity are not likely to play a role in living organisms, with their generally low vanadium concentrations. Decavanadate (Figure 2.7) may be an exception, but the building principles underlying this highly condensed vanadate can be traced back straightforwardly to mononuclear building blocks otherwise common with mononuclear vanadium. Examples of vanadium complexes belonging to the various structure types will essentially be provided in Section 2.3.2, ordered by the type of functions, and emphasising compounds of (potential) model character for biogenic vanadium systems. Additional model complexes will be introduced and discussed in later sections dealing with biogenic vanadium compounds.

2.3.1 Structural Features

In its coordination compounds, vanadium can attain the coordination numbers (*cn*) 4–8 in various coordination geometries (Figure 2.21). A tetrahedral (trigonal pyramidal)

arrangement is realised in the case of $cn = 4$; examples are $[V^{III}Cl_4]^-$, $V^{IV}Cl_4$ (**Ia**), $V^VO(OR)_3$ (esters of orthovanadic acid, **Ib**) or $[V^VO_2Cl_2]^-$ (**Ic**).

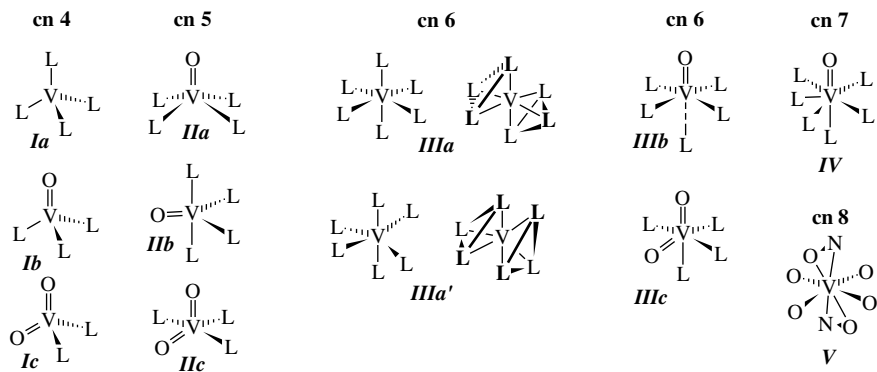
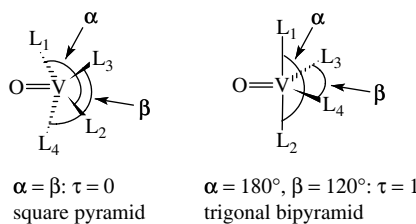


Figure 2.21

Structural variation in non-oxo (**a**), oxo- (**b**) and dioxovanadium complexes (**c**) with coordination number $cn = 4$ (**I**), 5 (**II**), 6 (**III**), 7 (**IV**) and 8 (**V**). For $cn = 6$, structure types **IIIa** and **IIIa'**, the antiprismatic (octahedral) and prismatic arrangements are additionally highlighted.

A large number of oxovanadium(IV) and -(V) complexes are pentacoordinate, i.e. $cn = 5$. The most common structure in this extended family is the square (tetragonal) pyramid, **IIb**, with the oxo group in the apex and the vanadium centre above the plane spanned by the four equatorial ligands. The distance of vanadium from this plane typically is around 0.3 Å; deviations from this average value in either direction are, however, common. In many instances, distortion towards the trigonal bipyramidal is observed; the about ideal trigonal-bipyramidal structure (**IIb**, present e.g. in the cofactor of vanadate-dependent haloperoxidases) is, however, rare. To quantify the degree of distortion, the angular parameter τ is in use, defined in Scheme 2.1: the angles α and β define the angles between mutually opposite ligands in the base of the square pyramid. In an ideal square pyramid (point symmetry C_{4v} if all of the ligands L are identical), α and β have the same size, and $\tau = 0$. In an ideal trigonal bipyramidal (point symmetry D_{3h}), one of the angles is 180° (the angle between the axial ligands) and the other is 120° (the angle between equatorial ligands), and τ becomes 1.



Scheme 2.1

Non-oxo pentacoordinated vanadium complexes can adopt the structure of a trigonal bipyramid $[VF_5]$; in accord with valence shell-electron pair repulsion (VSEPR) theory], or that of a square pyramid [predicted for $V(CH_3)_5$.^[33]

The octahedral arrangement ($cn = 6$) is realised in the aqua cations of V^{III}, $[V(H_2O)_6]^{3+}$ (**IIIa**),⁴ oxovanadium(IV), $[VO(H_2O)_5]^{2+}$ (**IIIb**) and dioxovanadium(V), $[VO_2(H_2O)_4]^+$, (**IIIc**). As in the dioxovanadium complexes with $cn = 5$ (**IIc**), the $\{VO_2\}$ moiety is exclusively in the *cis* configuration. In this configuration, the two strong π -donating O²⁻ ligands can make use of all of the three vanadium-d orbitals available for π interaction (d_{xz} , d_{yz} , d_{xy}). If the oxo groups were in *trans* positions, the d_{xy} would be left unused. The ligand *trans* to the V=O moiety is subjected to the *trans* influence, originating in competition for the same binding orbitals at vanadium. The *trans* influence, particularly effective in the monooxo vanadium species, weakens the V–L bond for the *trans* standing ligand with respect to the other bonds. The size of this effect differs. A V–O single bond, commonly between 1.8 and 2.0 Å (see also below), may become as long as 2.5 Å (and even more), classifying the *trans* ligand as a good leaving group, and suggesting easy conversion between type **IIIb** (octahedral) and **IIb** (square pyramidal) structures. The coordination environment of vanadium in the solid methyl ester $\{VO(OCH_3)_3\}_n$ depicted in Figure 2.11 (right), is an example for this intermediate situation between structure types **IIIb** and **IIb**. The *trans* influence (sometimes incorrectly termed ‘*trans* effect’) does in fact have consequences particularly for the solution chemistry of penta- and hexacoordinated vanadium complexes, since the sixth position, *trans* to the oxo group, can easily be occupied by or depleted of a solvent molecule (water, methanol, dimethyl sulfoxide, tetrahydrofuran, etc.), which in turn readily exchanges for a more potent ligand, most notably if this ligand function allows stabilisation through the chelate effect.

The O²⁻ function is a strong $\sigma + \pi$ donating ligand,⁵ giving rise to short V–O bonds. Typically, bond lengths are between 1.57 and 1.61 Å, represented by a strong IR absorption for the V=O stretch $\nu(VO)$ at $980 \pm 20 \text{ cm}^{-1}$. Bond lengths clearly exceeding 1.61 Å and $\nu(VO)$ clearly red shifted are indicative of additional interaction with ‘matrix’ molecules. These can be (i) neighbouring molecules in the crystal lattice, giving rise to V=O···V=O interactions, or (ii) hydrogen bonds to polar, hydrogen-bearing molecules or functions in the crystal lattice or the surrounding medium, i.e. interactions of the kind V=O···H–X. H₂O, HOR (R = aliphatic or aromatic residue), HO₂C–, H₂NR and HN=C– are potential candidates for comparatively strong hydrogen interactions with oxovanadium groups. This interaction can end up in a conversion of V=O to {V–OH⁺} (see also Figure 2.24 later). Protonation of the V=O group can occur on acidification of oxovanadium complexes. The extent to which the oxo group is involved in additional bonding interaction – or even is protonated – can be derived from the valence bond order s , defined by

$$s = \Sigma(d/R_0)^N \quad (2.18)$$

In this relation, originally derived by Brown,^[34] d is the experimental V–O distance, $R_0 = 1.78$ is a standardised length of a vanadium–oxygen bond of unit valence and the exponent $N = -5.1$ (a fitting constant) relates to binding of oxygen (ligands) to vanadium. The summation is carried out over all bonding interactions involving the oxygen, if there is more than one such interaction. This is the case when oxygen is part of a ligand function (alcoholate, etc.), or in multinuclear vanadium compounds such as decavanadate, where there are – in addition to the end-standing oxide – singly, doubly and hexuply

⁴ Note that we are dealing with octahedral *geometry*, and not with octahedral symmetry (point group O_h). $[V(H_2O)_6]^{3+}$, a d² system, has lower than O_h symmetry due to Jahn–Teller distortion.

⁵ With respect to the V=O bond order (double bond); see also footnote 1, in Section 2.1.3.

bridging oxygens (cf. Figure 2.7, left). The expected ideal bond order for oxygen is 2. Whenever s drops below ca 1.7, additional bonding interaction is likely to occur. Since ‘the sum of bond valences s at each atom is equal to the *atomic valence* [of this atom (here: vanadium)]’,^[34] this formalism can be employed to distinguish between V^{IV} (atomic valence 4) and V^V (atomic valence 5), e.g. in a mixed-valence vanadium compound.

The variations of V–O bond lengths in some octahedral (oxo and dioxo) and square-pyramidal (dioxo) complexes obtained from solid-state structures of vanadium oxides and oxovanadium phosphates are summarised in Figure 2.22. As already pointed out in the introductory remarks at the beginning of Section 2.3, the O=VO₄, O=VO₅, O=VO(O₄) and VO₆ units are also building blocks in condensed vanadium compounds, i.e. oligonuclear vanadium complexes containing ‘vanadium oxide’ cores, including bridging oxo functions, such as in polyoxovanadates, where these functions are in the junctions of corners, edges and faces shared by VO_n polyhedra. Thus, the Va and Vb sites in decavanadate (Figure 2.7) correspond to the structure type **IIIb** and the Vc sites to **IIIa** (Figure 2.21). The bond valence and atom valence schemes briefly outlined above can (and have been) effectively applied to such condensed species.

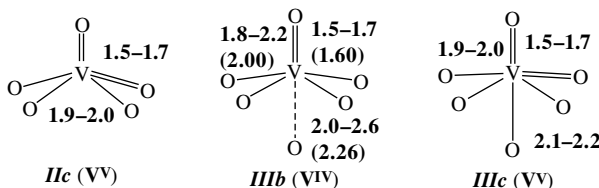


Figure 2.22

Coordination geometries ($cn = 5$, structure type **IIc**; $cn = 6$, structure type **IIIb** and **IIIc** in Figure 2.21) and bond lengths; modified from Ref. 35. Bond lengths in parentheses are average values.

An octahedron may also be seen as a trigonal antiprism. Instead of adopting the geometry of a trigonal antiprism (**IIIa**) as one of the extremes, the other extreme, an arrangement according to a trigonal prism (**IIIa'** in Figure 2.21) may be adopted. This rare coordination geometry is mainly realised in several non-oxo (‘bare’) vanadium(IV) complexes.

Seven coordination ($cn = 7$) gives rise to a pentagonal bipyramid, which is more or less a domain of peroxy chemistry: if, in an octahedral dioxovanadium complex (**IIIc**), the equatorial oxo ligand is replaced by a peroxy ligand, and if the peroxy ligand is taken as a bidentate ligand, this geometric arrangement is realised. There are only a few examples of type **IV** complexes without peroxy participation. Similarly, $cn = 8$ is restricted to selected examples, one of which is the non-oxo vanadium(IV) compound amavadin, occurring in *Amanita* mushrooms, and its V^{IV} and V^V model complexes, all containing two bidentate hydroxamido ligands mutually *trans*, as sketched in structure **V** in Figure 2.21.

In dinuclear⁶ oxovanadium complexes, the two oxovanadium centres may be bridged through one or two ligands. These can be O²⁻(μ -O), halides, in particular Cl⁻, or alcoholate functions OR⁻. The doubly bonded oxo group also can act as a bridging ligand (with a reduction in bond order as discussed above), mainly so if the mononuclear units are based on dioxovanadium species. The bridging mode can be symmetric in

⁶ It is usually not appropriate to refer to complexes containing two vanadium centres, each of which is in an equivalent environment, as a dimer (since, when broken down to the ‘monomers’, rearrangement and/or uptake of an additional ligand occurs). Rather, the term ‘dinuclear’ is appropriate.

the sense that, in the $\{V_2(\mu-O)\}$ or $\{V(\mu-O)\}_2$ core (this rhombic core is often termed ‘diamond core’), the V–O bond lengths to the two vanadium centres are alike, or ‘asymmetric’. In addition, the relative orientations of the doubly bonded oxo groups give rise to distinguishable cases, which are of fundamental importance for the magnetic behaviour of the diamond cores in case of V^{IV} complexes. The possible configurations for symmetrically mono-bridged and planar di-bridged dinuclear oxovanadium complexes^[36] are illustrated in Figure 2.23, which also contains the folded alternative realised for $\{[VO(O_2)_2](\mu-lac)_2\}^{2-}$ (Figure 2.13, right). Intermediate situations to those depicted in Figure 2.23 are known. The two vanadium centres may attain the same oxidation state (+IV or +V) or, less common, be in a mixed-valence situation.

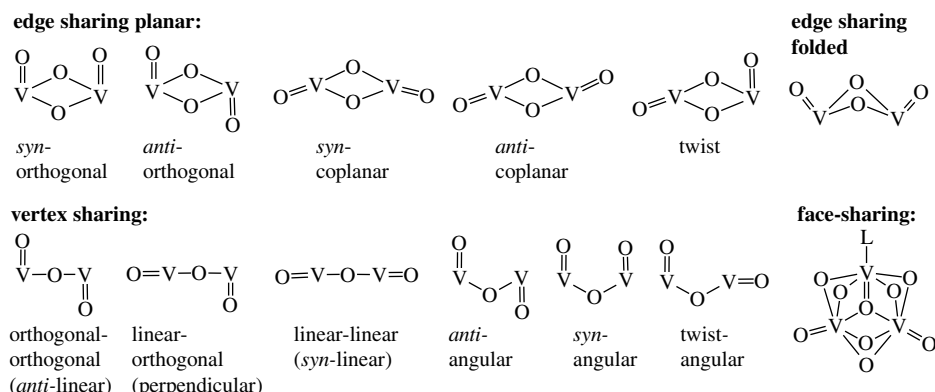


Figure 2.23

Configurations of the central $\{V=O(\mu-O)\}_2$ and $\{(V=O)_2\mu-O\}$ cores in binuclear oxovanadium complexes. The classifications follow the orientations of the terminal oxo groups with respect to the plane (edge-sharing units) or the V–O–V fragment (corner-sharing units), partly following ref. 36.

From the structural scheme provided by the central *cis*-dioxovanadium unit (**Ic**, **IIc** and **IIIc** in Figure 2.22), variations can be derived by either gradually protonating one of the oxo groups or by replacing one of the oxo groups by peroxide or superoxide (Figure 2.24). Protonation (*de facto* or formal) leads to the oxo–hydroxo and oxo–aqua cores, replacement of an oxo group by peroxide to an oxo–peroxo complex, in which the peroxo group is usually bonded in the symmetrically side-on fashion. Protonation of the peroxo group yields a hydroperoxo complex, discussed as an intermediate in haloperoxidase activity. Organic derivatives of this hydroperoxo intermediate can have the organic peroxide coordinated in the (somewhat asymmetric) side-on or in the end-on mode. The one-electron oxidation of the peroxo ligands results in the formation of an oxo–superoxo species^[37] (see also Section 3.3.3).

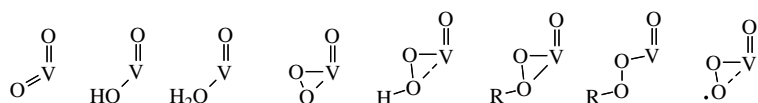


Figure 2.24

Variations of the *cis*-dioxovanadium core through (formal) protonation or substitution.

If a vanadium complex is devoid of an S_n axis (i.e. lacking an inversion centre i and a mirror plane σ), the vanadium centre is chiral. For a complex of coordination number 5 or 6, this is the case if there are two chelate-ring structures present, or if there are at least four different functions coordinated to vanadium. This is demonstrated in Figure 2.25. For complexes with chelating ligands, the symbols Λ and Δ are used to distinguish between the two enantiomers: when viewed along a threefold (pseudo-) axis, the chelate backbones may form a left-handed (Λ) or a right-handed (Δ) helix. The naturally occurring non-oxo vanadium compound amavadin is an illustrative example (Section 4.2). For oxovanadium complexes with at least four differing ligands, the C/A nomenclature to label the enantiomers has been recommended. The convention in this case is similar to the priority rule employed for chiral carbon centres, modified by the fact that a principal axis is defined, here by the $V=O$ bond director, pointing towards the observer. The rotational direction among the equatorial ligands follows their priority, starting with the ligand of highest priority [highest atomic number and, if directly bonded atoms are identical, the bonding partner(s) from the second coordination sphere, etc.]. For a right-handed rotation, the descriptor C (clockwise) is employed, and for the left-handed rotation the descriptor A (anti-clockwise). If, in addition to the chiral vanadium centre, chiral elements, i.e. chiral centres or planes, are present in the ligand system, diastereomers of differing physical (and chemical) properties are generated. Typically, this is the case if amino acids are constituents of ligand systems. For an example, see the Schiff base complex in Figure 2.26.

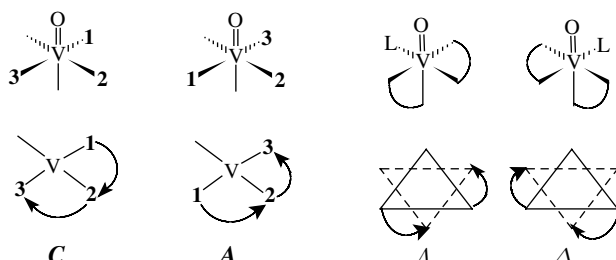


Figure 2.25

Chiral vanadium centres in 5–6-coordinated vanadium complexes with chelating structures (right) and at least four (including the oxo group) different ligands (left). The presentations in the bottom row are views along the pseudo-fourfold and -threefold axis. The numbers indicate priorities of the ligands; the oxo group points towards the observer.

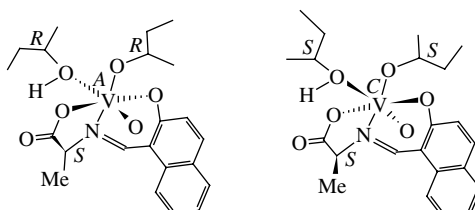


Figure 2.26

Two diastereomers of a vanadium Schiff base complex with a chiral vanadium centre plus three chiral centres in the ligand periphery.^[38] The constituents of the Schiff base are *o*-hydroxynaphthaldehyde and *S*-alanine; the additional monodentate ligands are *sec*-butanol and *sec*-butanolate.

2.3.2 Coordination Compounds with (Potential) Model Character for Biogenic Vanadium Systems

In this section, selected and representative vanadium coordination compounds will be introduced. The aim is to provide a first overview of those coordination modes which are related – or can be related – to the coordination of vanadium to biogenic ligands in its biologically relevant oxidation states +III, +IV and +V. Additional, and usually more complex, structures will be provided in those sections of Chapters 4 and 5, that are dedicated to model chemistry. For simplicity, the coordination compounds will be grouped according to the type of ligand functions dominating the coordination sphere:

1. alcohol, alcoholate and ether; keto- and enolate
2. phenolate and catecholate
3. carboxylate
4. thio-functional ligands
5. sulfur in multifunctional ligands
6. miscellaneous mixed ligand spheres.

This ordering also is hierarchical in the sense that ligands having two or more different functional groups will generally be dealt with in the group of higher count.

2.3.2.1 Coordination of *O*-Functional Ligands Derived from Alcohols, Alcoholates, and Ethers

As already pointed out in Section 2.1.3, simple alcohols form mono- and oligomeric alcoholato complexes, depending on the concentration and the nature of the alcohol. The oligomers, mainly dimers, are in equilibrium with the monomers (see also Figure 2.11); exchange rates are typically in the millisecond range. The solid-state structure of $\{\text{VO}(\text{O}i\text{Pr})_3\}_2$, **1** in Figure 2.27, typifies this class of complexes:^[17] two $\text{VO}(\text{O}i\text{Pr})_3$ units, with the $\text{O}i\text{Pr}$ substituents in the all-*cis* arrangement, are loosely attached via two semi-bridging⁷ OR^- to form a dimer. In more complex structures containing one or two alcohols or a diol in addition to other ligands, one of the alcoholic functions may remain protonated, as shown in Figure 2.26, and for the structure motif **5** in Figure 2.27. Alkoxyalkoxide ligands, i.e. ligands containing an ester and an alcoholate function, can employ both functionalities in coordination to vanadium (**2** in Figure 2.27).^[39] Diols and triols form oligonuclear complexes, such as represented by compounds **3**^[40] and **4**.^[41] In **4**, 3,3-dimethylpropanediolate coordinates to a vanadium centre in the bidentate fashion. One of the alcoholate groups also bridges to a second vanadium, thus forming a dinuclear unit, in which the two vanadium centres are additionally asymmetrically bridged by OH. Two of these dinuclear units are linked together to form a tetramer through weak bonds, including trebly bridging OH. The end-on plus bridging mode of a diol (fragment) (**6** in Figure 2.27) is a common feature as sugars or sugar derivatives coordinate to vanadium. Mononuclear, non-oxo vanadium(IV) complexes have been characterised with 1,3,5-triamino-1,3,5-tridesoxy-*cis*-inositol (taci), viz. $[\text{V}(\text{taci})_2]^{4+}$ (**7**),^[42] and with benzoin (**8**).^[43] In **8**, bis(deprotonated) benzoin coordinates out of its enedioliate form.

⁷ The term ‘semi-bridging’ is used here for OR groups giving rise to a normal V–O bond length, 1.9(1) Å, plus a weak V–O bond, 2.3(1) Å.

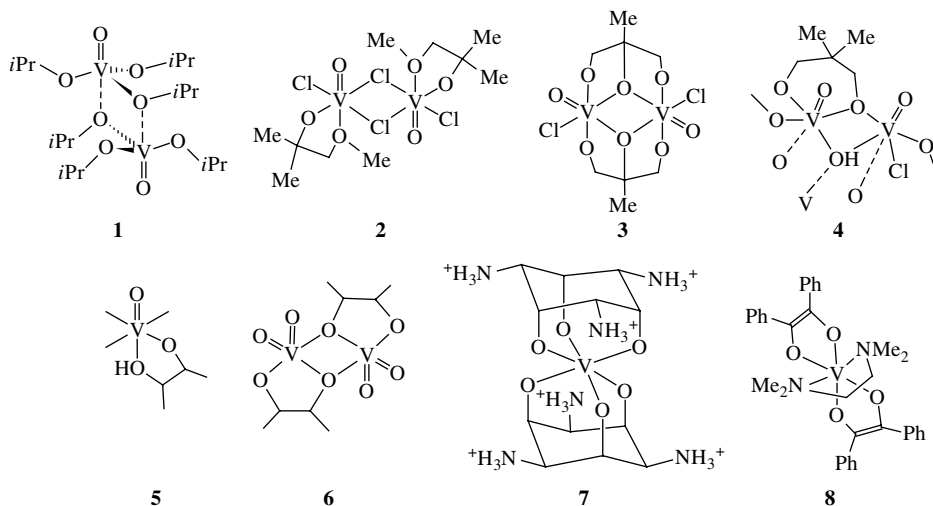
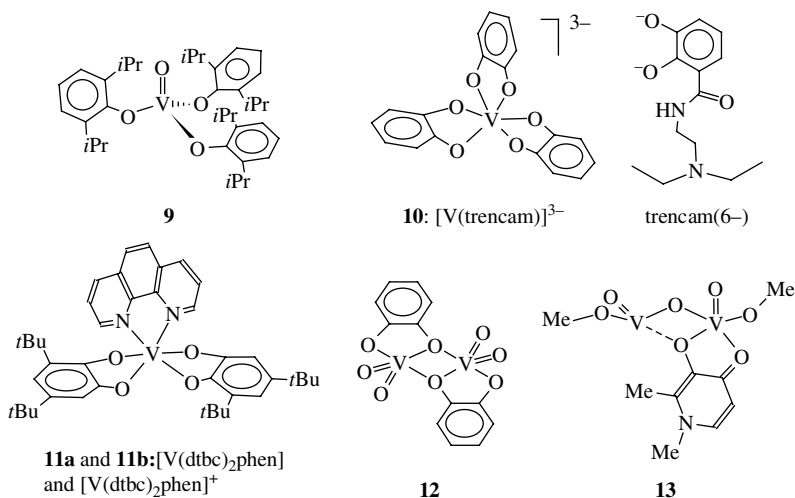


Figure 2.27
Examples for the coordination modes of alcoholates. See refs 17 and 39–43.

2.3.2.2 Coordination of *O*-Functional Ligands Derived from Phenolate, Catecholate and Enolate

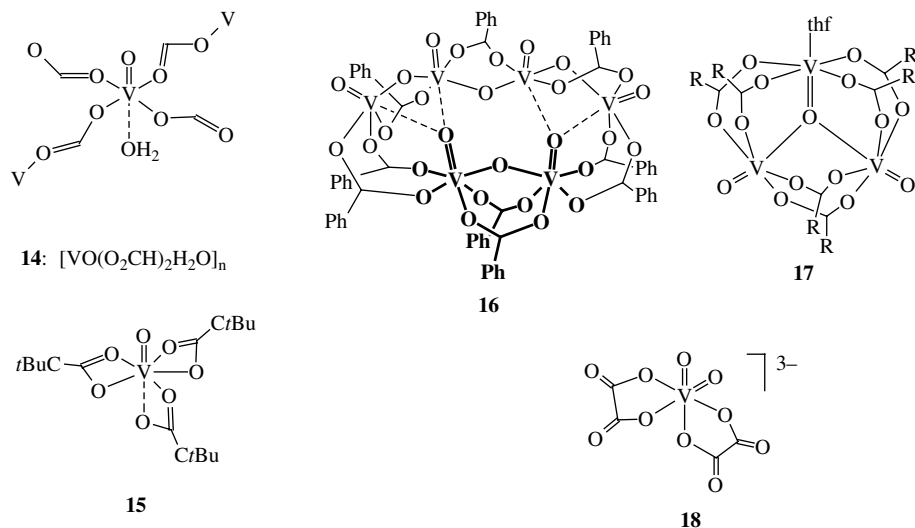
Phenols such as 1,6-bis(isopropyl) form esters derived from orthovanadic acids comparable to those observed with alcohols. Compound **9** in Figure 2.18 is an example.^[44] Catecholates (*o*-hydroquinones) coordinate to vanadium in the oxidation states +III, +IV and +V, and there is interesting redox chemistry related to the interaction between vanadium and tunichromes – naturally occurring catechol analogues – which will be considered in more detail in the context of vanadium in ascidians (Section 4.1). Catechols further model catechol-based siderophores such as enterobactin and azotochelin, which very effectively coordinate many metal ions, including V^{4+} and vanadate (cf. Section 4.5), and thus permit mobilisation of these metal ions from insoluble precipitates in the neutral and slightly alkaline pH range and from mineralised forms of the metals. The complex anion $[\text{V}^{\text{III}}(\text{trencam})]^{3-}$ (**10**) represents a homoleptic catecholatovanadium complex of distorted octahedral geometry.^[45] The trigonal twist angle is 41° . The ligand trencam(6–) contains an amine-tris(amide) backbone not directly participating in coordination to vanadium. The V^{IV} and V^{V} complexes **11a** and **11b** contain *o*-phenanthroline as an auxiliary ligand.^[46] Whereas the V^{V} complex attains the coordination geometry of a slightly distorted octahedron, the V^{IV} complex is trigonal prismatic (**IIIa** and **IIIa'**, respectively, in the classification in Figure 2.21). The complexes **11a** and **11b** again are representatives of the small family of non-oxo vanadium(IV) and -(V) complexes. Catecholate can also coordinate in the bridging mode (**12** in Figure 2.28)^[47] and thus in a manner analogous to vicinal diols. Complex **13** derives from pyrimidone(1–). The ligand coordinates via the keto and the enolate-O.^[48] The complex is dinuclear, containing the $\{\text{O}=\text{V}\}_2(\mu-\text{O})$ framework, with a $\text{V}-(\mu-\text{O})-\text{V}$ bond angle of 110.4° , and the two $\text{V}=\text{O}$ fragments in the perpendicular (linear-orthogonal; Figure 2.23) orientation. Pyrimidone complexes of vanadium, as the related maltolato complexes, exhibit insulin-enhancing properties (Section 5.1.1).

**Figure 2.28**

Selected examples of phenolato, catecholato and enolato complexes. See refs 44–48.

2.3.2.3 Coordination of *O*-Functional Ligands Derived from Carboxylates

Homoleptic carboxylatovanadium complexes are relatively scarce. Compounds **14–18** in Figure 2.29 are examples. In the polymeric VO^{2+} formate **14**, generated from metavanadate and formic acid, the octahedrally coordinated $[\text{VO}(\text{O}_2\text{CH})_2\text{H}_2\text{O}]$ units form interpenetrating double layers, in which the formate is in the $\eta^1:\mu_2$ bridging mode.^[49] The comparatively rare coordination number seven in the pentagonal bipyramidal arrangement (type **IV** in Figure 2.21) is realised with pivalate (*tert*-butyl acetate): complex **15** is a true mixed anhydride of orthovanadic and pivalic acid.^[50] The V–O bond *trans* to the doubly bonded oxo group is rather weak; the bond length is to 2.21 Å, compared with 1.98–2.08 Å for normal V–O(carboxylate) bonds. The hexanuclear mixed-valence $(\text{V}^{\text{V}})_5\text{V}^{\text{IV}}$ system **16**, containing benzoate, actually consists of a dinuclear and a tetranuclear unit derived from divanadate $[\text{H}_2\text{V}_2\text{O}_7]^{2-}$ and linear tetravanadate $[\text{HV}_4\text{O}_{13}]^{5-}$, respectively.^[50] The two subunits, each containing $\eta^1:\mu$ -carboxylate and symmetrically bridging oxo groups, are additionally linked together by two benzoates and $\mu_3-\text{O}^{2-}$ through weak (2.27–2.43 Å) bonding interaction. The asymmetrically trebly bridging oxo group is a common motif in trinuclear oxovanadium(IV) complexes of the general appearance shown for compound **17**, where R is a methyl or phenyl group. The light-blue type **17** complexes, ‘basic vanadium carboxylates’, readily form in solutions containing the vanadyl ion, carboxylate and (small amounts of) water. The bis(oxalato) complex **18** exemplifies homoleptic vanadium–carboxylato complexes containing a bifunctional – here a bis(carboxylate) – ligand capable of forming a stable chelate-ring structure.^[51] Bifunctional carboxylate complexes containing an alcoholato group in addition to the carboxylate, typically lactate and citrate, have been introduced in the context of speciation studies in aqueous solution (see Figures 2.13, 2.14 and 2.20). The coordination of carboxylate as a composite of a more complex ligand disposing of one to three additional ligand functions is a very common feature; see below and also Figure 2.15 for the coordination modus of dipeptides.

**Figure 2.29**

Carboxylatovanadium(IV and V) complexes. The divanadate unit in **16** is highlighted in bold. R in **17** is the methyl or phenyl group. See refs 49–51.

2.3.2.4 Coordination of S-Functional Ligands

There is some interest in the coordination of thiofunctional ligands to vanadium in the context of the interaction of vanadium with cysteine (and perhaps also with methionine) side-chains of peptides and proteins (Section 5.2.1), and the presence of vanadium as an integral part of the *M* cluster in the FeV cofactor of vanadium nitrogenase (Section 4.4). Thiofunctional ligands are soft and therefore do not readily ‘communicate’ with the hard vanadium(V) centre. Hence systems containing V^{V} and thio ligands are commonly redox labile, as has already been noted in Section 2.2.1 (see also Figure 2.17 in that section). The number of known vanadium(V) compounds containing thio ligands is restricted to a few inorganic examples, viz. the thio analogues of vanadate and divanadate, $[\text{VS}_4]^{3-}$ and $[\text{V}_2\text{S}_7]^{4-}$, the related thiophenolate $[\text{VS}_2(\text{S}_2)\text{SPh}]^{2-}$, **19** in Figure 2.30,^[52] and certain vanadate(V)-inhibited phosphatases, where incorporation of vanadate into the active site pockets impedes redox interaction (Section 5.2.1). The copper(I) salt of tetrathiovanadate occurs naturally as the mineral sultanite (Table 1.1). The disulfide⁸ ligand present in the anion **19** is also found in the vanadium(IV) mineral patronite, $\text{V}(\text{S}_2)_2$, and in several more complex vanadium compounds, such as the dinuclear tris(thiocarbonato) complex **20**^[52] and the trinuclear dithiocarbamato complex **21**^[53] in Figure 2.30. The oxidation state of vanadium in **20** is +IV; the two vanadium centres are, however coupled, and the compound is diamagnetic. In **21**, with formally two V^{III} and one V^{IV} , the $\text{V}_3(\mu_3-\text{S})(\eta^2-\text{S}_2)_3$ core is electronically delocalised, giving rise to an average oxidation number of 3.33 for each of the three vanadium centres. Four thiolato functions are present in the anionic, square pyramidal vanadium(IV) complexes $[\text{VS}(\text{SPh})_4]^{2-}$ (**22**)

⁸ The S_2^{2-} ligand is also termed ‘persulfido’ in analogy with the peroxy ligand O_2^{2-} .

and $[\text{VS}(\text{ethylenedithiolate})_2]^{2-}$ (**23**).^[54] The selenium analogue of **22**, $[\text{VSe}(\text{SPh})_4]^{2-}$, has also been characterised.

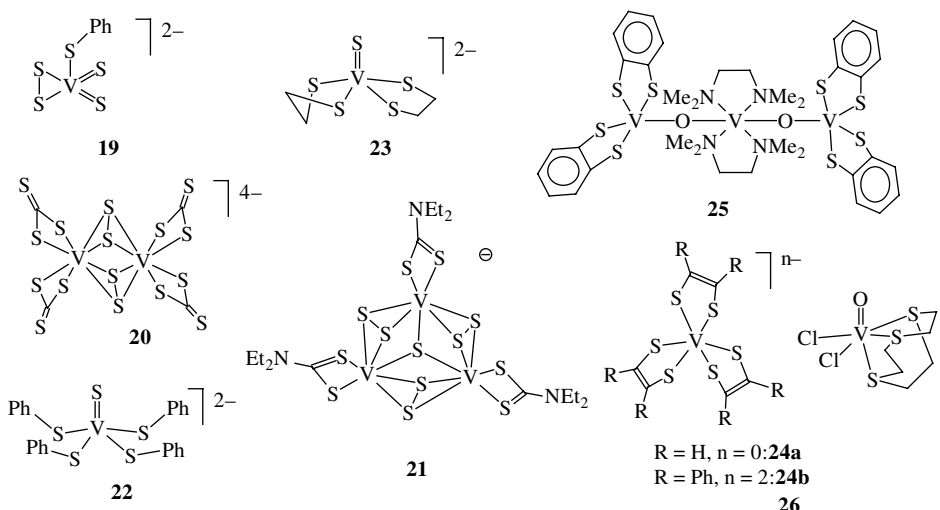
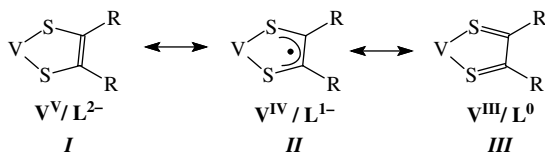


Figure 2.30
Vanadium complexes featuring the coordination of thiofunctional ligands. See refs 52–57a.

Dithiolene is an integral part of the molybdopterine cofactors in various molybdenum (and tungsten) based oxygenases and deoxygenases, a fact which has initiated extensive studies into the chemistry of model complexes containing the dithiolene ligand. Although corresponding vanadium systems have not (yet) been found in living organisms, the chemical similarity (diagonal relationship) between molybdenum and vanadium may well unearth vanadium analogues of the molybdopterines.⁹ The tris(dithiolene) complexes **24a** and **24b** in Figure 2.30 are distorted octahedral ($\text{R} = \text{H}$, **24a**) and slightly distorted trigonal prismatic ($\text{R} = \text{Ph}$, **24b**).^[55] Dithiolenes are well-established ‘non-innocent’ ligands, i.e. they can internally delocalise a maximum of two electrons per ligand towards the metal centre, hampering or even impeding allotment of a defined oxidation state to the metal and the ligand. The situation is illustrated in Scheme 2.2. The rather long C–C distance in the ligand backbone (1.41 Å in **24b**, 1.33 Å in **24a**), and the short C–S bond lengths (1.69 Å in **24b**, average of 1.72 Å in **24a**) account for sizable contributions of the resonance structure **II** in Scheme 2.2. The valence state of the vanadium centres in the two $\text{V}(\mu-\text{O})(\text{dtc})_2$ moieties ($\text{dtc} = \text{dithiocatecholate}$) of compound **25** formally is +V, if the ligand is considered dianionic.^[56] Since dithiocatecholate, as catecholate, can be non-innocent, the electronic situation may be different. Compound **26** is a rare example of thioether coordination.^[57a] The ligand is 1,4,7-trithiacyclononane, commonly abbreviated as [9]ane S₃. The V–S bond lengths, 2.470 and 2.634 Å, are fairly long when compared with V–thiolate (2.378 Å in **23**) and V–thiocatecholate (average 2.36 Å in **25**).

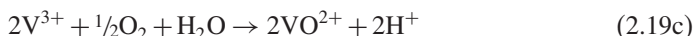
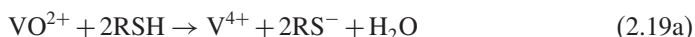
⁹ Reports on a nitrate reductase containing vanadium (but lacking the pterin cofactor), isolated from the chemo-litho-autotrophic bacterium *Thioalkalivibrio nitratireducens*, have appeared; see Section 4.4.2.



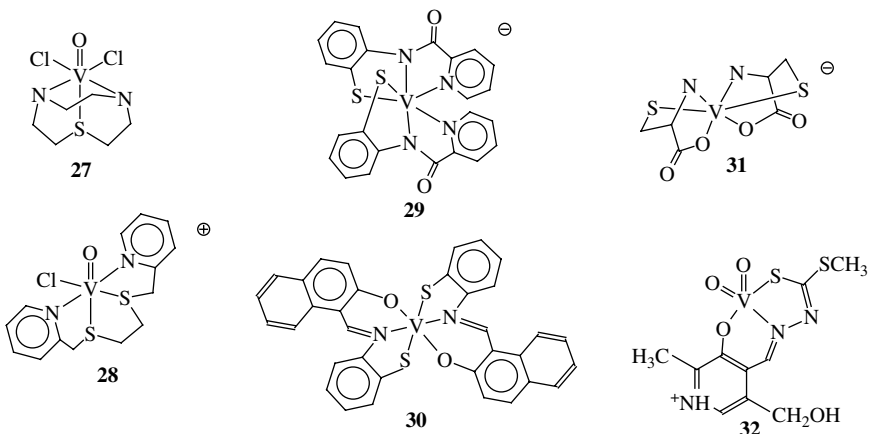
Scheme 2.2

2.3.2.5 Coordination of Sulfur-containing Multifunctional Ligands

The ligand 1-thia-4,7-diazacyclononane, [9]aneN₂S, forms an oxovanadium(IV) complex (**27** in Figure 2.31)^[57b] which corresponds to the complex obtained with [9]aneS₃ (**26** in Figure 2.30). The thioether function is in a *trans* position to the doubly-bonded oxygen; the bond length *d*(V–S) amounts to 2.69 Å. Thioether coordination, again to an oxovanadium(IV) centre, is also observed in the cationic complex **28**, representing a strongly distorted octahedron, with disordered Cl/O (65% O in the axial and 35% in the equatorial position) and *d*(V–S) = 2.530 and 2.597 Å.^[58a] In the anionic V^{III} complex **29**, a ligand sphere containing thiophenolate, carboamide and aromatic amine is realised.^[58b] The ligand is the picolinic acid amide of *o*-mercaptoaniline. The average *d*(V–S) is 2.37 Å. The Schiff base derived from *o*-mercaptoaniline and *o*-hydroxynaphthaldehyde forms the vanadium(IV) complex **30**.^[59] The two ligands are in a strongly distorted trigonal antiprismatic array. The complex represents a rare example in that (i) it represents a non-oxo vanadium(IV) complex and (ii) the Schiff base + thiolate functionalities are preserved at the expense of the tautomeric thiazoline form. Complex **30** is generated by the reaction between [VOCl₂(thf)₂], *o*-hydroxynaphthaldehyde and *o*-mercaptoaniline. More generally, the complex formation between vanadyl ions and thiols under aerobic conditions is often accompanied by deoxygenation of vanadium and oxidation of thiol to disulfide. In this reaction episode, the vanadyl ion can take over the role of an oxidation catalysts according to the reaction sequence depicted by Equations (2.18a–c).^[58b]



Concomitant coordination by thiolate, carboxylate and amide is realised in the anionic bis(cysteinato)vanadium(III) complex **31** in Figure 2.31. The V–S distance is 2.395 Å. Similar coordination modes have been found for oxovanadium(IV) in speciation studies in aqueous solution for cysteine-related ligands and ligands containing cysteine, such as glutathione. Complex **31** can therefore be considered a close model for the interaction of cysteine residues (along with other functional groups of protein constituents) with vanadium in its physiologically relevant oxidation states +IV and +V. Multi-functional coordination including sulfur can even stabilise dioxovanadium(V), as demonstrated for complex **32**, containing a ligand system composed of pyridoxal and *S*-methylthiocarbazate, providing phenolate-O and imine along with the sulfur function.

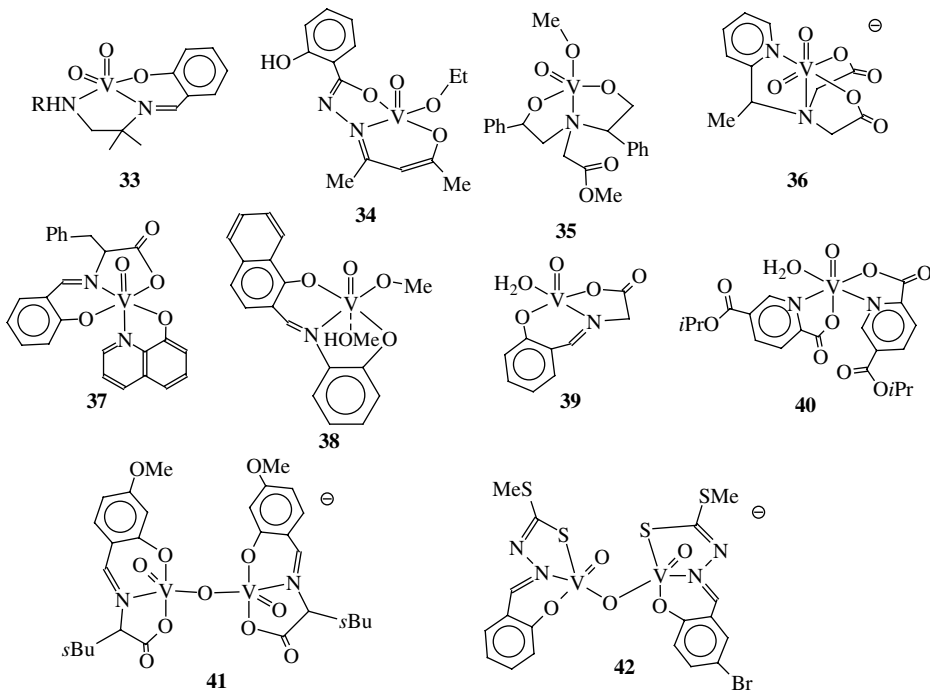
**Figure 2.31**

Selection of vanadium complexes with multifunctional ligands including sulfur. See refs 57b–61.

2.3.2.6 Miscellaneous Mixed Ligand Spheres

Oxovanadium(IV) and -(V) complexes containing a mixed *ON* or *ONS* coordination sphere are abundant and have been reviewed.^[62] A selection is provided by the mononuclear complexes **33–40** in Figure 2.32. Complexes **33–38** contain vanadium in the oxidation state +V and complexes **39** and **40** in the oxidation state +IV. Vanadium(V) complexes can be based on the VO_2^+ (**33**,^[63] **36**) or the VO^{3+} moiety (**34**, **35**,^[64] **38**), commonly with the coordination numbers $cn = 5$ (**33–35**) or 6 (**36**, **37**), or in between, i.e. with the sixth ligand only weakly coordinated, as shown for **38**, which contains a methanol ligand in the second axial position. A value of $cn = 5$ or 6 is also the most common in oxovanadium(IV) complexes, based on the VO^{2+} moiety (**39** and **40**).^[65] Independent of the oxidation state, the coordination geometry for the $cn = 5$ commonly is square pyramidal (**33**, **34**, **39**), usually slightly distorted, with an angular parameter τ of up to ca 0.2. (for the definition of τ , see Scheme 2.1 in Section 2.3.1). The trigonal bipyramidal arrangement is clearly less frequent. Compound **35** is an example; $\tau = 0.72$, i.e. **35** is somewhat distorted towards the square pyramid. Typical bi- to tetradentate ligands stabilising the oxo- and dioxovanadium centres contain the O-donors phenolate and carboxylate and the N-donors aromatic or aliphatic amine, and imine nitrogens of Schiff bases or hydrazones.

The anions **41** and **42** in Figure 2.32 are examples of dinuclear Schiff base complexes containing the $(\text{V}=\text{O})_2(\mu-\text{O})$ core in the *anti*-linear (**41**)^[66] and the *syn*-angular conformation (**42**)^[67]; Figure 2.23. In both complexes, the two halves of the molecule display the distorted square pyramidal coordination geometry. Both complexes are mixed-valence $\text{V}^\text{V}/\text{V}^\text{IV}$ species. Whereas there is rapid inter-valence exchange in **41**, the valence states in **42** are isolated and can be detected separately by ^{51}V NMR and EPR Spectroscopy^[68] (Chapter 3). The almost linear arrangement of the $\text{V}_2(\mu-\text{O})$ moiety in **41** (the $\text{V}-\text{O}-\text{V}$ angle is 170.9°) with the two oxo groups *trans* to each other (*cis* to the bridge), the d_{xy} orbitals of the two vanadium centres are almost coplanar, an orientation which allows for electronic interaction through the p_x orbital of the oxo bridge (x -axis). The vanadium

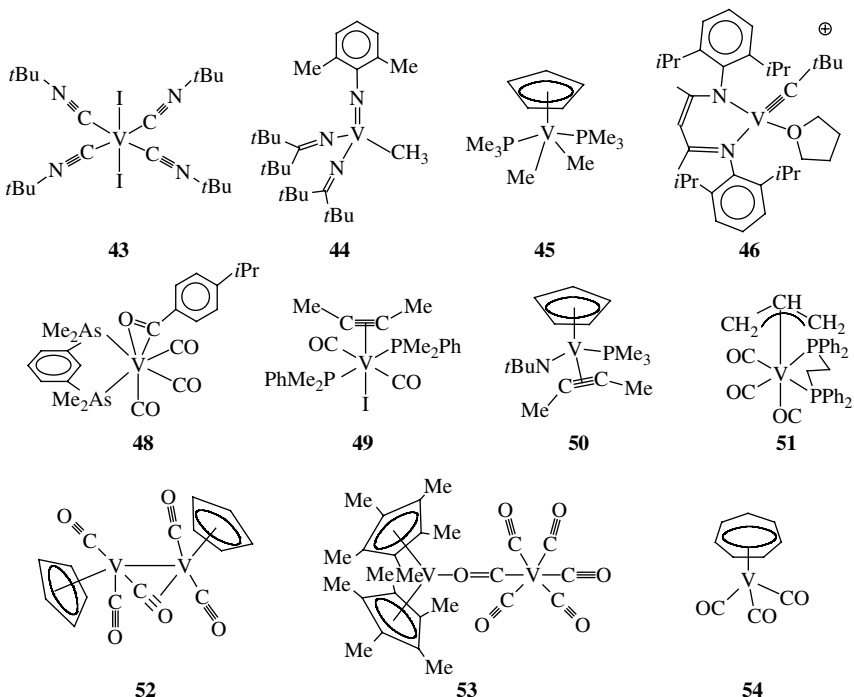
**Figure 2.32**

Vanadium compounds with oligodentate ON and ONS ligands. Each of the vanadium complexes represents an example of a specific subgroup. **33**, dioxo- V^{V} , square pyramidal (sqp); **34**, monooxo- V^{V} sqp; **35**, monooxo- V^{V} , trigonal bipyramidal; **36**, dioxo- V^{V} , octahedral (oct); **37**, monooxo- V^{V} , oct; **38**, monooxo- V^{V} , oct/sqp; **39**, monooxo- V^{IV} , sqp; **40**, monooxo- V^{IV} , oct. In the mixed-valence dinuclear complexes **41** and **42**, the two vanadium centres are indistinguishable (**41**) and isolated (**42**), respectively.

centre in both units of **41** is in the C configuration (Figure 2.25). In **42**, the $\text{V}-\text{O}-\text{V}$ angle is to 149.7° .

2.4 The Vanadium–Carbon Bond

In this section, selected coordination compounds containing at least one $\text{V}-\text{C}$ bond will be addressed. The $\text{V}-\text{C}$ bond has so far not been observed in Nature. There is, however, evidence for the formation of intermediates with the $\text{V}-\text{C}$ bond in the reductive protonation of alkynes, alkenes and isonitriles, catalysed by vanadium nitrogenase (Section 4.4). Further, the general ability of vanadium-based catalysts in redox, oxygenation, hydrogenation and polymerisation reactions, evident in the respective conversion of organic substrates in research and in technical processes,^[68] suggests that vanadium can attain a similar role in environmental transformations. Cyclopentadienylvanadium complexes have been shown to display cancerostatic properties (Section 5.1.2). A selection of structurally characterised complexes, representing basic concepts of organovanadium compounds, is shown in Figure 2.33.

**Figure 2.33**

Vanadium coordination compounds containing at least one V–C bond.

In its organic compounds, vanadium can attain all of the possible oxidation states. High to medium oxidation states are stable with σ -alkyl, alkylidene (Schrock-carbene; σ , π -donating) and alkylidyne (carbyne, σ , π_x , π_y -donating) ligands, represented by the V^{V} and V^{III} complexes **44** and **45**,^[69] which contain the methyl ligand, and the cationic V^{V} complex **46**, with an alkylidyne(3-) ligand.^[70] Carbonyl ligands and other ligands capable of delocalising (accepting) electron density from the metal via π back-bonding stabilise low oxidation states. Examples are the η^2 -alkyne complexes **49** and **50** (V^{I}),^[71] the isonitrile complex **43** (V^{II}),^[72] the η^2 -acyl complex **48** (V^{I})^[73a] and the η^3 -allyl complex **51** (V^{I}).^[73b] The oxidation state $-I$ is realised in the hexacarbonylvanadate anion $[\text{V}(\text{CO})_6]^-$ and in the sandwich complex **54**, containing three carbonyl ligands and the tropylum [cyclo heptatrienyl(1+)] cation in the η^7 bonding mode. In $[\text{V}(\text{CO})_5]^{3-}$, vanadium is in its lowest possible oxidation state, $-\text{III}$. The sandwiching η^5 -cyclopentadienyl(1-) (Cp ; compounds **45**, **50**, **52** and **53**) is a very common ligand, and the $\{\text{CpV}\}$ moiety is fairly stable throughout all vanadium oxidation states and also under physiological conditions.

The common coordination mode for carbonyl is end-on via the carbon, and the bonding interaction is usually described in terms of a synergistic σ -donor and π -acceptor interaction, leading to a strengthening of the metal-to-carbon bond and a weakening ('activation') of the carbon-to-oxygen bond. This bonding situation also applies to other ligands, isoelectronic with CO, such as isonitrile (RNC), the nitrosyl cation (NO^+) and dinitrogen (N_2) the activation of which plays a role in nitrogen fixation (by nitrogenase), denitrification (of NO) and side-reactions of nitrogenase (hydrogenation of RNC). Along with the common end-on bonding of the carbonyl ligand, the semi-bridging mode (**52**) and the bridging, isocarbonyl mode (**53**)^[74] have also been noted.

References

- [1] C. F. Baes and R. E. Messmer, *The Hydrolysis of Cations*, Wiley Interscience, New York, **1976**, pp. 197–210.
- [2] R. Meier, M. Boddin, S. Mitzenheim and K. Kanamori, in: *Metal Ions in Biological Systems* (H. Sigel and A. Sigel, Eds), Marcel Dekker, New York, **1995**, Ch. 2.
- [3] (a) L. Pettersson, B. Hedman, A. M. Nennen and I. Andersson, *Acta Chem. Scand., Ser.A* **1985**, *39*, 499; (b) H. Schmidt, I. Andersson, D. Rehder and L. Pettersson, *Chem. Eur. J.* **2001**, *7*, 251.
- [4] D. Wang, W. Zhang, C. Grüning and D. Rehder, *J. Mol. Struct.* **2003**, *656*, 79–91.
- [5] L. Pettersson, I. Andersson and O. W. Howarth, *Inorg. Chem.* **1992**, *31*, 4032–4033.
- [6] Y.-P. Zhang and R. H. Holm, *Inorg. Chem.* **1988**, *27*, 3875–3876.
- [7] I. Andersson, A. Gorzsás, C. Kerezsi, I. Tóth and L. Pettersson, *Dalton Trans.* **2005**, 3658–3666.
- [8] M. J. Gresser, A. S. Tracey and K. M. Parkinson, *J. Am. Chem. Soc.* **1986**, *108*, 6229–6241.
- [9] (a) M. E. Leonowicz, J. W. Johnson, J. F. Brody, H. F. Shannon, Jr. and J. M. Newsman, *J. Solid State Chem.* **1985**, *56*, 310–378; (b) M. Roca, M. D. Marcos, P. Amorós, J. Alamo, A. Beltrán-Porter and D. Beltrán-Porter, *Inorg. Chem.* **1977**, *16*, 3414–3421; (c) R. V. Panin, R. V. Shpanchenko, A. V. Mironov, Y. A. Velikodny and E. Antipov, *Chem. Mater.* **2004**, *16*, 1048–1055.
- [10] (a) P. Buglyó, T. Kiss, E. Alberico, G. Micera and D. Dewaele, *J. Coord. Chem.* **1995**, *36*, 105–116; (b) T. Kiss, E. Kiss, G. Micera and D. Sanna, *Inorg. Chim. Acta* **1998**, *283*, 202–210.
- [11] I. Andersson, S. Angus-Dunge, O. W. Howarth and L. Pettersson, *J. Inorg. Biochem.* **2000**, *80*, 51–58.
- [12] P. Schwendt, J. Tyršelová and F. Pavějčík, *Inorg. Chem.* **1995**, *34*, 1964–1966.
- [13] (a) S. J. Angus-Dunne, C. P. Paul and A. S. Tracey, *Can. J. Chem.* **1997**, *75*, 1002–1010; (b) P. C. Paul, S. J. Angus-Dunne, R. J. Batchelor, F. W. B. Einstein and A. S. Tracey, *Can. J. Chem.* **1997**, *75*, 429–440.
- [14] W. Prandl and L. Hess, *Z. Anorg. Allg. Chem.* **1913**, *82*, 103–129.
- [15] (a) A. S. Tracey and M. J. Gresser, *Proc. Natl. Acad. Sci. USA* **1986**, *83*, 609–613; (b) A. S. Tracey and M. J. Gresser, *Can. J. Chem.* **1988**, *66*, 2570–2574.
- [16] J. Spandl, I. Brüdgam and H. Hartl, *Z. Anorg. Allg. Chem.* **2000**, *626*, 2125–2132.
- [17] F. Hillerns, F. Olbrich, U. Behrens and D. Rehder, *Angew. Chem. Int. Ed. Engl.* **1992**, *31*, 447–448.
- [18] (a) D. C. Crans, R. A. Felty, H. Cheng, H. Eckert and N. Das, *Inorg. Chem.* **1994**, *33*, 2427–2438; (b) Q. Chen and J. Zubieto, *Coord. Chem. Rev.* **1992**, *114*, 107–167; (c) A. Müller, J. Meyer, H. Bögge, A. Stammmer and A. Botar, *Z. Anorg. Allg. Chem.* **1995**, *621*, 1818–1831.
- [19] S. Hati, R. J. Batchelor, F. W. B. Einstein and A. S. Tracey, *Inorg. Chem.* **2001**, *40*, 6258–6265.
- [20] A. Gorzsás, I. Andersson and L. Pettersson, *Dalton Trans.* **2003**, 2503–2511.
- [21] M. Biagioli, L. Strinna-Erre, G. Micera, A. Panzanelli and M. Zema, *Inorg. Chim. Acta* **2000**, *310*, 1–9.
- [22] P. Schwendt, P. Švančárek, I. Smatanová and J. Marek, *J. Inorg. Biochem.* **2000**, *80*, 59–64.
- [23] A. Gorzsás, K. Getty, I. Andersson and L. Pettersson, *Dalton Trans.* **2004**, 2873–2882.
- [24] (a) M. Kaliva, E. Kyriakakis and A. Salifoglou, *Inorg. Chem.* **2002**, *41*, 7015–7023; (b) M. Tsaramyris, M. Kaliva, A. Salifoglou, C. P. Raptopoulos, A. Terzis, V. Tangoulis and J. Giapintzakis, *Inorg. Chem.* **2001**, *40*, 5772–5779.
- [25] A. Gorzsás, I. Andersson, H. Schmidt, D. Rehder and L. Pettersson, *Dalton Trans.* **2003**, 1161–1167.
- [26] H. Schmidt, I. Andersson, D. Rehder and L. Pettersson, *Chem. Eur. J.* **2001**, *7*, 251–257.
- [27] A. Dörnyei, S. Marcão, J. Costa Pessoa, T. Jakusch and T. Kiss, *Eur. J. Inorg. Chem.* **2006**, 3614–3621.
- [28] P. C. Paul and A. S. Tracey, *J. Biol. Inorg. Chem.* **1997**, *2*, 644–651.

- [29] E. Garribba, E. Lodyga-Chruscinska, G. Micera, A. Panzanelli and D. Sanna, *Eur. J. Inorg. Chem.* **2005**, 1369–1382.
- [30] (a) E. Garribba, G. Micera and A. Panzanelli, *Inorg. Chem.* **2003**, *42*, 3981–3987; (b) G. Micera, D. Sanna, A. Dessì, T. Kiss and P. Buglyó, *Gazz. Chim. Ital.* **1993**, *123*, 573–577.
- [31] Á. Doernyei, E. Garribba, T. Jakusch, P. Forgo, G. Micera and T. Kiss, *Dalton Trans.* **2004**, 1882–1891.
- [32] T. Kiss, P. Buglyó, D. Sanna, G. Micera, P. Decock and D. Dewaele, *Inorg. Chim. Acta* **1995**, *239*, 145–153.
- [33] R. J. Gillespie, I. Bytheway, T.-H. Tang and R. F. W. Bader, *Inorg. Chem.* **1996**, *35*, 3954–3963.
- [34] I. D. Brown, *Structure and Bonding in Crystals*, Vol. II, Academic Press, New York, **1981**, Ch. 14.
- [35] M. Schindler, F. C. Hawthorne and W. H. Baur, *Chem. Mater.* **2000**, *12*, 1248–1259.
- [36] W. Plass, *Inorg. Chem.* **1997**, *36*, 2200–2205.
- [37] H. Kelm and H.-J. Krüger, *Angew. Chem. Int. Ed.* **2001**, *40*, 2344–2348.
- [38] R. Fulwood, H. Schmidt and D. Rehder, *J. Chem. Soc., Chem. Commun.* **1995**, 1443–1444.
- [39] E. C. E. Rosenthal, H. Cui, K. C. H. Lange and S. Dechert, *Eur. J. Inorg. Chem.* **2004**, 4681–4685.
- [40] J. Salta and J. Zubierta, *Inorg. Chim. Acta* **1997**, *257*, 83–88.
- [41] D. C. Crans, A. M. Marshman, M. S. Gottlieb, O. P. Anderson and M. M. Miller, *Inorg. Chem.* **1992**, *31*, 4939–4949.
- [42] B. Morgenstern, S. Steinhauser, K. Hegetschweiler, E. Garribba, G. Micera, D. Sanna and L. Nagy, *Inorg. Chem.* **2004**, *43*, 3116–3126.
- [43] M. Farahbakhsh, H. Schmidt and D. Rehder, *Chem. Commun.* **1998**, 2009–2010.
- [44] R. A. Henderson, D. L. Hughes, Z. Janas, R. L. Richards, P. Sobota and S. Szafert, *J. Organomet. Chem.* **1998**, *554*, 195–201.
- [45] A. R. Bulls, C. G. Pippin, F. E. Hahn and K. N. Raymond, *J. Am. Chem. Soc.* **1990**, *112*, 2627.
- [46] T. A. Kabanos, A. J. P. White, D. J. Williams and J. D. Woollins, *J. Chem. Soc., Chem. Commun.* **1992**, 17–18.
- [47] M. J. Manos, A. J. Tasiopoulos, C. Raptopoulos, A. Terzis, J. D. Woollins, A. M. Z. Slawin, A. D. Keramidas and T. A. Kabanos, *J. Chem. Soc., Dalton Trans.* **2001**, 1556–1558.
- [48] F. Avecilla, C. F. G. C. Geraldes, A. L. Macedo and M. M. C. A. Castro, *Eur. J. Inorg. Chem.* **2006**, 3586–3594.
- [49] T. R. Gilson, *J. Solid State Chem.* **1995**, *117*, 136–144.
- [50] D. Rehder, in: *Polyoxometalates: from Platonic Solids to Anti-Retroviral Activity*, M. T. Pope and A. Müller (Eds), Kluwer , Dordrecht, **1994**, pp. 157–166.
- [51] M.-H. Lee and K. Schaumburg, *Magn. Reson. Chem.* **1991**, *29*, 865–869.
- [52] S. C. Sendlinger, J. R. Nicholson, E. B. Lobkovsky, J. C. Huffman, D. Rehder and G. Christou, *Inorg. Chem.* **1993**, *32*, 204–210.
- [53] H. Zhu, Q. Liu, Y. Deng, T. Wen, C. Chen and D. Wu, *Inorg. Chim. Acta* **1999**, *286*, 7–13.
- [54] (a) J. K. Money, J. C. Huffman and G. Christou, *Inorg. Chem.* **1985**, *24*, 3297–3302; (b) J. R. Nicholson, J. C. Huffman, D. M. Ho and G. Christou, *Inorg. Chem.* **1987**, *26*, 3030–3034.
- [55] R. J. H. Clark and P. C. Turtle, *J. Chem. Soc., Dalton Trans.* **1978**, 1714–1721.
- [56] W. Tsagkalidis, D. Rodewald and D. Rehder, *J. Chem. Soc., Chem. Commun.* **1995**, 165–166.
- [57] (a) G. R. Willey, M. T. Lakin and N. W. Alcock, *J. Chem. Soc., Chem. Commun.* **1991**, 1414–1416; (b) U. Heizel, A. Henke and R. Mattes, *J. Chem. Soc., Chem. Commun.* **1997**, 501–508.
- [58] (a) H. Nekola, D. Wang, C. Grüning, J. Gätjens, A. Behrens and D. Rehder, *Inorg. Chem.* **2002**, *41*, 2379–2384; (b) D. Wang, A. Behrens, M. Farahbakhsh, J. Gätjens and D. Rehder, *Chem. Eur. J.* **2003**, *9*, 1805–1813.

- [59] M. Farahbakhsh, H. Nekola, H. Schmidt and D. Rehder, *Chem. Ber./Recl.* **1997**, *130*, 1129–1133.
- [60] H. Maeda, K. Kanamori, H. Michibata, T. Konno, K. Okamoto and J. Hidaka, *Bull. Chem. Soc. Jpn.* **1993**, *66*, 790–796.
- [61] M. R. Maurya, A. Kumar, A. R. Bhat, A. Azam, C. Bader and D. Rehder, *Inorg. Chem.* **2006**, *45*, 1260–1269.
- [62] M. R. Maurya, *Coord. Chem. Rev.* **2003**, *237*, 163–181.
- [63] E. Kwiatkowski, G. Romanowski, W. Nowicki, M. Kwiatkowski and K. Suwinska, *Polyhedron* **2003**, *22*, 1009–1018.
- [64] C. Wikete, P. Wu, G. Zampella, L. De Gioia, G. Licini and D. Rehder, *Inorg. Chem.* **2007**, *46*, 196–207.
- [65] J. Gätjens, B. Meier, Y. Adachi, H. Sakurai and D. Rehder, *Eur. J. Inorg. Chem.* **2006**, 3573–3585.
- [66] J. Costa Pessoa, M. J. Calhorda, I. Cavaco, I. Corriera, M. T. Duarte, V. Felix, R. T. Henriques, M. F. M. Piedade and I. Tomaz, *Dalton Trans.* **2002**, 4407.
- [67] S. K. Dutta, S. Samanta, S. B. Kumar, O. H. Han, P. Burckel, A. A. Pinkerton and M. Chaudhury, *Inorg. Chem.* **1999**, *38*, 1982–1988.
- [68] T. Hirao, *Chem. Rev.* **1997**, *97*, 2707–2724.
- [69] (a) J. Yamada and K. Nomura, *Organometallics* **2005**, *24*, 3621–3623; (b) G. Liu, D. J. Beetstra, A. Meetsma and B. Hessen, *Organometallics* **2004**, *23*, 3914–3920.
- [70] F. Basuli, B. C. Bailey, D. Brown, J. Tomaczewski, J. C. Huffman, M.-H. Baik and D. J. Mindiola, *J. Am. Chem. Soc.* **2004**, *126*, 10506–10507.
- [71] (a) H. Gailus, H. Maelger and D. Rehder, *J. Organomet. Chem.* **1994**, *465*, 181–185; (b) M. Billen, G. Hornung and F. Preuss, *Z. Naturforsch., Teil B* **2003**, *58*, 975–989.
- [72] C. Böttcher, D. Rodewald and D. Rehder, *J. Organomet. Chem.* **1995**, *496*, 43–48.
- [73] (a) J. Schiemann and E. Weiss, *J. Organomet. Chem.* **1983**, *255*, 179–191; (b) U. Francke and E. Weiss, *J. Organomet. Chem.* **1977**, *139*, 305–313.
- [74] J. H. Osborne, A. L. Rheingold and W. C. Trogler, *J. Am. Chem. Soc.* **1985**, *107*, 6292–6297.

This page intentionally left blank

3 Physico-chemical Methods for the Characterisation of Native and Model Vanadium Compounds

3.1 ^{51}V NMR Spectroscopy

3.1.1 General

In order to be accessible to ^{51}V NMR, a vanadium compound has to be diamagnetic. This is the case for V^{V} (d^0), low-spin V^{III} (d^2), low spin V^{I} (d^4), $\text{V}^{-\text{I}}$ (d^6) and $\text{V}^{-\text{III}}$ (d^8). In addition, dinuclear V^{IV} (d^1) centres with strong anti-ferromagnetic coupling are detectable by NMR. The presence of paramagnetic ‘impurities’, e.g. V^{IV} along with V^{V} formed by partial reduction of vanadium(V) in the presence of reducing agents, does not prevent the detection of the ^{51}V NMR signal of the V^{V} compound, provided that there is no exchange between the d^0 and d^1 systems. The signal-to-noise ratio, however, usually deteriorates and, depending on whether there are substantial contacts between the two systems, the chemical shift and linewidth may be influenced. Dinuclear mixed-valence $\text{V}^{\text{IV}}/\text{V}^{\text{V}}$ complexes can give rise to both a ^{51}V NMR signal and an EPR signal for the V^{V} and the V^{IV} centre, respectively, if the two centres are isolated (no inter-valence charge transfer). An example is complex **42** in Figure 2.32. Since vanadium(IV) is an excellent probe for EPR detection (Section 3.3), EPR and ^{51}V NMR are complementary and highly efficient analytical tools for the investigation of compounds containing vanadium in either of these two oxidation states.

Among the transition metal nuclei, ^{51}V is unique because of its excellent NMR properties (Table 3.1). Its receptivity is close to that of the proton, a consequence of the high natural abundance and the favourable magnetogyric ratio, the latter also accounting for its accessibility at a frequency close to that used for the detection of ^{13}C . The nuclear spin of the ^{51}V nucleus is $7/2$. Nuclei with a spin $> 1/2$ have a nonspherical distribution of the nuclear charge, giving rise to a quadrupole moment. The quadrupole moment of the ^{51}V nucleus, -4.8 fm^2 , is comparatively small, allowing for the acquisition of usually well-resolved spectra. The quadrupole moment gives rise to effective relaxation and thus to line broadening (see below), which may be considered a disadvantage when it comes to spectral resolution. Much of this disadvantageous situation is counterbalanced by the broad chemical shift range, covering roughly 4600 ppm. Even minor variations in the electronic status at the vanadium nucleus are thus detectable through variations of the chemical shift. Chemical shifts are temperature sensitive, i.e. comparison of δ values

requires their determination at about the same temperature. This is particularly important for low-valent vanadium compounds.

Table 3.1 NMR-relevant parameters of the two magnetic vanadium nuclei.

Nucleus	Nuclear spin I	Quadrupole moment Q (fm 2)	Abundance (%)	Magnetogyric ratio, $\gamma(10^7 \text{ rad s}^{-1} \text{ T}^{-1})$	Receptivity relative to ^{1}H	Frequency ν_0 (MHz) ^a
^{50}V	6	+21	0.24	+2.6721	1.3×10^{-4}	9.988
^{51}V	$7/2$	-4.8 ^b	99.76	+7.0492	0.38	26.350

^a Measuring frequency at 2.35 T (where ^{1}H in TMS resonates at 100 MHz).

^b The value for $Q(^{51}\text{V})$, commonly reported as -5.2 fm 2 , was recently revised.^[1]

Since the short relaxation times associated with a quadrupolar nucleus drastically reduce the time delay to be applied in an NMR experiment between two pulses, measuring times are short or, in other words, distinct ^{51}V NMR signals can often be detected with a limited time spent down to micromolar concentrations. Along with this apparent advantage, quadrupolar nuclei provide information in addition to the ‘classical’ parameters chemical shift (or shielding) and nuclear spin–spin coupling constants. Variations in linewidths for quadrupolar nuclei are another sensitive quantity allowing for the evaluation of the electronic and the steric situation in the first coordination sphere of a vanadium compound, its periphery, its (local) symmetry and its interaction with the matrix, i.e. counter-ions, solvent molecules and other constituents present in solution.

About 0.24% of the naturally occurring vanadium is present as ^{50}V , with clearly less favourable NMR properties (Table 3.1). This nucleus is therefore not commonly used in analytical NMR spectroscopy.

The reference applied in quoting ^{51}V chemical shifts is neat VOCl_3 , for which the chemical shift δ is set to zero. Since VOCl_3 is rather an aggressive liquid, which is readily hydrolysed in moist air, the use of a more easily manageable, ‘auxiliary’ standard may be useful. An aqueous solution of 1 M sodium metavanadate at pH 12 is sometimes employed, which contains the anions VO_4^{3-} ($\delta = -535.7$ ppm) and $\text{V}_2\text{O}_7^{4-}$ ($\delta = -559.0$ ppm). ^{51}V NMR spectroscopy has recently been reviewed.^[1]

3.1.2 Shielding in Isotropic Media

In this section, the shielding situation will be treated under conditions where the molecules or ions incorporating the ^{51}V nucleus are essentially freely mobile in solution, ‘essentially’ meaning that there are no preferential orientations, or any preferential orientation is averaged out on the NMR time-scale (milliseconds). The shielding situation encountered under slow-motion conditions, in mesophases (liquid crystals) and in the solid state will be addressed in Section 3.1.3. In the present section, the background theory of shielding will be dealt with, followed by examples of shielding ranges and specific shielding situations, allowing employment of this parameter as an analytical tool. Finally, two-dimensional exchange spectroscopy will briefly be addressed.

3.1.2.1 Background Theory

The terms ‘shielding σ ’ and ‘chemical shift δ ’ are often used side-by-side. They are related to each other by Equation (3.1), in which σ_{ref} is the shielding of the reference, VOCl_3 in our case:¹

$$\delta = \sigma_{\text{ref}} - \sigma \quad (3.1)$$

In this section, the reader will be confronted with and introduced to some comparatively elemental facts on the theory underlying interpretation of the shielding parameter accessible for ‘normal’ molecules in isotropic solutions, where normal refers to molecules which are not oversized (such as vanadium bound to proteins), and were we therefore are in the so-called ‘extreme narrowing limit’, characterised by the condition $2\pi\nu_0\tau_c \ll 1$, where ν_0 is the measuring frequency and τ_c the molecular correlation time, a measure of the mobility of a solute molecule in a solvent. ‘Extreme narrowing’ simply means that the molecule is freely mobile and the frequency applied to obtain NMR information does not influence the respective parameters. Although the term contains the component ‘extreme’, we are well in the domain of normal conditions.

Our training in the use of NMR spectra as an analytical tool is usually based on common nuclei such as ^1H and ^{13}C (and, perhaps, also ^{19}F and ^{31}P), and our training in understanding and interpreting NMR parameters is based more or less exclusively on ^1H NMR, which fact can lead to misconceptions of the factors influencing shielding in heavier nuclei, ‘heavier’ meaning all nuclei beyond ^1H and ^2H , ^6Li and ^7Li . Even for the lithium nuclei, the shielding concept automatically transferred from factors influencing proton shielding is just half of the truth. Addressing some basic conceptions of the background theory on shielding in the frame of this treatise might help to counteract superficial and thus incomplete or incorrect interpretations of trends in ^{51}V chemical shifts abundant in the literature. As an illustrative example, consider the following two series of shielding trends (EN = Allred–Rochow electronegativity):

	VOBr_3	VOCl_3	$\text{VO}(\text{OC}_3\text{H}_7)_3$	VOF_3
$\delta(\text{ppm})$	+432	0	-549	-757
EN	2.74	2.83	3.50	4.10
	$[\text{VSe}_4]^{3-}$	$[\text{VS}_4]^{3-}$	$[\text{VO}_4]^{3-}$	VF_5
$\delta(\text{ppm})$	+2570	+1574	-541	-895
EN	2.48	2.44	3.50	4.10

In both series, one might intuitively expect the shielding to decrease with increasing electronegativity (electron-withdrawing capability) of the substituents on vanadium. The contrary is the case, a fact which is sometimes referred to as ‘inverse electronegativity dependence’ of shielding.² Apparently, shielding is not explained as easily in these series.

¹ Although δ is a dimensionless quantity, and IUPAC does not recommend the use of ppm (parts per million) as a ‘dimension’, I will do so for clarity throughout.

² The ‘normal electronegativity dependence’, i.e. a decrease in shielding with increasing electronegativity of the donor atom of the ligand (or the group electronegativity of the ligand), is observed in ‘closed-shell’ vanadium complexes, e.g. $d^4(\text{V}^{+1})$ and $d^6(\text{V}^{-1})$. Since these oxidation states are of minor – if any – relevance to biological vanadium chemistry, the ‘normal dependence’ will not be addressed here. The interested reader is referred to ref. 1.

The anisotropic shielding constant is a 3×3 tensor, and its principal (diagonal) component, $\sigma = 1/3(\sigma_{xx} + \sigma_{yy} + \sigma_{zz})$, can be expressed by the sum of three terms:

$$\sigma = \sigma_{\text{dia}} + \sigma_{\text{para}} + \sigma_{\text{nl}} \quad (3.2)$$

The term σ_{nl} stands for non-local contributions, i.e. for contributions which do *not* stem from the immediate coordination sphere of vanadium. This term, mainly reflecting the influence of counter-ions and other matrix effects, is usually negligibly small in ^{51}V NMR. The local term σ_{dia} , the diamagnetic contribution, which governs variations in proton shielding, also accounts for substantial shielding variations in lithium NMR. In other nuclei, including ^{51}V , σ_{dia} is dominated by the core electrons, i.e. σ_{dia} is a sizable but essentially *constant* term, and thus hardly contributes to any variations in shielding. Hence we are left with the local paramagnetic term, σ_{para} . The choice of the term ‘paramagnetic’ in this context is somewhat unfortunate, because it may be confused with the paramagnetism originating from unpaired electrons, as in the paramagnetic V^{IV} (d^1) complexes. What are referred to by σ_{para} in the context of shielding are electronically excited ‘paramagnetic’ states, arising from an electronic situation where an electron from a doubly occupied diamagnetic ($S = 0$) ground state is promoted to an originally unoccupied state.

In the frame of ligand field theory, i.e. allowing for covalent bonding contributions between the vanadium centre and the ligands in its coordination sphere, quantified by, e.g., the LCAO (linear combination of atomic orbitals) coefficient c , σ_{para} can be expressed by the simplified but efficient (with respect to its message) Equation (3.3). In this equation, $(\Delta E)_{\text{av}}$ represents the mean (or averaged) excitation energy, i.e. the averaged ΔE of the contributing electronic transitions. The factor $\langle r^{-3} \rangle$ is the expectation value for r^3 , a measure of the extension of the 3d and, for V^{V} compounds, the 4p electron clouds.

$$\sigma_{\text{para}} = -\text{constant} \times (\Delta E^{-1})_{\text{av}} \langle r^{-3} \rangle c^2 \quad (3.3)$$

The term σ_{para} thus depends on

- the strength of the ligand field – via ΔE^{-1} ;
- the nephelauxetic effect, or softness, or polarisability of the ligands – via $\langle r^{-3} \rangle$;
- the covalency of the metal ligand bond – via c^2 ; for exclusive ionic (electrostatic) interaction, $c = 1$, otherwise $c < 1$.

Note that σ_{para} provides a negative contribution to shielding, i.e. σ_{para} is a deshielding term. Thus, as σ_{para} becomes small, overall shielding increases [Equation (3.3)]. A small σ_{para} term, and hence effective overall shielding, is to be expected as

- The ligand field is strong (large ΔE , small ΔE^{-1}).
- The ligands are soft (large $\langle r^{-3} \rangle$; small $\langle r^{-3} \rangle$).
- The covalent character of the vanadium-to-ligand bond dominates ($c \ll 1$).

These influences can counteract each other. In the two series of vanadium(V) compounds provided above, with the most electronegative substituent giving rise to the most effective overall shielding, the influence via the ligand strength is the most important. The prevalence of ΔE is demonstrated in Figure 3.1, showing a semi-quantitative molecular orbital scheme for the oxovanadium trihalides VOX_3 , $\text{X} = \text{Br}, \text{Cl}, \text{F}$. In the case of $\text{X} = \text{Cl}$ and Br , the main contributing HOMOs are the orbitals representing the $\pi(\text{V}=\text{O})$ ($3e$, 27% $\text{V}_{3\text{d}}$ population) and the σ_p ($\text{V}-\text{Cl}$) bonds ($4e$ and $5a_1$, 25% $\text{V}_{3\text{d}}$). For $\text{X} = \text{F}$, the only occupied level of relevance is $\pi(\text{V}=\text{O})$ ($5e$ and $5a_1$, 34% $\text{V}_{3\text{d}}$ character). In all

three cases, the LUMO essentially is represented by an unoccupied vanadium 3d level at approximately -10.5 eV . Nonbonding orbitals localised on the halogens, $n(\text{X})$, do not contribute due to a lack of vanadium contributions.

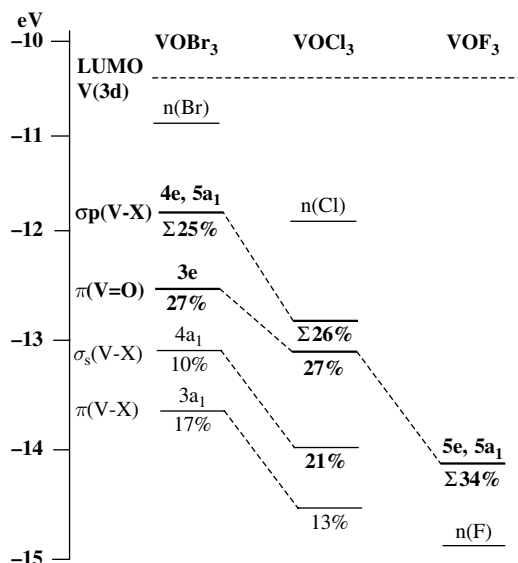


Figure 3.1

Semi-quantitative molecular orbital scheme for VOX_3 under C_{3v} symmetry; energy scale in electron-volts (eV). The LUMOs, at around -10.5 eV , are represented by essentially empty $\text{V}(3\text{d})$ levels. Main HOMOs contributing to ΔE are in bold. Indications underneath the energy level bars are percentages of $\text{V}(3\text{d})$ contributions to these levels. The nonbonding $n(\text{X})$ do not contribute. Redrawn from ref. 2.

3.1.2.2 Shielding Ranges

For inorganic vanadium compounds, the low-field limit³ of chemical shifts is marked by $[\text{VSe}_4]^{3-}$ (+2570 ppm) and the high-field limit by VF_5 (-895 ppm), i.e. by vanadium compounds with particularly soft (comparatively low electronegativity) and hard ligands (high electronegativity), respectively. For organic vanadium compounds, chemical shifts extend from +2382 ppm for $[(\text{CpV})_2\mu-\text{O}(\mu-\text{Te})(\mu-\text{Te}_2)]$ [$(\text{Cp} = \eta^5\text{-cyclopentadienyl}(1-))$] to -2054 for $[\text{CpV}(\text{CO})_3\text{SnPh}_3]^-$.^[1] The following empirical rules can be quoted:

1. *Electronegativity dependence.* As already noted above for shielding in the oxovanadium trihalides VOX_3 and the tetrachalcogenovanadates $[\text{VX}_4]^{3-}$, there is an apparent correlation between electronegativity and shielding: shielding increases with increasing electronegativity of ΣX in a series of comparable compounds. ‘Comparable’ are ‘innocent’ ligands [for the definition of ‘innocent’ in this context, see item 5 below], and excludes ligands coordinating side-on (η^2). Compounds with O^- and

³ Low-/high-field shift refers to the magnetic field.

N-functional ligands very generally will give rise to chemical shifts in the approximate range -400 to -600 ppm.^[2] Introducing a chloro ligand, or a simple thio ligand such as S^{2-} or RS^- , deshields the vanadium nucleus.

2. *Coordination number and coordination geometry.* In a series of complexes with identical ligand functions, such as VO_n ($n = 4-6$), shielding often decreases with increasing n . An illustrative example, displayed by the vanadium NMR spectrum in Figure 2.3 and the data in Table 2.3, is provided by the vanadates. The tetrahedral vanadates all resonate in the range -534 to -586 ppm; the actual shifts depend on the nuclearity and protonation state (Figure 3.2). In the peripheral vanadium centres of decavanadate, i.e. the C_{4v} sites V_a and V_b in Figure 2.7, the vanadium coordination environment can be described by $O=VO_4O'$, where the bond to O', *trans* to the doubly bonded oxygen, is weak. The coordination environment in these sites is in-between square pyramidal and square bipyramidal; the chemical shifts cluster around -500 ppm. An even more pronounced deshielding with respect to tetrahedral vanadates, $-420(2)$ ppm, is observed for the central vanadium sites in decavanadate, the O_h sites V_c.

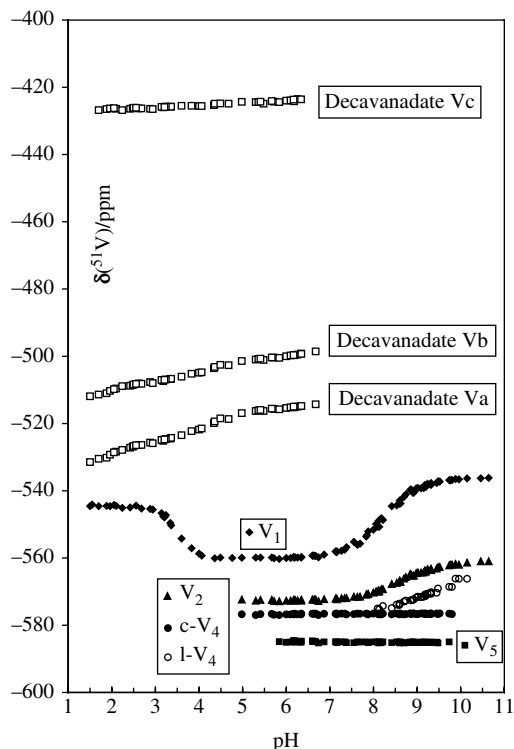


Figure 3.2

pH dependence of the chemical shifts of decavanadate (for the three vanadium sites, V_a, V_b and V_c; cf. Figure 2.7, left), monovanadate [$V_1 = H_x VO_4^{(3-x)-}$ and, below pH ≈ 2 , VO_2^+], divanadate [$V_2 = H_x V_2 O_7^{(4-x)-}$], cyclic tetravanadate (c-V₄ = $V_4 O_{12}^{4-}$), linear tetravanadate (l-V₄ = $V_4 O_{13}^{6-}$) and pentavanadate ($V_5 = V_5 O_{15}^{5-}$). See Figure 2.6 for the structures of V₁, V₂, c-V₄ and V₅. Courtesy of L. Pettersson, Umeå University, Sweden.

The relation between shielding and protonation state of monovanadate can be exploited to calculate the pH in an aqueous medium by the use of Equation (3.4):

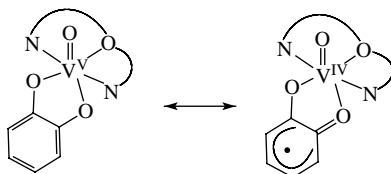
$$\text{pH} = \text{p}K_{\text{a}} + \log [(\delta_2 - \delta_{\text{obs}})/(\delta_{\text{obs}} - \delta_1)] \quad (3.4)$$

Where $\text{p}K_{\text{a}} = 8.17$ (K_{a} is the acid constant for $[\text{H}_2\text{VO}_4]^-$ in 0.15 M NaCl, i.e. isotonic conditions), and δ_1 and δ_2 refer to the chemical shifts for $[\text{H}_2\text{VO}_4]^-$ ($\delta_1 = -538.8$ ppm) and $[\text{H}_2\text{VO}_4]^-$ (-560.4 ppm); δ_{obs} is the chemical shift actually observed.

A second example for the influence of the coordination number on shielding is represented by the esters of orthovanadic acid, $\text{VO}(\text{OR})_3$. For spacious substituents R, or in dilute solutions, these esters are monomers, and the coordination number is 4 in a trigonal pyramidal environment. For less spacious substituents R and in sufficiently concentrated solutions, dimerisation and oligomerisation occur, leading to the coordination number 5 in a trigonal bipyramidal arrangement, as shown in Figure 2.11. The limiting shift values for, e.g., $\text{VO}(\text{OEt})_3$ are -605 ppm (for the monomer) and -573 ppm (for the oligomer).^[3]

3. *Steric effects.* Sterically demanding ligands induce upfield shifts in high-valent vanadium compounds. Examples are again the esters $\text{VO}(\text{OR})_3$. Thus, whereas for $\text{R} = \text{Et}$ δ is -605 ppm, a chemical shift $\delta = -623$ ppm has been reported for $\text{R} = \text{iPr}$ and $\delta = -681$ ppm for $\text{R} = \text{CMe}_3$.^[3] In complexes containing two or more elements of chirality, the different diastereomers are distinct in their chemical shifts. If vanadium itself is a centre of chirality (Figure 2.25), shift differences between diastereomers typically amount to 5–20 ppm, depending on the separation between the vanadium centre and the chiral element (centre or plane) in the ligand sphere; see also item 5 below.
4. *Peroxo and hydroxamido ligands.* These ligands coordinate almost exclusively side-on and consequently give rise to strained three-ring structures. The net effect upon shielding is an upfield shift by ca 50 ppm (and more) per peroxide (O_2^{2-} or RO_2^-) or hydroxamide (NR_2O^- , $\text{R} = \text{H}$ and/or alkyl; for functionalised R see item 5). Table 2.4 contains relevant data.
5. *Noninnocent ligands.* Ligands which are able to delocalise electron density towards the metal are termed ‘noninnocent’. This ligand-to-metal charge transfer (LMCT) gives rise to resonance hybrids of the kind shown in Scheme 3.1, resulting in substantial deshielding of the vanadium nucleus. Chemical shifts in fact correlate linearly with the energies of the LMCT band in the visible and near-infrared regions,^[4] i.e. with the ΔE term in Equation (3.3): low-energy LMCT transitions give rise to effective deshielding. Noninnocent ligands typically are hydroxamates and catecholates. For a demonstration, three complexes with a Schiff-base ligand derived from salicylaldehyde and aminoethylimidazole are compared with respect to their chemical shifts in Figure 3.3. Whereas the ‘innocent’ Schiff base ligand gives rise to a normal δ value, the hydroxamate and catecholate derivatives induce substantial deshielding, more dramatic for catecholate than for hydroxamide. Also noninnocent, although not to this extent, are calixarenes and functionalised hydroxamides NR_2O^- with substituents R terminated by carboxylates. This type of ligand is present in amavadin (Section 4.2). Figure 3.4 shows the ^{51}V NMR spectrum of the oxidised (i.e. V^{V}) form of an artificial amavadin obtained from the reaction of a vanadium precursor compound with racemic 2,2'-(hydroximino)diisopropionic acid. Along with the unprecedented low-field chemical shift of around -240 ppm, it is noteworthy that three signals are observed. These three signals correspond to three diastereomers, resulting from different combinations of

the *R*- and *S*-centres on the ligand, and the Δ and Λ antipodes associated with the orientation of the two ligands with respect to vanadium.



Scheme 3.1

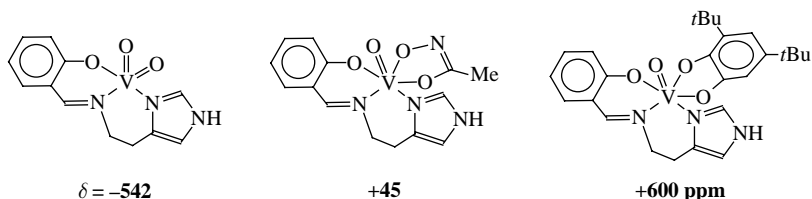


Figure 3.3

Chemical shifts $\delta(^{51}\text{V})$ for oxovanadium complexes carrying the innocent ligand salicylideneaminatoethylimidazole and (centre and right) the noninnocent methylhydroxamate and bis(*tert*-butyl)catecholate. The noninnocent ligands induce downfield shifts (deshielding).^[4]

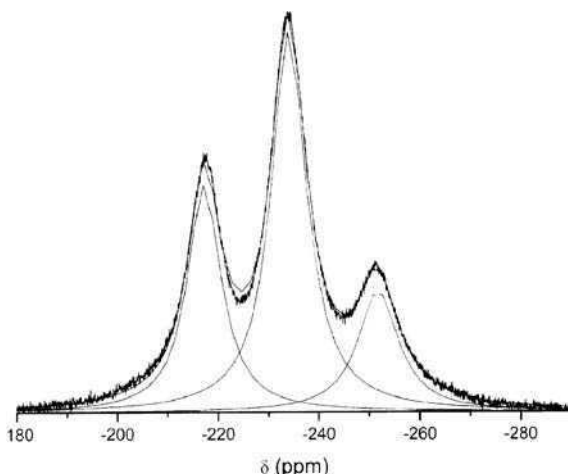


Figure 3.4

^{51}V NMR spectrum of a mixture of three diastereomers of oxidised amavadin in 0.1 M HCl. The chemical shifts are -217 , -234 and -252 ppm .^[5] Reproduced from J. Lenhardt *et al.*, *Chem. Commun.* **2006**, 4641–4643. Copyright (2006) with permission from The Royal Society of Chemistry.

3.1.2.3 Two-dimensional Exchange Spectroscopy

The chemical exchange rate(s) between two or more vanadium species can lie in about the same time window as the relaxation rates (lifetime of an excited state in an NMR

experiment), namely on the millisecond scale. This advantage, and the fact that on this time-scale the system in equilibrium commonly is beyond coalescence, often allows for the application of two-dimensional exchange spectroscopy (2D-EXSY). The aqueous vanadate system has thus been examined by EXSY, and the equilibria between mono-, di-, tetra- and pentavanadate shown in Figure 2.6 have been established.^[6] Figure 3.5 demonstrates the situation for the equilibria between mono- and dimeric esters of composition $\{\text{VO}(\text{OR})_3\}_n$ mentioned above (item 2 and also Figure 2.11). Critical in EXSY is the choice of the ‘correct’ mixing time, i.e. the time allowed for optimal magnetisation transfer from one of the exchanging species to the other. Depending on the specific system, these mixing times typically are in the range between 0.1 and 10 ms.

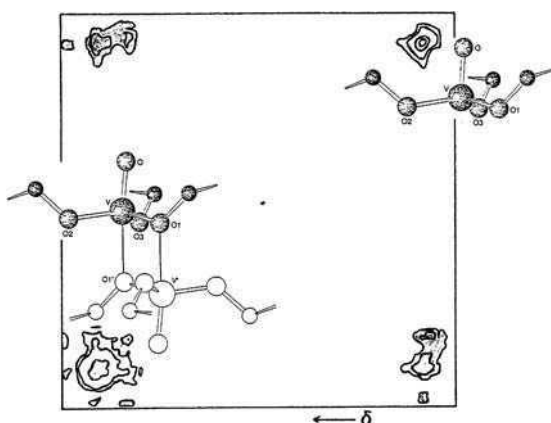


Figure 3.5

Two-dimensional, homonuclear ^{51}V exchange spectrum of $\{\text{VO}(\text{OEt})_3\}_n$, $n = 1$ and 2, at a mixing time of 1.5 ms. The off-diagonal peaks (cross peaks in the upper left and lower right corner) indicate exchange. The δ values are -573 ppm for the dimer and -605 ppm for the monomer.

3.1.3 Other ^{51}V NMR Parameters

Under isotropic conditions, linewidths and nuclear spin–spin coupling constants are additional parameters which can be employed in characterising vanadium compounds.

3.1.3.1 Linewidths

Linewidths are commonly measured at half-height of the signal and denoted $W_{\frac{1}{2}}$, in Hertz. Linewidths are inversely proportional to the relaxation time T . There are two relaxation mechanisms, distinguished as spin–lattice (or longitudinal) relaxation T_1 , and spin–spin (or transversal) relaxation T_2 . T_1 corresponds to an energy transfer from the excited nucleus to the environment. For a quadrupolar nucleus, this energy transfer, which ‘relaxes’ its excited to the ground state, quadrupole interaction via electric field gradients is the main contributor to relaxation. T_2 corresponds to an entropy transfer; under isotropic conditions, $T_2 \approx T_1$. The relaxation process can be described by Equation (3.5):

$$W_{\frac{1}{2}} = (\pi T)^{-1} = 0.041\pi^2 \times C_Q(1 + \eta^2/3)\tau_c \quad (3.5)$$

where C_Q stands for the quadrupole coupling constant, $C_Q = e^2 q_{zz} Q / h$, Q being the quadrupole moment (-4.8 fm^2), e and h the elementary charge and Planck's constant, respectively, and q_{zz} the electric field gradient in the zz direction. The quadrupole coupling constant describes the extent of interaction between the ^{51}V nucleus in its specific coordination environment and electric fields generated by the matrix. It is sensitive towards the electronic properties of the directly coordinating ligand functions and the local symmetry. The local symmetry also influences the asymmetry parameter η , which is zero for axial symmetry. Finally, the molecular correlation time τ_c is an important factor when it comes to variations in linewidths. This factor denotes the extent to which the molecule under consideration is freely mobile in the medium where it is dissolved. Large molecules, in particular large molecules deviating from an (approximately) spherical shape, tumble slowly, i.e. the time they are 'correlated' with the solvent dipoles is comparatively long, which facilitates energy transfer and thus decreases T and increases $W_{\frac{1}{2}}$. The influences on the width at half-height can be categorised as follows:

1. An increase in viscosity increases $W_{\frac{1}{2}}$ via τ_c . Viscosity increases with, *inter alia*, decreasing temperature and increasing concentration.
2. An increase in the ligand bulkiness induces an increase in $W_{\frac{1}{2}}$.
3. Ring strains in complexes with chelate structures give rise to line broadening.
4. The narrowest lines are observed for cubic symmetry (T_d , O_h) and in ligand arrangements close to cubic symmetry. Vanadates, including their protonated forms, are typical examples. Narrow lines also arise for many systems with local C_{nv} symmetry, e.g. VOX_3 (C_{3v}).
5. In compounds of the same build-up, hard ligands (strong σ -donors) induce narrower signals than soft donors. Examples are $[\text{VO}_4]^{3-}$ vs $[\text{VS}_4]^{3-}$ and VOF_3 vs VOBr_3 .

In practice, linewidths are determined by a complex pattern of all of these influences, and it is therefore hardly possible to assign 'typical' linewidth ranges to specific classes of complexes. On a very general basis, linewidths range between 30 and 3000 Hz, with T_d and C_{3v} compounds approaching the lower limit and low-symmetry compounds with bulkier ligands the upper limit. To obtain optimal resolution, influences via points 1 and 2 above can be minimised by appropriate choices of the solvent, temperature and concentration. These factors are also important when it comes to preventing relaxation decoupling (see the next section).

As already mentioned at the beginning of this chapter, the presence of paramagnetic VO^{2+} may further deteriorate the situation. Finally, it should be noted that linewidth influences via Equation (3.5) can be counteracted by linewidth variations encountered in systems in dynamic chemical equilibrium. Thus, the decrease in linewidth to be expected on increasing the temperature (decreasing the viscosity), may be overpowered by an increase in linewidth on approaching coalescence when increasing the exchange rates with increasing temperature.

3.1.3.2 Nuclear Spin–Spin Coupling

Nuclear spin–spin coupling J , also termed scalar coupling, between the vanadium nucleus V and a ligand nucleus L , is dominated by the Fermi contact term [Equation (3.6)].

This term describes the isotropic contribution of the interaction between the magnetic moments of the nuclei and the electrons.

$$J_{VL} \propto \gamma_V \gamma_L ({}^3\Delta E)^{-1} |S(0)_V|^2 |S(0)_L|^2 \sigma(s)^2 \quad (3.6)$$

where γ_V and γ_L are the magnetogyric ratios of the two coupling nuclei and $|S(0)_V|^2$ and $|S(0)_L|^2$ represent the s-electron densities at the respective nuclei. $({}^3\Delta E)^{-1}$ is the mean triplet excitation energy [note that, in quantifying J , the *triplet* energy is relevant, whereas in the respective equation for the paramagnetic deshielding, Equation (3.3), the singlet energy is involved]. $\sigma(s)^2$ describes the σ contribution to the V–L bond, including synergistic effects arising from π interactions. According to Equation (3.6), one should expect effective coupling (large coupling constants) for

- strongly electronegative ligands (mainly through an increase in $|S(0)_L|^2$ by contraction of the s orbitals);
- strengthening of the V–L interaction by increasing the $\sigma(s)$ character of the V–L bond.

Depending on the number of bonds between the V and L nuclei, one- or two-bond couplings, 1J or 2J , can be observed or, more generally, nJ , where the size of J decreases rapidly with increase in n . A major problem in evaluating coupling is relaxation. Efficient relaxation broadens the resonance lines to the extent where coupling is not resolved, or even does not exist due to relaxation decoupling, i.e. relaxation is too fast to allow communication between the two nuclei. Decreasing the viscosity (see above) can improve the situation. An example of a well-resolved coupling pattern is the ${}^{51}\text{V}$ NMR spectrum of ${}^{17}\text{O}$ -enriched orthovanadate in Figure 3.6 (left). The nucleus ${}^{17}\text{O}$ has a spin $5/2$ and thus gives rise to six equidistant lines of equal integral intensity. Also, resorting to the L nucleus (instead of ${}^{51}\text{V}$) can help: if the L nucleus has a spin = $1/2$ (such as ${}^{19}\text{F}$ and ${}^{31}\text{P}$), the spectrum, if resolved, shows eight equidistant lines. Fully effective, although unresolved, coupling may result in a plateau-like signal, the envelope of the eight-line pattern, from which the coupling information can still be extracted. The ${}^{31}\text{P}$ NMR spectrum in Figure 3.6 (right) is an example.^[7] The depression in the plateau is due to the fact that the uppermost left and right components of the (unresolved) eight-line pattern are narrower than those of the central components.

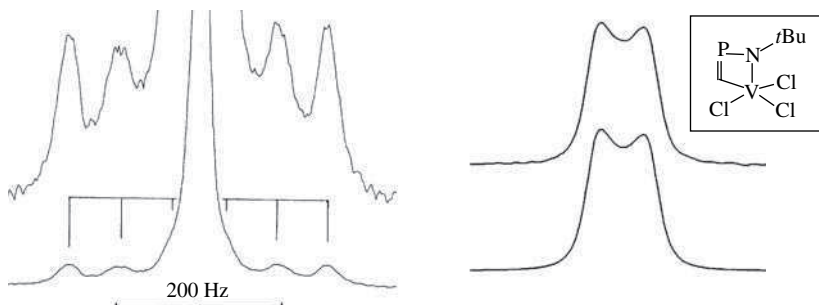


Figure 3.6

Left: 23.7 MHz ${}^{51}\text{V}$ NMR spectrum of $[\text{VO}_4]^{3-}$, enriched in ${}^{18}\text{O}$ (50.7%) and ${}^{17}\text{O}$ (8.3%). The main (central) resonance is due to $[\text{V}^{16,18}\text{O}_4]^{4-}$; the coupling pattern due to ${}^1J({}^{51}\text{V}-{}^{17}\text{O}) = 62$ Hz is superimposed. Right: ${}^{31}\text{P}$ NMR spectrum of a cyclic imidovanadium complex (inset), showing the envelope of the ${}^2J({}^{31}\text{P}-{}^{51}\text{V})$ coupling = 30.3 Hz. Top, experimental; bottom, simulation. From ref. [7]. Reproduced from D. Gudat *et al.*, *Magn. Reson. Chem.* 40, 139–146, Copyright (2002), with permission from John Wiley & Sons, Ltd.

3.1.4 NMR Parameters Under ‘Confined’ Conditions

Under anisotropic conditions, NMR lineshapes for a quadrupolar nucleus are dominated by chemical shielding and (first and second order) quadrupolar interactions. Dipolar interaction is usually a minor contribution only. First-order quadrupole interaction lifts the degeneracy of the allowed $2I$ (i.e. seven in the case of ^{51}V ; $I = 7/2$) Zeeman transitions as shown in Figure 3.7, giving rise to seven equidistant lines, viz. a central line ($m_I = +1/2 \rightarrow -1/2$, unaffected by quadrupole interaction) and six satellite lines. The overall breadth of the spectrum is determined by the size of the nuclear quadrupole coupling constant C_Q ; the deviations from axial symmetry and hence the shape of the spectral envelope are governed by the asymmetry parameter. Static solid-state NMR thus provides additional parameters, in particular the quadrupole coupling constant, which correlates with the electronic situation in a vanadium compound.^[1,8] The central component reflects the anisotropy of the chemical shift.

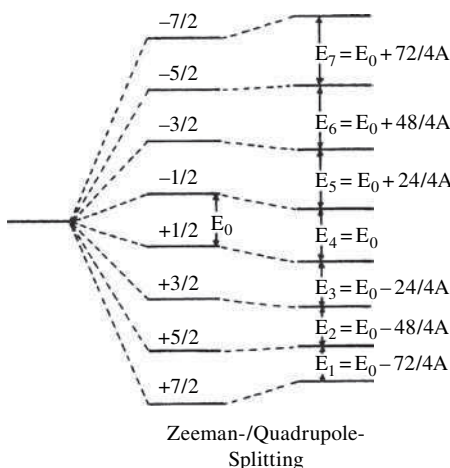
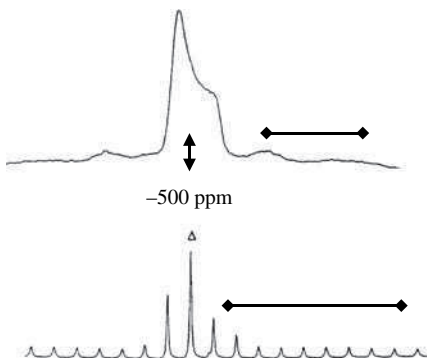


Figure 3.7

Zeeman and first order quadrupole splitting for the nucleus ^{51}V (nuclear spin $I = 7/2$). $A = C_Q(3\cos^2\Theta - 1)/8hI(2I - 1)$.^[8] The angle Θ defines the orientation of the principle axis of the (crystalline) sample with respect to the field direction.

The quadrupole perturbation term contains the factor $(3\cos^2\Theta - 1)$ which becomes zero for $\Theta = 54.7^\circ$, the ‘magic angle’. Magic angle spinning (MAS) of the sample thus removes first-order quadrupole interactions, and a spinning sideband manifold is obtained, from which the central transition δ_σ can be sorted out as the band the position of which remains unchanged when altering the spinning frequency. The quantity δ_σ is related to the isotropic chemical shift δ_{iso} by $\delta_\sigma = \delta_{zz} - \delta_{\text{iso}}$, where $\delta_{\text{iso}} = 1/3(\delta_{xx} + \delta_{yy} + \delta_{zz})$. A typical example, the static and MAS spectra of the ester $\text{VO}(\text{CH}_2\text{CH}_2\text{Cl})_3$, is shown in Figure 3.8.^[9] In Table 3.2, chemical shift data under isotropic and anisotropic conditions are compared for selected oxovanadium alkoxides. Table 3.2 also contains nuclear quadrupole coupling constants.

Seven separate and equidistant resonance lines are also observed in partially ordered systems, such as represented by mesophases (liquid crystals, lyotropic bilayer systems).

**Figure 3.8**

Static (top) and MAS ^{51}V NMR spectrum (bottom) of solid $\text{VO}(\text{OCH}_2\text{CH}_2\text{Cl})_3$. The central component in the MAS spectrum is indicated by Δ .^[9] The bars represent a spectral width of 500 ppm. Reproduced from D. C. Crans *et al.*, *Inorg. Chem.* 33, 2427–2438. Copyright (1994), with permission from the American Chemical Society.

Table 3.2 Isotropic and anisotropic NMR parameters for oxovanadium(V) alkoxides.

Compound	δ in isotropic media ^a pentane // neat	δ_{iso} in solid samples ^b	Quadrupole coupling constant, C_Q (MHz)
$\text{VO}(\text{OnPr})_3$	-604 to -587 // -555		4.4 ^c
$\text{VO}(\text{O}i\text{Pr})_3$	-624 // -628		5.2 ^d
$\text{VO}(\text{O}t\text{Bu})_3$	-681	-666.5	2.1 ^b
$\text{VO}(\text{CH}_2\text{CH}_2\text{Cl})_3$	-609 to -586	-500.6	2.6 ^b

^aRoom temperature. Where a range is indicated, δ is concentration dependent: the first entry is in ca. 15 mM, and the second entry in ca 350 mM solution; from ref. 3.

^bSolid state spectra; ref. 9.

^cStatic solid-state spectrum; ref. 3b.

^dIn nematic phase 4; ref. 8a.

The splitting $\Delta\nu$ again reflects first-order quadrupole interaction, but also the degree of order in the mesophase, quantified by the ordering factor S_a . The two quantities are connected by Equation (3.7).

$$\Delta\nu = S_a \times 3C_Q/4I(2I - 1) \quad (3.7)$$

Evaluation of the spectra thus provides the nuclear quadrupole coupling constant C_Q for the vanadium compound dissolved in the mesophase and the order parameter of the liquid crystalline phase. In Figure 3.9, two typical spectra are shown. The left-hand series of spectra were obtained for vanadate in a lyotropic mesophase prepared from tetrade-cyltrimethylammonium bromide and potassium dodecanoate in water.^[10] Monovanadate $[\text{HVO}_4]^{2-}$ (the signal at low field) undergoes weak interaction with the micellar surface throughout the range of composition of the cationic and anionic components of the mesophase, whereas the high-field component, $[\text{V}_2\text{O}_7]^{4-}$, interacts at higher fractions of dodecanoate only. The right-hand spectrum represents the situation for $\text{VO}(\text{O}i\text{Pr})_3$ dissolved in the liquid crystal MBBA.

Even in the absence of any order confining the molecules, isotropic molecular motion can be slowed to the extent where the system under consideration is far from extreme

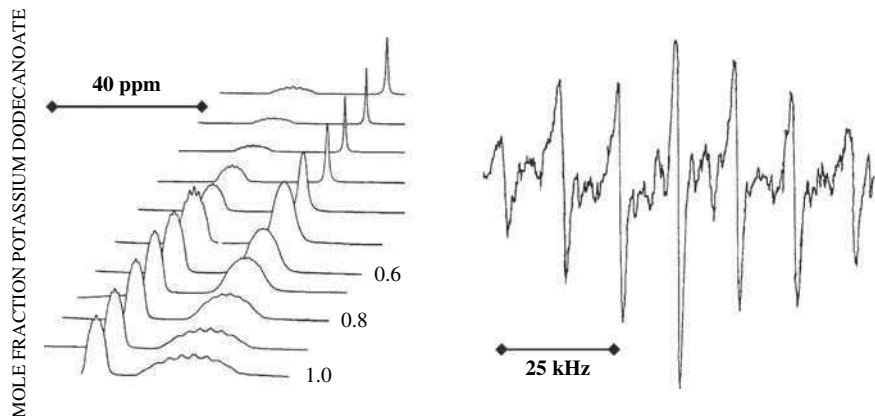


Figure 3.9

Left : ^{51}V NMR spectra of vanadate in a lyotropic mesophase (dodecanoate + tetradecyltrimethylammonium at varying ratios of the two components).^[10] The two components correspond to mono (low field) and divanadate (high field). Right: first-derivative ^{51}V NMR spectrum of $\text{VO}(\text{O}i\text{Pr})_3$ dissolved in the liquid crystal MBBA (4-methoxybenzylidene-4'-butylamine) at a concentration of 8.3%.

narrowing, a situation which is encountered with macromolecules, such as V^{V} firmly coordinated to a protein. Under these conditions, only the fairly sharp central transition ($m_l = +\frac{1}{2} \rightarrow -\frac{1}{2}$) is observed, and the NMR parameters δ and $W_{\frac{1}{2}}$ become a function of the strength of the applied magnetic field B_0 , as demonstrated for vanadate bonded to human serum transferrin:^[11]

$$B_0 = 7.05 \text{ T. C-lobe : } \delta = -536.0 \text{ ppm, } W_{\frac{1}{2}} = 418 \text{ Hz;}$$

$$\text{N-lobe : } \delta = -536.0 \text{ ppm, } W_{\frac{1}{2}} = 418 \text{ Hz.}$$

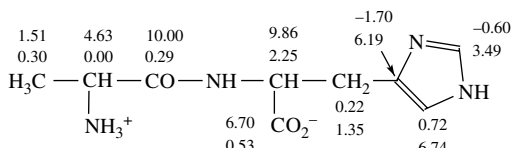
$$B_0 = 11.7 \text{ T. C-lobe : } \delta = -529.9 \text{ ppm, } W_{\frac{1}{2}} = 190 \text{ Hz;}$$

$$\text{N-lobe : } \delta = -531.4 \text{ ppm, } W_{\frac{1}{2}} = 268 \text{ Hz.}$$

3.2 NMR of Other Nuclei

In diamagnetic vanadium complexes, information on the mode of coordination of the ligand(s) can be obtained from magnetic nuclei in the coordination sphere by both one- and two-dimensional (homo- and heteronuclear) methods. In model complexes for bio-relevant vanadium compounds, informative spin probes are the spin- $\frac{1}{2}$ nuclei ^1H , ^{13}C and ^{15}N (the last preferably in ^{15}N -enriched samples), and the quadrupolar nuclei ^2H ($I = 1$), ^{14}N ($I = 1$) and ^{17}O ($I = \frac{5}{2}$). ^{17}O NMR is a powerful tool in characterising peroxovanadium complexes. Generally, the closer a ligand function is to the vanadium centre, the more its chemical shift deviates from that in the uncoordinated ligand. The shift difference $\Delta\delta = \delta(\text{complex}) - \delta(\text{free ligand})$, the so-called coordination-induced shift (CIS), is particularly helpful in assigning coordination modes via ^{13}C NMR. An illustrative example is provided in Scheme 3.2 for the coordination of the dipeptide alanyl-histidine to vanadate and peroxovanadate, respectively: For the vanadate complex, the CIS values

(upper entries in Scheme 3.2) indicate coordination via the terminal carboxylate and amino groups plus the deprotonated amide-N, excluding the imidazolyl moiety [cf. V(ala-his) in Figure 2.15]. Conversely, in the case of peroxovanadate [cf. V(O₂)₂(ala-his) in Figure 2.15], coordination occurs exclusively through the imidazolyl-*N* (lower entries in Scheme 3.2).^[12]



Scheme 3.2

Paramagnetic vanadium(III) possesses excellent NMR contact shift properties (very short electron-spin relaxation times and large hyperfine coupling constants), severely shifting proton NMR signals of ligands attached to vanadium, a fact which can be exploited (and has been exploited in the case of elucidating the nature of vanadium in the vanadocytes of ascidians; Section 4.1) to analyse V^{III} complexes via chemical shifts and intensities of paramagnetically shifted ¹H resonances. This includes systems where rapid ligand exchange takes place, e.g. between coordinated water and ‘free’ water in the coordination environment, where the solvent water ‘retains the paramagnetic contact information’. In such a case, the shift difference between water in contact with the paramagnetic centre and pure water is proportional to the amount of exchangeable coordination sites available at the vanadium centre (and the vanadium concentration); see section 4.1.2 for details.^[13] In complexes with nonexchangeable ligands, such as β-diketonates and β-ketoamines, isotropic contact interaction produces chemical shifts of the ligand protons of ca +150 to –60 ppm.^[14]

Whereas V^{III} gives rise to ¹H resonances which are substantially shifted but still sufficiently sharp to be detected, V^{IV} greatly broadens signals but does not cause appreciable shifts.^[15]

3.3 EPR Spectroscopy

3.3.1 General

Electron paramagnetic resonance (EPR) spectroscopy is virtually complementary to NMR spectroscopy: Whereas EPR detects the energy needed to switch the electron spin in a magnetic field (and the related relaxation phenomena), NMR addresses the corresponding effects associated with the spin of the nucleus (if the nucleus is magnetic, i.e. does have a spin). The main difference is the energy scale: gigahertz in EPR versus megahertz in NMR. Also note that, whereas in (modern) NMR the magnetic field is kept constant and the frequency modulated so as to adapt to the energy necessary to induce a transition, the classical EPR experiment is a continuous-wave method (constant frequency, variable magnetic field).

In order to be able to detect an EPR signal, a resulting overall spin *S* for the electron shell is necessary, provided by an odd number of electrons or, in the case of an even

number of electrons, a high-spin situation. For vanadium, the simplest case is represented by vanadium(IV), a d¹ system ($S = \frac{1}{2}$). In dinuclear complexes containing the (V^{IV})₂ μ -O or (V^{IV}V^V) μ -O core, the complex provides an EPR signal, the structure of which depends on the presence or absence of communication between the two centres. In the case of vanadium(III), or d², the overall spin is either $S = 0$ (low-spin; EPR inactive) or $S = 1$ (high spin). In principle, these $S = 1$ systems are susceptible to EPR measurement. In practice, the energies of the EPR transitions are outside the range that can be observed with the generally available spectrometers, as frequently observed with even numbers of unpaired electrons. In addition, relaxation is often fast to the extent where the signal broadens beyond detectability. High-spin V^{II} (d³, $S = \frac{3}{2}$) behaves similarly. Whereas low spin V^{II} ($S = \frac{1}{2}$) again can be a feasible EPR probe. The oxidation state of choice in EPR of vanadium compounds is certainly V^{IV}. Since the energy necessary to excite an electron in an external magnetic field largely depends on the specific electronic situation imparted by the nature of the functions attached to vanadium, an EPR spectrum provides sensible information on vanadium's coordination environment – as NMR does in V^V compounds – ignoring the bulk of the protein. The main protagonist of applications of EPR in biological systems containing vanadium is Chasteen, who reviewed the method and its applications almost three decades ago.^[16] For a more recent and comprehensive treatment of EPR (including ESEEM and ENDOR; see section 3.4, a review by Smith, LoBrutto and Pecoraro is recommended.^[17]

The condition for resonance in an EPR experiment is defined by Equation (3.8), in which v is the frequency, h is Planck's constant, β is the Bohr magneton, B is the magnetic field and g is the so-called g factor:

$$hv = g\beta B \quad (3.8)$$

The free electron value of the g factor is $g = 2.0023$. In V^{IV} complexes, g is below this value, typically between 1.94 and 1.98. To some extent, the g value corresponds to the chemical shift δ in an NMR experiment; it is, however, less meaningful (because it is less susceptible to changes in the ligand-induced electronic situation) than δ . Sufficiently more significant is the hyperfine coupling constant A , which quantifies the extent of coupling of the electron spin to the nuclear spin. Since the spin of the ⁵¹V nucleus is $I = \frac{7}{2}$, EPR lines of mononuclear V^{IV} complexes are split (if resolved) into $2I + 1 = 8$ lines. The electronic ground state ($S = \frac{1}{2}$), under the influence of the magnetic field, splits into two electronic states characterised by $m_S = +\frac{1}{2}$ and $-\frac{1}{2}$. Additional splitting occurs through the eight different magnetic orientations of the nuclear spin, characterised by m_I . The selection rules, $\Delta m_S = \pm 1$ and $\Delta m_I = 0$, give rise to eight allowed transitions. Under isotropic conditions an eight-line pattern is thus observed, flanked by the $m_I = -\frac{7}{2}$ transition at low field and the $m_I = +\frac{7}{2}$ transition at high field. The eight lines in the EPR spectrum are equidistant only in a first approximation. Actually, the separation between the lines gradually increases with increasing magnetic field.

Under conditions where isotropic tumbling of the molecules is restricted or annealed, as in frozen solutions, powders and other solid-state situations, anisotropic spectra are observed, i.e. additional splitting complicates the spectra, but also provides highly valuable information on the electronic nature and orientation of the ligand set. In the case of vanadyl complexes, the dominant V=O unit defines the primary axis (the z direction). In this case of so-called axial symmetry, two sets of eight lines are observed with differing g and

A values, denoted g_{\parallel} and g_{\perp} , and A_{\parallel} and A_{\perp} , respectively. The parallel component is the one coinciding with the V=O director and the direction of the magnetic field B . In a tetragonal complex (octahedral, square pyramidal), $g_{\parallel} < g_{\perp}$ and $A_{\parallel} > A_{\perp}$. A typical axial spectrum is shown in Figure 3.10. The anisotropic parameters are connected with the isotropic parameters by $A_{\text{iso}} = \frac{1}{3}(A_{\parallel} + 2A_{\perp})$ and $g_{\text{iso}} = \frac{1}{3}(g_{\parallel} + 2g_{\perp})$. If all three axes in the molecular frame are distinct, a ‘rhombic’ spectrum arises, with three different splittings characterised by A_x , A_y and A_z , and g_x , g_y and g_z , where the z component corresponds to A_{\parallel} and g_{\parallel} . The differences between the x and y components are usually small and hardly resolved in the central part of the overall spectrum.

For roughly assessing g_{\parallel} and A_{\parallel} , the two flanking lines (exhibiting the widest splitting) are employed; g_{\parallel} is obtained from Equation (3.8) with the magnetic field B of the centre of the spectrum. Dividing the separation between the two flanking resonance lines by seven provides A_{\parallel} . Refinement of the g and A values thus obtained by computer simulation is essential.

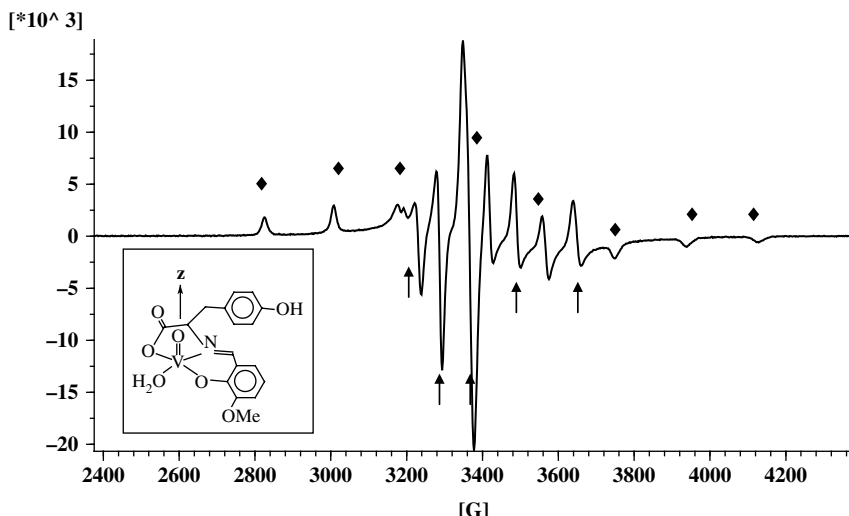


Figure 3.10
A typical anisotropic axial EPR spectrum of an oxovanadium(IV) complex (inset) in frozen THF. The ligand is a Schiff base derived from vanillin and tyrosine. Diamonds indicate the eight components of A_{\parallel} (the parallel hyperfine coupling constant; parallel defined by the z direction, which is the direction of the magnetic field). Arrows indicate the five inner components of A_{\perp} . Abscissa; magnetic field strength (G); ordinate, intensity (arbitrary units).

3.3.2 Applications

The parallel component A_{\parallel} of the hyperfine coupling constant is particularly sensitive to the nature of the equatorial ligand set of a square pyramidal or octahedral oxovanadium complex, the most common geometry of oxovanadium(IV) complexes. This is a consequence of the electronic ground state, d_{xy} , of the complexes, allowing interaction of the single vanadium electron with the donor functions in the equatorial plane. Although this ground state is essentially non-bonding, some delocalisation of the electron density towards π -type ligand-dominated molecular orbitals can occur, quantified by the

ground-state orbital population parameter (β^*)². This parameter, describing the population of the d_{xy} orbital, equals 1 (i.e. 100% population) if the electron is not delocalised at all, and becomes <1 in case of delocalisation. The lowest (β^*)² of 0.84 has been reported for ligand sets containing sulfur donors, which π -interact particularly easily. Since the amount of delocalisation correlates with the communication between the electron in the d_{xy} orbital and the ^{51}V nucleus, low (β^*)² will give rise to low $A_{||}$. An approximately linear correlation has been noted between $A_{||}$ and (β^*)², allowing for a first estimate of the donors in the equatorial plane.^[18]

A more sensitive tool for a correct assignment of the equatorial ligand set is provided by the additivity relationship, according to which $A_{||}$ is the sum of the contributions of the four equatorial ligands i . These contributions are quantified by the partial hyperfine coupling constants $A_{||}(i)$. Typical $A_{||}(i)$ vary between 32×10^{-4} and $46 \times 10^{-4} \text{ cm}^{-1}$; they are given in Table 3.3. In many cases (but not in all; see below), comparison of the measured and the calculated $A_{||}$ allows for an unambiguous decision on the nature of the equatorial ligand set.

Table 3.3 Partial parallel hyperfine coupling constants $A_{||}(i)$ for various binding groups i , taken from refs 16–18.

Binding group	$A_{ }(i)(10^{-4} \text{ cm}^{-1})$
H_2O	45.7
Imidazole $=\text{N}-$	40–46 ^a
Imine (Schiff base) $=\text{N}-$; average (range)	41.6 (38.1–43.7)
Cl^-	44.2
Amide C=O	43.5
SCN^-	43.2
Dimethylformamide	43.7
Carboxylate RCO_2^-	42.7–41.8
Phosphate PO_4^{3-}	42.5
Aromatic N	40.7
Amine RNH_2	40.1
Phenolate RO^-	38.9
Acetylacetone $=\text{C}-\text{O}^-$	37.6
Aliphatic RO^-	35.3
Thiophenolate RS^-	35.3
Amide $-\text{C}(\text{O})\text{NR}^-$; average (range)	35 (29–43) ^b
Aliphatic thiolate RS^-	31.9

^aDepending on the orientation of the imidazole ring; see text.

^bDepending on the overall charge of the ligand of which the amide group is a constituent (larger value for higher charge; for details, see text) and the coordination number.

The lowest $A_{||}(i)$ have been noted for the deprotonated amide nitrogen as a constituent of a multidentate ligand system, in particular if the overall charge of the ligand is low. Mean values are $32.7(\text{charge} - 1)$, $35.5(-2)$, $38.3(-3)$ and $40.9 \times 10^{-4} \text{ cm}^{-1}(-4)$.^[19] This strong reduction of A has been traced back to variations in the ionicity/covalency of the bond between the deprotonated nitrogen and vanadium: the covalency is more pronounced if the overall charge is -1 , leading to more effective electron delocalisation, i.e. smaller (β^*)² and low $A_{||}(i)$. Another factor influencing the size of A is the orientation of an (aromatic) ligand with respect to the V=O vector. This

has been worked out in detail for the imidazole ligand, which, as a constituent of histidine, coordinates to vanadium in the vanadate-dependent haloperoxidases both in the native vanadium(V) form (one histidine) and the inactive vanadium(IV) form (two histidines). The situation is illustrated in Figure 3.11 for two oxovanadium(IV) compounds representing extremes. On the left-hand side of Figure 3.11 the imidazole and the oxovanadium moiety are in the same plane (in a parallel orientation). The p orbital on N (the aromatic MO of imidazole) is perpendicular to the imidazole plane and can thus effectively interact with the d_{xy} orbital of vanadium. As a consequence, the $A_{||}$ electron is delocalised towards the ligand, and $A_{||}(\text{imidazole})$ is comparatively small. On the right-hand side of Figure 3.11, the imidazole is perpendicular to the V=O vector. The p orbital on N thus is parallel to the vanadyl bond and competes with the strong π -donating oxo group in interaction with the donating nitrogen orbital. Hence there will be only a marginal interaction with the donating nitrogen orbital. The $A_{||}(\text{imidazole})$ values have been shown to be a function of $\sin(2\theta - 90)$, where θ is the dihedral angle defined by the vanadium atom, the coordinated imidazole N and the carbon next to it, as shown in the central part of Figure 3.11.^[20] Similar explanations may hold for the range covered by $A_{||}(\text{imine})$ in Table 3.3.

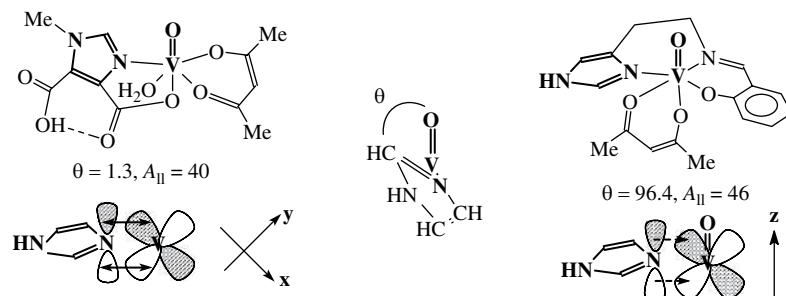
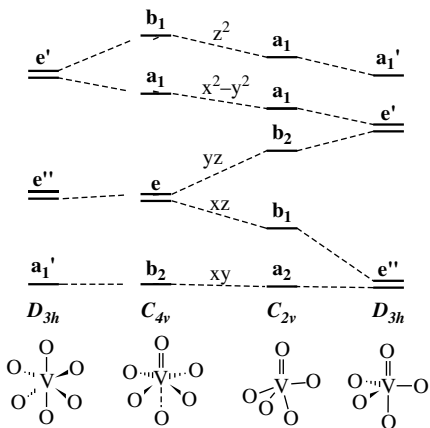


Figure 3.11

Dependence of the partial parallel hyperfine coupling constant on the orientation of the imidazole ring relative to the V=O vector. Left: parallel orientation leads to effective interaction between the p (aromatic) N donor orbital and V(d_{xy}). Right: perpendicular orientation leads to ineffective ligand-to-metal interaction due to competition with the strong π -donating axial oxo group. For the definition of the dihedral angle θ , see centre. See ref. 20.

A square pyramidal vanadyl complex ideally has local C_{4v} symmetry (d_{xy} ground state) and thus represents an axial system. Distortions reduce this symmetry to C_{2v} , giving rise to a rhombic system and thus further splitting of $A_{\perp} (\rightarrow A_x \text{ and } A_y)$, correlated with a lifting of the degeneracy of the e level (Figure 3.12). The difference between A_{xx} and A_{yy} reflects the extent of the distortion. The effect has been noted for, *inter alia*, oxovanadium complexes with α -hydroxycarboxylic acids H₂L of composition [VOL₂]²⁻, where $|A_{xx} - A_{yy}|$ ranges between 8.0×10^{-4} (L = glycolate) and $12.2 \times 10^{-4} \text{ cm}^{-1}$ (L = benzilate).^[21] The distortion can finally end up in a trigonal bipyramidal complex (C_{3v} symmetry), with a doubly degenerate ground state (d_{xz}, d_{yz}). In general, the additivity relation for the parallel component of A still holds despite these distortions, but the experimental $A_{||}$ (or A_z) are somewhat smaller than the calculated values.

This situation changes as octahedral complexes are distorted towards a trigonal prism (left part of Figure 3.12), typically observed in six-coordinated non-oxo vanadium(IV) complexes (**IIIa'** in Figure 2.21).^[22,23] This change in the arrangement of the ligand

**Figure 3.12**

Orbital correlation diagram for the transformation of a square pyramid to a trigonal bipyramidal ($C_{4v} \rightarrow C_{2v} \rightarrow D_{3h}$) and an octahedron to a trigonal prismatic ($D_{3h} \leftarrow C_{4v}$) under idealised local symmetries. Spin-orbit coupling has been neglected.

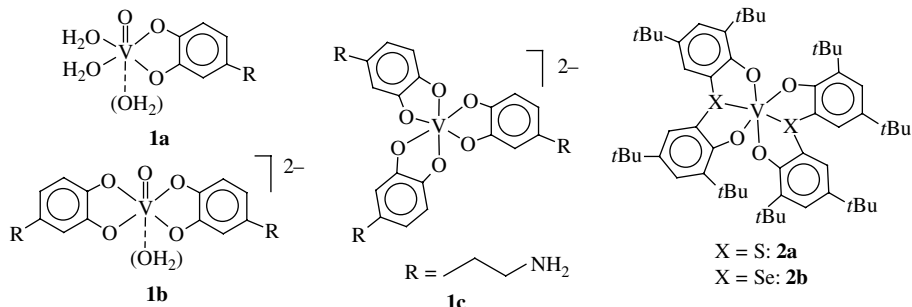
array is connected with a change in the ground state from d_{xy} in ‘normal’ oxovanadium complexes to $d(z^2)$ in a typical non-oxo trigonal prismatic vanadium complex such as **1c** and **2** in Figure 3.13, leading to dramatic consequences for the g and A parameters (for concrete examples, see Table 3.4):

oxovanadium (tetragonal; idealised C_{4v}):

$$\begin{aligned} \text{all } g \text{ values } < 2; g_{||}(g_z) &< g_{\perp}(g_x \approx g_y) \\ A_{||}(A_z) &>> A_{\perp}(A_x \approx A_y) \end{aligned}$$

non-oxo vanadium (trigonal prismatic; idealised D_{3h}):

$$\begin{aligned} g_{||}(g_z) &> g_{\perp}(g_x \approx g_y); g_z \approx 2 \\ A_{||}(A_z) &<< A_{\perp}(A_x, A_y) \end{aligned}$$

**Figure 3.13**

Oxovanadium (**1a**, **1b**) and non-oxo vanadium complexes (**1c**, **2a** and **2b**), for which EPR parameters are reported in Table 3.4. The ligand in the complexes **1a–c** is dopamine. The complexes **2** have been structurally characterised; the formulae for the complexes **1** are suggested structures.

Table 3.4 Selection of EPR parameters of oxo and non-oxo vanadium(IV) complexes. H_2L is dopamine, H_2L' and H_2L'' are monothio- and -selenocatechols, respectively; see Figure 3.13 for structures. Data from refs 22^a and 23. A values in units of 10^{-4} cm^{-1} .

Complex	$g_{ }(g_z)$	$g_{\perp}(g_x/g_y)$	$A_{ }(A_z)$	$A_{\perp}(A_x/A_y)$
VO(L) 1a	1.943	1.985	169	69
[VO(L) ₂] ²⁻ 1b	1.953	1.995	155	57
[V(L) ₃] ²⁻ 1c	~2	1.943	— ^b	109
VL' ₂ 2a	1.991	1.961/1.957	13.1	50.0/129.3
VL'' ₂ 2b	1.982	1.958/1.982	19.3	49.7/128.5

^aReassigned.

^bToo small for detection.

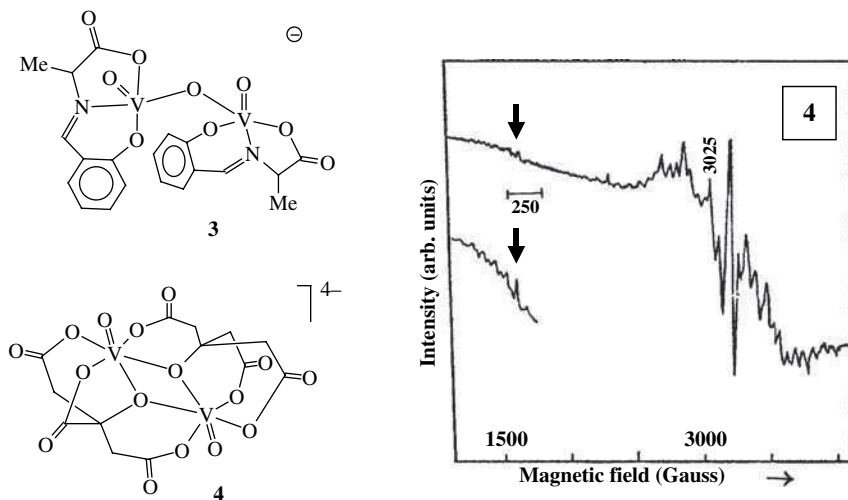
An interesting case also from the EPR spectroscopic point of view is dinuclear vanadium complexes containing one or two V^{IV} centres (for data see Table 3.5). In the mixed valence case, i.e. V^V/V^{IV}($S = 1/2$), two limiting situations can be encountered, viz. (i) valence localisation and (ii) rapid exchange of the electron between the two vanadium sites. Valence localisation gives rise to spectra of the same appearance as in mononuclear complexes, i.e. an eight-line pattern (for each of the spectral components, parallel and perpendicular) is observed. Complex **42** in Figure 2.32 and **3** in Figure 3.14 are examples. The localisation is a result of the *syn*-angular (**42** in Figure 2.32) and almost orthogonal conformation (**3** in Figure 3.14) of the (VO)₂ μ -O core. The localised state of **3** is only observed in the solid state and in frozen solutions. Solutions of **3** at room temperature exhibit a 15-line pattern, indicating that the electron is coupled to both vanadium nuclei.^[24] This situation is realised for the dinuclear mixed-valence complex **41** (Figure 2.32) already at low temperatures. In **41**, the (VO)₂ μ -O core is in the *anti*-linear conformation: The almost linear V–O–V arrangement allows for facile exchange of the electron between the two vanadium centres.

Table 3.5 EPR parameters for dinuclear vanadium complexes. A values in units of 10^{-4} cm^{-1} .

Complex	Comments	$g_{ }(g_z)$	$g_{\perp}(g_x, g_y)$	$A_{ }(A_z)$	$A_{\perp}(A_x, A_y)$
41 (Figure 2.32)	V ^{IV} /V ^V , 77 K, 15 lines	1.949	1.978	168	60.8
3 (Figure 3.14)	V ^{IV} /V ^V , 77 K, 8 lines	1.95	1.98	180	67
4 (Figure 3.14)	V ^{IV} /V ^{IV} , 77 K, 15 lines	1.95 ^a	1.98	83	25

^aIn addition, there is a half-field signal at $g \approx 4$; cf. Figure 3.14.

In the dinuclear citrato complex **4** in Figure 3.14, both vanadium centres – in the *anti*-coplanar conformation – are in the +IV state. There is only marginal ferromagnetic spin coupling; the coupling constant amounts to 0.065 cm^{-1} . The overall spin state is $S = 1$, giving rise to a 15-line pattern with unusually low coupling constants (Table 3.5). Interestingly, the ‘forbidden’ electronic transition corresponding to $\Delta m_s = \pm 1$ is also observed at half-field, i.e. a g factor of ca 4.^[25] The complete spectrum is shown in Figure 3.14.

**Figure 3.14**

A dinuclear V^{IV}V^V complex (**3**, $S = \frac{1}{2}$; localised spin state in the solid state and in frozen solution) and V^{IV}V^{IV} complex (**4**, $S = 1$). For complex **4**, the EPR spectrum is shown. The spectrum, composed of 15 overlapping lines for both the parallel and perpendicular components, is centred at ca 3200 G. The forbidden half-field signal at ca 1600 G (arrow) is also present. Reproduced from S. Mondal *et al.*, *Inorg. Chem.* **36**, 59–63, Copyright (1997), with permission from the American Chemical Society.

3.3.3 Other Paramagnetic Centres

Ligands such as catechols/*o*-quinones can redox interact with vanadium to form semiquinone intermediates, a reaction of interest in the context of the possible interaction of vanadate(V) with tunichromes in ascidians (Scheme 4.1 in Section 4.1). Under certain conditions, the semiquinone can be stabilised by complexation. Complex **5** in Figure 3.15 is an example, where vanadium(V) is coordinated to two catecholate(2-) and one semiquinone(1-) ligands. The single electron is localised; the *g* value of 2.004 is characteristic of an organic radical. The EPR spectrum, a 10-line pattern, reveals coupling to one proton ($A^H = 4.2 \times 10^{-4} \text{ cm}^{-1}$) and the ⁵¹V nucleus ($A^V = 2.1 \times 10^{-4} \text{ cm}^{-1}$), represented by a 10-line pattern.^[26] In the light of the role of vanadium in the production and conversion of the oxygen species O₂, O₂⁻ and O₂²⁻, the formation of the superoxo complex **6b** from the peroxy complex **6a** (Figure 3.15) is of great interest. The superoxo complex **6b** is generated electrochemically in acetonitrile at -30 °C by one-electron reduction of the peroxy ligand.^[27] The single electron is confined to a superoxo-associated molecular orbital. Coupling with the ⁵¹V nucleus leads to a distinct eight-line pattern with $A^V = 2.50 \times 10^{-4} \text{ cm}^{-1}$, centred at $g = 2.0119$. Warming to room temperature yields the oxovanadium(IV) complex **6c** and molecular oxygen, i.e. V^V is reduced by the superoxo ligand. Complex **6c** provides an EPR spectrum typical of oxovanadium complexes: $g_{\parallel} = 1.952$, $g_{\perp} = 1.986$; $A_{\parallel} = 161.3 \times 10^{-4}$, $A_{\perp} = 58.8 \times 10^{-4} \text{ cm}^{-1}$. The starting peroxy complex **6a** can be recovered by reacting **6c** with oxygen in acetonitrile-tetrahydrofuran, a two-electron reduction of oxygen, where one electron is delivered by V^{IV} and the second one by tetrahydrofuran.

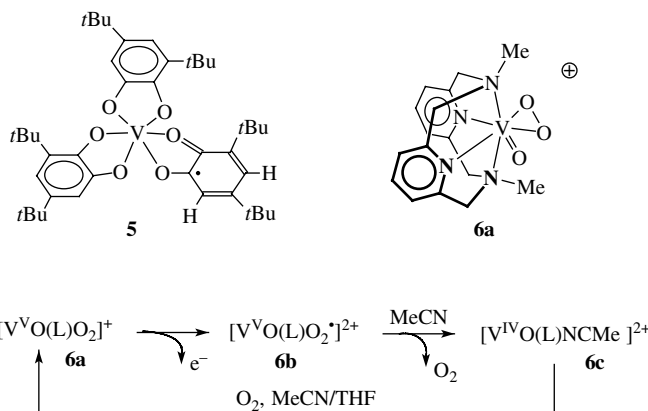


Figure 3.15

Two complexes with paramagnetic centres in the ligand system. The electron of the semiquinone radical (complex **5**, proposed structure) couples with a proton and vanadium,^[26] and the electron on the superoxo ligand (**6b**) with vanadium. The disposition of **6b** is based on the structurally characterised complex **6a**.^[27]

3.4 ESEEM and ENDOR Spectroscopies

Relaxation times in EPR are on the nanosecond scale and thus at least three orders of magnitude shorter than in NMR. Consequently, lines are considerably broader; typically, linewidths are around 1 mT. This precludes, in most cases, resolution of couplings of the unpaired electron on vanadium to nuclei in the ligand sphere, quantified by the superhyperfine coupling constant A^L (L for ligand). A^L of ligands directly connected to vanadium are typically around 1 MHz for ^1H (in, e.g., water ligands) and 5–7 MHz for ^{14}N coupling, but vary with the nature and orientation of the ligand. ESEEM and ENDOR are variants in EPR spectroscopy which can provide the superhyperfine coupling information.^[28]

ESEEM, short for electron spin echo envelope modulation, is a *pulsed* EPR technique. The simplest (and more commonly applied) technique is a two-pulse sequence: the sample, in a magnetic field set at a specific component of the EPR spectrum so as to permit resonance, is first subjected to a short and intense $90^\circ(\pi/2)$ pulse, upon which the electron spin magnetisation is flipped from the z orientation into the xy plane. After a delay time τ , a second, $180^\circ(\pi)$ pulse is applied, causing the spins to refocus and to emit, after a time interval of 2τ counted from the first pulse, a transient signal, called the spin echo. The situation is depicted in Figure 3.16 (left). The amplitude of the echo is measured as a function of τ . If there is no additional interaction, the amplitude of the echo decays exponentially. If, however, the electron is coupled to ligand nuclei with a spin $I > 0$, this exponential decay is superimposed, or modulated, by a *cosine* function for each of the nuclear interactions. Fourier transformation of the decay converts the spectrum from the time domain into the more familiar frequency domain. An example is displayed in Figure 3.16 (right). The spectrum, of vanadyl-bound vanabin, a vanadium-binding protein isolated from ascidians (Section 4.1), shows spin echoes produced by coupling of the electron to the amine group of lysine side-chains, $A^N = 4.5$ MHz.^[29] Superhyperfine coupling constants due to coupling to imidazole-N are around 7 MHz.

Other pulse sequences are in use such as the three-pulse sequence (Figure 3.16) and hyperfine sublevel correlation (HYSCORE) spectroscopy, the latter being a two-dimensional technique.^[17,30]

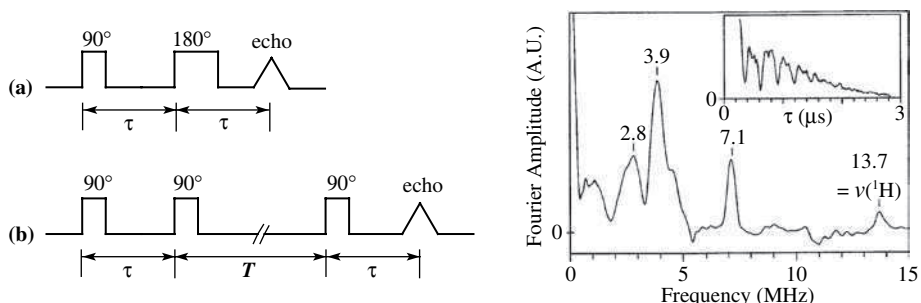


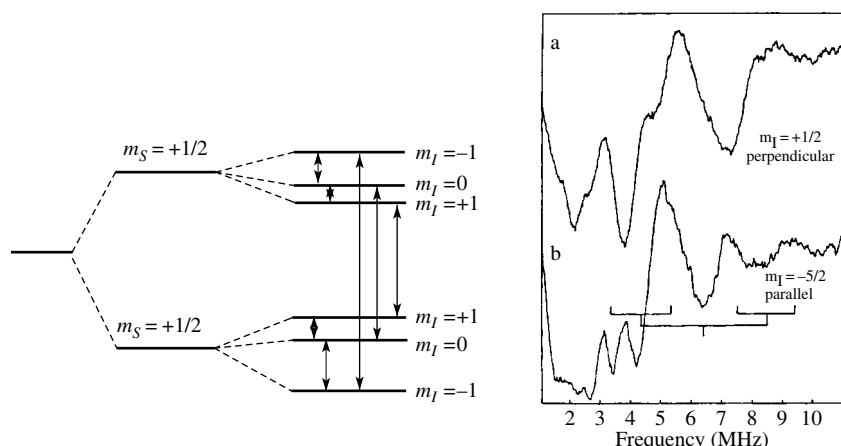
Figure 3.16

Left: two-pulse [(a) primary ESEEM] and three-pulse [(b) stimulated echo ESEEM] sequences; τ is the (fixed) delay time between pulses one and two and T is a variable delay time. Right: frequency domain and time domain (inset) of the two-pulse ESEEM spectrum of VO^{2+} – vanabin, recorded at the $m_I = -1/2$ line, at 77 K and a pulse width of 20 ns.^[29] The superhyperfine coupling constant $A^N = 4.5$ MHz (obtained from the ^{14}N double-quantum lines at 3.9 and 7.1 MHz) is in accord with amine nitrogen provided by lysines of the vanadium-binding protein. The spin echo due to proton coupling, at 13.7 MHz, was also observed. Reproduced from K. Fukui *et al.*, *J. Am. Chem. Soc.* 125, 6352–6353. Copyright (2003), with permission from the American Chemical Society.

'ENDOR is a powerful tool for the study of complexes containing paramagnetic ions such as VO^{2+} , primarily because inhomogeneous line broadening in conventional EPR spectra often hides hyperfine splittings that arise from ligand nuclei. ENDOR can sometimes recapture this lost resolution.'^[17] ENDOR is a double-resonance technique combining EPR and NMR, i.e. nuclear (NMR) transitions are observed by detecting an EPR signal. In an ENDOR experiment, the magnetic field is set to one of the components of the EPR spectrum, and a microwave power is applied which allows for partial saturation of the EPR transition. Subsequently, keeping the magnetic field constant, a suitable radiofrequency for the nucleus to be investigated (usually ^1H , ^{14}N or ^{31}P in the ligand sphere of the vanadium compound) is applied and swept over the range of probable resonances. In the case of resonance, a relaxation path is provided to the electron coupled to the nucleus, and the EPR signal regains intensity by relief of the saturation, which constitutes an ENDOR signal in the spectrum.

If the nucleus under investigation is a quadrupolar nucleus, such as ^{14}N with a nuclear spin of $I = 1$, quadrupolar disturbance of the nuclear hyperfine levels m_I leads to an asymmetric splitting of these levels and thus, with the selection rule for NMR transitions ($m_I = \pm 1$), to four ENDOR resonances, as depicted in the energy diagram in Figure 3.17 (left) and the ^{14}N ENDOR spectrum of vanadyl-substituted D-xylose isomerase^[31] in Figure 3.17 (right). The ENDOR frequency ν_{ENDOR} is related to the NMR frequency of the ligand nucleus ν_L and the superhyperfine coupling constant A^L by Equation (3.9). The quantity C_Q is the nuclear quadrupole coupling constant (Section 3.1.3). The C_Q term vanishes for spin- $1/2$ nuclei. The spectral pattern in Figure 3.17, the $A^N = 13.2$ MHz and the $C_Q = 0.72$ MHz obtained from the ENDOR spectrum set at the parallel $m_I = 5/2$ EPR line strongly suggest histidine binding to the vanadyl ion.

$$\nu_{\text{ENDOR}} = |\nu_L \pm A^L/2 \pm 3C_Q/2| \quad (3.9)$$

**Figure 3.17**

Left: energy splitting diagram for an $S = 1/2$ system. The electronic Zeeman interaction provides the electronic levels $m_S = \pm 1/2$. Nuclear Zeeman interaction plus quadrupole perturbation (by a nucleus of spin $I = 1$) gives rise to the m_I levels as indicated. The transitions (arrows) are determined by the selection rules, i.e. $\Delta m_I = 0$ for EPR, and $\Delta m_I = 1$ for ENDOR (bold arrows). Right: ^{14}N ENDOR spectrum of VO^{2+} -substituted D-xylose isomerase (site B), with the magnetic field set at the perpendicular $m_I = +1/2$ (a) and the parallel $m_I = -5/2$ EPR line (b).^[31] Reproduced from R. Bogumil *et al.*, *Eur. J. Biochem.* 196, 305–312. Copyright (1991), with permission of the Federation of the European Biochemical Societies (FEBS).

A comparatively recent new development in ENDOR spectroscopy is electron spin echo ENDOR (ESE-ENDOR), where nuclear spin transitions are detected by their effect on a transient EPR signal (the spin echo) generated by a two- or three-pulse excitation.^[32]

3.5 Optical Spectroscopies

3.5.1 UV-Vis

Electronic absorption spectra from the near-infrared (NIR) to the visible region (Vis) and ultraviolet region (UV) may result from intra-metal d-d transitions (parity forbidden), metal-to-ligand charge transfer (MLCT), ligand-to-metal charge transfer (LMCT), intra-ligand transitions and, in complexes containing more than one vanadium centre with the vanadium centres in different oxidation states, inter-valence charge transfer (IVCT). The more intriguing information on the electronic situation of the metal comes from the d-d transitions. Extinction coefficients ε for the ‘allowed’ LMCT, MLCT and IVCT transitions commonly are several thousand $1\text{ mol}^{-1}\text{ cm}^{-1}$, whereas the ‘forbidden’ d-d transitions give rise to ε values approximately in the range $20\text{--}200\text{ }1\text{ mol}^{-1}\text{ cm}^{-1}$.

Vanadium(V), which does not contain d electrons, obviously is restricted to intra-ligand and LMCT absorptions. Simple V^{V} compounds such as vanadate are colourless, because the LMCT bands lie in the UV region. Decavanadate, and also vanadate-dependent haloperoxidases (which contain vanadate additionally coordinated to a side-chain imidazole of the protein matrix), are yellow, because the LMCT tails from the UV into the violet range. More complex vanadium(V) complexes can be very colourful when the LMCT

shifts into the visible region. Examples are hydroxamate complexes, which can be used to for the colorimetric quantitative determination of vanadium(V), and other complexes with noninnocent ligands, such as catecholato–vanadium complexes with low-energy ligand-to-metal transitions.^[4]

Particularly clearly laid out is the situation in vanadium(IV), i.e. d¹ complexes, normally containing the VO²⁺ centre. Under ideal conditions, the complex has C_{4v} symmetry. An example is the vanadyl species present in sufficiently acidic solutions, [VO(H₂O)₅]²⁺. The orbital splitting has already been dealt with in Section 3.3.2 (Figure 3.12): the energetically most stable orbital, accommodating the electron, is d(xy) of symmetry b₂. The electron can be exited into the doubly degenerate e level (d_{xz}, d_{yz}), the a₁ [d(x² - y²)] or the b₁ [d(z²)] level, consequently giving rise to three bands. Under more realistic conditions, distortion occurs, and the degeneracy of the e level is lifted. Consequently, the lowest energy band splits into two components. The situation is shown below for C_{4v} and C_{2v} symmetries together with the approximate positions of the absorption bands in nanometers; see Figure 3.12 for the energy level diagrams.

C _{4v}	C _{2v}	
b ₂ → e d(xy) → d(xz, yz)	900–620 a ₂ → b ₁ d(xy) → d(xz)	band IA
	a ₂ → b ₂ d(xy) → d(yz)	band IB
b ₂ → a ₁ d(xy) → d(x ² - y ²)	690–530 a ₂ → a ₁ d(xy) → d(x ² - y ²)	band II
b ₂ → b ₁ d(xy) → d(z ²)	480–330 a ₂ → a ₁ d(xy) → d(z ²)	band III

Bands IA and IB are often unresolved and appear as one broad band. Band III is, in many cases, covered by the intense charge-transfer (CT) bands, or appears just as a shoulder on the low-energy side of the CT band. This is particularly so if there is sizable π interaction between vanadium and its ligand system. A characteristic spectrum showing all of the four bands is presented in Figure 3.18 for the 1:2 complex formed between the vanadyl ion and quinic acid at pH 7.9.^[21]

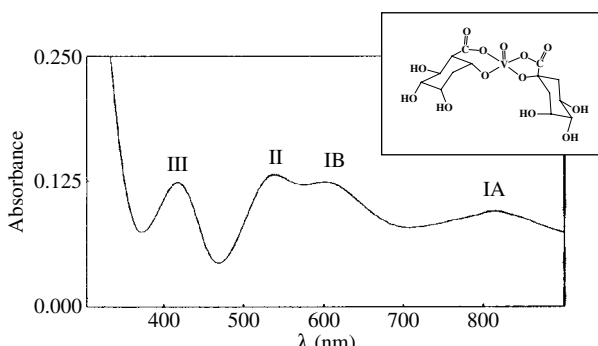


Figure 3.18
Electronic absorption spectrum of the VO²⁺-D-quinate system at pH 7.9, a ligand-to-metal ratio of 10:1, and an absolute vanadium concentration of 4 mM. The structure shown in the inset is based on EPR evidence.^[21] For the assignment of the bands, see the text. The appearance of a split band I is a consequence of trigonal distortions, which also are reflected in the EPR data. Reproduced from E. Garribba *et al.*, Inorg. Chem. 42, 3981–3987. Copyright (2003), with permission from the American Chemical Society.

The d^2 configuration in vanadium(III) complexes makes things more complicated due to inter-electronic repulsion. Considering again an ideal case, O_h symmetry (approximately realised in $[V(H_2O)_6]^{3+}$), the ground state is $(t_{2g})^2 = {}^3T_{1g}$. Exited states for allowed electronic transitions (only triplet-triplet transitions are allowed) can be $(t_{2g})^1(e_g)^1 = {}^3T_{1g}$ and ${}^3T_{2g}$, and $(e_g)^2 = {}^3A_{2g}$, and hence there are three transitions which occur, for $[V(H_2O)_6]^{3+}$, at 580, 391 and 263 nm (17 200, 25 600 and 38 000 cm^{-1}). The UV–Vis spectra of lower symmetry V^{III} complexes are sufficiently less concise and the spectra are accordingly of restricted significance for structure elucidation.

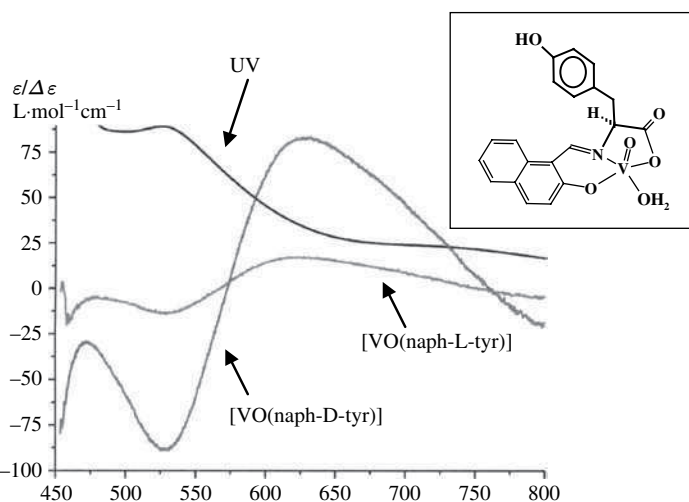
3.5.2 Circular Dichroism

Circular dichroism (CD) occurs in a UV–Vis spectrum if there is a chiral element, commonly a centre of chirality, in the compound. The centre of chirality may be represented by the coordination centre, i.e. the metal itself, or by a chiral ligand. Chiral compounds rotate the plane of linearly polarised light passing through the compound. Linearly polarised light can be treated as being composed of two (enantiomorphous) circularly polarised components of equal amplitude and phase, a left and a right circularly polarised wave, the electric vector of which rotates uniformly around the direction of propagation. The two components propagate at a different pace through the chiral medium (they have different refractive indices), resulting in a rotation of the plane of polarisation by an angle α . This phenomenon is termed optical rotary dispersion (ORD). In addition, the two components have different absorption coefficients ε in the absorption range. After passage through the optically active medium, the two vectors of the oppositely circularly polarised waves have different norms as a consequence of the differing extents of absorption. Their superposition hence does not re-provide linearly polarised light, but elliptically polarised light instead. The difference between the molar absorption coefficients for left and right circularly polarised light, $\Delta\varepsilon = \varepsilon_L - \varepsilon_R$, is called circular dichroism (CD). $\Delta\varepsilon$ can be calculated from the ellipticity. CD and ORD together are known as the Cotton⁴ effect. The CD effect can only be observed within the absorption band. In CD spectra, $\Delta\varepsilon$ is plotted as a function of the wavelength λ in nanometres; the maxima occurring in CD curves can be positive or negative.

CD can be a versatile tool in speciation analyses of aqueous solutions containing vanadate or VO^{2+} and chiral ligands,^[33] and for assigning a chiral compound the correct configuration. Figure 3.19 illustrates the latter situation for the optical antipodes of the complex $[\text{VO}(\text{naph-tyr})]$, where naph-tyr is the Schiff base formed from *o*-hydroxynaphthaldehyde and tyrosine.^[34]

Paramagnetic molecules (such as those containing the VO^{2+} unit) which are not optically active, when placed in a magnetic field perpendicular to the direction of propagation of polarised light, also show CD, termed magnetic circular dichroism (MCD), in this case. The origin of MCD lies in the Zeeman splitting of degenerate energy levels and the mixing of their electronic states by a magnetic field. The background theory and selected applications for vanadyl complexes pointing out the suitability of MCD for, *inter alia*, correct assignments of the electronic states from which electronic transitions occur, have been surveyed.^[35] The method is not commonly employed in vanadium chemistry.

⁴ Aimé Cotton, 1895.

**Figure 3.19**

UV (with band I at 712 nm and band II at 529 nm) and CD spectra of $[VO(\text{naph-tyr})]$ (inset; the L-isomer is shown). The scale for $\Delta\varepsilon$ is expanded 200-fold with respect to that for ε . Reproduced from M. Ebel and D. Rehder, *Inorg. Chem.* 45, 7083–7090. Copyright (2006), with permission from the American Chemical Society.

3.6 X-ray Absorption Spectroscopy

3.6.1 Background and General

With the availability of intense X-ray synchrotron radiation in the mid-1970s, X-ray absorption spectroscopy (XAS) emerged as an increasingly powerful tool for the elucidation of structural features of fine crystalline powders and amorphous samples, and thus as a complementary method to single-crystal (and powder) X-ray diffraction (XRD). By choosing atom-specific energy windows from the synchrotron radiation, selective excitation of a specific element in a complex compound is achieved, providing detailed information on its electronic structure and its environment. In a metalloprotein, e.g. vanadium nitrogenase and vanadate-dependent bromoperoxidase, the target element of choice is the vanadium centre and/or a characteristic binding site such as sulfide (in nitrogenase) and/or a substrate, such as bromide (in bromoperoxidase). Energy calibration is necessary and, in the case of vanadium XAS, this is usually done by referencing against a vanadium metal foil with the first inflection point set to 5465 eV.^[36]

Depending on the region under investigation, one distinguishes between X-ray absorption near-edge structure (XANES), also termed near-edge X-ray absorption fine structure (NEXAFS), and extended X-ray absorption spectroscopy (EXAFS). As implied by these terms, XANES addresses the region near to and associated with the absorption edge, whereas EXAFS refers to the extended (higher energy) part (Figure 3.20, top). The ‘edge’ commonly looked at in vanadium XAS is the K-edge, i.e. that part of the spectrum where an electron is exited from the K shell (the 1s orbital). In presenting data, it is common to quote the point of inflection of the K-edge and/or its maximum, assigned the dipole-allowed $1s \rightarrow 4p$ transition. Absorption features may additionally arise from valence p states and multiple scattering. In many cases, there is also present

a pre-edge⁵ (i.e. lower energy) feature, associated with the $1s \rightarrow 3d$ promotion. This extra feature is not found in ideally octahedral complexes, because the respective transition is parity forbidden (both states, s and d, are *gerade*). An example is vanadium(II)oxide (Table 3.6). As the symmetry is lowered from O_h , the inversion centre is broken; 3d–4p mixing occurs and the transition becomes partially allowed. The pre-edge peak is also commonly absent or has very low intensity in non-oxo vanadium complexes. Examples are $[V(ONO)Br_2]$ in Table 3.6 and amavadin and its model compounds (Figure 4.10). Amavadin is a naturally occurring, eight-coordinated non-oxo vanadium complex with carboxylate and hydroxamate coordination, present in *Amanita* mushrooms.

Information available from the energy position of the edge and the pre-edge encompass the formal oxidation state z of the metal, the ‘ionicity’ i (representing the difference in electronegativities of the metal and its ligand set) and the coordination number n . These quantities define the ‘coordination charge’ η as given by Equation (3.10).^[36,37] In Table 3.6, examples are collated which exemplify these influences on the position of the pre-edge and the edge: Increasing energy of the pre- and the K-edge with increasing

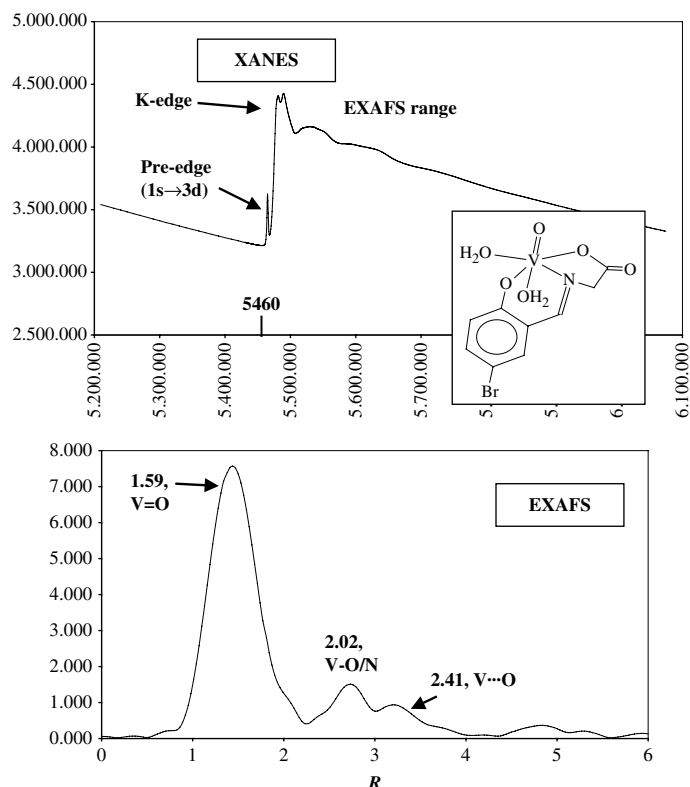


Figure 3.20

Top: XAS spectrum of the vanadium(IV) complex shown in the inset. Bottom: Fourier transform EXAFS spectrum of the same complex. R is the distance in Å. The spectrum shows three peaks, assigned as indicated. The $V \cdots Br$ distance has not been detected.

⁵ Also termed ‘white band’ or ‘white line’ in the older literature.

Table 3.6 XANES data on selected vanadium compounds. Energy positions are given in eV relative to vanadium metal foil (pre-edge = 5465.0 eV).

Entry no.	Compound (oxidation state of V, coordination environment) ^a	Pre-edge (1s → 3d)	K-edge (point of inflection)	K-edge (1s → 4p)	Ref.
1	VO (V ^{II} , 8O)	—	8	20.4	36
1	V ₂ O ₃ (V ^{III} , 6O)	3.4	10.7	23.5	36
1	V ₂ O ₄ (V ^{IV} , 6O)	4.5	14	26.2	36
1	V ₂ O ₅ (V ^V , 5O)	5.6	15.1	30.1	36
2	[V(nta) ₂] ³⁻ (V ^{III} , 2N + 4O)	3.9 ^b			37
2	[VO(nta)(H ₂ O)] ²⁻ (V ^{IV} , 1N + 5O)	4.7			37
2	[V ₂ O ₃ (nta) ₂] ³⁻ (V ^{IV,V} , 1N + 5O)	5.2			37
3	Native bromoperoxidase (V ^V , 1N + 4O)	4.0	8.0		39
3	Reduced bromoperoxidase (V ^{IV} , 2N + 4O)	3.1	5.7		39
4	[VO(OH)(dtc) ₂](V ^V , 2O + 4S)	4.68			38
4	[VO(OEt)(mal) ₂](V ^V , 6O)	5.88			38
5	[V(ONO)Br ₂](V ^{IV} , 1N + 2O + 2Br)	—	12.52		40
5	[VO(ONO)(H ₂ O)](V ^{IV} , 1N + 5O)	4.41	14.73		40

^a Abbreviations for ligands: nta = nitrilotriacetate; dtc = dithiocarbamate; mal = maltolate, *ONO* = a tridentate, carboxylate- and phenolate-terminated Schiff base.

^b Very low intensity.

oxidation number of vanadium is reflected by entries 1, 2 and 3, and entries 4 and 5 demonstrate an increase in energy with increasing ionicity (electronegativity of the ligand set). In addition to its energy position, the pre-edge feature provides information on the coordination geometry of a vanadium complex: Since the 3d set is split depending on the symmetry of the complex, the pre-edge peak is a composite of several overlapping components.^[38]

$$\eta = z - (1 - i)n \quad (3.10)$$

The EXAFS region contains information on the interactions of the electron, removed by ionisation, with the electron shells of surrounding atoms. If this electron is taken as an electron wave, this interaction can be described in terms of a reflection of the wave by the electron shells of neighbouring atoms (the ‘scatterers’). Oncoming and reflected waves interfere, and the patterns of interference are analysed. From the analysis, information on distances *R* (e.g. bond lengths) can be extracted to a high accuracy, almost matching that of XRD. The mean square variation in *R* is represented by the Debye–Waller factor σ^2 , a quality factor for the accuracy of the determined bond length. Spectra are collected in the *k* space and Fourier transformed for convenience, yielding a radial distribution function of the atomic arrangement, i.e. the information is provided in an intensity–*R* diagram as depicted in Figure 3.20 (bottom), providing, in principle, a specific peak for each shell which, in practice, often overlap.⁶ Indirectly, information on the nature of the (nearest) neighbours is thus also available – with similar restrictions as in XRD. Further information is the *number* of nearest neighbours, i.e. the coordination number, but with lower

⁶ Often, the *R* values in these Fourier-transformed presentations are ‘apparent *R* values’, which have to be corrected (by addition of ca 0.1–0.2 Å, depending on the actual size of *R*) to arrive at the ‘real’ *R* values.

accuracy than in XRD. Coordination numbers usually are determined, with an uncertainty of ± 1 , from the amplitudes of the EXAFS peaks. By combining the EXAFS information on coordination number and distances with the XANES information on the intensity and substructure of the pre-edge feature, indirect information on the coordination geometry is also available.

Some theoretical aspects and experimental details on XAS of vanadium compounds have been reviewed.^[41]

L-edge X-ray absorption can provide information in addition to that obtained from K-edge spectra. The energy by which electrons are exited from the L shell into the valence-3d level and further into the continuum is by an order of magnitude less than in K-edge XAS. Figure 3.21 exemplifies the situation for two low-valent (+II and +III), octahedral vanadium compounds containing a tetradeятate neutral N_2S_2 and two bromo ligands. Due to spin-orbit coupling, the p level of the L shell is split, giving rise to two bands, viz. $\text{L}_3(2\text{p}_{3/2} \rightarrow 3\text{d})$ at low energy and $\text{L}_2(2\text{p}_{1/2} \rightarrow 3\text{d})$ at high energy. Figure 3.21 reveals (i) the low-energy shift for the V^{II} (d^3) as compared with the V^{III} (d^2) complex and (ii) extensive fine structure of both peaks in the L features of the V^{II} complex.

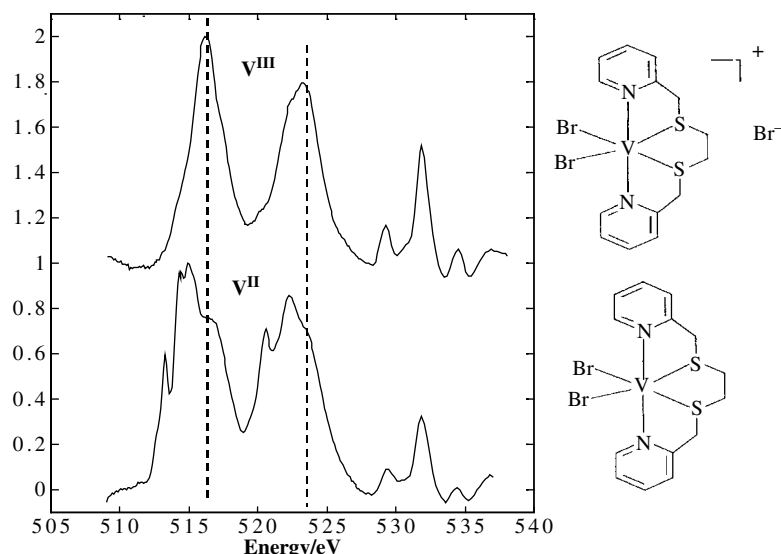


Figure 3.21
L-edge XAS features of two vanadium complexes with identical coordination environment but different oxidation number (+III and +II), showing L_3 (left) and L_2 (centre). The weak bands to the right correspond to the excitation of oxygen (H. Nekola, Ph.D. thesis, Hamburg 2001; communicated by T. Funk and S. P. Cramer, Stanford Synchr. Rad. Lab., CA).

3.6.2 Biological Applications

Applications to specific biological systems containing vanadium will be addressed in some detail in the context of the respective subsections of Chapter 4 on naturally occurring vanadium compounds: vanadium in sea squirts (e.g. Figure 4.3), vanadate-dependent haloperoxidases (e.g. Table 4.5) and vanadium nitrogenases (e.g. Table 4.8). The central messages, including key references, are briefly summarised here.

In the case of the sea squirts (ascidians), vanadium XAS^[42] plus sulfur XAS studies^[43] have revealed the nature of vanadium present in the highly acidic medium of the vanadium-containing blood cells, the vanadocytes. Vanadium is in oxidation state +III and in a coordination environment exclusively consisting of (or dominated by) oxygen donors; the most likely composition of the predominant species present is $[V(H_2O)_5(HSO_4)]^{2+}$.

XAS of vanadium nitrogenase isolated from the bacterium *Azotobacter* has been particularly useful, since it provides sweeping evidence for the very close relationship of this ‘alternative’ nitrogenase with the structurally characterised molybdenum pendant.^[39] The relation extends to the number and nature of (distances to) the donor atoms directly bonded to vanadium/molybdenum, and the iron–iron distances of the cofactor cage, indicating an identical topology which has been successfully modelled by hetero-cubane clusters of the general composition $[VL_3Fe_4S_4]^q$.

The V XAS investigations of vanadium nitrogenase additionally exemplify the inconspicuous pre-edge feature typical of non-oxo vanadium complexes (i.e. vanadium complexes lacking the apical V=O moiety) otherwise characteristic of amavadin from *Amanita* mushrooms. The oxidation state +IV for vanadium in amavadin and the lack of an (originally postulated) oxo group had clearly been backed up by XANES and EXAFS^[44] of this interesting molecular compound long before direct structure evidence from diffraction data became available.

XAS of the native and reduced vanadate-dependent bromoperoxidase from the marine alga *Ascophyllum nodosum* clearly showed that the coordination environment of vanadium drastically changes on reduction (see also entry 3 in Table 3.6), providing an explanation for the inactivity of the reduced enzyme.^[39] General features for the native (V^V) enzyme are consistent with the vanadate–His centre in the active site later found by XRD. In particular, pH and the addition of the substrate bromide did not influence the XAS parameters, whereas H_2O_2 changed the absorption features, indicative of its direct coordination to vanadium.^[45] Vanadium^[40] and bromine XAS^[46] studies of the peroxidase plus its substrate bromide indicate the presence of Br^- at a non-bonding distance of ca 4 Å from vanadium, and a bonding distance of 1.88 Å corresponding to bromine binding to a light scatterer, presumably C(sp³).

References

- [1] D. Rehder, T. Polenova, M. Bühl, *Annu. Rep. NMR Spectrosc.* **2007**, *62*, 49–114.
- [2] (a) W. Priebsch and D. Rehder, *Inorg. Chem.* **1985**, *24*, 3058–3062; (b) D. Rehder, C. Weidemann, A. Duch and W. Priebsch, *Inorg. Chem.* **1988**, *27*, 584–587.
- [3] W. Priebsch and D. Rehder, *Inorg. Chem.* **1990**, *29*, 3013–3019.
- [4] C. R. Cornman, G. J. Colpas, J. D. Hoeschele, J. Kampf and V. L. Pecoraio, *J. Am. Chem. Soc.* **1992**, *114*, 9925–9933.
- [5] J. Lenhardt, B. Baruah, D. C. Crans and M. D. Johnson, *Chem. Commun.* **2006**, 4641–4643.
- [6] D. C. Crans, C. D. Rithmer and L. A. Theisen, *J. Am. Chem. Soc.* **1990**, *112*, 2901.
- [7] D. Gudat, U. Fischbeck, F. Tabellion, M. Billen and F. Preuss, *Magn. Reson. Chem.* **2002**, *40*, 139–146.
- [8] (a) K. Paulsen and D. Rehder, *Z. Naturforsch., Teil A* **1982**, *37*, 139–149; (b) W. Basler, H. Lechert, K. Paulsen and D. Rehder, *J. Magn. Reson.* **1981**, *45*, 170–172.
- [9] D. C. Crans, R. A. Felty, H. Chen, H. Eckert and N. Das, *Inorg. Chem.* **1994**, *33*, 2427–2438.
- [10] A. S. Tracey and K. Radley, *Can. J. Chem.* **1985**, *63*, 2181–2184.
- [11] J. A. Saponja and H. J. Vogel, *J. Inorg. Biochem.* **1996**, *62*, 253–270.

- [12] H. Schmidt, I. Andersson, D. Rehder and L. Pettersson, *Chem. Eur. J.* **2001**, *7*, 251–257.
- [13] R. M. K. Carlson, *Proc. Natl. Acad. Sci. USA* **1975**, *72*, 2217–2221.
- [14] (a) F. Röhrscheid, R. E. Ernst and R. H. Holm, *Inorg. Chem.* **1967**, *6*, 1607–1613; (b) K. Hiraki, M. Onishi, Y. Nakashima and Y. Obayashi, *Bull. Chem. Soc. Jpn.* **1979**, *52*, 625–626.
- [15] J. Reuben and D. Fiat, *J. Am. Chem. Soc.* **1969**, *91*, 4652–4656.
- [16] N. D. Chasteen, in: *Biological Magnetic Resonance* (L. J. Berliner and J. Reuben, Eds), Vol. 3, Plenum Press, New York, **1981**, pp. 53–119.
- [17] T. S. Smith, II, R. LoBrutto and V. L. Pecoraro, *Coord. Chem. Rev.* **2002**, *228*, 1–18.
- [18] A. J. Tasiopoulos, A. N. Troganis, A. Evangelou, C. P. Raptopoulou, A. Terzis, Y. Deligiannakis and T. A. Kabanos, *Chem. Eur. J.* **1999**, *5*, 910–921.
- [19] E. Garribba, E. Lodyga-Chruscinska, G. Micera, A. Panzanelli and D. Sanna, *Eur. J. Inorg. Chem.* **2005**, 1369–1382.
- [20] T. S. Smith, II, C. A. Root, J. W. Kampf, P. C. Rasmussen and V. L. Pecoraro, *J. Am. Chem. Soc.* **2000**, *122*, 767–775.
- [21] E. Garribba, G. Micera and A. Panzanelli, *Inorg. Chem.* **2003**, *42*, 3981–3987.
- [22] P. Buglyó, A. Dessi, T. Kiss, G. Micera and D. Sanna, *Dalton Trans.* **1993**, 2057–2063.
- [23] T. K. Paine, T. Weyhermüller, L. D. Slep, F. Neese, E. Bill, E. Bothe, K. Wieghardt and P. Chaudhuri, *Inorg. Chem.* **2004**, *43*, 7324–7338.
- [24] S. Mondal, P. Ghosh and A. Chakravorty, *Inorg. Chem.* **1997**, *36*, 59–63.
- [25] M. Velayutham, B. Varghese and S. Subramanian, *Inorg. Chem.* **1998**, *37*, 1336–1340.
- [26] M. E. Cass, D. L. Greene, R. M. Buchanan and C. G. Pierpont, *J. Am. Chem. Soc.* **1983**, *105*, 2680–2686.
- [27] H. Kelm and H.-J. Krüger, *Angew. Chem. Int. Ed.* **2001**, *40*, 2344–2348.
- [28] N. D. Chasteen, *Methods Enzymol.* **1993**, *227*, 232–244.
- [29] K. Fukui, T. Ueki, H. Ohya and H. Michibata, *J. Am. Chem. Soc.* **2003**, *125*, 6352–6353.
- [30] S. S. Eaton and G. R. Eaton, in: *Vanadium in Biological Systems* (D. N. Chasteen, Ed.), Kluwer, Dordrecht, **1990**, Ch. XI.
- [31] R. Bogumil, J. Hüttermann, R. Kappl, R. Stabler, C. Sudfeldt and H. Witzel, *Eur. J. Biochem.* **1991**, *196*, 305–312.
- [32] H. Thomann and M. Bernardo, in: *Biological Magnetic Resonance* (L. J. Berliner and J. Reuben, Eds), Vol.13, Plenum Press, New York **1993**, pp. 275–322.
- [33] (a) H. Bauer, J. Brun, A. R. Hernanto and W. Voelter, *Z. Naturforsch., Teil B* **1989**, *44*, 1464–1472; (b) J. Costa Pessoa, I. Tomaz and R. Henriques, *Inorg. Chim. Acta* **2003**, *356*, 121–132; (c) J. Costa Pessoa, S. Marcão, I. Correira, G. Gonçalves, A. Dörnyei, T. Kiss, T. Jakusch, I. Tomaz, M. M. C. A. Castro, C. F. G. C. Castro and F. Avecilla, *Eur. J. Inorg. Chem.* **2006**, 3595–3606.
- [34] M. Ebel and D. Rehder, *Inorg. Chem.* **2006**, *45*, 7083–7090.
- [35] D. J. Robbins, M. J. Stillman and A. J. Thomson, *J. Chem. Soc., Dalton Trans.* **1974**, 813–820.
- [36] P. Wong, F. W. Lytle, R. P. Messmer and D. H. Maylotte, *Phys. Rev. B* **1984**, *30*, 5596–5610.
- [37] K. H. Hallmeier, R. Szargan, G. Werner, R. Meier and M. A. Sheromov, *Spectrochim. Acta, Part A* **1986**, *42*, 841–844.
- [38] J. M. Arber, E. de Boer, C. D. Garner, S. S. Hasnain and R. Wever, *Biochemistry* **1989**, *28*, 7968–7973.
- [39] C. Weidemann, D. Rehder, U. Kuetgens, J. Hormes and H. Vilter, *Chem. Phys.* **1989**, *136*, 405–412.
- [40] U. Christmann, H. Dau, M. Haumann, E. Kiss, P. Liebisch, D. Rehder, G. Santoni and C. Schulzke, *Dalton Trans.* **2004**, 2534–2540.
- [41] C. D. Garner, D. Collison and F. E. Mabbs, in: *Metal Ions in Biological Systems* (H. Sigel and A. Sigel, Eds), Marcel Dekker, New York, **1995**, Ch. 19.
- [42] P. Frank and K. O. Hodgson, *Inorg. Chem.* **2000**, *39*, 6018–6027.
- [43] P. Frank, B. Hedman and K. O. Hodgson, *Inorg. Chem.* **1999**, *38*, 260–270.

- [44] (a) C. D. Garner, P. Baugh, D. Collison, E. S. Davies, A. Dinsmore, J. A. Joule, E. Pidcock and C. Wilson, *Pure Appl. Chem.* **1997**, *69*, 2205–2212; (b) E. M. Armstrong, A. L. Beddoes, L. J. Calviou, J. M. Charnock, D. Collison, N. Ertok, J. H. Naismith and C. D. Garner, *J. Am. Chem. Soc.* **1993**, *115*, 807–808.
- [45] U. Küsthhardt, B. Hedman, K. O. Hodgson, R. Hahn and H. Vilter, *FEBS Lett.* **1993**, *329*, 5–8.
- [46] (a) H. Dau, J. Dittmer, M. Epple, J. Hanss, E. Kiss, D. Rehder, C. Schulzke and H. Vilter, *FEBS Lett.* **1999**, *457*, 237–240; (b) D. Rehder, C. Schulzke, H. Dau, C. Meinke, J. Hanss and M. Epple, *J. Inorg. Biochem.* **2000**, *80*, 115–121.

4 Naturally Occurring Vanadium Compounds

4.1 Vanadium in Ascidians and Polychaete Worms

4.1.1 Ascidians: History, Speculations and Facts; An Introduction and Overview

In 1911, the German physiologist Martin Henze discovered high levels of vanadium (which he termed ‘chromogen’ because of the variations in colour) in blood cells of the blood from the sea squirt, or ascidian, *Phallusia mamillata* Cuv., collected in the Gulf of Naples, Mediterranean Sea.^[1] At that time, vanadium was still considered a rare element, and against this background, Henze’s findings may be considered a key discovery in the history of the biological chemistry of vanadium, described by Michibata *et al.* in a review on the reduction and accumulation of vanadium in ascidians in the following way:^[2]

‘His [Henze’s] discovery attracted the interdisciplinary attention of chemists, physiologists and biochemists, in part because of the considerable interest in the possible role of vanadium in oxygen transport as a third possible prosthetic group in respiratory pigments in addition to iron and copper [see, however, below], and in part because of the strong interest in the extraordinarily high levels of vanadium never before reported in other organisms. Much of the interest developed because vanadium was found in ascidians, which phylogenetically belong to the chordata.’

Ascidians,¹ also called sea squirts, belong to the Ascidiacea, a class of the subphylum Urochordata, or Tunicata. The last term indicates that these animals feature a tunic, a tough outer mantle. This outer covering consists of a mucopolysaccharide–protein ground substance, blood cells and tunicin fibres. The fibres contain cellulose. Tunicates in turn belong to the phylum Chordata and are classified as protochordates: while the adult individuals do not contain a vertebral column, the juvenile larvae show features in common with vertebrates. In particular, the larvae do have a prevertebral column, a so-called notochord (and a dorsal nerve cord, another characteristic of vertebrates). Ascidians are thus at the fringe of the most developed life forms, a fact which has inspired several researchers to suggest that it was ‘decided’ in this specific class of animals whether vanadium or iron should predominantly be employed in electron transfer processes, an

¹ The name derives from the Greek *askidion*, meaning ‘small wine-skin’, referring to the sac-like body form of the ascidians.

assumption which was nourished by findings according to which certain phylogenetically more advanced ascidians (the order Stolidobranchia) accumulate iron instead of vanadium, whereas vanadium is predominantly accumulated by species belonging to the more primitive orders Aplousobranchia (mainly present as V^{IV}) and Phlebobranchia (mainly V^{III}). Stolidobranchia in fact contain considerably less vanadium than the other two suborders (Table 4.1).

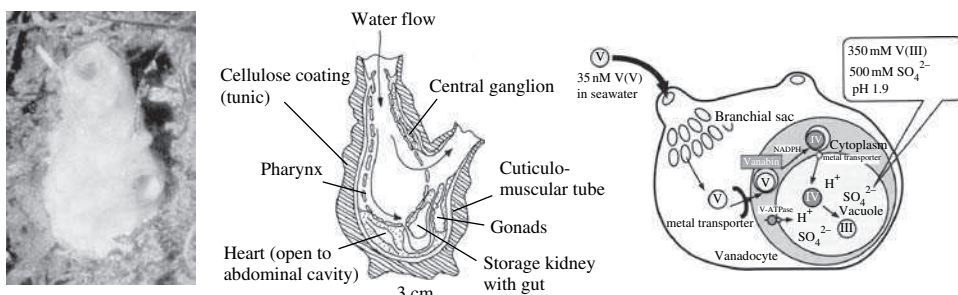
The amount of vanadium found in tunicates also appears to correlate with the pH (more vanadium at lower pH). Individuals belonging to the Phlebobranchia usually also contain tunichromes, whereas Aplousobranchia are devoid of this hydroxy-DOPA-based oligopeptide pigment (see below). The vanadium is present in special blood cells, called vanadocytes, essentially represented by two cell types: the signet ring cells and the vacuolated amoebocytes.^[2,3] They accumulate vanadium from sea water [$c(V) \approx 30 \text{ nm}$] by a factor of up to 10^8 .

Table 4.1 Vanadium concentrations (mM) in different tissues of several ascidians (from ref. [2]).

Species	Tunic	Mantle	Branchial	Serum	Vanadocytes
Suborder Phleobranchia					
<i>Ascidia gemmata</i>					347.2
<i>Ascidia ahodori</i>	2.4	11.2	12.9	1.0	59.9
<i>Ascidia sydneiensis</i>	0.06	0.7	1.4	0.05	12.8
<i>Phallusia mamillata</i>	0.03	0.9	2.9		19.3
<i>Ciona intestinalis</i>	0.003	0.7	0.7	0.008	0.6
Suborder Stolidobranchia					
<i>Styela plicata</i>	0.005	0.001	0.001	0.003	0.003
<i>Halocynthia roretzi</i>	0.01	0.001	0.004	0.001	0.007

The larvae in their early state are mobile, but they settle to solid substrates prior to metamorphosis. The adult individuals are almost exclusively sessile. Most are solitary, but some form colonies. Water, including food and solutes, is taken in through the oral siphon and enters the animal via the branchial sac, and the filtered water is released through the atrial siphon (Figure 4.1). When disturbed, they squeeze out jets of water. Sea squirts are very commonly distributed over the rocky ocean shores and are particularly frequent in salt-rich shallow bays and harbour areas.

Henze himself introduces his findings on the blood of ascidians in the following way: ‘There is almost no information on the blood of ascidians. Nonetheless I think that, with this communication, I will be able to show that this subject reveals plenty of interesting aspects, deviating from what we are generally used to.’ Henze then refers to earlier work of Harless and Krukenberg, according to which carbon dioxide, when passed through the blood of *Phallusia*, causes a blue colouration which disappears as oxygen is applied: ‘colour changes which are by no means observable’. Henze further makes it clear that ‘remarks on the respiratory importance, connected to the above-mentioned colour changes, are by no means supported by experiment and are thus speculative.’ Winterstein had in fact shown previously, based on applying ‘exact methods’, that there is no specific binding ability for oxygen connected with the blood of *Phallusia*, and that consequently there is no parallelism to iron-based haemoglobins and the copper-based haemocyanins.

**Figure 4.1**

Left: *Phallusia mamillata*, the sea squirt originally studied by Henze. The two ‘openings’ correspond to the oral and atrial siphon. Centre: schematic drawing of *P. mamillata*; redrawn from ref. 9. Right: schematic drawing of an ascidian and a vanadocyt (signet ring cell),^[2] illustrating the route of transport of vanadium: intake in the form of vanadate(V) is through the oral siphon and the branchial sac. In the cytoplasm of the vanadocyt, vanadate(V) is reduced to V^{IV} and bound to the cytoplasmatic carrier protein vanabin. After transport into the vacuole, reduction to V^{III} occurs. The high proton concentration is provided by a vacuole-type proton ATPase (V-ATPase). Reproduced from H. Michibata *et al.*, *Coord. Chem. Rev.* 237, 41–51. Copyright (2003), with permission from Elsevier.

The issue of whether tunicate blood cells are involved in oxygen uptake and transport could, of course, be settled by experimentation. This challenge was met for tunicate specimens collected from both Atlantic^[4a] and Pacific ocean waters,^[4b] using an oxygen electrode to measure dissolved dioxygen concentrations. It was found that the oxygen-binding capacity of tunicate blood cells was indistinguishable from that of sea water.

In the light of these early findings, it is surprising that there are still a sizable number of individuals in the scientific community who think of ascidian blood in terms of oxygen transport. This may be due to the introduction, about three and a half decades after Henze’s work, of the term ‘haemovanadin’² for the vanadium compound(s) present in ascidian blood cells. This term appears to have turned up for the first time in a report by Califano and Caselli, published in 1947, on *Ricerche sulla emovanadina – dimostrazione di una proteina*^[5] (Research on haemovanadin – demonstration of a protein³), dealing with ‘haemolysed’ blood from the same organism Henze had investigated. In their summary, Califano and Caselli state that⁴

‘...the term haemovanadin is proposed to indicate this organic compound for which three states can be identified: (1) native haemovanadin (*emovanadina nativa*) of a faint green colour found in the vanadocytes and thus functionally active; (2) red haemovanadin (*emovanadina rossa*), corresponding to Henze’s *braune Lösung* [brown solution], which is found when vanadocytes are haemolysed; and (3) blue haemovanadin (*emovanadina azurra*), corresponding to Henze’s chromogen, and obtained by oxidation of red haemovanadin.’

² At this point I would like to thank Kenneth Kustin, who helped me a lot in tracing back (historical) facts on the blood of ascidians.

³ The notion of haemovanadin being a protein or any other organic compound later turned out to be erroneous.

⁴ Translation adapted to the Italian summary of the original article.

The vanadium contents in the chromogen, according to Henze's quantitative analysis, amounted to 'more than 15% Vd₂O₅'.⁵ The subsequent assumption of Henze^[6a] and others,^[6b] according to which – based on the high reducing power – V₂O₂(and thus V^{II}) was supposed to be present, is incorrect. 'Native haemovanadin' actually contains V^{III} (for details, see below). Vanadium(III) precipitates to form brownish V^{III} hydroxides at pH > 3 (Henze's *braune Lösung*). Aerial oxidation leads to 'blue haemovanadin' with V^{IV}O²⁺.

The role of vanadium in the blood of ascidians remains elusive. An interesting hypothesis was proposed by Smith almost three decades ago,^[7] namely that the low oxidation state of vanadium and the low pH are the result of an

'... accommodation to the end product problem during anoxia by providing an alternative electron and proton sink, the final result being to generate a resilient tunic from polymerised tunichrome [comparable to sclerotisation in the insect imperium].

... Therefore I submit that vanadocytes enable ascidians to sustain periods of oxygen deprivation (anoxia), in contradistinction to proposals suggesting that they serve as oxygen carriers.'

The idea of vanadate (and vanadyl, the first reduction product of vanadium after vanadate had entered the ascidian) acting as electron acceptors is an attractive view in the light of vanadate actually being a primary electron acceptor for the bacterium *Shewanella oneidensis* (Section 4.5).

The early suggestion of Henze, according to which 'also in the chemistry laboratory represented by the cell, this [vanadium] compound may infer oxidations,'^[1] may or may not be correct, a suggestion which was based on the (even at that time) well-established ability of 'vanadic acid' to catalyse oxidations, e.g. aniline to aniline black. Almost three decades later, Webb stated in an article on 'Observations on the blood of certain ascidians':^[8] 'It may be confessed at the start that it has been found impossible to suggest any plausible explanation of the function of the vanadium compound, and that only a little progress has been made towards elucidating its chemical nature'. The chemical nature of haemovanadin nowadays is well established, but with respect to its function we are no better off than we were almost 100 years ago.

4.1.2 Ascidians: The Present Stand

The blood of ascidians contains up to 11 blood cell types, differentiated primarily by their morphology and to a lesser extent by their function. For some time, the morula cells were believed to be those containing vanadium, due to their greenish appearance, which actually is due to the high contents of tunichromes (see below). The real vanadocytes, as already pointed out in the preceding section, are the signet ring cells and the vacuolated amoebocytes, the latter containing less vanadium than the former. Two other types of blood cells, the type II compartment cells and the granular amoebocytes, might also take up vanadium.

The signet ring cells contain a large vacuole (Figure 4.1, right), and it is this vacuole which contains the vanadium. The pH can be as low as 1.9. By far the most predominant anion is sulfate, present at this pH in about equal amounts of SO₄²⁻ and hydrogensulfate,

⁵ For an unknown reason, Henze used *Vd* as the chemical symbol for vanadium.

HSO_4^- ($\text{p}K_a = 1.96$). The strongly acidic reaction of lysates of the blood cells, already noted by Henze, is thus due to the intracellular sulfuric acid.

The nature of the vanadium in the vanadocytes has been under debate for a considerable time space. Complexes with protein fractions, porphinogenic compounds and catecholates had been proposed as chelators for vanadium. Catecholates are known to be effective binders for vanadium in the oxidation states III and IV (and V), and the presence of tunichromes⁶ in most of the ascidians belonging to the suborder Phlebobranchia^[9] has transiently enforced the notion of tunichromes being the primary reducing agents for incoming vanadate, and the primary ligands to stabilise the vanadyl ion formed by reduction. Tunichromes (Figure 4.2) are small tri- or dipeptides consisting of DOPA and hydroxy-DOPA units (DOPA is short for 3,4-dihydroxyphenylalanine). All these theories had, however, to be tuned down or even abandoned. Porphinogens have not been found in ascidians, and the tunichromes are not associated with the vanadocytes. Furthermore, they are absent in ascidians belonging to the Aplousobranchia suborder. Most of the vanadium, when in the oxidation state +III, is actually present in the form of aqua-sulfato complexes and therefore, in principle, in a form already proposed in 1953 by Bielig and Bayer, who suggested a ‘proteinium salt of the disulfatovanadium(III) acid, $[\text{Prot} \cdot \text{NH}_3]^+ [\text{V}(\text{SO}_4)_2]^-$.^[10]

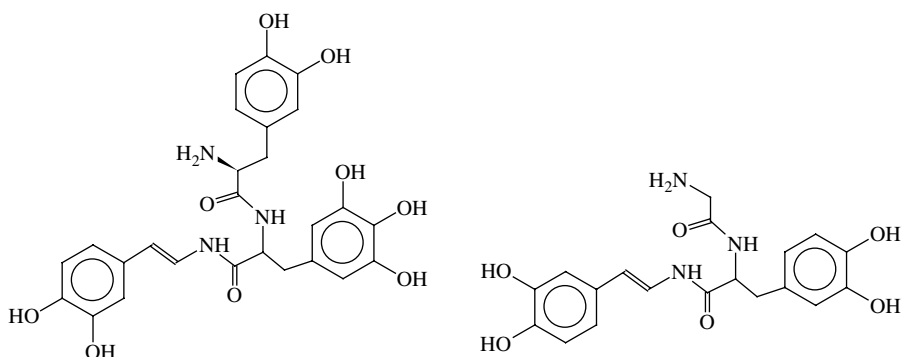


Figure 4.2

Examples of tunichromes from *Ascidia nigra* (suborder Phlebobranchia) (left) and *Molgula manhattensis* (suborder Stolidobranchia) (right).

Vanadium(III) in Phlebobranchia ascidians with a high acidity in the signet ring cell vacuoles (e.g. *Ascidia gemmata*) makes up about 98% of the overall vanadium present in blood cells. The $\text{V}^{\text{III}} : \text{V}^{\text{IV}}$ ratio decreases with increasing pH. According to magnetic measurements, $\text{V}^{\text{III}}(\text{d}^2)$ is in its high-spin state ($S = 1$)^[11a] and normally not accessible to electron paramagnetic resonance (EPR) due to efficient relaxation. The excellent contact shift properties of high-spin V^{III} (Section 3.2) were employed, at an early stage, to provide convincing evidence that the coordination sphere of vanadium in the vanadocytes

⁶ The existence of tunichromes in tunicates was not always discussed without controversy. Transiently, tunichromes were considered artefacts, derived from faulty preparations. In 1992, however, Bayer *et al.*^[9a] unambiguously isolated and characterised a tunichrome in *Phallusia mammillata*, the tunicate in which Henze discovered vanadium.

is dominated by water ligands.^[11b] Living vanadocytes from *Ascidia ceratodes* exhibit a signal at 21.5 ppm, paramagnetically shifted to low (magnetic) field with respect to plasma water by ca 17 ppm. The intensity and linewidth (1.3–1.4 kHz) of the 21.5 ppm signal indicated that it cannot be due to protons in a stable vanadium coordination compound. Rather, the signal represents water protons in rapid exchange between water coordinated to vanadium and surrounding solvent water. Quantitative analysis yielded a probable composition $\{V^{III}(H_2O)_5L\}$.

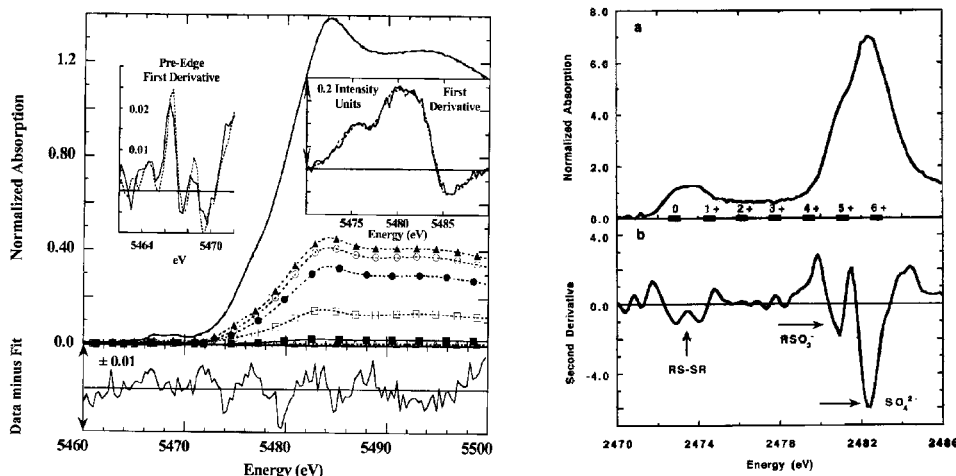
These results are in fairly good agreement with more recent studies based on vanadium K-edge X-ray absorption spectroscopy (XAS).^[12] As outlined in Section 3.6, the energy position of the K-edge (reflecting the energy necessary for the excitation of an electron from the K shell) is sensitive to the oxidation state and the ligand electronegativities. In Figure 4.3 (left), the spectrum of blood cells from a single individual of *A. ceratodes* is shown, including subspectra (dashed lines connecting symbols) employed for optimum fitting. Optimum fitting could be achieved with the following percentage composition for the predominant vanadium species:⁷

$[V(H_2O)_6]^{3+}$	38.7%
$[V(HSO_4)(H_2O)_5]^{2+}$	34.0%
$[V(HSO_4)_2(H_2O)_4]^+$	10.3%
$[V(SO_4)(H_2O)_3(OH)_2]^-$	9.9%
$[V(H_2O)_5OH]^{2+}$	2.7%
Other	4.5%

These results clearly indicate that, at least in *A. ceratodes*, the average composition of vanadium corresponds to $[V(HSO_4)(H_2O)_5]^{2+}$ {or $[V(SO_4)(H_2O)_5]^+$ } and thus is in accord with Bielig and Bayer's early suggestion of sulfate being coordinated to vanadium. The composition varies between individuals of the same species, and between different species. In part, these variations go along with variations in pH. Higher pH, e.g. pH 2.7 in *Ascidia ahodori*, will favour the formation of sulfato–hydroxo complexes such as $[V(SO_4)(H_2O)_4OH]$ and $[V(SO_4)(H_2O)_3(OH)_2]^-$. For *Phallusia nigra*, sulfato complexes have not been detected. For this species, there appears to be evidence that, along with the hexaquavanadium(III) cation, sizable amounts of $[V(\text{catecholate})_3]$ are present. These findings, if not due to an artefact (such as partial lysis of the blood cells), might reactivate the notion of part of the vanadium being bound to tunichromes, at least in this specific ascidian.

The results obtained from vanadium K-edge XAS of *A. ceratodes* have essentially been corroborated by sulfur K-edge XAS. Sulfur XAS also indicates the presence of aliphatic sulfonate and low-valent sulfur, the latter possibly stemming from organic disulfide (Figure 4.3, right). As an example, the three sulfur species detected in *A. ceratodes* whole blood cells are in the ratio 1.0:0.9:0.4 (sulfate: sulfonate: low-valent sulfur), total concentration 250 mM.^[13] There is therefore a possibility that, along with sulfate, also sulfonate coordinates to V^{III} , generating $[V(H_2O)_5(OSO_3)]^{2+}$. The detection of low-valent sulfur (in the oxidation state –I) is interesting in the light of the large number of cystine links found in vanabin2 (see below).

⁷ In the original work,^[12b] the complexes are formulated with SO_4^{2-} instead of HSO_4^- .

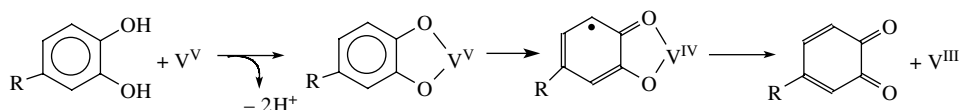
**Figure 4.3**

Vanadium (left) and sulfur (right) K-edge XAS spectrum of blood cells from *Ascidia ceratodes*. Left: the solid line represents the experimental spectrum, the dashed lines indicate the components of the fit: ▲, $c(V^{III}) = 50 \text{ mM}$, $c(SO_4^{2-}) = 523 \text{ mM}$, pH = 1.8; ○, $c(V^{III}) = 100 \text{ mM}$, $c(SO_4^{2-}) = 150 \text{ mM}$, pH = 1.8; ●, $c(V^{III}) = 50 \text{ mM}$, pH = 0.04; □, $c(V^{III}) = 50 \text{ mM}$, pH = 3.0; ■, 0.1 M VOCl_2 in 0.1 M HCl. The insets show the first derivatives of the pre-edge feature (left) and the K-edge (dashed lines: fit). The bottom trace is the difference between the experimental and the fit. Reproduced from P. Frank *et al.*, *Coord. Chem. Rev.*, 237, 31–39. Copyright (2003), with permission from Elsevier. Right: top, absorption spectrum; bottom, first derivative. The arrows indicate disulfide, sulfonate and sulfate. The K-edge maxima of the various sulfur oxidation states are marked on the central horizontal line. Reproduced from P. Frank *et al.*, *Inorg. Chem.* 38, 260–270. Copyright (1999), with permission from the American Chemical Society.

Vanadate likely enters the organism through anion (phosphate, sulfate) channels.^[14a] Early investigations of the uptake of vanadium by *Phallusia mamillata*, using ^{48}V -labelled vanadate, have shown that vanadium primarily accumulates in the branchial sac.^[14b] The radioactive ^{48}V is a β^- (half-life 16.2 days) and γ emitter. Uptake by tissue is slow and depends on the age of the individual; in fully mature individuals, only 2% of the overall vanadium is found in the vanadocytes after 2 days. In contrast, incorporation into the blood cells is a rapid process ($t_{1/2} = 57 \text{ s}$ at 0°C). Vanadate migrates into the cytoplasm of the vanadocyte through phosphate channels^[14a] and/or is translocated by a metal transporter (cf. Figure 4.1, right), where it is picked up by vanabins [vanadium-binding proteins (see below)] and reduced to the +IV state, in the form of vanadyl ions [oxovanadium(IV), VO^{2+}], bonded to vanabin.^[2,15] Another metal transporter conveys the vanadyl ions into the vacuole, where further reduction to the +III state takes place. A vacuole-type ATPase (V-ATPase) powers the translocation of protons into the vacuole, providing the unusually low pH.

It appears to be well established by now that the reductant responsible for the conversion of vanadate(V) to oxovanadium(IV) is nicotine adenine dinucleotide phosphate (NADPH), produced in the pentose phosphate pathway.^[2] Further reduction to V^{III} in the vacuoles of the vanadocytes of Phlebobranchia ascidians remains elusive. Several reductants have been proposed and shown to be effective in the *in vitro* and/or *in vivo* reduction of V^V to V^{IV} and/or V^{IV} to V^{III} , including tunichromes. Selected investigations of the related redox chemistry of vanadium can be briefly summarised as follows:

- In neutral aqueous media, the *M. manhattensis* tunichrome (Figure 4.2) reduces V^V and V^{IV} to V^{III}.^[15] The generation of V^{III} is more facile from V^V than from V^{IV}, suggesting an electron transfer pathway (with or without coordination of vanadium to the catecholate moiety), as shown in Scheme 4.1.

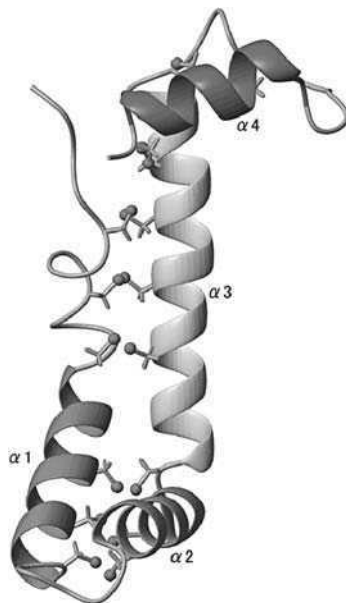


Scheme 4.1

M. manhattensis does not, however, accumulate vanadium. No appreciable reduction to V^{III} was found with the tunichrome from *A. nigra*, an effective vanadium accumulator (Table 4.1). On the other hand, reaction of [VO(acac)₂] with 2,4-di(*tert*-butyl)catechol yields [V(semiquinone)₃].

- [VO₂(edta)]³⁻ is slowly reduced to [VO(edta)]²⁻ by NADPH at neutral pH [where edta = ethylenediaminetetraacetate(4-)]. Reduction is markedly accelerated as the pH is lowered to 3.
- Simple inorganic vanadium(V) compounds are reduced by thiolates such as cysteine and cysteinemethyl ester (CysMe) to VO²⁺. Further reduction to V^{III} by CysMe is achieved on addition of H₂(edta)²⁻, which stabilises the V^{III} state by formation of [V^{III}(edta)H₂O]⁻. For this reduction to occur it is crucial that less than 1 equivalent of edta is employed, apparently in order to provide a site of direct interaction between VO²⁺ and the thiol function. CysMe is oxidised to cystine. Cysteine does not reduce VO²⁺ to V^{III} under these conditions. Low-valent sulfur (with the sulfur in the oxidation state -I) is present in the vacuoles of vanadocytes (see above). This type of reaction has nourished the assumption that a vanadium reductase might be present in the intermembrane face of the singlet ring cells, disposing of an N₂O₄ ligand set for vanadium coordination, i.e. a ligand set comparable to edta.^[12c]

One of the most exciting developments of late in ascidian chemistry is the discovery of the vanabins, the vanadium-binding proteins, by Michibata's group. So far, at least five vanabins have been identified in *Ascidia sydneiensis samea* (and *Ciona intestinalis*), named vanabin1–4 and vanabinP. Four of the vanabins are contained in the vanadocytes. Vanabin1, vanabin2 and vanabin3 are cytosolic and vanabin4 is located in the cytoplasmatic membrane. VanabinP is constituent of the coelomic fluid (blood plasma).^[16] The structure of the *A. sydneiensis* vanabin2 has recently been solved by multinuclear and -dimensional NMR of ¹⁵N-enriched material, revealing a new class of metal binding proteins, viz. a bow-shaped conformation with four α -helices connected by nine disulfide bonds.^[17] Figure 4.4 illustrates features of vanabin2; Figure 4.5 provides the amino acid sequence of vanabin1–4. The high number of disulfide bridges (nine in vanabin2), which is reminiscent of intracellular proteins of thermophilic archaea, stabilises the protein and is essential for optimal binding capacity for vanadyl ions. The molecular weight of vanabin2 is 10 467 Da. Of the 91 amino acids, 14 constitute lysine and thus a basic amino acid having available a side-chain amino group. The lysines are exclusively located on one side of the

**Figure 4.4**

Solution structure of vanabin2 as obtained from NMR spectroscopy. The ‘solid’ backbone, representing the four α helices (amino acids 18–70), is shown in ribbon presentation. The two halves of the bow-shaped molecules are linked by nine cystines. Courtesy H. Michibata, Hiroshima University, Japan.

Vanabin 1	1	- - M V [S] K F T I L [L G] V [V V] L M A L S - - V N A Y E S E [F] D D E T	30
Vanabin 2	1	- - - M [S] K V I F A L [V L] V V V L V A C - - I N A T Y V E F E E A Y	29
Vanabin 3	1	M A S K [L] F L L L F L G [M] F V L I A A S D E S F D E E E D [F] E D E V	34
Vanabin 4	1	M V T K [S] H I I F F L G M [V V] V I V G C P A F E K F V S K N E E S V	34
Vanabin 1	31	F E K G - - P G [C] - - K [C] Q S V [C] G E V K K [C] G V K [C] F R S [C] N G D	60
Vanabin 2	30	A P V D - - - C K G Q C T T P C E P L T A C K E K C A E S C F T S	59
Vanabin 3	35	M A Q S Y Y P E C D - - C R Q E C G T F R N C R A T C R A N C G D G	66
Vanabin 4	35	I V [D] S - - - C K T N C S T E C L P L K N C T E N C T E H [C] E G L	64
Vanabin 1	61	R [D] - - C T K D C A [K] A K [C] G K V P N A G D [C] G H [C] M L S [C] E G K	91
Vanabin 2	60	A [D] K K T [C] R R N C K [K] A D [C] E - - P Q D K V C D A C R M K C H K A	91
Vanabin 3	67	R - - - C R R E C K R T K C I N - - M K S Q C R N C N G D C R E R	94
Vanabin 4	65	S [D] K K A C H Q N C R [K] V T C K - - A E D G Q C R A C K K K C K D E	96
Vanabin 1	92	C R A D H C A [S] A [C] P G [K] V S [K] A P A [C] L D C M K L [N] C V - - -	120
Vanabin 2	92	C R A A N C A [S] E C P K H E H K S D T C R A C M K T [N] C K - - -	120
Vanabin 3	95	C R S K Y C S K P C Y - K S L K V R K C V R C M V V S C H L R F	125
Vanabin 4	97	C [K] K A N C K [S] S C E E K A M K S P A C K S C M E K [N] C H - - -	125

Figure 4.5

Aligned amino acid sequences of vanabins1–4, demonstrating the high degree of conservation. Conserved residues are in boxes. The framed part indicates the protein region employed as the antigen in the generation of monoclonal antibodies. 18 cysteine (C) residues act as disulfide linkers. The lysine (K) and arginine (R) amino side-chains in vanabin2 are involved in vanadyl binding. Reproduced from N. Yamaguchi *et al.*, Zool. Sci. 23, 909–915. Copyright (2006), with permission from the Zoological Society of Japan.

protein, and these are the sites where VO^{2+} binds, as evidenced by ^{15}N HSQC (heteronuclear single quantum coherescence) perturbation experiments after addition of vanadyl sulfate to the protein, and the comparatively small ^{14}N isotropic hyperfine coupling constant of 4.5 MHz obtained from ESEEM (electron spin-echo envelope modulation; cf. Section 3.4) experiments.^[18]

Vanabin1 and vanabin2 are metallochaperone proteins transporting vanadyl ions from the cytoplasm to the vacuole, as shown schematically in Figure 4.1 (right). They can bind up to 20 VO^{2+} , also classifying them as storage proteins. In contrast to the well-known storage proteins for iron(III) (ferritins) and zinc (thioneins), cluster formation does not take place. Rather, all (or practically all) of the vanadium centres are isolated. The binding constant, ca. $4.5 \times 10^4 \text{ M}^{-1}$, is not particularly large, allowing for a stabilisation of available VO^{2+} in the about neutral cytoplasm, i.e. preventing precipitation of vanadyl hydroxides, and allowing delivery of vanadium to the vacuoles. Incidentally, the binding constants are comparable to those reported for other metal chaperones, such as those for nickel and copper ions. Vanabin2 also binds Fe^{3+} and Cu^{2+} . The secondary structure of the protein is essentially invariant with pH in the pH range 7.5–4.5. The affinity of VO^{2+} to the protein decreases on acidification. At pH 4.5, the binding constant is $1.1 \times 10^4 \text{ M}^{-1}$ and the maximum binding number decreases from 20 (at pH 7.5) to 5. A further decrease in pH leads to protonation of the binding sites and release of VO^{2+} . The vanadyl carrier vanadinP, present in the blood plasma and closely related to the other vanabins, can bind a maximum of 13 VO^{2+} (binding constant $3.6 \times 10^4 \text{ M}^{-1}$).

Along with the vanabins, a vanadium-binding protein particularly abundant in the digestive system of *A. sydneiensis*, with a striking homology to glutathione transferases (GST), has been isolated.^[19] GSTs comprise an ancient superfamily of enzymes that utilise glutathione in detoxification processes. They catalyse the conjugation of electrophilic substrates to glutathione, have peroxidase and isomerase activities and are able to bind noncatalytically a wide range of endogenous and exogenous ligands. The ascidian GST analogue is a dimer (25.6 kDa per subunit) which exhibits vanadium-binding activity. The protein coordinates up to 16 $\text{V}^{\text{IV}}/\text{V}^{\text{V}}$ centres, with binding constants of $5.6 \times 10^3 (\text{VO}^{2+})$ and $8.3 \times 10^3 (\text{H}_2\text{VO}_4^-) \text{ M}^{-1}$. In the light of the uptake of vanadium in the form of vanadate from sea water, the affinity for vanadate is particularly interesting. The dual role, to act as a vanadate/vanadyl binder and carrier and as a transferase for glutathione, is intriguing in the light of the ability of glutathione to reduce V^{V} to V^{IV} .

4.1.3 Polychaeta Fan Worms

The marine fan worm *Pseudopotamilla occelata*, belonging to the polychetes (bristle worms) and thus to the phylum Annelida (annelids), is the second marine organism which has been shown to accumulate vanadium.^[20] Vanadium contents are between 320 and $1350 \mu\text{g/g}^{-1}$ dry weight of the whole body, which compares with $1550 \mu\text{g/g}^{-1}$ dry weight for *Ascidia ahodari* and $260 \mu\text{g/g}^{-1}$ for *A. sydneiensis samae*. Other species belonging to the genus *Pseudopotamilla* also accumulate vanadium. About 90% of the overall vanadium is found in the bipinnate radioles of the branchial crown (Figure 4.6), concentrated in vacuoles of the outer (apical) part of the epidermal cells, and associated with high amounts of sulfur, predominantly present in the form of sulfate. XAS analysis of living specimens of *P. occelata* revealed the presence of vanadium essentially in the oxidation state +III in an $\text{V}\{\text{O}\}_6$ environment [$d(\text{V}-\text{O}) = 2.00 \text{ \AA}$, compared with 1.99 \AA in *A. ceratodes*]. Together with the coexistence of sulfate in the vanadium-containing epidermis vacuoles,

this is convincing evidence for a comparable speciation – $[V(H_2O)_5HSO_4]^{2-}$ and related complexes – in ascidians and polychaete fan worms. A similar mechanism may work on the accumulation of vanadium in Ascidiaceae and Polychaeta, suggested by locating the same antigens in *P. occelata* and *A. sydneiensis*, recognised by vanadium-associated proteins of the latter.

As in the case of the ascidians, the function of vanadium in the fan worms is elusive.

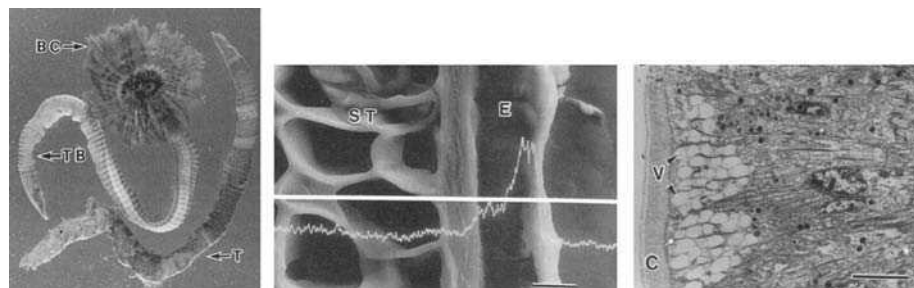


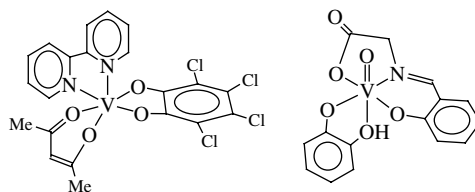
Figure 4.6

Left: view of *Pseudopotamilla occelata*, extracted from its tube (T). TB = trunk body; BC = branchial crown, where (in the bipinnate radioles) most of the vanadium accumulates. Centre: longitudinal section of a bipinnate radiole. ST = supporting tissue; E = epidermis. Vanadium is concentrated in the outer layer of the epidermis, as shown by a clear peak in the X-ray microanalysis. Scale bar 10 μm . Right: transmission electron micrograph of the apical portion of a bipinnate radiole, showing the vacuoles (V) containing V^{III} and sulfate. Some vanadium is also contained in the cuticle (C). Scale bar 3 μm . Reproduced from T. Ishii, in: *Vanadium in the Environment, part 1: Chemistry and Biochemistry* (J. O. Nriagu, Ed.) Copyright (1998), with permission from John Wiley & Sons, Ltd.

4.1.4 Model Chemistry

The presence of high amounts of vanadium and tunichromes in certain ascidians had initiated extensive studies into the chemistry of vanadium–catechol and –pyrogallol complexes until, about 10 years ago, it became clear that there is possibly no direct chemistry between these two ingredients, located in different body tissues and compartments. Catechols form stable complexes with vanadium in its biologically relevant oxidation states +V, +IV and +III. The complexes can be homoleptic, or they contain additional ligands, such as bipyridine, *o*-phenanthroline, acetylacetone or Schiff bases. Examples were provided in Section 2.3.2 in Figure 2.28, compounds **10–12**. Since the amide backbone of the tunichromes is comparatively rigid, it is unlikely that homoleptic complexes are formed with vanadium. Possible coordination environments may be represented by the two complexes depicted in Figure 4.7, containing, in addition to the catecholate, bipyridine and acetylacetone, or a Schiff base ligand. The latter complex also accounts for the possibility that, under acidic conditions, the coordinated catecholate can be present in its monoprotonated form.

Catechols (and pyrogallols) readily reduce vanadium(V) to vanadium(IV) and, in some instances, further to vanadium(III). In the context of tunichromes as the presumed reducing agents in ascidians, the redox chemistry of catecholatovanadium complexes has been investigated to some extent.^[21] Results on reduction potentials for the V^V/V^{IV} and

**Figure 4.7**

Two possible models for putative vanadium–tunichrome interaction in ascidians: $[V^{III}acac(bipy)catCl_4]$ [$acac = \text{acetylacetone}(1-)$; $bipy = \text{bipyridyl}$; $catCl_4 = \text{tetrachlorocatecholate}(2-)$]^[21] and $[V^{IV}O(\text{gly-sal})cat]$ [$\text{gly-sal}(1-)$ is the Schiff base formed from glycine and salicylaldehyde; $cat = \text{catecholate}(1-)$].^[22]

V^{IV}/V^{III} couples are summarised in Table 4.2. In contrast to catecholato complexes of, e.g., chromium and iron, where the redox processes usually are ligand centred, they are metal centred in the case of catecholatovanadium complexes. As noted above, some of the vanadium present in *Phallusia nigra* can be modelled by catecholate and keto–enolate binding, and thus be attributed to vanadium coordinated to tunichrome. Catecholates form rather stable complexes with vanadium in aqueous solution. Speciation studies in the VO^{2+} –catechol system have shown that mono- and bis-ligand complexes form, starting at pH values of ca 2.5. In addition, mainly at higher V:catechol ratios, non-oxo V^{IV} complexes containing three catecholato ligands are obtained in the slightly acidic range [Equation (4.1)].^[23]

Table 4.2 Reduction potentials $[E_{1/2}$ (V vs NHE^a)] for selected catecholatovanadium complexes.^{b,c}

Complex	Solvent	V^V/V^{IV}	V^{IV}/V^{III}
$[V(\text{trencam})]^d$	Dimethylformamide	+0.53	-0.54
$[V(\text{trencam})]$	Water		-0.37
$[V(dtbc)_2\text{phen}]$	Acetonitrile	+0.52	-0.79
$[V(Cl_4\text{cat})_2\text{bipy}]$	Acetonitrile	+0.52	-0.75
$[V(Cl_4\text{cat})_2\text{bipy}]$	Dichloromethane	+0.43	-0.90
$[V(\text{cat})(\text{acac})_2]$	Acetonitrile		-0.22
$[V(dtbc)(\text{acac})_2]$	Acetonitrile		-0.38
$[V(Cl_4\text{cat})(\text{acac})\text{bipy}]^e$	Dichloromethane	-0.36	-0.90

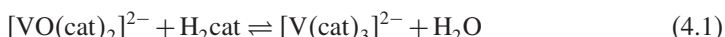
^aNHE = normal hydrogen electrode.

^bFrom ref. 21 and literature cited therein.

^cAbbreviations: dtbc = 2,4-di(*tert*-butyl)catecholate(2-); cat = catecholate(2-); $Cl_4\text{cat} = 2,3,4,5$ -tetrachlorocatecholate(2-); phen = *o*-phenanthroline; bipy = 2, 2'-bipyridyl; acac = acetylacetone(1-).

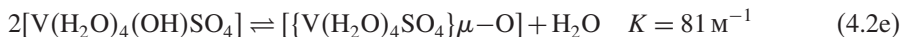
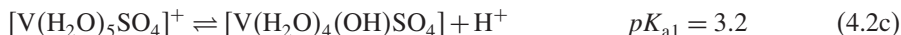
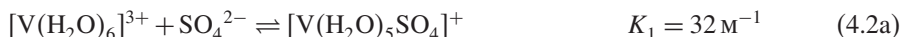
^dFor the tris(catecholate) trencam(6-), see **13** in Figure 2.28.

^eSee Figure 4.7.



The presence of vanadium(III) complexes in the very acidic medium of the vacuoles of the signet ring cells in *Ascidia ceratodes*, containing one or two sulfato/hydrogensulfato ligands, has focused interest on sulfatovanadium complexes as model systems.^[24] Whereas VO^{2+} readily forms a 1:1 complex with sulfate ($K = 300 \text{ M}^{-1}$), the affinity of V^{III} to sulfate is less pronounced. Selected stability constants and pK_a values obtained from

speciation studies based on redox measurements and spectrophotometric titrations are provided in the following equations:^[25]



A number of sulfatovanadium(III, IV and V) complexes have been structurally characterised, demonstrating the versatility of the coordination modes that the sulfate ligand can attain. Selected structures of purely inorganic complexes on the one hand and complexes containing a multidentate organic co-ligand on the other hand are collated in Figure 4.8. Inorganic sulfatovanadium complexes are commonly synthesised by hydrothermal methods, and in most cases are stable only in the solid state, forming polymeric two- and three-dimensional patterns, in which sulfate coordinates in the end-on or bridging (μ_2 and μ_3) fashion. An example for unidentate coordination in the presence of a co-ligand is the neutral complex $[\text{VO}(\text{H}_2\text{L})\text{SO}_4]$, where H_2L derives from a deprotonated tetraaminodiphenolate, coordinating the vanadyl ion through two phenolate oxygens and two secondary amino functions.^[26] The dinuclear complex $[\{\text{VO}(\text{sal-aebmz})\}_2(\mu-\text{SO}_4)]$ in Figure 4.8 exemplifies the bridging mode of sulfate.^[27] The ligand sal-aebmz(2–) represents a Schiff base derived from salicylaldehyde and ethylaminobenzimidazole, which forms a second bridge between the two vanadium centres via the phenolate group.

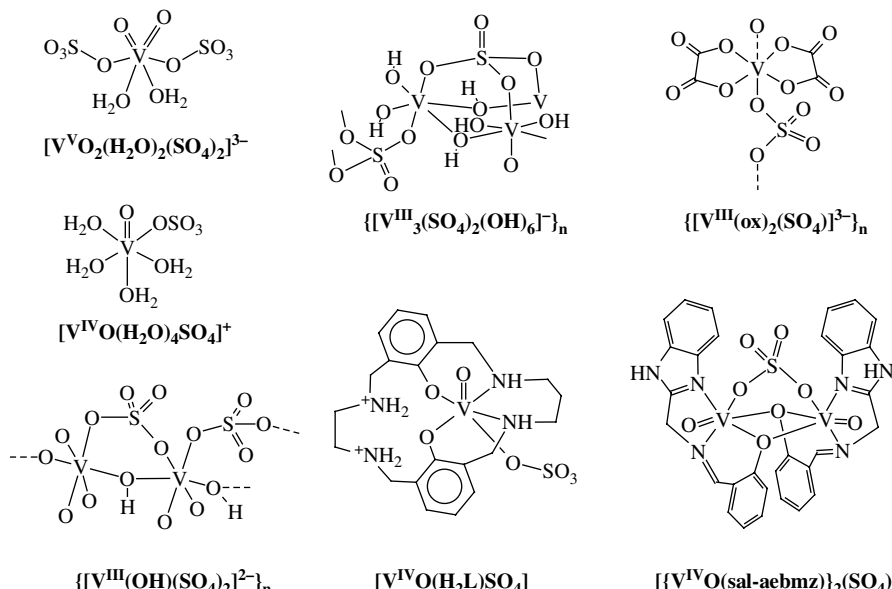


Figure 4.8

Examples of structurally characterised sulfatovanadium complexes with and without co-ligands, exemplifying different coordination modes of sulfate. See refs 24, 26 and 27.

4.2 Amavadin

'One fascinating aspect of bioinorganic chemistry is that of metal accumulation by living organisms, for example, to provide an appropriate concentration for the use of the metal in one or more specific biochemical functions and/or as a means of protection against toxicity that arises from an excess of metal. A striking example of metal accumulation is provided by . . . *Amanita muscaria*, the "fly agaric", . . . [which] concentrates vanadium to levels up to 400 times those typically found in plants.'

These are the introductory words in a communication on the structural characterisation of amavadin by Garner and co-workers in 1999.^[28] The discovery of high amounts of vanadium in *A. muscaria* dates back to 1931:^[29] in an article '*Sur la répartition du molybdène dans la nature*' [on the distribution of molybdenum in nature], the comparatively high amounts of vanadium found in *A. muscaria* (3.3 mg kg^{-1})⁸ and garlic (0.8 mg kg^{-1}) are noted.⁹ The vanadium compound present in *Amanita muscaria*, known as fly agaric or toadstool, was first isolated and characterised in 1972 by Bayer from mushrooms collected in the Black Forest (Germany), and named amavadin:^[30]

'[Amavadin is isolated by] addition of methanol to the frozen mushroom. The thawed mixture is ground and filtered, the filtrate acidified with acetic acid (to 0.1 N). DEAE cellulose is added and the slurry stirred overnight. The cellulose is then placed in a chromatography column, washed with 0.5 M acetic acid, and the amavadin eluted with 0.2 N phosphate buffer (pH 5.8). The eluate is [. . .] absorbed on Sephadex A25, and the amavadin eluted with 0.4 N phosphate buffer (pH 5.8). The lyophilised amavadin is extracted with methanol and further purified on Dowex and Sephadex.'^[30a]

Later, amavadin was also found, in comparably high concentrations, in two other species belonging to the genus *Amanita*, viz. *A. regalis* and *A. velatipes*. Most *Amanita* mushrooms and mushrooms belonging to related genera do not show any significant enrichment in vanadium. The amounts of vanadium in *A. muscaria* are independent of the vanadium content in the soil; the accumulation increases, however, with age, and vanadium is irregularly distributed: particularly rich in vanadium are the bulb (up to 1000 mg kg^{-1} dry weight) and the lamellae (up to 400 mg), whereas spores contain only 1–2% of the lamellar vanadium.^[31]

Due to its intensely red coloured cap covered with whitish flecks, the fly agaric (Figure 4.9), commonly associated with pine plantations, is possibly the most eye-catching and best known poisonous mushroom. Its 'poison' muscarin (occasionally used as a hallucinogenic intoxicant) is not in any known relationship with amavadin.

In Table 4.3, characteristics of amavadin are summarised.¹⁰ Amavadin is a low molecular mass, anionic non-oxo vanadium(IV) complex derived from the dichiral ligand *N*-hydroxyimino-2,2'-diisopropionic acid, *S, S*–H₃hidpa (**A** in Figure 4.10, in its trebly deprotonated form, hidpa(3–)). Solutions of amavadin are light blue, such as those of simple vanadyl salts such as vanadyl sulfate. The optical and EPR features, and the

⁸ These specifications are possibly related to 1 kg weight of the fresh vegetable.

⁹ On p. 499 of ref. 29.

¹⁰ For various aspects of amavadin see also: T. Hubregtse, Proefschrift (Ph.D. thesis), **2007**, Technical University Delft, The Netherlands.

**Figure 4.9**

The amavadin-containing mushroom *Amanita muscaria* (fly agaric, toadstool) is easily recognisable by its bright red cap, covered with white warts.

Table 4.3 Physico-chemical characteristics of amavadin.

$\lambda_{\max}/\text{nm}(\varepsilon/\text{dm}^3 \text{mol}^{-1} \text{cm}^{-1})$:	775(23), 699(22), 565(25) ^{a[34a]}
EPR: $g_{ } = 1.925$, $g_{\perp} = 1.987$; $A_{ } = 154$, $A_{\perp} = 47 \times 10^{-4}$ T	^[34a]
$\delta(^{51}\text{V})/\text{ppm}$ of the oxidised (V^{V}) form:	-281(Δ isomer) ^{b[34b]}
$\nu(\text{C}-\text{CH}_3)$ = 985 cm ⁻¹ [misinterpreted as $\nu(\text{V}=O)$] ^[30]	
XAS: K -edge at 5480.8 eV ^[34b]	
Stability constant: $\log \beta_2 = 23(1)^{[32]}$	
$\text{V}^{\text{IV}}/\text{V}^{\text{V}}$ redox couple, E/V vs NHE:	0.27 (DMSO), 0.81 (water, pH 7) ^[35]
Self-exchange rate ($\text{V}^{\text{IV}} \rightleftharpoons \text{V}^{\text{V}} + \text{e}^-$) $k_{22}/\text{l}^3 \text{mol}^{-1} \text{s}^{-1}$:	$(1 \pm 0.5) \times 10^5$ ^[36]

^aCorresponding to the transitions from the electronic ground state $d(x^2 - y^2)$ to $d(xz)$, $d(xy)$ and $d(z^2)$, respectively.

^bFor the chemical shifts of diastereomers of synthetic amavadin, see ref. 36 and Figure 3.4.

presence of an intense band at 985 cm⁻¹ in the infrared region, otherwise typical of the V=O stretching vibration in vanadyl complexes, led to the early (incorrect) structural assignment **B** in Figure 4.10.^[30b,c] Later, this structure was reassigned by Bayer *et al.*,^[32] mainly based on comparative studies of the stability constants, and supported by distinct differences in the EPR parameters and redox behaviour of VO^{2+} complexes with model ligands on the one hand and amavadin on the other, and further by the fact that the pre-edge peak and V–O distances typical of the vanadyl fragment are lacking in the X-ray absorption spectrum of amavadin. This second structure proposal by Bayer *et al.* was backed up by the structure elucidation of the model complex with *N*-hydroxyiminodiacetic acid, H₃hida (**C** in Figure 4.10),^[33] by the structure of the V^{V} form of amavadin, the monoanion $[\Delta-\text{V}\{(S,S)-\text{hidpa}\}_2]^-$,^[34] and finally by the calcium salt of amavadin itself, $[\text{Ca}(\text{H}_2\text{O})_5][\Delta-\text{V}\{(S,S)-\text{hidpa}\}_2] \cdot 2\text{H}_2\text{O}$ ^[28] (**D** in Figure 4.10), where Ca^{2+} is coordinated to one of the carboxylate oxygens not

bonded to vanadium. There are no structural changes on going from amavadin to its oxidised form. In the crystals of amavadin, vanadium is in the Δ configuration (see also Figure 2.25). A phosphoric acid derivative, with vanadium in the Λ configuration, $[\Lambda\text{--V}\{(S,S)\text{--Hidpa}\}_2] \cdot \text{H}_3\text{PO}_4 \cdot \text{H}_2\text{O}$, has also been structurally characterised. In the isolated form of natural amavadin, approximately equal amounts of the Δ and Λ forms are present. Complexation of $(S,S)\text{--Hidpa}$ to vanadium yields a Δ to Λ ratio of amavadin of 2.3 directly after synthesis. Epimerisation occurs, and the ratio decreases to 0.80 after equilibrium has been reached.^[37a] For the stability in aqueous solution and against oxidation, the ligand motif provided by the trianionic hidpa(3 $-$) appears to be essential.^[37b]

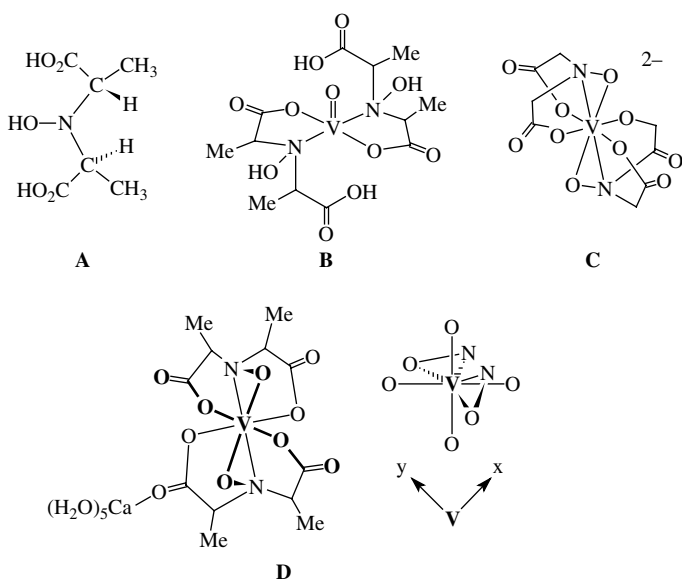
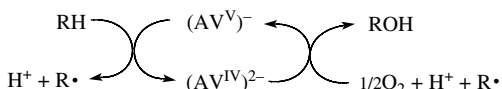


Figure 4.10

A, The ligand present in amavadin, *N*-hydroxyimino-2,2'-diisopropionic acid (*S,S*-H₃hidpa); B, $[\text{VO}(\text{Hhidpa})_2]$, the first proposal for the structure of amavadin;^[30b] C, a structurally characterised model compound, $[\text{V}(\text{hida})_2]^{2-}$ ($\text{H}_3\text{hida} = \text{N}$ -hydroxyiminodiacetic acid)^[35] D, structure of the calcium salt of the Δ enantiomer of amavadin, $[\text{Ca}(\text{H}_2\text{O})_5][\Delta\text{--VO}\{\text{S},\text{S}\text{--}(\text{hidpa})\}_2] \cdot \text{H}_2\text{O}$. The idealised coordination geometry as viewed along the z axis is also shown. The orbital accommodating the single electron, the SOMO (semi-occupied molecular orbital) has $d(x^2 - y^2)$ character.^[33a]

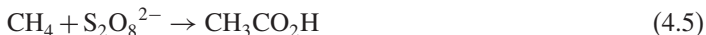
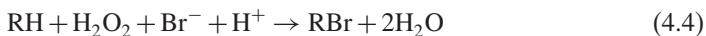
As in the case of ‘haemovanadin’ in the ascidians, the role of amavadin in the fly agaric is elusive. In the light of the diagonal relationship between molybdenum and vanadium, and the well-established role of molybdenum in oxygenases and deoxygenases, it is attractive to assume that amavadin has been a component of a primitive redox-active enzyme, a remainder of, e.g., an evolutionary overcome oxidase^[38a] or oxygenase in a reaction such as shown in Equations (4.3a) and (4.3b), and working as illustrated in Scheme 4.2.





Scheme 4.2
AV = amavadin.

In any case, amavadin and amavadin models can be efficient catalysts in oxidation, oxo transfer and oxidative C–C coupling reactions. The calcium salts of synthetic amavadin $\{\text{Ca}[\text{V}(\text{hidpa})_2]\}$ and the amavadin model $\text{Ca}[\text{V}(\text{hida})_2]$ (**C** in Figure 4.10) catalyse the oxidation, by H_2O_2 , of cyclohexane in acidic media to form cyclohexanol [Equation (4.3b)], along with some cyclohexanone.^[38b] In the presence of bromide, bromocyclohexane is obtained [Equation (4.4)], a reaction which is reminiscent of the enzymatic bromination by vanadate-dependent bromoperoxidase to be dealt with in the next section. Amavadin-based complexes also catalyse the oxidation, by peroxodisulfate, of methane to acetic acid [Equation (4.5)] and, in the presence of carbon monoxide, of alkanes and cycloalkanes to the corresponding carboxic acids [Equation (4.6)] (note that reactions (4.5) and (4.6) are formulated non-stoichiometrically).^[39] In the context of redox interactions with the participation of cysteine-containing peptides and proteins, it is of interest that the amavadin analogues $[\text{V}(\text{hida})_2]^{2-}$ and $[\text{V}(\text{hidpa})_2]^{2-}$ act as electron-transfer mediators in the electrocatalytic oxidation of thiols HSR (e.g. cysteine) to disulfides (e.g. cystine) [Equation (4.7)], an inner-sphere oxidation via a short-lived ($t_{1/2} \approx 0.3$ s) $\{\text{V}^{\text{V}} \cdot \text{HSR}\}$ intermediate.^[40]



Model chemistry on amavadin has been directed towards (i) the exploration of the exclusive field of non-oxo vanadium(IV and V) complexes and (ii) the coordinating properties of simpler versions of the ligand H_3hidpa (**A** in Figure 4.10), which, from an inorganic chemist's point of view, is a derivative of hydroxylamine, NH_2OH .

Ligands stabilising the non-oxo vanadium(IV) centre are supposed to 'compensate' for the $\sigma + \pi$ donating ability of the oxo group otherwise characteristic in V^{IV} complexes, i.e. they have to be able to donate sufficient electron density (σ and π) to the metal. Alternatively, if a non-oxo V^{IV} centre is formed intermittently in a reaction course, such as the reaction sequence Equation (2.19) in Section 2.3, this may be intercepted by the ligand if the resulting complex is particularly stable (as in the case of amavadin; Table 4.3). Inositol derivatives (**7** in Figure 2.27) and benzoin (**8** in Figure 2.27) can form non-oxo vanadium(IV) complexes, and catecholates show a pronounced tendency to form non-oxo complexes; an example is **11** in Figure 2.28. More generally, multidentate ligands containing phenolate functions can stabilise non-oxo vanadium(IV). Figure 4.11 shows three examples, where phenolate coordinates along with amide (**1**),^[41a] azo-nitrogen (**2**)^[41b] and amine (**3**).^[41c] Complex **30** in Figure 2.31 is another example: here, the

coordination sphere is occupied by two phenolate-O, two thiophenolate-S and two neutral imine functions. The coordination geometry is slightly distorted octahedral (**3**), (distorted) trigonal prismatic (**1** and **2** in Figure 4.11, **11a** in Figure 2.28 or in-between these two situations (**30** in Figure 2.31). See also the coordination schemes **IIIa** vs **IIIa'** in Figure 2.21.

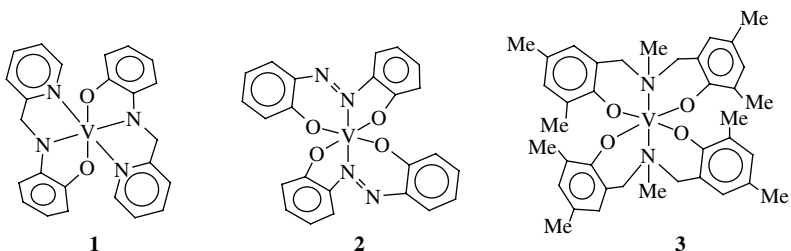
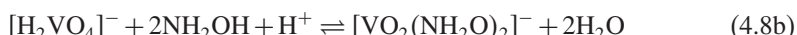
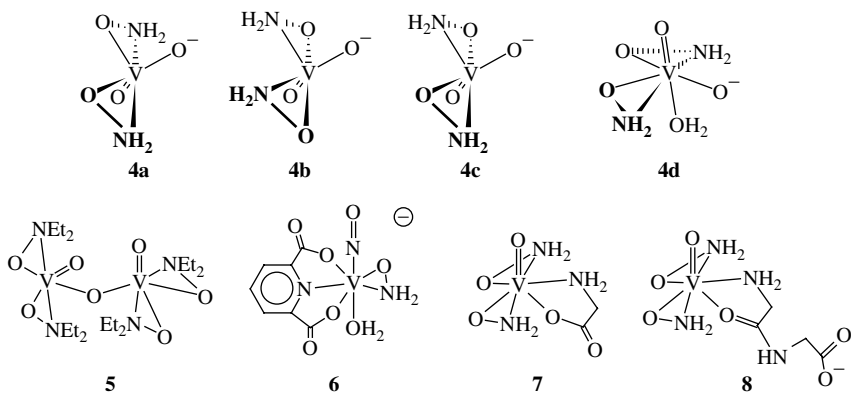


Figure 4.11

Non-oxo ('bare') vanadium(IV) complexes,^[41] modelling the non-oxo character of amavadin. For additional examples, see **11** in Figure 2.28 and **30** in Figure 2.31.

In all of these non-oxo complexes, the coordination number is 6. The unusual coordination number 8 in amavadin comes about by the side-on (η^2) coordination of the hydroxamido moieties, in addition to the coordination of the four carboxylate functions. The η^2 coordination mode of hydroamides($1-$) has already briefly been addressed in Section 2.1.2 in connection with more general aspects of the aqueous inorganic vanadium chemistry. Aqueous solutions of vanadate and hydroxylamines, NH_2OH , NHMeOH and NMe_2OH , undergo condensation reactions of the kind shown in Equations (4.8a) and (4.8b), i.e. they form vanadates in which one or two OH groups from the original orthovanadate are replaced by $\eta^2-\text{NR}_2\text{O}^-$. In the case of the bis(hydroxamido) species, several isomers have been shown, by ^{51}V NMR, to exist simultaneously in solution. Four of these isomers, **4a-d**, are depicted in Figure 4.12; the structure assignments follow suggestions by Tracey's group.^[42] A dinuclear species containing the $\{\text{VO}_2\mu-\text{O}\}$ core in the twist-angular conformation (cf. Figure 2.23), viz. compound **5** in Figure 4.12, has been structurally characterised.^[43] In water, this dinuclear complex is unstable. The complexes **6**, **7** and **8** in Figure 4.12 are examples of complexes containing, in addition to one or two hydroxamides, other ligands. In the anionic dipicolinato-nitrosyl complex **6**, which was structurally characterised as the caesium salt, vanadium is in a distorted pentagonal bipyramidal environment. Considering the nitrosyl ligand as NO^- , vanadium is formally in the oxidation state +III.^[44] Complexes **7** and **8** contain glycinate and glycyllglycinate as coligands. Whereas the former coordinates through the amine and the (monohapto) carboxylate, the latter employs, along with the amine terminus, the carbonyl oxygen of the peptide bond in chelation of vanadium,^[45] i.e. a coordination mode also observed, along with amide-N coordination, in other vanadate-dipeptide systems (see, e.g., Figures 2.15 and 2.18).



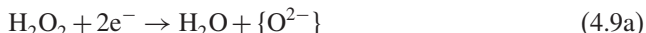
**Figure 4.12**

Hydroxamido complexes of vanadium(V) (**4**, **5**, **7**, **8**) and formally vanadium(III) (**6**). The ‘mixed anhydrides’ **4** are present in solution in equilibrium with vanadates. Complexes **5–8** have been structurally characterised.

4.3 Vanadate-dependent Haloperoxidases

4.3.1 History, Background and General Aspects

Peroxidases are oxidases or oxygenases acting on peroxide as electron acceptor. Equation (4.9a) represents the oxidase and Equation (4.9b) the oxygenase activity (AH is an inorganic or organic substrate). Three classes of peroxidases are usually distinguished: non-haeme peroxidases, haeme peroxidases (containing iron in a porphinogenic environment) and vanadate-dependent peroxidases. Whereas the last type were characterised only a quarter of a century ago,^[46] haeme and non-haeme peroxidases have a long-standing tradition. One of the most systematically studied enzymes, the haeme peroxidase from horseradish, has already been investigated thoroughly by Willstätter. In contrast to the haeme peroxidases, which are oxidatively deactivated by excess H₂O₂, the vanadate-dependent peroxidases, commonly termed vanadate-dependent haloperoxidases, VHPO, are surprisingly robust, i.e. they readily survive in excess H₂O₂ and in organic solvents, remain active even at temperatures as high as 70 °C and are insensitive to synchrotron radiation, properties which facilitate their isolation and characterisation. VHPOs are widely distributed, mainly in marine brown algae.



The historical background of peroxidases has been reviewed.^[47a] The existence of an enzyme (actually a haloperoxidase) in marine algae, capable of oxidising iodide to iodine, was established by Kylin in 1929. The enzyme was originally termed iodide oxidase, because it was thought to rely on oxygen as the electron acceptor. Later it was suggested that the oxidation of iodide was due to the combined action of a dehydrogenase and a haeme component. A few years earlier, in 1926, Sauvageau discovered free bromine in marine algae and found that the cells were able to brominate fluorescein to eosin (tetra-bromofluorescein). In 1966, Hager showed that a chloroperoxidase (a haeme peroxidase

containing ferriprotoporphyrin IX as prosthetic group) isolated from the fungus *Caldariomyces fumago* was able to introduce halogens, in the presence of H₂O₂, into a variety of organic compounds.^[47b]

Hans Vilter, who revealed the nature of the first representative of the large family of VHPOs, a bromoperoxidase (VBrPO) present in the marine brown alga *Ascophyllum nodosum*, described the history of his discovery in the following way:¹¹

'We were interested in antibiotics from marine organisms. Some of these are phlorotannins, and it was assumed that these tannins are polymerised due to the activity of peroxidases. There were available only a few, very preliminary, studies on peroxidases in seaweeds. The enzymes had been detected in crude extracts from the algae, but none of these enzymes had been purified, and no spectroscopy had been done. In those days, the general opinion was that peroxidases from higher plants were haeme-containing enzymes, and it was reasoned that peroxidases from seaweeds should be haeme-containing enzymes too, and that it was thus not worthwhile to waste time in their study. I thus intended to spend only a few weeks on this project, doing a rapid purification and demonstrating, using electron absorption spectroscopy,¹² that the algal peroxidase in fact is a haeme enzyme. I ran into several problems, however, and it turned out that the project lasted a couple of years. [. . .] During the early purification experiments, there was a partial loss of enzyme activity, although, when handling the enzyme preparations with a Hamilton syringe, an increase of activity was observed.¹³ Dialysing the enzyme preparations, using EDTA-containing citrate/phosphate buffers, yielded inactive preparations. This prompted me to study the effect of metal ions on the enzyme activity. This study eventually revealed that the apoenzyme could be reconstituted to the active holoenzyme with vanadate. There was no reconstitution of the activity with iron or other metal ions. The reactivation by vanadate was inhibited by phosphate, due to the structural similarity of phosphate and vanadate.'

The algal peroxidases are located in the transitional region between cortex and medulla of the cells forming the cell wall, which are particularly rigid in order to allow survival of the alga under the harsh conditions in the tidal zones, where the algae are subjected to tractive and shear forces. The rigidity of the thallus wall is due to cellulose fibres embedded in a matrix of phycocolloids such as alginates, hampering the isolation of the enzyme. In addition, tannins and (poly)phenols are abundant, which can modify proteins in the course of the separation processes from the bulk algal material. All these difficulties had finally been overcome,^[46c] although the isolation of the native enzyme is still an ongoing process. Depending on the source, about 100 mg of fully active enzyme can be recovered from 10 kg of finely chopped and freeze-dried algal material. Reactivation of the apoenzyme is slow, and complete reconstitution takes hours. For reconstitution, vanadium has to be present as vanadate(V); VO²⁺ is not taken up, and the reduced (VO²⁺ form of the holoenzyme is inactive. Vanadate concentrations to restore half-maximal reactivation are ca 35 nM, which is the vanadate concentration present in sea water.

¹¹ Slightly modified from Vilter's script prepared for a lecture on occasion of the 3rd International Symposium on the Chemistry and Biological Chemistry of Vanadium in Osaka, 2001, presented orally on behalf of Hans Vilter by the author of this book.

¹² The so-called Soret band, a strong absorption at ca 410 nm, is typical of haeme enzymes.

¹³ The cannulae of Hamilton syringes contain a vanadium-doped steel.

The enzyme shows typical absorption in the near-UV region at 310 nm, leaching out to about 360 nm, giving rise to a faint yellow colouration. The marine alga *A. nodosum*, also known as pig-weed or knobbed wreck, belongs to the division Phaeophyta (brown algae). It is widely spread across the tidal zones of rocky shores of the North Atlantic and Pacific. VHPOs are common among the brown algae, but have also been found sporadically in red algae (such as *Corallina pilulifera* and *Cor. officinalis*), in a green alga (*Halimeda* sp.), the fungi *Curvularia inaequalis*^[48a] and *Botrytis cinerea*^[48b] and in the terrestrial lichen *Xanthoria parietina*,^[49] a more or less rust-coloured leafy lichen growing on rocks, walls and tree bark, common in temperate zones. Some of the organisms mentioned here are illustrated in Figure 4.13.

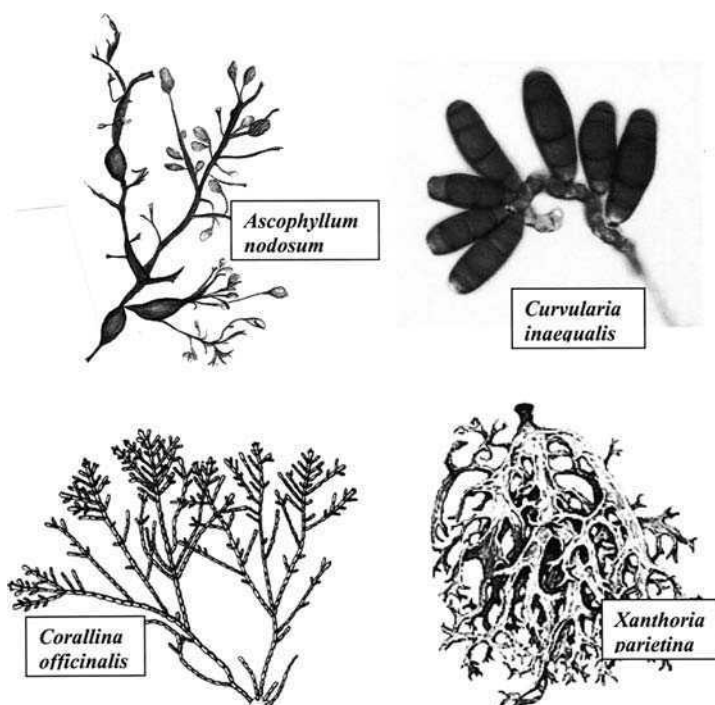


Figure 4.13

Organisms containing vanadate-dependent haloperoxidases. The enzymes from the algae *A. nodosum* and *Cor. officinalis* and the lichen *X. parietina* are bromoperoxidases, and the fungal enzyme (*Cur. inaequalis*, shown with sporangia) is a chloroperoxidase.

The concentration of the halides X^- in sea water is in the molar ($\text{Cl}^-, 0.55 \text{ M}$), millimolar ($\text{Br}^-, 0.8 \text{ mM}$) and the micromolar range ($\text{I}^-, 0.4 \mu\text{M}$). Hydrogen peroxide is formed in daylight, and its concentration in superficial sea water is micromolar. The basic reaction catalysed by the enzyme is the two-electron oxidation/oxygenation of halide X^- to an $\{X^+\}$ species, where $\{X^+\}$ is X_2 , X_3^- and/or XOH , i.e. hypohalous acid. The reaction is illustrated in Equation (4.10a) for the formation of hypobromous acid from bromide. In a successive step, hypohalous acid nonenzymatically halogenates organic substrates [Equation (4.10b)]. In the absence of substrate, singlet oxygen forms [Equation (4.10c)]. Depending on the substrate specificity, the enzymes are termed iodo-, bromo- or

chloroperoxidases. Iodoperoxidases (VIPO) can oxidise (or oxygenate) iodide only, bromoperoxidases (VBrPO) iodide and bromide. At sufficiently high chloride concentrations, the VBrPOs also show some chloroperoxidase activity. Chloroperoxidases (VCIPO) are able to oxidise all three halides, covering a surprising range of redox potentials, namely 0.53–1.36 V (vs NHE). The algal enzymes are iodo- or (mostly) bromoperoxidases and the fungal enzyme is a chloroperoxidase. The differing substrate specificities hint at different functions: the algae possibly use the halogenated compounds as a defence against epiphytes and endophytes. Apart from the direct bactericidal and fungicidal action, the hypohalous acid also prevents biofilm formation on the surface of the algae by destruction of bacterial communication signals. On the other hand, hypochlorous acid produced by the fungi *Cur. inaequalis* and *B. cinerea* (both are major plant pathogens) possibly allows access of the fungus to its ‘host’ by oxidative degradation of the plant cell walls.



A large variety of halogenated compounds in sea water going back to the activity of algal VHPOs have been detected, including complex compounds^[50] (for a selection, see Figure 4.14, **9–11**), but also basic compounds such as CHBr_3 (bromoform), CHBr_2Cl and CH_3I . Halomethanes contribute to the ozone degradation and thus to the global ozone balance. The amount of bromoform produced by marine algae constitutes some 10^4 tons per year and thus is comparable to the anthropogenic input.^[51]

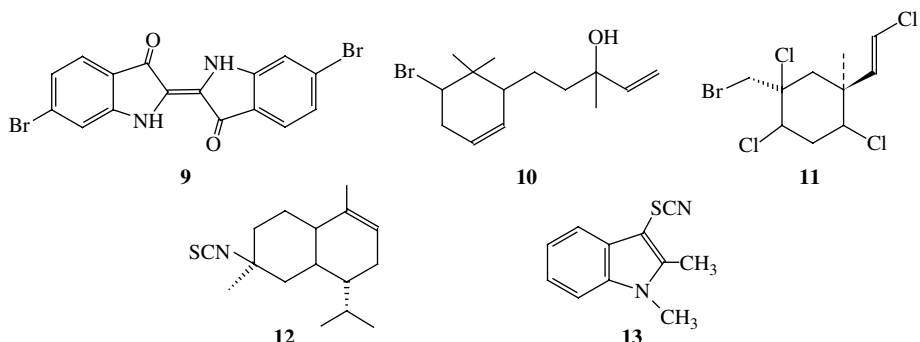


Figure 4.14

Examples for complex halogenated organic compounds found in marine environments. **9**, 6,6'-dibromoindigo; **10**, α -synderol; **11**, violacene.^[51] The organic thiocyanato derivative **12** is a marine natural product; compound **13** is a synthetic product generated in the $\text{VBrVO}-\text{SCN}^--\text{H}_2\text{O}_2-1,2$ -methylindole system.^[52]

VHPOs also accept the pseudohalides CN^- and SCN^- as alternative substrates, and even oxidise cyanide and thiocyanate preferentially to bromide.^[52] Thiocyanate is generated *in vivo* by thiosulfate sulfur transferase in the process of cyanide detoxification, and is present in concentrations comparable to that of bromide. Organic thiocyanato compounds have been discovered in marine environments (**12** in Figure 4.14, suggesting that their formation is also catalysed by, *inter alia*, VHPOs. Laboratory experiments have shown

that algal bromoperoxidases in fact catalyse, in the presence of H_2O_2 , the thiocyanation of organic substrates such as 1,2-dimethylindole (**13** in Figure 4.14). Another group of substrates for VHPOs are organic sulfides (thioethers) and disulfides. Prochiral sulfide is enantioselectively oxidised to chiral sulfoxide and some sulfone (below), a reaction of prime interest in organic synthesis and for pharmaceutical applications. Among additional substrates ‘accepted’ by VHPOs are indoles and monoterpenes (below). Instead of peroxide, peracids can be employed as an oxygen source in the oxygenation of bromide by VBrPO. In contrast, oxidation or singlet oxygen formation is not catalysed with alkyl hydroperoxides (ROOH) as a potential oxygen source, which otherwise can replace H_2O_2 in model reactions (see Section 4.3.3).

The pseudohalide azide N_3^- inhibits VCIPO. The first structurally characterised VHPO had in fact been crystallised in its azide-inhibited form. Inhibition has also been noted with hydroxylamine and hydrazine. Further, structural analogues of vanadate, such as $[\text{AlF}_4]^-$ and phosphate, are potent inhibitors. In turn, vanadate inhibits many phosphatases (and other phosphate-metabolising enzymes). On the other hand, apo-VHPOs can exhibit some phosphatase activity, and vanadate-inhibited phosphatases show some haloperoxidase activity. These phenomena will be discussed in Section 5.2.1.

The ability of vanadate-dependent haloperoxidases to catalyse the introduction of halogens at specific sites of organic acceptor molecules has prompted investigations into the use of these enzymes (and vanadium complexes modelling their active site) in organic syntheses. This field of application, and the potential use of VHPOs as anti-fouling agents in, e.g., marine paints, has initiated investigations into the directed evolution of mutants of the VCIPO from *Cur. inaequalis* by site-directed mutagenesis,^[53] in particular with respect to an increase in the activity in the slightly alkaline range (the activity maximum of the native VHPOs lies in the mildly acidic range). In the case of *Cur. inaequalis*, this task has considerably been facilitated by the successful expression of the enzyme in *Escherichia coli*^[53b] and beer yeast, *Saccharomyces cerevisiae*. A dramatic increase in activity, by a factor of 100, has been achieved for the triple mutant P395D/L241V/T343A, where the notation P395D stands for the exchange of proline (position no. 395 in the amino acid sequence) in the native enzyme for aspartate (D in the one-letter code) in the mutant.^[14] In Table 4.4, activity characteristics for the native enzymes from *A. nodosum*

Table 4.4 Kinetic and thermodynamic characteristics for the oxidation of bromide catalysed by wild-type VHPOs and a mutant (ref. 53).^a

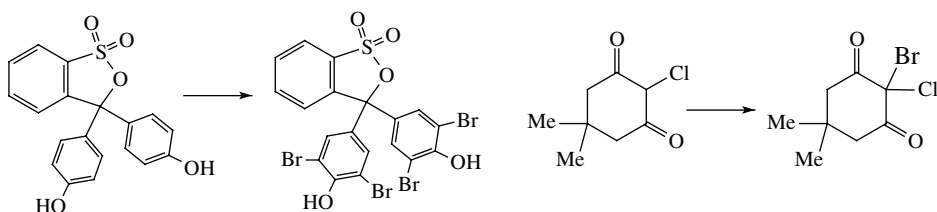
Enzyme	$k_{\text{cat}}(0.5\text{mMBr}^-)$, pH 5 (s ⁻¹)	$k_{\text{cat}}(1\text{mMBr}^-)$, pH 8 (s ⁻¹)	$k_{\text{cat}}(100\text{mMBr}^-)$, pH 8 (s ⁻¹)	$K_M(\text{Br}^-)$, pH 8 (mM)	$K_M(\text{H}_2\text{O}_2)$, pH 8 (μM)
VBrPO		5	50	16	22
VCIPO (wild type)	100	1	1	0.12	<5
VCIPO mutant ^b	575	40	100	3.1	16

^a k_{cat} is the rate constant for the catalytically conducted bromination of monochlordimedone; cf. Scheme 4.3, right. K_M is the Michaelis constant (a measure of the affinity of the enzyme to its substrate).

^b See text.

¹⁴ L = leucine, V = valine, T = threonine and A = alanine.

and *Cur. inaequalis* and its triple mutant are contrasted. Activity data are usually collected on the basis of an assay based on the bromination of phenol red to bromophenol blue or, more conveniently, monochlorodimedone to its brominated derivative (Scheme 4.3, left and right, respectively).



Scheme 4.3

4.3.2 Structural and Catalytic Features

Single-crystal X-ray structures are available for the enzymes isolated from *A. nodosum* (holoenzyme),^[54] *Cur. inaequalis* (apoenzyme and tungstate variant,^[55a] sulfate variant,^[55b] azide form of the holoenzyme^[55c] and the native holoenzyme plus its peroxy form^[55d]), *Cor. officinalis* (phosphate variant) and *Cor. pilulifera* (phosphate variant).^[56] The *Cor. pilulifera* peroxidase also contains a structural Ca^{2+} ion. The enzymes from the red algae are hexamers of dimers with 595 amino acids per monomeric subunit, the

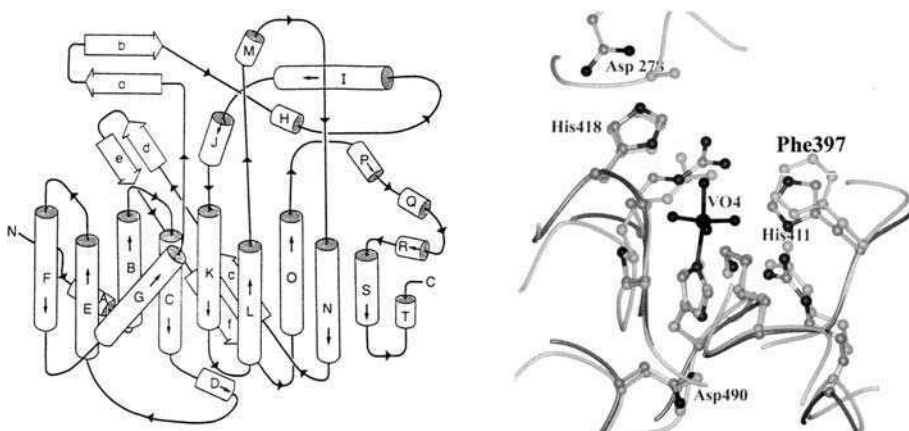


Figure 4.15

Left: schematic representation of the build-up of the chloroperoxidase from *Cur. inaequalis*. Helices are drawn as cylinders and β -strands as broad arrows. The C and N termini are indicated.^[55c] Reproduced from A. Messerschmidt and R. Wever, *Proc. Natl. Acad. Sci. USA* 93, 392–396. Copyright (1996), with permission from the National Academy of Sciences, USA. Right: superposition of the active sites of the algal (*A. nodosum*) bromoperoxidase (dark) and the fungal (*Cur. inaequalis*) chloroperoxidase (light).^[54] Reproduced from M. Weyand *et al.*, *J. Mol. Biol.* 293, 595–611. Copyright (1999), with permission from Elsevier.

A. nodosum enzyme is a homodimer (551 amino acids) and the *Cur. inaequalis* enzyme is a monomer constituting 609 amino acids. The tertiary structures are dominated by helical elements, arranged in bundles of four helices. Figure 4.15 (left) provides a schematic view of the fungal VClPO. The dodecameric VBrPO from *Cor. officinalis* attains cubic symmetry, with each of the faces of the cube occupied by a dimer. This arrangement leaves a cavity of 26 Å in diameter; the outer diameter of the protein amounts to 150 Å. The monomeric *Cur. inaequalis* enzyme has a cylindrical shape with the dimensions 80 × 55 Å.

The overall amino acid homology between the three types of haloperoxidases is comparatively low: there is 33% identity between the *A. nodosum* and *Cor. officinalis* enzymes and 21.5% identity between the *A. nodosum* and the *Cur. inaequalis* enzymes. There is, however, close homology in the active site regions. In the algal bromoperoxidases, the active site is situated at the bottom of a substrate cleft or funnel, 20 Å deep and 14 Å wide in the case of *Cor. officinalis*, and 15 Å deep and 12 (entrance) to 8 Å (bottom) wide in the case of *A. nodosum*. The inside of the funnel is lined by hydrophilic and hydrophobic amino acids, allowing, in principle, access of a broad variety of substrates.

In all of the VHPOs, the prosthetic group vanadate (H_2VO_4^-) is bonded to the protein via the Nε of a histidine ('proximal histidine'). In contrast, neither phosphate, tungststate or molybdate in the correspondingly reconstituted forms of the enzymes form a covalent bond to histidine. Vanadium is in the centre of a slightly distorted trigonal bipyramidal. The second axial position is occupied by an OH group, the three equatorial positions by OH, O⁻ and a doubly bonded oxo group, as shown in Figure 4.16 for the *A. nodosum* (a) and *Cur. inaequalis* (b) enzymes. The vanadate centre is further in

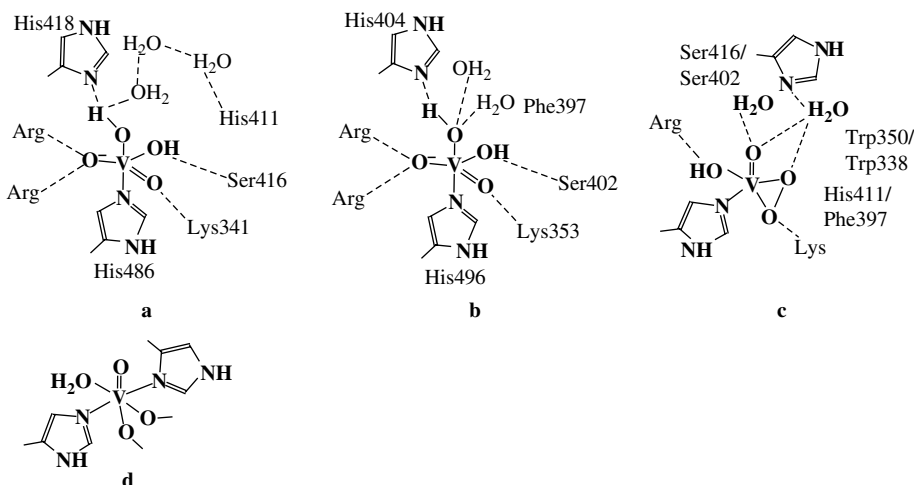


Figure 4.16

The active sites of the bromoperoxidase from *A. nodosum* (a), the chloroperoxidase from *Cur. inaequalis* (b) and its peroxy form (c). In (c), amino acids proposed to play a role in the activation of peroxide are indicated. Tryptophan (Trp350/Trp338) is replaced by arginine (Arg395) in the bromoperoxidase from the red alga *Cor. officinalis*. The structure in (d) is based on XAS and EPR data for the reduced, inactive form of the *A. nodosum* enzyme. See Table 4.5 for structure parameters and references.

contact with a couple of amino acid side-chains at the active site through salt bridges (arginine) and, mainly, hydrogen bonds. In particular, the axial hydroxo group bridges to a ‘distal histidine’ (His418 and His404, respectively) plus water through hydrogen bonding interactions. Selected bond lengths for covalent and noncovalent interactions are listed in Table 4.5 for the VBrPO from *A. nodosum* and the VCIPo from *Cur. inaequalis*.

Table 4.5 Selected bond lengths (in Å) for vanadate-dependent peroxidases from single crystal X-ray diffraction analysis (XRD) and X-ray absorption spectroscopy (XAS). See Figure 4.16a–d for structure representations and numbering of the amino acids.

	<i>A. nodosum</i> (a), XRD ^[54]	Reduced <i>A. nodosum</i> . (d), XAS ^[58]	<i>Cur. inaequalis</i> (b), XRD ^[55d]	Peroxo form of <i>Cur. inaequalis</i> (c), XRD ^[55d]
V–O _{ax}	1.77 ^a	1.63 (1O)	1.93	1.86 (pseudoaxial peroxy-O)
V–O _{eq}	1.54–1.60 ^a	1.91 (3O)	~ 1.65	1.89 (peroxy-O) 1.60 and 1.93
V–N	2.11 ^a	2.11 (2N)	1.96	2.19
His418/404	3.07, 3.11		2.97	Not bonded to {VO ₄ N}
Lys341/353	2.87		3.19	2.67
Ser416/402	2.86, 2.67		2.79	2.90
Arg	2.93–3.28		2.98–3.03	2.77–3.03
H ₂ O			2.59, 2.92	3.01, 3.03

^aThe d(V – O/N) values obtained from XAS of the enzyme + bromide at pH 8 are 1.62 (1O) and 1.72–2.07 Å (3O + 1N).^[57b]

The similar arrangement within the active centres of the algal and the fungal peroxidases is also demonstrated by the superposition of the active site structures in Figure 4.15 (right). The two sites are close to congruent. The main difference is the exchange of hydrophilic histidine (His411) in the bromoperoxidase for hydrophobic phenylalanine (Phe397) in chloroperoxidase. Apparently, this difference makes up for the differing substrate specificities of the two enzymes, i.e. the fact that chloride is oxidised by the fungal but not (at ambient chloride concentration) by the algal peroxidases.

Dithionite reduction of the VHPOs generates the reduced V^{IV} forms, which are inactive. This deactivation on reduction goes along with an apparently irreversible structure change. According to XAS^[58] (Table 4.5 and EPR studies,^[59] the vanadium centre in the reduced form is in a square pyramidal or (more likely) octahedral coordination environment (structure **d** in Figure 4.16). The coordination sphere is formed by a doubly bonded oxo group, two nitrogens (almost certainly stemming from histidines), and two to three oxygen functions. Candidates for the oxygen-functional ligands are serinate, aspartate and water. The EPR spectroscopic hyperfine coupling constants change with pH, indicating that changes in pH give rise to a change in the coordination environment:

$$\begin{array}{lll} \text{pH}8.4 : & A_{||} = 160.1 & A_{\perp} = 50.2 \times 10^{-4} \text{ cm}^{-1} \\ \text{pH}4.2 : & A_{||} = 167.5 & A_{\perp} = 55.1 \times 10^{-4} \text{ cm}^{-1} \end{array}$$

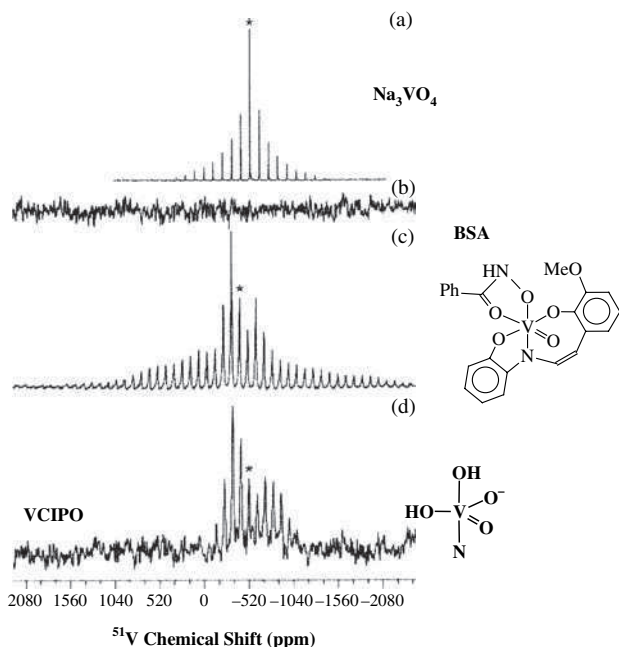
A possible explanation is a reorientation of one of the imidazole moieties (from parallel to perpendicular with respect to the V=O vector) on acidification (cf. Figure 3.11 in Section 3.3). Alternatively, protonation of one of the ligands at lower pH may take place.

The $pK_a = 5.4$ obtained from an EPR titration favours protonation of a histidine or carboxylate. The presence of a water ligand is strongly supported by a decrease in the linewidths of the hyperfine components in the EPR, as H_2O is exchanged for D_2O , and an increase in the linewidths on dissolving the reduced enzyme in $H_2^{17}O$.^[59a] As outlined in Section 3.3, one of the factors influencing EPR linewidths is unresolved superhyperfine coupling of the paramagnetic metal centre with magnetic nuclei such as 1H , 2H , ^{14}N and ^{17}O . This interaction is sufficiently less pronounced for deuterium than for protium, and particularly effective if nonmagnetic ^{16}O is substituted for the quadrupolar ^{17}O . The presence of water is further supported by ESEEM (electron spin-echo envelope modulation; Section 3.3.4; investigations which show an intense and characteristic 1H modulation on the central EPR line at 13.8 MHz (magnetic field $B_0 = 0.324\text{ T}$).^[59b] In addition, ESEEM revealed the presence of nitrogen in the coordination sphere through four ^{14}N transitions at 3.1, 4.2, 5.3 and 8.1 MHz, very much in accord with model compounds containing imidazole-based ligands in a VO^{2+} complex, such as **14** in Figure 4.20 in the following section.^[59c]

On coordination of the oxidant peroxide to the vanadium centre in the native enzyme, the geometry changes from trigonal bipyramidal to a structural arrangement in-between trigonal bipyramidal and square pyramidal (**c** in Figure 4.16). Structural data are given in Table 4.5. As will be detailed below, the active species in halide oxidation is probably a hydroperoxo intermediate, and lysine possibly acts as a mediator for protonation of the coordinated and thus activated peroxide. As far as the delivery of the halide is concerned, tryptophan (Trp350/338) and histidine (His411)/phenylalanine (Phe397) have been proposed to impart the transport of Br^-/Cl^- to the peroxy ligand in the *A. nodosum* VBrPO and *Cur. inaequalis* VCIPO, respectively. In the *Cor. officinalis* VBrPO, where Trp350 is replaced by Arg395, this arginine should be involved. Alternatively, or additionally, serine or histidine may come in as a halide director. Evidence for this assumption comes from bromine and vanadium K-edge EXAFS studies of bromide binding to the *A. nodosum* peroxidase.^[57a] The Br-EXAFS revealed a first bromine shell corresponding to light scatterers (such as carbon, nitrogen or oxygen) at a distance of 1.88 \AA , corresponding to a covalent bond between bromine and the light scatterer, and a second shell at 2.89 \AA , again representing light scatterers. In the V-EXAFS,^[57b] a shell at 4.1 \AA was modelled with bromine. Direct bonding of bromide to vanadium could therefore definitely be ruled out by this study. In an X-ray diffraction study on *Cor. pilulifera* soaked with bromide, a V–Br distance of 3.6 \AA was found.¹⁵

The presence of two OH groups (one axial and one equatorial), and hence of H_2VO_4^- in the active centre, cannot unambiguously be concluded from X-ray diffraction data. Convincing proof has been provided by a combination of quantum mechanical density functional theory (DFT) calculations combined with solid-state ^{51}V NMR measurements [under magic angle spinning (MAS) conditions] on the resting state of the *Cur. inaequalis* peroxidase.^[60] Figure 4.17 illustrates NMR spectra and Table 4.6 provides a comparison of the experimental NMR parameters and those obtained from DFT calculations on the best (and most reasonable) model. The chemical shift $\delta(^{51}\text{V}) \approx -520\text{ ppm}$ is in the range expected for vanadate attached to a nitrogen-functional ligand. The considerably more

¹⁵ J. A. Littlechild, University of Exeter, personal communication.

**Figure 4.17**

MAS ^{51}V spectra (14.1 T) of recombinant *Cur. inaequalis* VCIPO (bottom trace, with the best model for the vanadium environment indicated). For comparison, the solid-state NMR spectra of a model compound (centre), sodium orthovanadate (top) and bovine serum albumin [BSA, trace (b)] are also shown. An asterisk indicates the isotropic peak. Reproduced from N. Pooransingh-Margolis *et al.*, *J. Am. Chem. Soc.* 128, 5190–5208. Copyright (2006), with permission from the American Chemical Society.

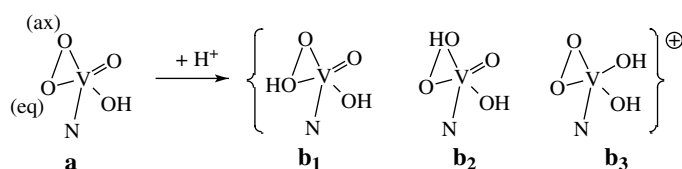
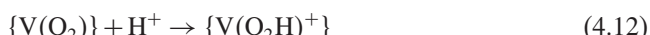
Table 4.6 Experimental and calculated (for the best model; inset in the bottom trace of Figure 4.17) MAS NMR data for the *Cur. inaequalis* chloroperoxidase.^[59] For the meaning of the NMR parameters, see Section 3.1.4.

	Quadrupole coupling constant C_Q (MHz)	Asymmetry parameter η_Q	Chemical shift δ_σ
Experimental	10.5(1.5)	0.55(0.15)	-520(13)
Calculated (DFT)	11.3	0.44	-568

effective shielding of the ^{51}V nucleus in the *A. nodosum* bromoperoxidase, -931 ppm,^[61] remains to be explained.

The consumption of protons in the conversion of halide to hypohalous acid, [Equation (4.10a)], and the fact that protons are needed as a co-catalyst in the oxygenation of sulfides to sulfoxides [Equation (4.11)] is suggestive of an essential role of protonation in the activation of the peroxy form of the haloperoxidases; [Equation (4.12)]. For the peroxy form, the best agreement between calculations and structural data is obtained for a strongly distorted trigonal bipyramidal, with the Ne of the imidazole moiety in the axial and one of the peroxy oxygens in the pseudoaxial position (**a** in Scheme 4.4).^[62] Protonation can occur on the pseudoaxial or the equatorial peroxy oxygen, or on the second

equatorial oxo group (**b**₁–**b**₃ in Scheme 4.4). All three possibilities are energetically about alike. Substrate (halide or sulfide) binding does not *directly* involve, according to DFT calculation, a protonated site. Since attack of the substrate (modelled by Br[−] and SMe₂) is clearly favoured at the pseudoaxial peroxy oxygen, the intermediate **b**₁ in Scheme 4.4 is the most likely candidate in catalytic turnover. The various successive steps in bromide and sulfide oxygenation are summarised in the catalytic cycles depicted in Figure 4.18. Evidence has been provided that the formation of hypobromous acid can also involve a hypobromito intermediate.^[63]



Scheme 4.4

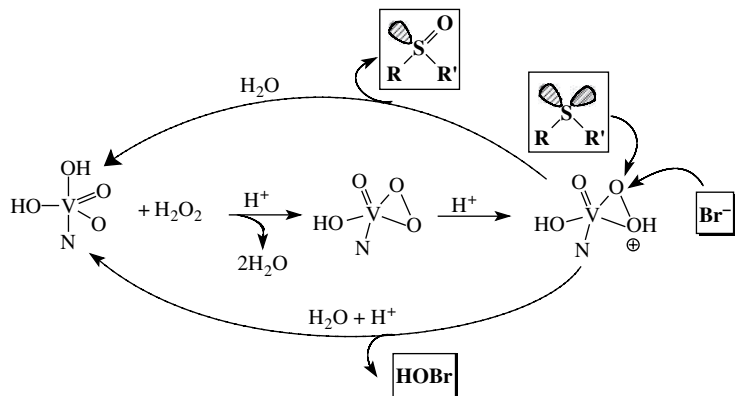


Figure 4.18

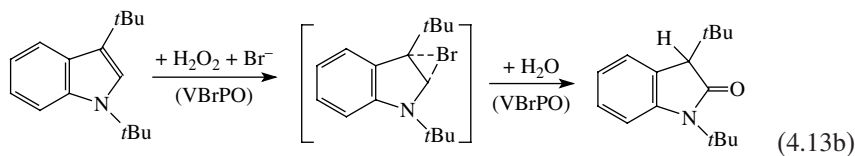
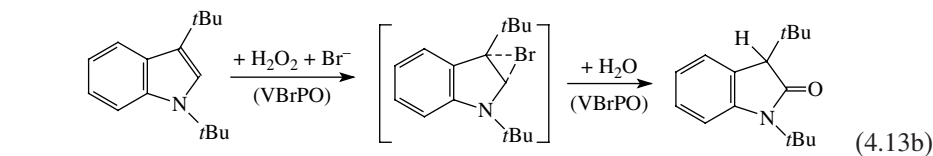
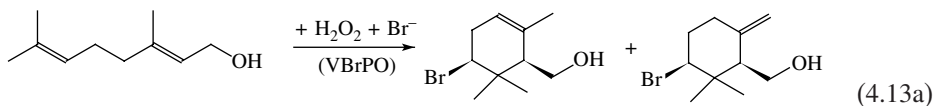
Activation of peroxide through formation of a peroxy and hydroperoxy intermediate (centre), and catalysis of the oxygenation of bromide (bottom) and sulfide (top). In both reaction paths, a hydroperoxy complex is the active catalyst and oxygen transfer occurs through direct attack of the substrate to the nonprotonated peroxy oxygen (Scheme 4.4^[62], and Scheme 4.9).

As mentioned above, sulfides are also substrates for the VBrPOs. Scheme 4.5 summarises selected results obtained by oxidation of prochiral sulfides with H₂O₂ in mixtures of water and alcohol. Yields and enantiomeric excess (e.e.) are subject to large variations, depending on the source of the bromoperoxidase (*Cor. officinalis* vs *A. nodosum*) and

the nature of the sulfide.^[64] Since the active centre itself is achiral, the chiral induction is indicative of intermittent substrate binding to the multi-chiral active site pocket. Terpenes, terpene analogues and indoles undergo oxidative cyclisation in the presence of H₂O₂ and bromide, catalysed by the bromoperoxidases form *A. nodosum* or *Cor. officinalis*.^[65] The bromoperoxidative cyclisation of geraniol shown in Equation (4.13a) is an illustrative example. The respective oxidation of 1,3-di-*tert*-butylindole to the indolinone, Equation (4.13b), is of particular interest since this reaction is regiospecific. The presence of bromide is indispensable, suggesting the intermediate formation of a {Br⁺} species which electrophilically attacks the double bond in the pyrrole moiety of the indole derivative.

	<i>Cor. offic.</i>	<i>A. nodosum</i>	<i>Cor. offic.</i>	<i>A. nodosum</i>	<i>Cor. offic.</i>	<i>Cor. offic.</i>
Yield / %	7	ca. 95	57	90	76	99
e.e. / %	-	96	11	6	93	90
Configuration		R	S	R	S	S

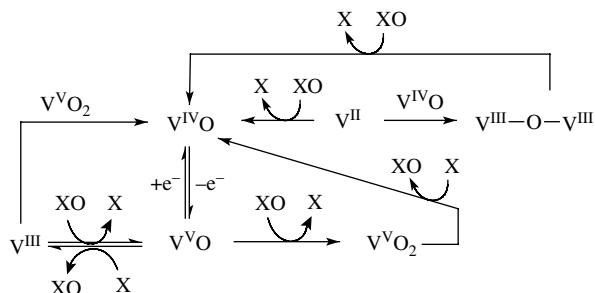
Scheme 4.5



4.3.3 Model Chemistry

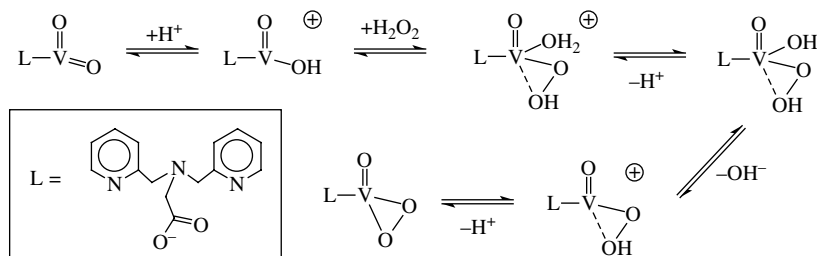
Basically, vanadium is an efficient mediator of oxo transfer reactions accompanied by reduction/oxidation processes. Equation (2.19) in Section 2.3, related to the oxidation of thiolate, is a specific example where oxo and non-oxo vanadium are involved in a catalytic cycle. More generally, selected vanadium-mediated oxo transfer reactions from or to a substrate, and involving the vanadium oxidation states +II to +V, can be summarised as depicted in Scheme 4.6,^[66] where X can be dimethyl sulfide, iodobenzene, triphenylphosphine and other substrates.

In the vanadate-dependent haloperoxidases, an oxo group of the vanadate centre is exchanged for peroxide prior to oxo transfer, referred to as an activation of peroxide, and oxo transfer to a substrate such as halide or R₂S is afforded by nucleophilic attack of the substrate to the activated (hydro)peroxide as shown in Figure 4.18. Generally, peroxovanadium complexes can thus be considered to model the active catalytic site in the haloperoxidases. A mechanism for the peroxovanadium complex formation as depicted in Equation (4.14), proposed by Pecoraro and co-workers^[67] on the basis of



Scheme 4.6

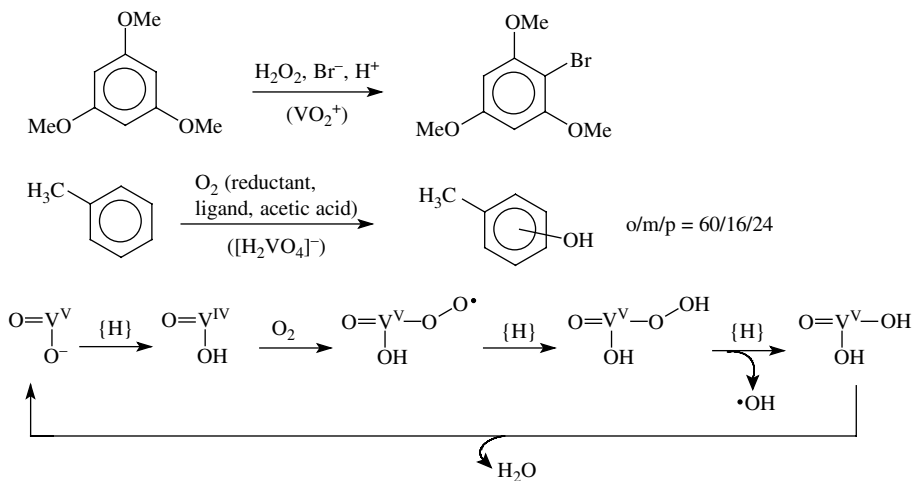
kinetic investigations, is shown in Scheme 4.7. An associative mechanism is suggested, in which peroxide binds to a protonated form $\text{VO}(\text{OH})\text{L}$ of a vanadium model complex VO_2L , followed by the loss of hydroxide (or water) as the rate-determining step.



Scheme 4.7

The simplest conceivable models are the dioxovanadium cation $\text{VO}_2^+ \{ = [\text{VO}_2(\text{H}_2\text{O})_4]^+ \}$ at $\text{pH} \approx 2$ and below, and vanadate ($[\text{H}_2\text{VO}_4]^-$ at $\text{pH} \approx 7$; $[\text{HVO}_4]^{2-}$ at $\text{pH} \approx 9$). VO_2^+ catalyses the monobromination of 1,3,5-trimethoxybenzene in the presence of bromide and hydrogen peroxide (Figure 4.19, top) under strongly acidic and hence non-physiological conditions.^[68] The turnover numbers are, however, orders of magnitude lower than in the corresponding bromination by *A. nodosum* bromoperoxidase, viz. 15 mol of brominated compound per mole of catalyst per hour for VO_2^+ at $\text{pH} < 3$ vs 4.7×10^5 for the enzyme at a pH optimum of ca 6. As in the case of the enzymatic pathway, singlet oxygen forms in the absence of the substrate.

The formation of superoxo and hydroperoxo intermediates has been suggested for the hydroxylation of aromatic hydrocarbons such as toluene, catalysed by vanadate (in the form of $[\text{Bu}_4\text{N}]^+[\text{H}_2\text{VO}_4]$) under aerobic conditions in acetonitrile-acetic acid; (Figure 4.19, centre).^[69] A primary reductant, ascorbic acid or zinc, is necessary for the intermediate formation of oxovanadium(IV), which is the virtual activator of oxygen. In addition, an N-donating ligand, pyridine or pyrazine-2-carboxylic acid, has to be added. Apparently, this ligand stabilises the intermediate vanadium species very much in the manner in which vanadate is stabilised by the proximal histidine in the VHPOs.

**Figure 4.19**

Oxidation reactions catalysed by simple vanadium catalysts. Top: oxidative bromination of trimethoxybenzene catalysed by dioxovanadium(V) in strongly acidic solution.^[67] Centre: oxidation of toluene by oxygen, catalysed by vanadate in the presence of a ligand, e.g. ascorbic acid and pyridine. All three isomeric cresols are formed.^[68] Bottom: the reaction sequence for the formation of hydroxyl radicals, supposedly the actual oxidant; modified from the respective scheme provided in ref. 68.

A reaction sequence, based on ref. 68, delivering a hydroxyl radical as the actual oxidant, is proposed in Figure 4.19, (bottom).

In modelling active centres of metalloenzymes, one commonly distinguishes between structural and functional models. Structural models are those which are good ‘copies’ of the active centre with respect to the nature of the ligand functions, the arrangement of the ligand set and the spectroscopic properties. Functional models, on the other hand, mimic the native reaction catalysed by the enzyme. Functional models may or may not be good replicas of the actual build-up of the active centre. If they are, i.e. in cases where function *and* structure are reproduced by the model compound, the synthetic mimic is considered to be a good overall model. But even then, two limiting cases can be considered: in case 1, the model system allows reproduction of the enzymatic reaction, but is consumed in the course of reaction, i.e. the model takes part in a stoichiometrically conducted reaction; in case 2, the model system actually catalyses the reaction. The truth often lies in-between, i.e. the ‘good model’ survives a couple of turnovers before it is consumed in side-reactions. In certain (rare) instances it is possible to reconstitute the ‘catalyst’, e.g. electrochemically, in a secondary process coupled to the basic reaction.

In this part of the section on the model chemistry of haloperoxidases, the following scenarios will be addressed:

1. structural models of the reduced enzyme;
2. peroxyvanadium complexes;
3. structural and functional models of the native enzymes, including applications in organic synthesis;
4. hydrogen bonding and supramolecular features.

4.3.3.1 Structural Models of Reduced Haloperoxidases

In the reduced, inactive VHPOs, the oxovanadium(IV) centre is coordinated to four to five light ligand functions, two of which supposedly are the aromatic imidazolyl nitrogens of two histidines in the active site pocket. As far as electronic properties are concerned, the imine nitrogen in Schiff bases is comparable to the imidazolyl-N (depending, however, on the orientation of the imidazolyl ring with respect to the V=O axis; see Section 3.3), and complexes with either ligand function coordinated to the VO^{2+} core can be considered suitable structural models. Examples, depicted in Figure 4.20, encompass the coordination of two imidazoles along with two carboxylates (**14**)^[59c] imidazole + Schiff base N (along with phenolate, carbonyl-O and enolate; **15**)^[70a] and two Schiff base N (plus two phenolates; the dichiral complex **16**).^[70b] The structure of **16** is in-between a trigonal bipyramidal and square pyramid; the τ parameter, defined in Scheme 2.1 (Chapter 2), is 0.43. All three complexes exhibit structural and/or EPR parameters also found for the reduced enzyme. Of particular interest is the comparability of the ^{14}N ESEEM features of **14** and reduced VHPO. As outlined in Section 4.3.2, the EPR parameters of reduced VHPO are pH dependent, suggesting the release of one of the ligands by protonation at lower pH. This trend is modelled by the complexes **17a** (high-pH form) and **17b** (low-pH form) in Figure 4.20,^[70a] with hyperfine coupling constants well in agreement with those found for reduced VHPO:

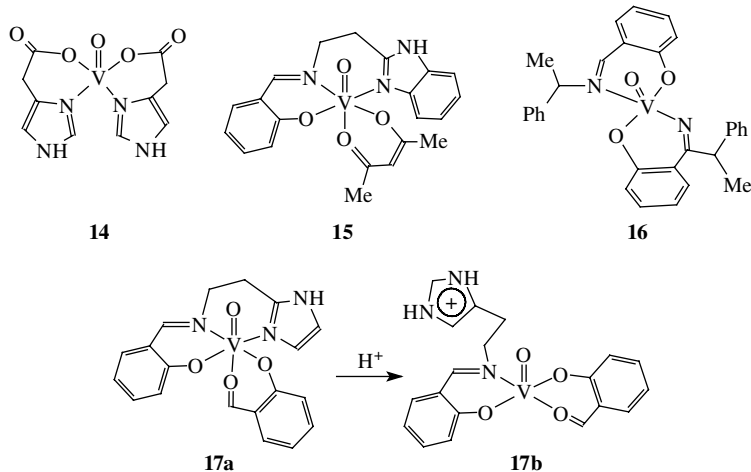
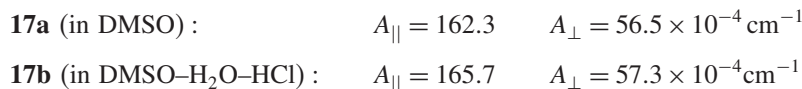


Figure 4.20

Complexes which model structural and spectroscopic features of the reduced (VO^{2+}) form of vanadate-dependent haloperoxidases.

4.3.3.2 Peroxovanadium Complexes

Although peroxovanadium complexes are abundant, none actually structurally models the active centre of the peroxy form of the structurally characterised chloroperoxidase from the

fungus *Cur. inaequalis* (**c** in Figure 4.16), which is a monoperoxo complex with coordination number 5 and displays a distorted square-pyramidal arrangement of the O_4N ligand set. The majority of synthetic peroxyvanadium complexes attain the coordination number 7 in pentagonal bipyramidal geometry, and the ligand set either without any nitrogen or more than one nitrogen. Typical pentagonal bipyramidal monoperoxo complexes with just one nitrogen donor are the mixed picolinato–oxalato complex **18**^[71] and the ethanolamine–diacetato complex **19**^[72] in Figure 4.21. The dipicolinato complex **20** has a labile water ligand in one of the axial positions and may therefore be considered to approach coordination number 6 in a pentagonal pyramid arrangement.^[73] This also applies to the iminodiacetato complex **21**,^[74] in which a carboxylate oxygen group from a neighbouring molecule occupies a seventh position (*trans* to the doubly bonded oxo group). Two aqua ligands are contained in the picolinato complex **22**, one *trans* to the oxo group [at a distance $d(V-O) = 2.307 \text{ \AA}$ and thus labilised] and the other in the equatorial plane with $d(V-O) = 2.046 \text{ \AA}$.^[75] A genuine pentagonal pyramidal case is represented by the imidazole–bis(peroxo) complex **23**.^[76] The coordination number 5 finally is realised in the peroxy–bis(silanolato) complex **24**,^[77] which attains the geometry of a rhombic pyramid. Distances $d(V-O_{\text{peroxide}})$ are typically between 1.78 and 1.93 \AA , clustering around 1.87 \AA , and the coordination of the peroxy group is essentially symmetric, with a $d(O-O)$ of or close to 1.44 \AA .

For complexes such as **18** in Figure 4.21, with one peroxy group (in the pseudo-pentagonal plane) and two bidentate donor ligands, the following two ‘rules’ (following Schwendt and Sivák^[71]) can be noted. (i) The ligand carrying the higher charge (L^1) occupies equatorial sites, the ligand with the lower charge (L^2) equatorial + axial positions. L^2 can be neutral (e.g. bipyridyl or picolylamide) and L^1 monoanionic (e.g. picolinate), or L^2 can be monoanionic and L^1 dianionic (e.g. oxalate). (ii) If L^2 (the ligand occupying equatorial + axial positions) has an O and N donor function, the oxygen goes into the axial position, e.g. the carboxylate-O of picolinate(1–), or the carbonyl-O of picolylamide.

The speciation in the aqueous system containing vanadate, H_2O_2 and L-alanyl-L-histidine (ala-his) as a ligand modelling the VHPOs’ active site histidine (see also Figure 2.15) has

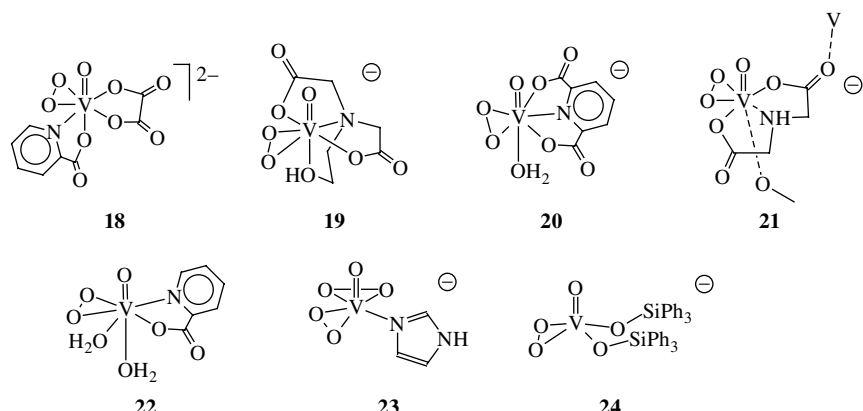
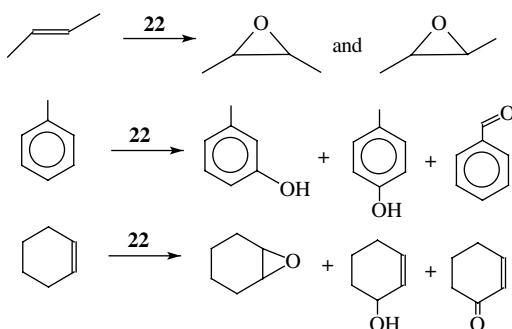


Figure 4.21

Examples of peroxyvanadates stabilised by ligands containing one *N*-function and a variable number of *O*-donors. The selection of complexes shown here has been carried out so as to approach as closely as possible the active centre in the peroxy form of the *Cur. officinalis* chloroperoxidase, $\{VO(OH)(O_2)N\}$ (Figure 4.16c).

been exhaustively investigated by a combination of ^{51}V NMR and H^+ -potentiometry.^[78] This investigation has revealed the presence of eight neutral and anionic ternary (vanadate-peroxo-ala-his) complexes containing one or two peroxo ligands and one ala-his, the latter coordinated via the histidine- $\text{N}\varepsilon$, as shown for $\{\text{V}(\text{O}_2)_2(\text{ala-his})\}^-$ in Figure 2.15.

Despite the fact that synthetic peroxovanadium complexes do not model satisfactorily the active centre of the VHPOs in the sense outlined above, most of them are effective oxidants under mild conditions, or even catalysts for, or active intermediates in the catalysis of, oxygenation reactions using hydrogen peroxide as the oxo transfer agent.^[63] Examples of oxo transfer reactions to organic substrates carried out via peroxovanadium complexes – the hydroxylation of alkanes, alkenes and aromatic compounds by the picolinato complex **22** (Figure 4.21) – are depicted in Scheme 4.8.



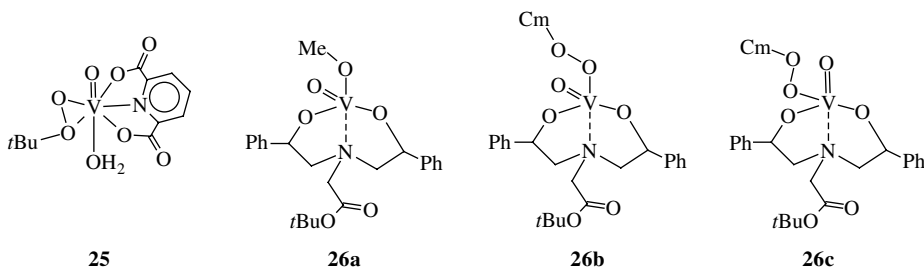
Scheme 4.8

For complex **22**, see Figure 4.21.

In nonprotic solvents, organic hydroperoxides RO_2H can be more efficient oxidants – again mediated by vanadium – than H_2O_2 . The structurally characterised neutral *tert*-butylperoxo complex **25** in Figure 4.22 exhibits the same general features^[79] as the anionic peroxo complex **20** in Figure 4.21, with the exception that the coordination mode of the organic peroxo ligand $t\text{BuO}_2^-$ is slightly asymmetric: the bond lengths to the peroxo oxygens are $d(\text{V}-\text{O}) = 1.872$ and $d(\text{V}-\text{O}t\text{Bu}) = 1.999 \text{ \AA}$. In sulfoxidation reactions with cumyl hydroperoxide CmO_2H , catalysed by the trigonal bipyramidal complex **26a** (Figure 4.22), a close model of the active site of the VHPOs, peroxo intermediates have been shown by ^{51}V NMR to be the active oxo transfer species. In these peroxo complexes, which form by substitution of the axial methoxo group in **26a** by CmO_2^- , DFT calculations suggest that the peroxo ligand coordinates in an end-on rather than a side-on fashion, **26b** and **26c**.^[80] The variant with the peroxide in the axial position (**26b**) is more stable than that with the peroxide in the equatorial position (**26c**) by 17.6 kJ mol^{-1} . The bond length $d(\text{V}-\text{O}_{\text{peroxo}})$ is 1.827 \AA in **26b** and 1.833 \AA in **26c**, and hence in the ‘normal’ range for vanadium–peroxo bond lengths. In both complexes, the bond between vanadium and the axial N is rather weak (2.38 and 2.57 \AA , respectively).

4.3.3.3 Structural and Functional Models of the Native Enzymes, Including Applications in Organic Synthesis

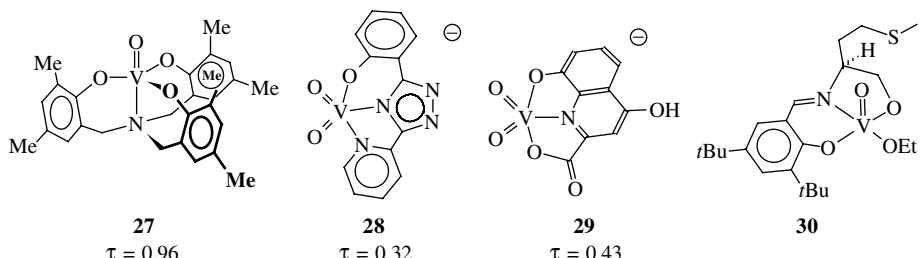
In Section 2.2.1 and Figure 2.15, the binding characteristics of alanylhistidine to vanadate under about physiological conditions were addressed, showing that the tendency of ala-his

**Figure 4.22**

Vanadium complexes containing organic peroxides in the (slightly asymmetric) side-on bonding mode, **25**^[79] and the end-on bonding mode, **26b** and **26c** (Cm = cumyl).^[80] The latter derive from the methoxo complex **26a** by reaction with CmO_2H .

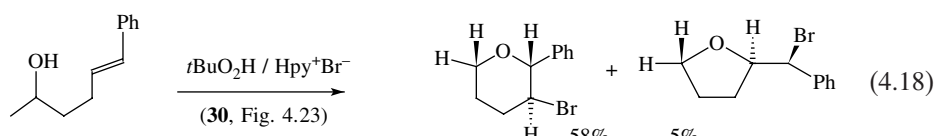
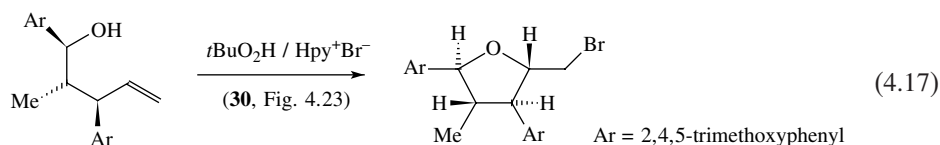
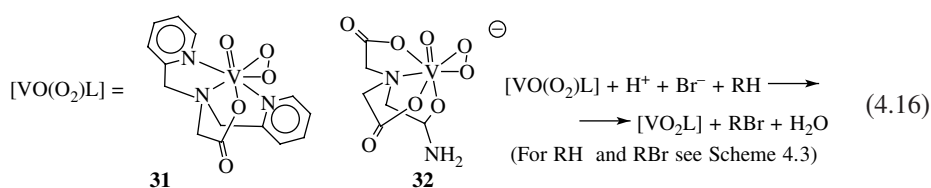
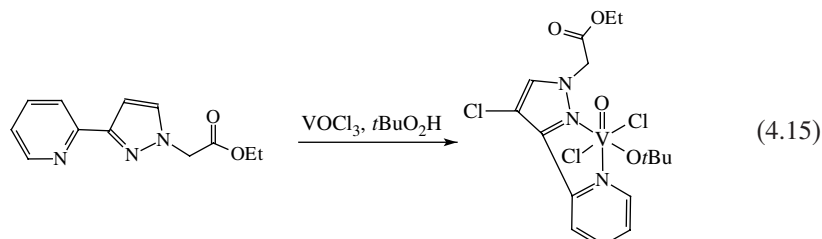
to coordinate to vanadate in the binary system vanadate – ala-his is not very pronounced, in contrast to the ternary vanadate – ala-his – peroxide system (see also above), in which peroxide (i) enhances the affinity of ala-his to coordinate to vanadium and (ii) promotes the coordination through the imidazolyl moiety. In the two vanadate complexes formed with ala-his in aqueous solution, a neutral and an anionic complex, coordination is achieved through the terminal amino and carboxylate functions plus the deprotonated amide-N, a coordination mode certainly not in accord with that in the native peroxidases.

As depicted by structures **a** and **b** in Figure 4.16, vanadium in the VHPOs actually is in a trigonal bipyramidal ligand array. Synthetic oxovanadium complexes with coordination number 5 tend to attain the square pyramidal geometry (Figure 2.32); vanadium complexes modelling the trigonal bipyramidal arrangement of the $\text{O}=\text{V}(\text{O}_3\text{N})$ motif are therefore rare. An example is compound **26a** in Figure 4.22, containing an axial methoxo group (modelling the axial OH) and an axial amine nitrogen (modelling the histidine-N), which is part of a tridentate, dianionic ligand, viz. a chiral aminodiethanolate, providing the two equatorial oxygen functions. The third equatorial ligand is the doubly bonded oxo group. This complex further mimics, through the chiral centres in the ligand periphery, the chirality of the protein pocket incorporating the active centre.^[80] In Figure 4.23, a selection of additional complexes fulfilling several of the criteria for adequate structural models are presented.^[81–84]

**Figure 4.23**

Selected oxovanadium(V) complexes modelling specific features of the active centre of haloperoxidases, such as the (distorted) trigonal bipyramidal NO_4^- ligand array. See also **26a** in Figure 4.22. From refs 81 (**27**), 82 (**28**), 83 (**29**) and 84 (**30**).

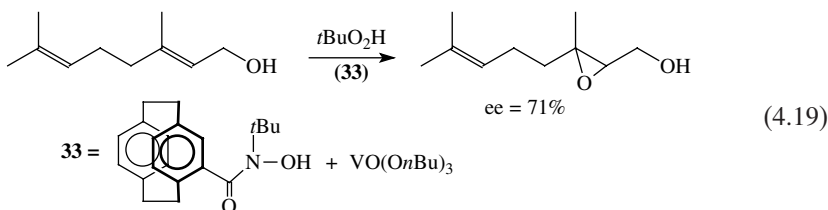
Functional models of peroxidases are of particular interest when it comes to organic synthesis, pharmaceutical and industrial applications. In Figure 4.14, naturally occurring brominated and chlorinated compounds were introduced, which probably go back to the oxidative bromination ability of VHPOs, and with Equations (4.13a) and (4.13b) (see above), examples of the potential of VBrPO in organic syntheses were illustrated. Equations (4.15)–(4.18) represent halogenations of organic compounds modelling reactions catalysed by haloperoxidases. The active chlorinating species for the pyrazole moiety in Equation (4.15), chlorine atoms or *tert*-butyl hypochlorite (*t*BuOCl), is generated in a reaction simulating VCPO.^[85] The peroxy complexes **31** and **32** in Equation (4.16) contain the supporting ligand bis(methylpyridyl)glycinate(1–) (**31**) and (amidomethyl)iminodiacetate(2–) (**32**). These complexes catalyse the bromination of phenol red (RH) to bromophenol blue (RBr) (cf Figure 4.14) by *tert*-butyl peroxide (*t*BuO₂H) in acetonitrile in the presence of an equimolar amount of perchloric acid, and the generation of oxygen in the absence of substrate. The bromination reaction is first order in both peroxyvanadium complex and bromide; the maximum rate, however, depends on the amount of acid added.^[86] The prospective broad potential for organic syntheses including natural products is revealed by the bromocyclisation of alkenols to pyran and furan derivatives; [Equations (4.17) and (4.18)].^[84] Of particular interest is the formation of the diastereomerically pure all-*trans* tetrahydrofuran derivative in Equation (4.17). The catalyst employed here, the square pyramidal vanadium(V) complex **30** in Figure 4.23, contains a chiral Schiff base derived from a substituted salicylaldehyde and a chiral amino alcohol.

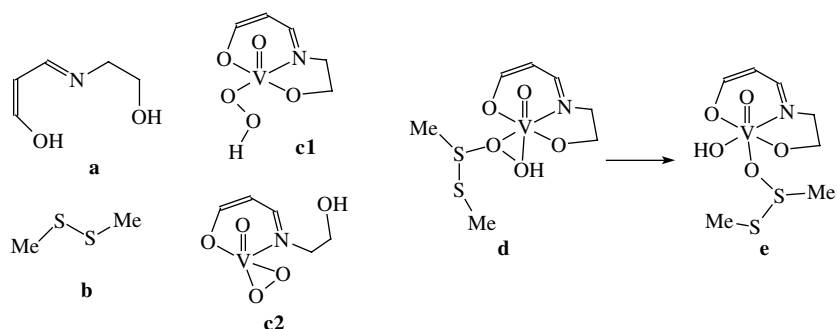
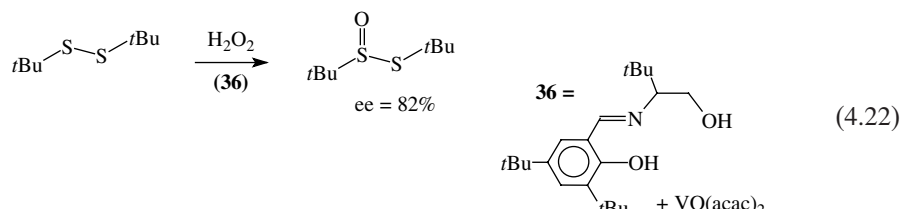
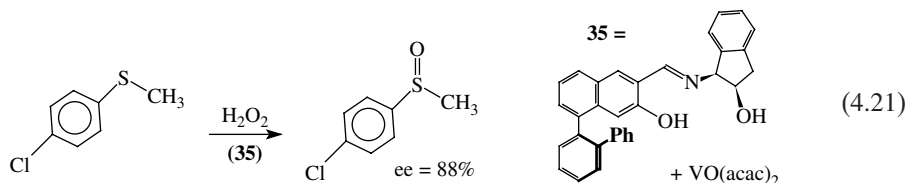
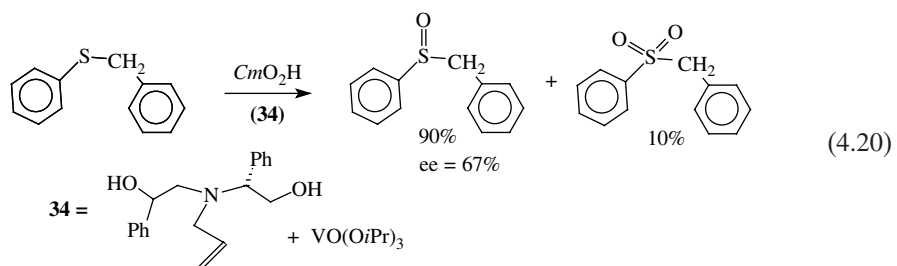


Apart from oxidative halogenations, the use of model systems of the VHPOs has focused on the enantioselective oxidation of substrates such as alkenes or sulfides. The corresponding *enzymatic* reactions were depicted in Equation (4.13) for oxidations in general and in Scheme 4.5 for sulfoxxygenations. Equation (4.19) is a model reaction for the epoxidation of geraniol, yielding the epoxide selectively in the 2,3-position and with an enantiomeric excess (e.e.) of 71%. The oxidant is *t*BuO₂H. Interestingly, it is not necessary to synthesise a preformed catalyst precursor; the active catalyst is generated *in situ* from VO(OnBu)₃ and a chiral hydroxamic acid.^[87] The *in situ* formation of the active catalyst from an oxovanadium(V) or -(IV) species, typically VO(OR)₃ and VO(acac)₂ [acac = acetylacetone(1–)], is also a characteristic feature in the oxygenation of sulfides, thioacetals and disulfides, [Equations (4.20)–(4.23)]. Enantiopure sulfoxides are of prime interest because of their potential as chiral synthons in organic synthesis and as pharmaceuticals (e.g. Sulindac®).

Oxygenation of prochiral sulfides, exemplified by Equations (4.20)^[88] and (4.21),^[89] more or less selectively results in the formation of the sulfoxide with medium to good e.e. Some sulfone is commonly formed along with the sulfoxide. Results similar to those obtained with the *in situ* catalyst have been observed with the ‘intact’ catalyst, the peroxy complexes **31** and **32** in Equation (4.16), which are active not only in bromide oxidation but also in sulfide oxygenation,^[86b] and with the procatalyst, e.g. **26a** in Figure 4.22. As noted above, procatalysts of the latter type convert to the active peroxy species (**26b**) under turnover conditions.^[80,88] The sulfoxxygenation reaction is also transferable to disulfides, [Equation (4.22)]^[90] and thiocetals [Equation (4.23)].^[91] In either case, only one of the sulfurs is oxygenated.

Computational chemistry can be a valuable complement to experiment for the elucidation of reaction mechanisms in homogenous catalysis. As an example, the reaction path for the bromoperoxidation, as made plausible by DFT calculations, was presented in Section 4.2.2 (Scheme 4.4 and Figure 4.18). A thorough computational analysis has also been carried out on the sulfide peroxidation represented by Equation (4.22), employing the model ligand **a** and substrate **b** in Scheme 4.9.^[92] For the nature of the catalyst, several isomers of hydroperoxy and peroxy complexes can be considered, all within a span of ca 20 kJ/mol⁻¹. All of the isomers of the hydroperoxy intermediate contain the hydroperoxy group in the η^1 coordination mode (which has also been shown to be the energetically favoured one in the case of the alkylperoxy intermediates; **26b** and **26c** in Figure 4.22). The most stable isomer of the hydroperoxy variant is **c1** in Scheme 4.9. The most stable peroxy variant, **c2**, is less stable than **c1** by 18.4 kJ mol⁻¹. Based on these results, the transition state **d**, corresponding to a direct transfer of the peroxy oxygen to the sulfur, has been proposed to represent the ‘correct’ reaction path, excluding an insertion mechanism where the sulfide coordinates to vanadium prior to the oxo transfer. Structure **d** relaxes to structure **e**, which is the rate-limiting step in the overall reaction.





Scheme 4.9

4.3.3.4 Hydrogen Bonding and Supramolecular Features

The vanadate centre in the haloperoxidases not only is covalently bonded to a histidine, but also is in electrostatic contact with arginine and, through a hydrogen bonding network, with lysine, histidine, serine and water (Figure 4.16). The ionic interaction

between vanadate and the guanidinium residue of arginine is modelled by the host – guest compound **37** in Figure 4.24, with tris(2-guanidiniumethyl)amine acting as a supramolecular receptor for HVO_4^{2-} .^[93] The binding constant for **37** is $1.1 \times 10^3 \text{ M}^{-1}$; the adduct has a characteristic UV absorption at 307 nm, which compares well with the 312 nm for the VCIPO from *Cur. inaequalis*.

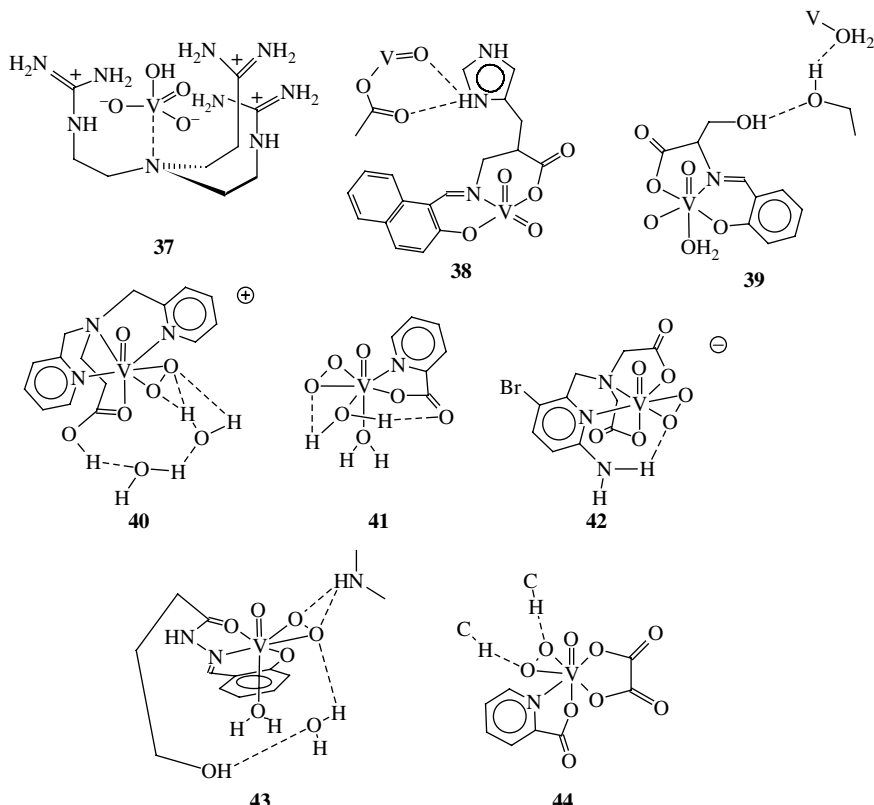
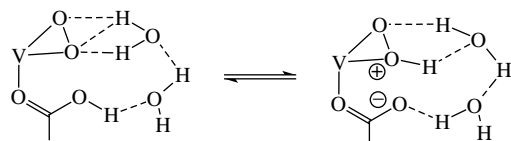


Figure 4.24

Complexes modelling supramolecular features such as salt interaction (**37**), classical intermolecular hydrogen bonds (**38–40**, **43**), intramolecular hydrogen bonding (**41** and **42**) and nonclassical intermolecular hydrogen interaction (**44**). For bond distances, see Table 4.7; for references, see text.

Inter- and intramolecular hydrogen bonding interactions between vanadate/peroxovanadate and proton-active amino acid side-chains or water in the surroundings of vanadate can be effective mediators for the delivery of protons, which are indispensable for the catalytic oxo transfer process to a substrate. The complexes **38**^[94a] and **39**^[94b] (Figure 4.24) are examples of intermolecular hydrogen bonding involving serine (**39**) and protonated histidine (**38**). In both cases, the amino acid is constituent of a tridentate *ONO* Schiff base, coordinating through the carboxylate-O, the imine-N and the phenolate-O, leaving the amino acid side-chain dangling and thus available for interaction with neighbouring molecules. Bond lengths for the relevant interconnections are summarised with those of other model compounds in Table 4.7. The cationic complex **40** is a β -alanine derivative in which the nonprotonated oxygen of the carboxylic acid

function coordinates to vanadium.^[95] The carboxylic acid proton is hydrogen bonded to a water, of crystallisation, which binds to a second water which finally interacts with the coordinated peroxide. The situation can be interpreted in terms of a frozen-in switch-on/switch-off mechanism for the delivery of a proton to the peroxy group (Scheme 4.10). The four participating oxygens (carboxylate, two water molecules and peroxide) are in an about tetrahedral arrangement.¹⁶ In the picolinato complex **41**,^[75] one of the coordinated water molecules (the one in the equatorial plane), which is hydrogen bonded to peroxide and carboxylate, plays a comparable role. The role of lysine as a mediator for peroxide protonation is modelled by the anionic complex **42**: an intramolecular hydrogen bond is present between the peroxy ligand and the amino group.^[96] The ligand derives from iminodiacetate; the hydrogen-bonded amino group is attached to a methylpyridyl substituent at the imino-N. A situation representing features of both **40** and **42** is represented by complex **43**, containing an *ONO* ligand derived from salicylaldehyde and the hydrazide of γ -hydroxybutyric acid.^[97] As in the case of the serine derivative **39**, the alcoholic functionality does not participate in coordination, but is involved in a hydrogen bond network, tying it to the peroxy ligand via an interstitial water molecule. The acidic NH of the hydrazide moiety, hydrogen bonded to the peroxide of an adjacent complex, may be considered to model active site lysine.



Scheme 4.10

Table 4.7 Listing of selected bond lengths involving hydrogen bonds in model complexes of VHPOs. For the numbering of the complexes, see Figure 4.24.

Complex	Bond	Bond length (Å)	Bond	Bond length (Å)
38 ^[94a]	(His)N–H \cdots O(carboxylate)	2.699	(His)N–H \cdots O=V	2.980
39 ^[94b]	(Ser)O–H \cdots O(Ser)	2.697	(Ser)O–H \cdots OH ₂ (coord.)	2.647
40 ^[95]	$-\text{C}(\text{O})\text{O}-\text{H}\cdots\text{OH}_2$	2.550	HO–H \cdots OH ₂ (inter water)	2.711
	OH ₂ \cdots O ₂ (peroxide)	2.860, 2.995, 3.250		
41 ^{a[75]}	OH ₂ \cdots O ₂ (peroxide)	2.55	(coord.)OH ₂ \cdots O(carboxylate)	2.40
42 ^[96]	NH ₂ \cdots O ₂ (peroxide)	2.640		
43 ^[97]	(alcoholic)O–H \cdots OH ₂	2.86	NH \cdots O ₂ (peroxide)	2.80, 2.05
	OH ₂ \cdots O ₂ (peroxide)	2.99		
44 ^[71]	(pyr)C–H \cdots O ₂ (peroxide)	2.444, 2.488		

^aThe H \cdots O distances are given.

¹⁶ A situation which is reminiscent of the preactivation step of the substrate urea by nickel urease.

In addition to classical hydrogen bonds, C–H \cdots X bonds have also been recognised to play an important role in protein structure and stability. Although no such structure elements have been reported decisively for the structures of vanadate-dependent haloperoxidases, a compound, **44**, is included in Figure 4.24 that contains intermolecular hydrogen-bonding interactions between the coordinated peroxide and aromatic CH groups of a picolinato ligand in a related molecule.^[71]

4.4 Vanadium and the Nitrogen Cycle

To date, only the role of vanadium in biogenic nitrogen fixation has been established unambiguously. In addition, there are a few reports on a putative importance of vanadium in (bacterial) nitrate reductases, otherwise a domain of molybdenum. These reports are based on investigations which remain to be backed up. They are nonetheless briefly addressed, with a question mark, in Section 4.4.2.

4.4.1 Vanadium Nitrogenases

This section is subdivided as follows:

1. history and background;
2. structure and function;
3. alternative substrates (such as alkynes, nitriles, isonitriles and azide);
4. model chemistry.

4.4.1.1 History and Background

In a ‘Brief note on the catalysis of the biological nitrogen fixation’ from 1933, Hans Bortels communicated the following observation:^[98a]

‘In a previous communication we demonstrated that molybdenum strongly fosters the fixation of nitrogen by *Azotobacter chroococcum* [. . .]. Based on these findings, I have argued that fertility parallels the molybdenum contents of the soil. Meanwhile, and independently of these investigations, the correctness of the mentioned notion has been proven by Ter Meulen on the basis of numerous analyses. [. . .] Searching for elements capable of substituting molybdenum in its effect on *Azotobacter*, and following a friendly hint by Prof. Goldschmidt from Göttingen [. . .], I found out in 1930 that vanadium compounds almost match molybdenum with respect to their positive effect on nitrogen fixation by *Azotobacter*. Except for molybdenum and vanadium, and sometimes tungsten (with a weak impact only), all other elements coming into question proved ineffective’.

Bortels ended his note by announcing a more elaborate publication on the matter at a later point in time ‘because presently other work is more exigent’. A more detailed account was published years after these findings, entitled ‘Further investigations into the importance of molybdenum, vanadium, tungsten and other earthen ashes for nitrogen-fixing and other microorganisms’.¹⁷^[98b] In the abstract to this paper he states that:

¹⁷ Weitere Untersuchungen über die Bedeutung von Molybdän, Vanadium, Wolfram und anderen Erdaschenstoffen für stickstoffbindende und andere Mikroorganismen.

'Molybdenum and vanadium promote nitrogen fixation by *A. chroococcum*, *A. vinelandii* and *Bac. amylobacter*, [in the case of] molybdenum up to the 100-fold of the amount accomplished in the absence of these elements by *Azotobacter*. From this it is concluded that without molybdenum or vanadium there is no possibility for any appreciable nitrogen fixation.'

A role of tungsten could later be ruled out, and earlier findings of minor effects by tungsten were traced back to impurities of tungsten present in the culture media, due to the difficulty of separating molybdenum and tungsten completely.

The findings of Bortels were later confirmed by other researchers,^[99] and extended to studies of nitrogen fixation by several strains of *Clostridium butyricum* in a particularly detailed investigation carried out by Jensen and Spencer in 1947.^[100] *C. butyricum* is an obligate anaerobic bacterium living in soil and the intestines of humans and animals. Unlike *Azotobacter*, its primary function is not nitrogen fixation. Rather, it produces butyric acid (and other short-chain carbonic acids) by fermentation of carbohydrates and thus helps in counter-acting diarrhoea and inflammatory bowel diseases such as ulcerative colitis and Crohn's disease. *C. butyricum* strains tested for their ability to reduce nitrogen did so in the presence of molybdate and, in many cases, also vanadate or vanadyl sulfate at concentrations $c(V) \approx 40 \text{ nM}$, with a detectable stimulation still at $c(V) = 4 \text{ nM}$. In their General Conclusion, Jensen and Spencer stated that:

'The experimental results show quite clearly that although molybdenum and vanadium have some influence on the general metabolism of the chlostridia, their effect consists pre-eminently in an acceleration of the nitrogen-fixation process, as in *Azotobacter*. It is reasonable to assume that both kinds of bacteria may possess a nitrogen-fixing enzyme ("nitrogenase") that requires molybdenum as an activator, with vanadium as a less effective substitute; a certain difference in the enzymes seems to exist, in so far as in some of the clostridia they are not activated by vanadium'.

The final breakthrough was achieved by the Sussex Nitrogen Fixation Group in the period 1980–86, culminating in a paper ('The alternative nitrogenases of *Azotobacter chroococcum* is a vanadium enzyme'), published and highlighted (by Cammack) in *Nature*,^[101] the commenting paper with a somewhat exaggerated heading ('A role for vanadium at last'), in the light of the fact that a vanadate-dependent bromoperoxidase from the marine alga *Ascophyllum nodosum* had been characterised – and thus a biochemical role for vanadium established – 3 years before.^[46] In the original paper, the findings are summarised as follows:

'*Azotobacter vinelandii* [...] has two systems for nitrogen fixation: a conventional nitrogenase involving molybdenum and an alternative system which functions under conditions of Mo deficiency and does not require the functional genes for conventional nitrogenases. [...] Recently, an alternative nitrogen fixation system has been demonstrated in *Azotobacter chroococcum* strain MCD1155, in which the structural genes for conventional nitrogenases are deleted. We demonstrate here that nitrogen fixation by this strain depends on vanadium and we show that its purified nitrogenase is a binary system in which the conventional molybdoprotein is replaced by a vanadoprotein'.

Biogenic nitrogen fixation converts dinitrogen to ammonia (or ammonium ions), making available nitrogen for assimilation by plants. Along with free-living bacteria such as *Azotobacter*, *Clostridium*, *Klebsiella* and *Rhodospirillum*, cyanobacteria (blue-green algae such

as *Anabaena*) and bacteria involved in symbiosis contribute to N₂ conversion. *Rhizobium* associated with legumes (Papilionaceae) and *Francia* associated with the alder (*Alnus*) are examples of symbiotic N₂-fixing bacteria. Biogenic reductive nitrogen fixation is part of the global nitrogen cycle (Figure 4.25). The triple bond in dinitrogen makes this molecule a particularly stable one; the enthalpy of formation is ΔH = −946 kJ mol^{−1}. Apart from bacterial reductive bioactivation, nonbiogenic oxidative activation can occur by splitting N₂ into nitrogen atoms, followed by reaction with oxygen to form nitrogen oxides and finally nitric acid/nitrate. The energy to break the dinitrogen bond can be provided by electric discharges (thunderstorms) and by short-wavelength UV irradiation or cosmic rays in the stratosphere. Nitrate and ammonia are redox-interconvertable (ammonification; nitrification), and nitrate can be built back to dinitrogen by stepwise reduction (denitrification). All of these processes are essentially carried out by specialised bacteria, employing enzymes which contain metal ions (Fe, Cu, Mo) in their active centres.

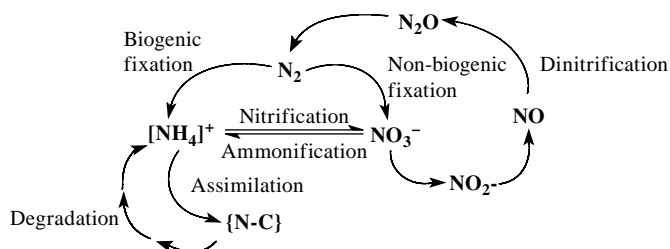


Figure 4.25

Several essential steps within the global nitrogen cycle. Vanadium is involved in biogenic nitrogen fixation and, perhaps (Section 4.4.2), in the first step of denitrification.

A third and increasingly important supply of ammonia (and nitrate) is provided by anthropogenic nitrogen fixation, based on the Haber–Bosch (and Ostwald) process. Biogenic and anthropogenic reductive N₂ conversion are compared in Table 4.8:

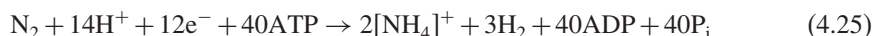
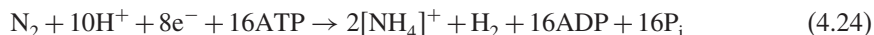
Table 4.8 Comparison of biogenic and anthropogenic nitrogen fixation.

	Biogenic N ₂ fixation	Anthropogenic N ₂ fixation
Educts	N ₂ , [H]	N ₂ , H ₂
Products	[NH ₄] ⁺ , H ₂	NH ₃
Yield	50–75%	ca 15%
Temperature	Ambient (energised by MgATP)	500 °C
Pressure	1 bar	200–500 bar
Catalyst	Nitrogenase ({Fe ₇ S ₉ Mo/V})	α-Fe + Al ₂ O ₃ + K ₂ O + ...
Turn over per year	ca 10 ⁸ t	ca 10 ⁸ t

The comparison shows that biogenic fixation is more effective, less energy consuming and proceeds under clearly milder conditions than the Haber–Bosch process, a fact which has encouraged world-wide research directed towards a better understanding of the biological process and towards modelling the active centre (see below) in an effort to have available a catalyst allowing one to copy the bacterial nitrogen conversion, a goal which is still far from being reality.

4.4.1.2 Structure and Function of Vanadium Nitrogenase

The net reaction for N₂ reduction catalysed by molybdenum nitrogenase (MoNase) is represented by Equation (4.24) and the corresponding reaction catalysed by vanadium nitrogenases (VNase) by Equation (4.25). In either case, molecular hydrogen is produced along with ammonium ions, i.e. the nitrogenases also exhibit hydrogenase activity. MoNase is more efficient than VNase in the sense that 75% of the reduction equivalents are used for N₂ reduction (50% in the case of VNase), and only two ATP are consumed per electron transferred (3–4 in the case of VNase). Consequently, the microorganisms preferentially employ the ‘conventional’ MoNase. The ‘alternative’ VNase is activated in case of Mo deficiency, or at low temperatures where it becomes the more efficient one. *Azotobacter* also has available an ‘iron-only’ nitrogenase, independent of Mo and V, but genetically related to the Mo and V variants.



Vanadium nitrogenase comprises an iron protein (Fe-protein) and a vanadium–iron protein (VFe-protein), encoded by structural genes homologous to, but distinct from, those of molybdenum nitrogenase. Despite the biochemical similarity, the vanadium system thus does not simply arise from substitution of Mo by V in the MoFe protein.^[102] Whereas the MoFe-protein has an $\alpha_2\beta_2$ substructure (overall molecular mass $M = 200$ kDa), the VFe-protein from *A. chroococcum* attains an $\alpha_2\beta_2\delta_2$ subunits structure (Figure 4.26, top) of $M = 240$ kDa.^[103] The α subunits accommodate the so-called **M** cluster (also termed FeVco, for iron–vanadium–cofactor), which is likely the site of N₂ activation. At the interface of the α and β subunits, a **P** cluster is located, linked to two cysteinate residues of each of the subunits. The **P** clusters, involved in electron shuttle, basically consist of two fused [4Fe,4S] cubanes, the composition of which in the reduced state is $[\{\text{Fe}_4\text{S}_3(\text{Cys})_2\}_2(\mu-\text{S})_2(\mu-\text{Cys})_2]$. The overall arrangement of subunits and clusters of the VFe-protein is such that it attains C_2 symmetry; the distance between **M** and **P** cluster is 21 Å and the distance between the two **M** and the two **P** clusters is 70 Å. Electron delivery to the VFe-protein is incurred by the Fe-protein ($M = 60$ kDa), which contains a [4Fe,4S] ferredoxin, and MgATP attached to it, which power the electron flux.

The vanadium nitrogenase from *A. vinelandii* has the same $\alpha_2\beta_2$ subunit structure as the Mo enzyme. Interestingly, a second VNase has been isolated from *A. vinelandii*, lacking one of the α subunits and consequently one of the **M** clusters and half of one of the **P** clusters. This incomplete $\alpha\beta_2$ variant is still active.^[104] VNases in general are less stable than their Mo counterparts, leading to a larger variability and pronounced problems when it comes to crystallisation.

To date, structural information on vanadium nitrogenase from X-ray diffraction data is not available, but all of the indirect information obtained from genetics and spectroscopic studies, e.g. Mössbauer, X-ray absorption, MCD and EPR, account for a comparable build-up of the **M** clusters.^[102] Accordingly, vanadium is part of a cluster system containing, in addition to V, seven iron ions and nine inorganic, bridging sulfide ions (Figure 4.26, bottom). Vanadium is additionally coordinated to a histidine and the vicinal hydroxide and carboxylate of homocitrate. An intriguing feature of this cluster from a coordination chemist’s point of view is the coordination number 3 for six of the iron centres. Recent high-resolution X-ray diffraction data have revealed residual electron density in the cage formed by these six irons. This electron density can be fitted to a light atom, and it is

tempting to assign it to a nitrogen atom. Even if this assignment turns out to be correct,¹⁸ the question remains of where and how the rupture of the dinitrogen bond occurs, and whether bond breakage is preceded by protonation (as suggested by model investigations; see below).

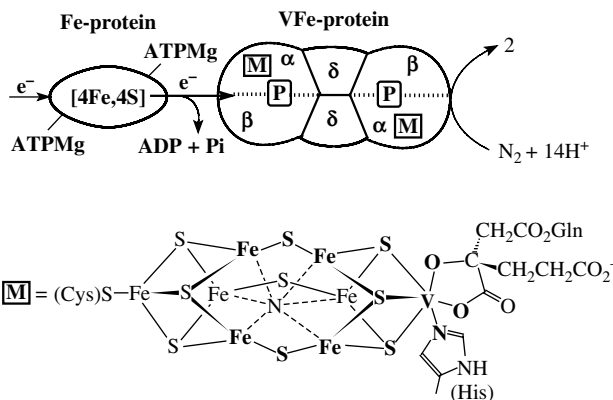
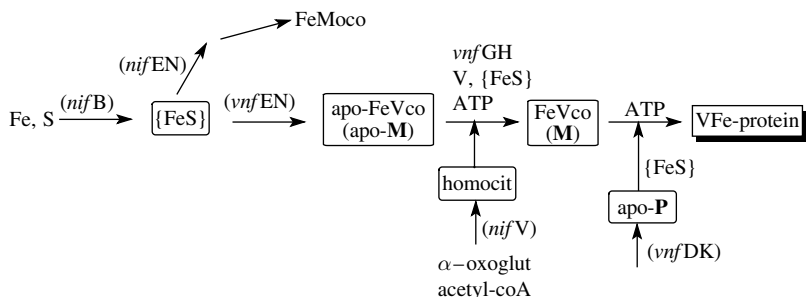


Figure 4.26

Organisation of the vanadium nitrogenase from *Azotobacter* and the structure of the **M** cluster (FeVco), the latter in analogy to findings for the FeMoco of molybdenum nitrogenase. The assignment of the electron density within the Fe_6 cage to a nitrogen atom is of preliminary nature.

Before going into spectroscopic detail, supporting the structure shown in Figure 4.26, let us briefly consider genetic aspects of the biosynthesis of the VFe-protein, summarised schematically in a simplified manner in Figure 4.27. A number of nitrogen fixation genes (termed *nif* for the molybdenum enzyme and *vnf* for the vanadium enzyme) have been shown to play roles in the biosynthesis of the Mo- and the V-protein. The gene cluster encoding MoNase is *nifHDK* and for VNase *vnfH/vnfDGK*.^[103] Also required for the synthesis of the Mo and V proteins is the cluster *nif/vnfEN*. Despite of the similarity of the final proteins, the genetic build-up branches at an early point. The gene *nifB* triggers the formation, from a pool containing iron and sulfur, of a low molecular weight cluster constituting iron and acid-labile (i.e. inorganic) sulfur, {FeS}, and possibly comparable to iron–sulfur clusters of the ferredoxin type which also form by self-assembly, [Equation (4.26)]. At this point, bifurcation between the paths leading to the MoFe- and the VFe-proteins occurs: whereas *nifEN* takes care of the assemblage of the FeMoco, *vnfEN* initiates the synthesis of the apo-**M**, the template-protein for accommodation of the FeVco (the **M** cluster). With recourse to {FeS}, a vanadium source, homocitrate and ATP, the complete FeVco (**M** cluster) is assembled. Homocitrate is synthesised from α -oxoglutarate and acetyl-coenzyme-A by a homocitrate synthase, which is encoded in *nifV*. The formation of the template for the **P** cluster, apo-**P**, is triggered by the gene *vnfDK*; incorporation of {FeS} establishes the **P** cluster and the complete VFe-protein.^[102] The small δ subunit is the product of *vnfG*.

¹⁸ Theoretical calculations both support and relativise the assumption that the central atom is nitrogen. For a critical overview, see, e.g., ref. 113b.

**Figure 4.27**

Genes (*nif* and *vnf*) involved in the biosynthesis of the VFe-protein. {FeS} is a low molecular weight iron–sulfur cluster used in both the synthesis of the VFe- and MoFe-protein. The gene for homocitrate synthase (*nifV*) is equally used in both systems. Modified from ref. 102. For the M cluster and the complete protein, see Figure 4.26.



The *vnf* genes have also been reported for other bacteria, and in the cyanobacteria *Anabaena variabilis* and *A. azotica*, the latter from Chinese rice fields. These cyanobacteria express a vanadium nitrogenase which, as the bacterial VNases, also reduces ethyne to ethene and further to ethane.^[105]

Structure information on the FeVco of vanadium nitrogenases has been obtained from iron and vanadium K-edge X-ray absorption spectroscopy (XAS) (for background information, see Section 3.6.), in particular so from the extended (EXAFS) region.^[106] In Table 4.9, selected results are presented for the dithionite-reduced VNases from *A. vinelandii*, *A. chroococcum* and a model complex for the FeVco, the anionic heterocubane $[\text{V}(\text{dmf})_3\text{Fe}_3\text{Cl}_3]^-$, **60** in Figure 4.36; see Section 4.4.1.4. The data provide (i) similarity with structural information directly obtained (i.e. via X-ray diffraction) for the Mo-protein of MoNase, and thus the presumed similarity of the cofactors of the two enzymes including octahedral coordination of the heterometal (V/Mo), and (ii) similarity between the FeVco and the model cubane. From the energy position of the pre-edge

Table 4.9 Selected data from XAS investigations of vanadium nitrogenases from *Azotobacter*. The number of scatterers (next neighbours to vanadium) *n* and the distances *d* are provided. For the model compound, data from single-crystal structure results (XRD) are added for comparison. Data from refs. 102 and 106a. See also text.

	<i>A. vinelandii</i>		<i>A. chroococcum</i>		$[\text{V}(\text{dmf})_3\text{Fe}_3\text{Cl}_3]^-$ (60 in Figure 4.36)		XRD
	<i>n</i>	<i>d</i> (Å)	<i>n</i>	<i>d</i> (Å)	<i>n</i>	<i>d</i> (Å)	
V – O/N	2–3	2.15	3 ± 1	2.15	3	2.12	2.13
V – S	3–4	2.33	3 ± 1	2.31	3	2.35	2.33
V – Fe	3 ± 1	2.76	3 ± 1	2.75	3	2.73	2.77

(3 eV) and the K-edge inflection (10 eV), it was further concluded that vanadium in the cofactor is in oxidation state II–IV.

Additional, although less stringent, structure information comes from other spectroscopic techniques: EPR spectra of the enzyme are complex. The EPR spectrum of the VNase from *A. vinelandii* shows three signals.^[107] The first signal of axial symmetry at $g \approx 2$ is typical of a spin $S = 1/2$ system of a reduced iron-sulfur cluster. The second signal is a composite signal centred at $g = 5.5$, representing the low-field inflections of the ground-state and first excited-state transitions of an $S = 3/2$ spin system. This signal can be assigned to the FeVco. A third signal in the $g \approx 2$ region, only observed under specific measuring conditions, remains elusive. The paramagnetic $S = 3/2$ spin state (i. e. three unpaired electrons) of the FeVco has also been inferred from magnetic circular dichroism (MCD) spectra,^[108] and from the magnetic hyperfine structure of one of the spectral components in the Mössbauer spectrum.^[109] The EPR parameters are further in accord with those of model clusters containing the $[\text{VFe}_3\text{S}_4]^{2+}$ core (see model chemistry). Although all these studies do not provide proof, they strongly suggest, along with the genetic evidence, the presence of **P** and **M** clusters in the VFe-protein of VNase (Figure 4.26) analogous to those of the MoFe-protein in the MoNase.

4.4.1.3 Alternative Substrates for Reduction by Vanadium Nitrogenases

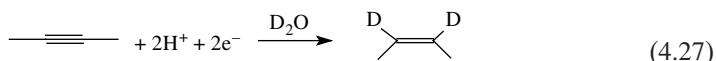
Dinitrogen and protons [Equation (4.25)] are not the only substrates reduced by nitrogenases. Furthermore, the product spectrum obtained as the reduction is catalysed by VNase differs from that catalysed by MoNase. This includes N_2 reduction: Whereas wild-type MoNase cleanly converts N_2 to ammonia, VNase also produces some hydrazine.^[110] Substrates and educts for the two nitrogenases are compared in Table 4.10

Table 4.10 Comparison of substrates and educts for VNase and MoNase.

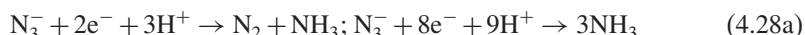
Substrate	Products (VNase)	Products (MoNase)
N_2	$\text{N}_2\text{H}_4, \text{NH}_3$	NH_3
C_2H_2	$\text{C}_2\text{H}_4, \text{C}_2\text{H}_6$	C_2H_4
HCN	$\text{CH}_3\text{NH}_2, \text{HCHO}, \text{CH}_4, \text{NH}_3$	$\text{CH}_3\text{NH}_2, \text{CH}_4, \text{NH}_3$
$\text{CH}_2=\text{CHCN}$	$\text{C}_3\text{H}_6, \text{C}_3\text{H}_8$	$\text{C}_3\text{H}_6, \text{C}_3\text{H}_8$
CH_3CN	$\text{CH}_3\text{NH}_2, \text{C}_2\text{H}_4$	$\text{C}_2\text{H}_6, \text{NH}_3$
CH_3NC	$\text{C}_2\text{H}_4, \text{C}_2\text{H}_6, \text{CH}_4, \text{CH}_3\text{NH}_2$	$\text{C}_2\text{H}_4, \text{CH}_4, \text{CH}_3\text{NH}_2, (\text{CH}_3)_2\text{NH}$
HN_3		$\text{N}_2\text{H}_4, \text{NH}_3$
N_3^-	$\text{N}_2, \text{N}_2\text{H}_4, \text{NH}_3$	N_2, NH_3

The formation of hydrazine in the case of VNase may hint at a different activation mechanism of the N_2 molecule, i.e. protonation prior to bond dissociation (VNase) versus bond dissociation prior to protonation (MoNase). However, the intermediate formation of hydrazine has also been detected in shock-frozen MoNase. The reduction of ethyne to ethene (followed by further reduction to ethane in the case of VNase), when carried out in D_2O , leads to the formation of the *Z* (*cis*) isomer (*Z*)-1,2-deuteroethene, [Equation (4.27)], very much suggesting activation of ethyne by side-on coordination to the metal

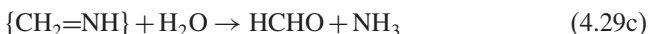
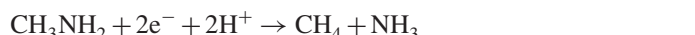
centre. I will come back to this point in the next section.



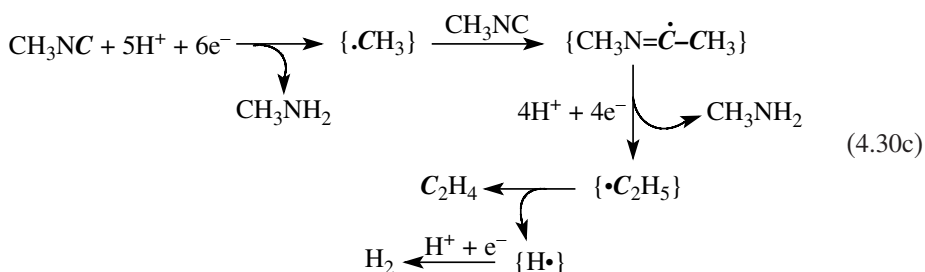
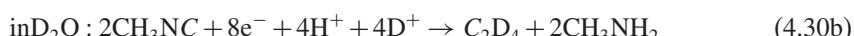
The propensity of VNase to release partially reduced intermediates was exploited to obtain insight into the reduction products and reduction paths observed as hydrogen cyanide and azide are reduced.^[111] As in N₂ reduction, hydrogen is formed as a by-product in all of these reaction. Equation (4.28) summarises the results for azide reduction by VNase.



The pattern of the reaction products observed in HCN/CN⁻ reduction suggests that the first step is the two-electron reduction to methyleneimine CH₂=NH, [Equation (4.29a)], which can either be further reduced to methylamine and methane plus ammonia, [Equation (4.29b)], or be hydrolysed to formaldehyde and ammonia, [Equation (4.29c)].



Of particular interest is the formation of ethene (and ethane) as a minor product in the reduction of methyl isocyanide according to Equation (4.30). Both carbon atoms of the reduction product result from the isocyanide-carbon [emphasised in bold italics in Equation (4.30a)], proven by the fact that, when the reaction is carried out in D₂O, the completely deuterated ethene is obtained, [Equation (4.30b)]. A possible mechanism, including radical intermediates and insertion (C–C coupling), is formulated in Equation (4.30c).



4.4.1.4 Model chemistry

Extensive research activities have been directed towards elucidating the actual site of activation and reduction of dinitrogen. Extended Hückel molecular orbital calculations carried out on idealised models (Figure 4.28, 45a) of the cofactors FeMco (M = Mo, V, Fe) of the three nitrogenases suggest, based on the similarity of the electronic structures,

that the heterometal M attains a stabilising function of the cluster only.^[112] Coordinating dinitrogen end-on to four of the iron centres of the Fe₆ trigonal prismatic cage (**45b** in Figure 4.28) reveals a very small HOMO – LUMO gap in the case of M = Mo and V, with the lowest lying LUMOs exhibiting considerable π^* contributions from dinitrogen. From these results, it is inferred that the three electrons necessary to reduce one nitrogen can easily be filled in. One should keep in mind, however, that the models employed in this (and other) calculations are grossly simplified, in particular with respect to the coordination sphere of the heterometal. Protonation of the histidine or carboxylate function coordinated to Mo and V can occur and make available a binding site for N₂. The differences in activity and in product specificity between vanadium and molybdenum nitrogenase pointed out in the previous section further support an ‘active’ role of the heterometal. Finally, the less pronounced inhibition of VNase-catalysed nitrogen reduction (but not of the evolution of hydrogen) by carbon monoxide appears to be correlated with the weaker binding of CO to V than to Mo.

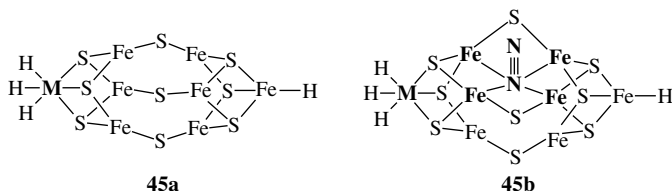


Figure 4.28

Model complexes employed in extended Hückel MO calculations on the activation of dinitrogen.

Irrespective of the question of which metal centre is the one that activates N₂, the possible mechanistic path for the reduction and protonation of N₂ has recently been approached by the energy profile,^[113] obtained from DFT calculations, of the Yandulov–Schrock cycle, to date the only process mimicking, to some extent,¹⁹ catalytic N₂ reduction at a molybdenum centre. The central component of the Yandulov–Schrock cycle^[114] (Figure 4.29) is a dinitrogen–Mo^{III} complex containing a tripodal tetradentate amine ligand NN₃ with spacious aryl substituents shielding the site of nitrogen binding. The reducing agent is decamethylchromocene, Cp^{*}₂Cr, and the proton source a 2,6-lutidinium borate. According to these calculations, protonation and one-electron reduction steps alternate. Since the first protonation step for N₂ is strongly endergonic, activation is afforded, provided by coordination of N₂ to the metal. Also endergonic is the last reduction step, by which ammonia is released and the low oxidation state of molybdenum restored. The most exergonic step is the cleavage of the N–N bond in the postulated intermediate {Mo(NNH₃)⁺}. A plausible mechanism for the reduction of N₂ to NH₃ by the enzyme and model compounds thereof is depicted for the vanadium systems in Scheme 4.11. Branching at the diazenido(1–) intermediate ({V–N=NH}) yields hydrazine as a by-product by additional electron transfer and protonation steps.

Model chemistry directed towards mimicking the structure and function of vanadium-nitrogenase has been reviewed.^[115]

¹⁹ Six cycles have been achieved, with an overall yield of 65% ammonia.

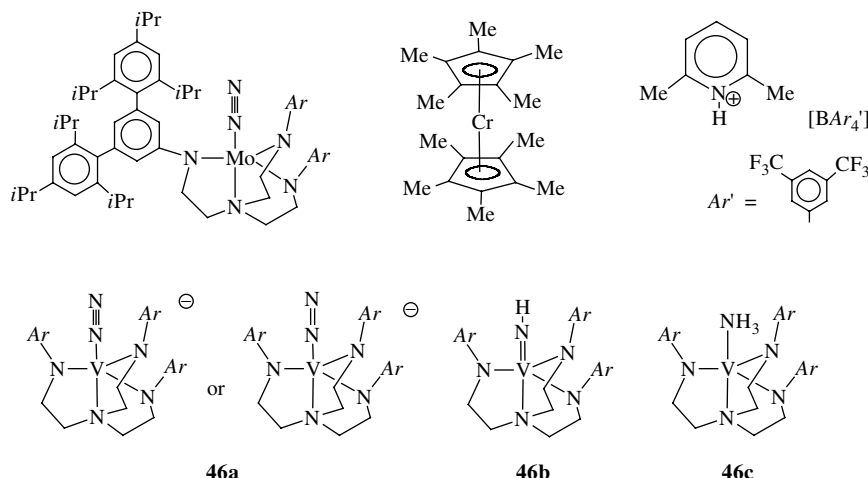
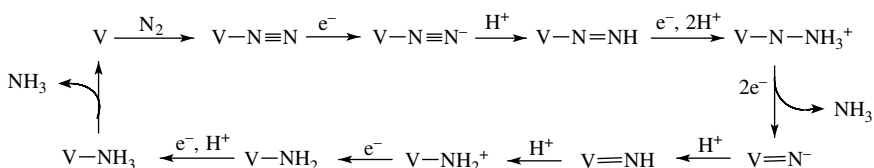


Figure 4.29

Top row: the three components of the Yandulov–Schrock cycle for catalytic dinitrogen reduction. Left: the catalyst with the substrate N₂ coordinated to Mo (Ar refers to the aryl substituent drawn in detail for one of the nitrogens). Centre: the reductant bis(pentamethylcyclopentadienyl)chromium, Cp*₂Cr. Right: the proton source 2,6-lutidinium borate. Bottom row: vanadium complexes with intermediates of nitrogen reduction: activated dinitrogen or diazenido(2-) (**46a**), imide (**46b**) and ammonia (**46c**).



Scheme 4.11

The Schrock system just described for molybdenum has equally been applied to vanadium, and complexes containing species involved in nitrogen activation and reduction, viz. dinitrogen [or diazenido(2-)], imide and ammonia, complexes **46a–c** in Figure 4.29, have been characterised.^[116] Although the imide complex **46b** and the dinitrogen complex **46a** produce ammonia on reduction with Cp*₂Cr and lutidinium as proton source, atmospheric nitrogen could not be activated, i.e. the vanadium system does not work catalytically. Complex **46c** has been obtained by reacting [VCl₃(thf)₃], in the presence of the tripodal NN₃ ligand, with potassium graphite or sodium naphthalide.

Other tetradentate, tripodal ligands have been employed successfully to stabilise substrates of VNase and intermediates along the reduction pathway of N₂. Examples with NS₃ and PS₃ ligands are provided in Figure 4.30. The complexes **47** contain vanadium in the oxidation states +III (neutral ligands such as hydrazine and isonitrile), +IV [monoanionic ligands such as methyldiazenido(1-) and cyanide(1-)] and

+V (the imide complex **47d**).^[117] The hydrazine complex $[\text{V}(\text{NS}_3)\text{N}_2\text{H}_4]$ **47b** disproportionates on heating in THF to form the ammonia complex **47a** and dinitrogen according to (the non-stoichiometric) Equation (4.31); the complex does not, however, act as a catalyst for the disproportionation of hydrazine. The anionic complexes **48** contain a PS_3 ligand set; the overall composition is $[\text{V}(\text{PS}_3)\text{L}]$.^[118a] For L = chloride, i.e. $[\text{V}(\text{PS}_3)\text{Cl}]^-$, catalysis of the reduction of hydrazine to ammonia has been observed in CH_3CN in the presence of cobaltocene, Cp_2Co , as reducing agent and 1,6-lutidinium hydrochloride for the proton delivery. The reaction probably proceeds via the formation of an acetonitrile derivative $[\text{V}^{\text{III}}(\text{PS}_3)\text{NCMe}]$, which is reduced by Cp_2Co to $[\text{V}^{\text{II}}(\text{PS}_3)\text{NCMe}]^-$, which then exchanges acetonitrile by hydrazine (formation of $[\text{V}^{\text{II}}(\text{PS}_3)\text{N}_2\text{H}_4]^-$) prior to reduction to ammonia. Conversion is slow, and this is attributed to a competing reaction by which $[\text{V}^{\text{III}}(\text{PS}_3)(\text{N}_2\text{H}_4)_3]$ (**49**) is formed. The hydrazine of **49** is not susceptible to reduction. Complex **49** has been structurally characterised; stabilisation is achieved by hydrogen bonding contacts between the coordinating thiolate and the exposed NH_2 moieties of the hydrazines.^[118b] Another family of trigonal bipyramidal and tetrahedral vanadium complexes containing intermediates of the N_2 reduction derives from 1,6-diisopropylphenolate as stabilising ligand.^[119] The compounds **50** and **51** in Figure 4.31 are examples.

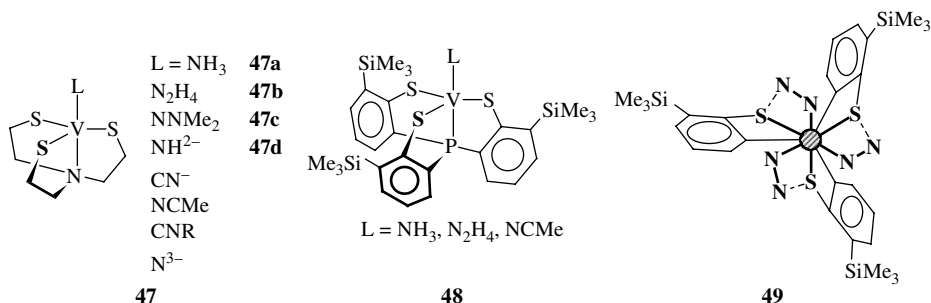
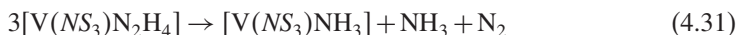
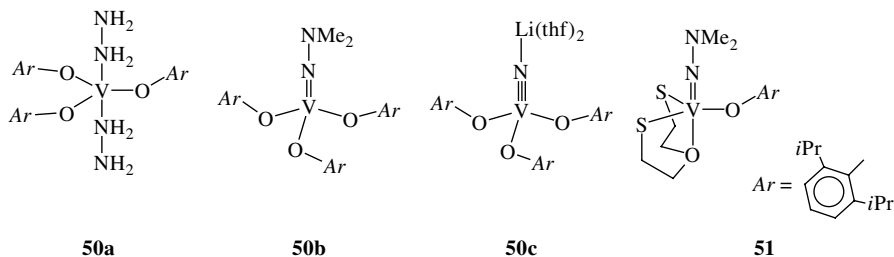


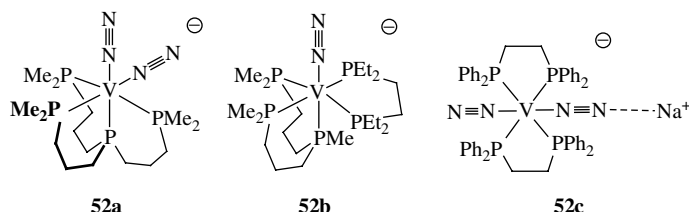
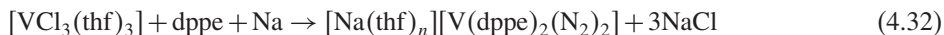
Figure 4.30

47: Complexes with tetradentate tripodal ligands which stabilise substrates [N_2H_4 , CN^- , NCMe , CNR (R e.g. *t*Bu)], intermediates (N_2H_4 , NNMe_2^- , NH^{2-}) and products (N_2H_4 , NH_3) of vanadium nitrogenase.^[118] $[\text{V}(\text{PS}_3)\text{NCMe}]$ (**48**) is catalytically active in N_2H_4 reduction (see text). The tris(hydrazine) complex **49** is viewed ‘from the top’ along the P–V axis (shadowed central circle).

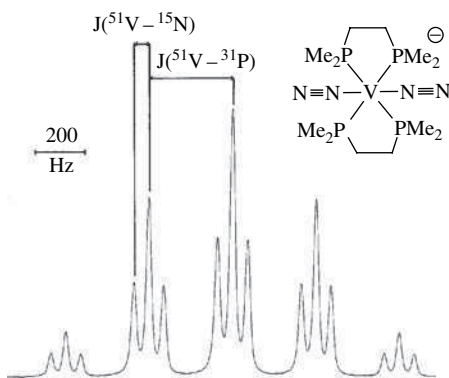
Chelating phosphine ligands are suited to stabilise oxidation states of vanadium as low as $-\text{I}$. This is certainly not an oxidation state of biological relevance. The dinitrogen complexes of $\text{V}^{-\text{I}}$ are of interest, however, since to date (i) they are the only completely characterised vanadium complexes containing the dinitrogen ligand bonded in the end-on fashion and (ii) they intrinsically reduce the nitrogen to ammonia + hydrazine [and are thus comparable to Hidai’s and Chatt’s famous phosphine-stabilised dinitrogen-molybdenum(0) complexes].^[120] Three examples, containing the tripodal, tetradentate PP_3 (**52a**), a tridentate + bidentate phosphine (**52b**) and two bis(diphenylphosphinoethane) ligands (dppe, **52c**) are displayed in Figure 4.32. The examples have been chosen so as to demonstrate how the number of coordinating dinitrogens and the configuration (*cis*)

**Figure 4.31**Aryloxovanadium(III) and -(V) complexes modelling intermediates in N_2 fixation.^[119]

vs trans) can be influenced by the choice of the phosphine ligand(s). Complexes with oligodentate phosphines, and more basic phosphine functions (alkyl vs phenyl substituents on phosphorus), show increased stability against incidental loss of N_2 . The complexes are prepared by reduction of $[\text{VCl}_3(\text{thf})_3]$ with sodium or lithium in the presence of the phosphine under an N_2 atmosphere, as shown in Equation (4.32) for the synthesis of **52c**. The activation of dinitrogen becomes apparent when considering the drastic low-frequency shift of the NN stretching frequency. The $\nu(\text{NN})$ values typically are between 1720 and 1880 cm^{-1} , as compared with 2331 cm^{-1} for free dinitrogen and 1883 cm^{-1} for **46a** in Figure 4.29. Most of the complexes are stable in solution at ambient temperature, where they can unequivocally be characterised by their ^{51}V NMR patterns (Figure 4.33). The complexes are additionally stabilised by contacts between the anion $[\text{V}(\text{P})_n(\text{N}_2)_{6-n}]^-$ and the counter ion $[\text{Na}(\text{thf})_x]^+$ or $[\text{Li}(\text{thf})_y]^+$. In solution, this is demonstrated by the pattern of the ^7Li NMR spectra. In the solid state, the complex *trans*- $[\text{Na}(\text{thf})][\text{V}(\text{dppe})_2(\text{N}_2)_2]$ (**52c**), exhibits a direct contact between Na^+ and N_2 in the $(\text{thf})\text{Na} \cdots \text{N} \equiv \text{N} - \text{V}$ moiety, $d(\text{Na} \cdots \text{N}) = 2.445(11)\text{ \AA}$. The distance $d(\text{N}-\text{N}) = 1.30(16)\text{ \AA}$ is about the same as in free N_2 (1.098 \AA), within the limits of error. Addition of HBr to THF solutions of complexes such as **52** gives rise to reductive protonation according to the net reaction represented by Equation (4.33) for $[\text{V}(\text{dmpe})_2(\text{N}_2)_2]^-$ [$\text{dmpe} = \text{bis}(\text{dimethylphosphino})\text{ethane}$].

**Figure 4.32**Anionic dinitrogen complexes stabilised by phosphines.^[120] The counter-ions are solvated (by THF) Na^+ or Li^+ .

Other ‘dinitrogen’ vanadium complexes have been introduced in the last two decades, all of which are dinuclear and contain dinitrogen (originally stemming from aerial N_2) in the

**Figure 4.33**

^{51}V NMR (94.73 MHz) spectrum of a THF solution containing the anion $\text{trans}-[\text{V}(\text{N}_2)^2(\text{dmpe})_2]^-$ (inset). The spectrum shows the quintet due to one-bond ^{51}V - ^{31}P coupling (four equivalent ^{31}P); each of the quintet components is additionally split into a triplet by one-bond ^{51}V - ^{15}N coupling (two equivalent ^{15}N). Two-bond couplings are not resolved.

bridging $\mu, \eta^1 : \eta^1$ coordination mode. A selection of these dinitrogen-bridged complexes, **53–57**,^[121–125] is presented in Figure 4.34. Vanadium-nitrogen and nitrogen-nitrogen bond lengths are summarised together with those for **46**, **47** and **49–52** (Figures 4.29–4.32 in Table 4.11. The bond lengths $d(\text{N–N})$ in all of these complexes are between 1.21 and 1.26 Å, i.e. in-between a triple bond as in the complex **52c** with the nitrogen in the end-on

Table 4.11 Vanadium–nitrogen and nitrogen–nitrogen bond lengths (in Å) with standard deviations for dinitrogenvanadium complexes. The compounds are arranged in order of increasing oxidation state of nitrogen.

Complex	$d(\text{N–N})$	$d(\text{V–N})$	Nature of ligand	Vanadium oxidation state ^a	Ref.
46c (Figure 4.29)	—	2.1623(8)	NH_3	III	116
47a (Figure 4.30)	—	2.154(7)	NH_3	III	117
47d (Figure 4.30)	—	2.234(2)	NH^{2-}	V	117
50c (Figure 4.31)	—	1.565(5)	$\text{N}^3\text{-}[\text{Li}(\text{thf})_2]^+$	V	119
47b (Figure 4.30)	1.48(2)	2.180(9)	N_2H_4	III	117
49 (Figure 4.30)	av. 1.455	av. 2.225	N_2H_4	III	118b
50a (Figure 4.31)	1.467(6)	2.161(4)	N_2H_4	III	119
47c (Figure 4.30)	1.305(5)	2.214(3)	NNMe ₂ or NNMe ₂ ²⁻	III or V ^b	117
51 (Figure 4.31)	1.467(6)	2.161(4)	NNMe ₂ or NNMe ₂ ²⁻	III or V ^b	119
57 (Figure 4.34)	1.235(6)	1.756(5)	$\mu-(\text{N}=\text{N})^{2-}$	III	125
53 (Figure 4.34)	1.259(6)	1.777(3)	$\mu-(\text{N}=\text{N}^2-)$	"II"	121
54 (Figure 4.34)	1.222(4)	av. 1.773	$\mu-(\text{N}=\text{N})^{2-}$	III	122
55 (Figure 4.34)	1.228(4)	1.833(3)	$\mu-(\text{N}=\text{N})^{2-}$	"II"	123
56 (Figure 4.34)	1.212(8)	av. 1.767	$\mu-(\text{N}\equiv\text{N})$ or $\mu-(\text{N}=\text{N})^{2-}$	I or "II"	124
52c (Figure 4.32)	1.130(16)	1.915(11)	$\text{N}_2 \cdots [\text{Na}(\text{thf})]^+$	-I	120b

^aOxidation states are a matter of debate, depending on the electron count, i.e. the nature attributed to the nitrogen ligand coordinated to vanadium. The oxidation states assigned here do not in all cases agree with those proposed in the original literature.

^bNeutral isodiazene ($\text{N}=\text{NMe}_2$) or hydrazido($2-$).

bonding mode and the single bond for the hydrazine complexes **47b**, **49** and **50a**, classifying the ligand as the two-electron reduction product of $\text{N}\equiv\text{N}^{2-}$, viz. the diazenido($2-$) ligand $[\text{N}=\text{N}]^{2-}$. This view is supported by the rather short $d(\text{V}-\text{N})$ (1.76 – 1.83 Å), indicative of double bond character in the vanadium–nitrogen bond. Consequently, the cumulenic structure has been chosen throughout for the $\text{V}(\mu-\text{N}_2)\text{V}$ units in Figure 4.34, also in accord with $\text{V}-\text{N}-\text{N}$ angles of about 180° or close to 180° (162.4° for **53**, 171.6° for **55**).

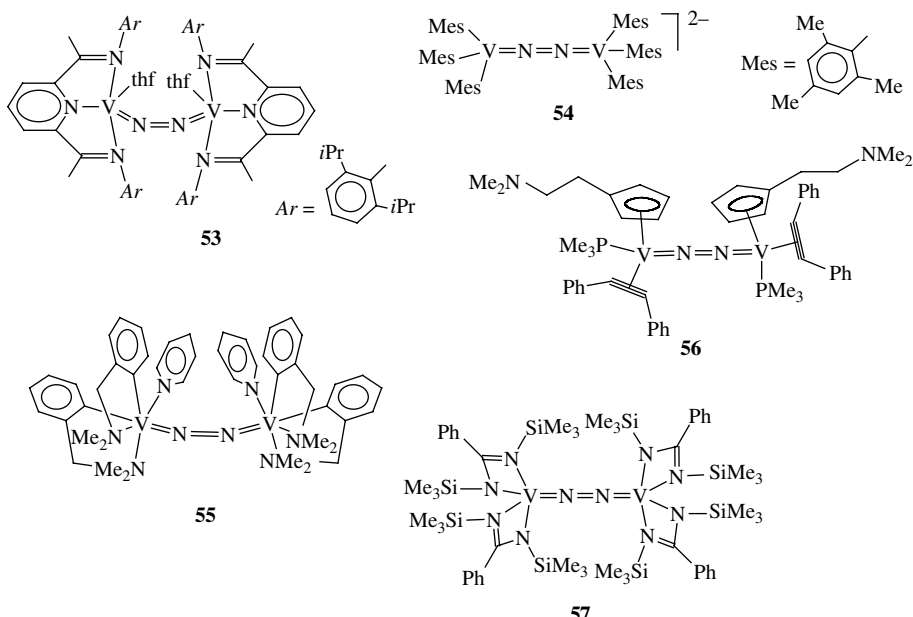
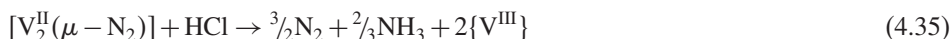
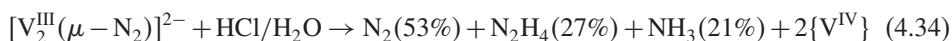


Figure 4.34

Dinuclear vanadium complexes with bridging diazenido($2-$). The ligands are 2,6-bis(1-iminoethyl)pyridine (**53**),^[121] mesityl(1-)^[122] 2-dimethylaminophenyl(1-) and pyridine (**55**),^[123] tolane, trimethylphosphine and dimethylamino-Cp(1-)^[56],^[124] and benzamidinate(1-)^[57].^[125] The complexes **54** and **55**, containing σ -alkyls, produce ammonia and hydrazine on protonation.

Whereas the dinuclear, diazenido-bridged complexes containing N -functional ligands such as bis(imino)pyridine and benzamidinate (**53** and **57**) do not give ammonia or hydrazine on protonation, vanadium complexes with σ -alkyl bonds (**54** and **55**) evolve NH_3 or $\text{NH}_3 + \text{N}_2\text{H}_4$ along with N_2 with acids, as shown in Equations (4.34) and (4.35) for $[\text{V}_2^{\text{III}}(\mu-\text{N}_2)]^{2-}$ (**54**)^[121] and $[\text{V}_2^{\text{II}}(\mu-\text{N}_2)]$ (**55**).^[123b] In these reactions, the vanadium centre is the intrinsic electron donor (reducing agent), i.e. these processes do not proceed catalytically.



Reduction of aerial N_2 promoted by low-valent vanadium does not, in fact, rely on the presence of ‘complicated’ co-ligands. Alkaline solutions containing V^{2+} and Mg^{2+}

(or, rather, the hydroxidic structures of these ions) can very effectively reduce N_2 to ammonia and hydrazine, as was shown by Shilov and co-workers almost four decades ago, [Equation (4.36)].^[126a] At room temperature and an N_2 pressure of 1 bar, the main product formed was hydrazine. Elevating the temperature to 70°C resulted in predominant production of ammonia. In more recent reports, the Shilov group showed that, from N_2 reducing alcoholic solutions containing V^{2+} and catechols, an active anionic complex of composition $\{\text{V}^{\text{II}}(\text{cat})_2\}^{2-}\}_4$ can be isolated and characterised by its $\text{V}^{\text{II}}(\text{d}^3)$ zero-field splitting EPR features.^[126b] The proposed active unit present in solution, including the substrate N_2 for activation, **58**, is provided in Figure 4.35. Even later, a cubane-type catecholato complex containing the cubane core $[\text{V}_2^{\text{II}}\text{V}_2^{\text{III}}(\text{OMe})_2(\text{cat})_2]^2-$, supposedly responsible for the reduction of N_2 to ammonia and of H^+ to hydrogen, was isolated and structurally characterised.^[126c] While the Shilov systems are active in alkaline solutions and in the presence of catechols, acidic solutions (pH 4.5) containing V^{2+} and α, ω -dicarboxylates $-\text{O}_2\text{C}(\text{CH}_2)_n\text{CO}_2^-$ effectively reduce dinitrogen to hydrazine, [Equation (4.37)].^[127] Optimal activity is achieved for $n = 5$ and 6, and this is related to an optimal conformation for picking up and activating N_2 (**59** in Figure 4.35). Interestingly, polycarboxylates obtained by copolymerisation of styrene and cinnamic acid are also active.

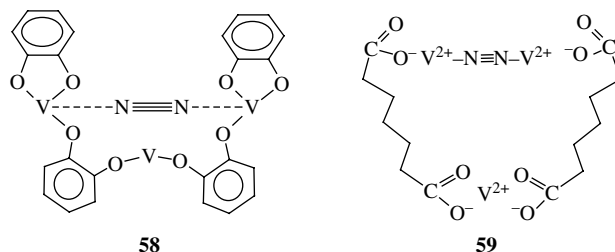
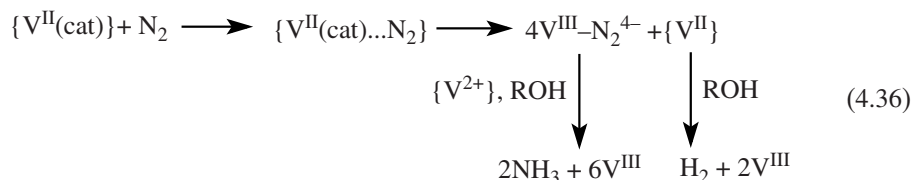


Figure 4.35
Proposed activation of dinitrogen in the V^{II} -catecholate^[126b] and V^{II} -dicarboxylate systems.^[127]

All of these beautiful model complexes for nitrogen fixation have one disadvantage in common: they do not represent any of the structural features of the iron–vanadium cofactor in the nitrogenase. In contrast, cubane clusters constituting the vanadium–iron–sulfur moiety of the FeMoco are expedient structural models, with the disadvantage, however, that they do not catalyse the reduction of N_2 .

Cubanes such as **60**^[106b] in Figure 4.36 have been successfully employed to match XAS data of VNase to structural parameters obtained from single-crystal X-ray diffraction; Table 4.9 in Section 4.4.1.2. Cluster **60** is able to impart the reduction of hydrazine

to ammonia with cobaltocene as the electron source and lutidinium hydrochloride for proton delivery. Related to **60** are the heterocubanes **61** and **62**,^[128] with a protective tris(pyrazolyl)hydroborate (**61**) or tris(pyrazolyl)methanesulfonate (**62**) coordinated to the vanadium site. Cluster **61** can be described in terms of a $[\text{V}^{\text{III}}, \text{Fe}^{\text{III}}, \text{Fe}_2^{\text{II}}\text{S}_4]^{2+}$ ($S = \frac{3}{2}$) core with respect to approximate charge distribution. Its one-electron oxidation leads to a diamagnetic ($S = 0$) core with charge distribution $[\text{V}^{\text{III}}, \text{Fe}_2^{\text{III}}, \text{Fe}^{\text{II}}\text{S}_4]^{3+}$. The charge localisation is backed up by Mössbauer spectra, which show two overlapping quadrupole doublets. Cluster **62** can reversibly be oxidised and reduced in a one-electron step, [Equation (4.38)], with redox potentials $E_{1/2}(\text{ox}) = -0.23$ and $E_{1/2}(\text{red}) = -1.34$ V vs NHE. The cluster **60** readily forms by self-assembly from ferrous chloride and tetrathiovanadate(V). The pyrazolyl and thiolate ligands in **61** and **62** are introduced into **60** by ligand substitution reactions.

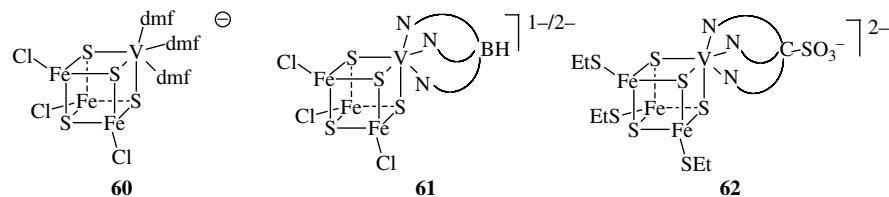
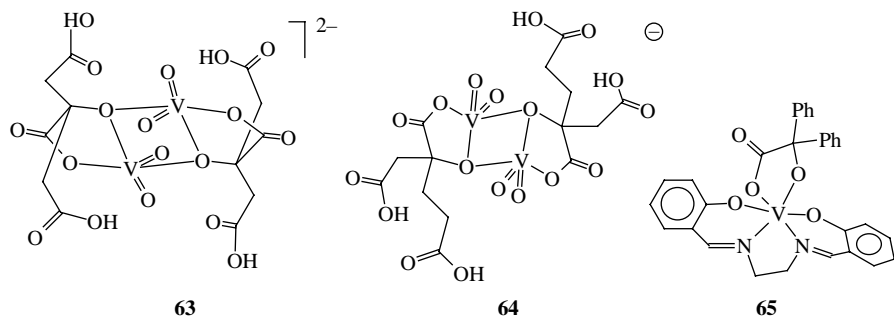


Figure 4.36

Heterocubane clusters containing the $[\text{VFe}_3\text{S}_4]$ core modelling the iron–vanadium site in the iron–vanadium cofactor (FeVco, or **M** cluster) of vanadium nitrogenase (Figure 4.26). The tridentate ligand N_3BH^- is tris(pyrazolyl)borate, the ligand N_3CSO_3^- , tris(pyrazolyl)methanesulfonate.

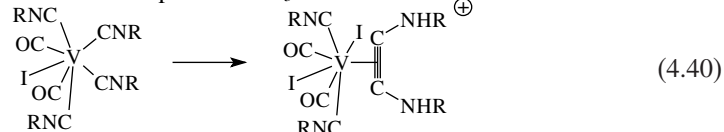
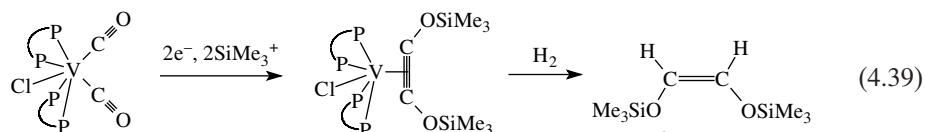
Another structural feature of the FeVco is the coordination of histidine and homocitrate to vanadium. Coordination both of imidazole and imidazole derivatives (including histidine) and of hydroxycarboxylic acids to vanadium in its oxidation states +IV and +V is not uncommon, and has been dealt with in previous sections: for hydroxycarboxylates, see Figures 2.13, 2.14, 2.19 and 2.20; for histidine, see Figures 2.15 and 2.18; for other imidazole derivatives, see Figure 4.20. The citratovanadium(V) complex **63** in Figure 4.37 is an additional example. Here, citrate coordinates through the vicinal carboxylate plus alkoxides, i.e. in the mode postulated for the FeVco. This also applies to the homocitratovanadium(V) complex **64**. None of these structures meets the requirements for a ‘good’ model, however, since they are *dinuclear* complexes of *dioxovanadium* whereas the vanadium centre in the vanadium containing cofactor is mononuclear and lacks the oxo group. A closer approach is the benzilatovanadium(IV) complex **65**, which also models histidine binding by the electronically related Schiff-base imine-N.

In the context of alternative substrates for nitrogenases, in particular alkynes, [Equation (4.27)], model compounds are of interest in which the alkyne is coordinated side-on to vanadium. The side-on or π coordination implies a weakening of the triple bond by π -back-donation from vanadium-d into the π^* orbitals of the ligand, and hence an activation. The activated siloxyacetylene in the complex $[\text{CIVdmpe}]_2\eta^2-(\text{Me}_3\text{SiOC}\equiv\text{COSiMe}_3)]$ [dmpe = bis(dimethylphosphino)ethane] is reduced by hydrogen to the respective ethene, [Equation (4.39)]. The precursor acetylene complex is formed by

**Figure 4.37**

Complexes modelling the coordination of vicinal carboxylate plus hydroxide in the FeVco. The ligands are dihydrogencitrate(2-) (**63**),^[129] dihydrogenhomocitrate(2-) (**64**)^[130] and benzilate(2-) (**65**).^[131] The non-oxo complex **65** is additionally stabilised by a double Schiff base ligand derived from ethylenediamine and salicylaldehyde.

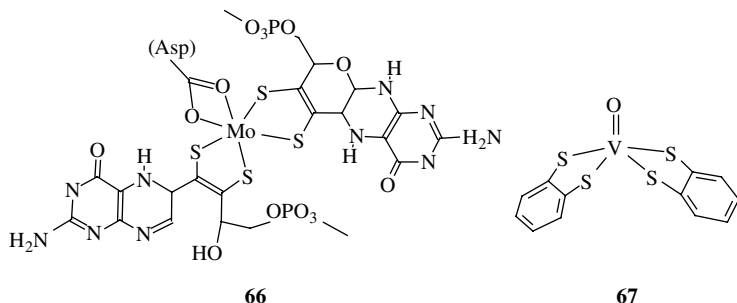
reductive two-electron coupling of two carbon monoxide ligands. This C–C bond formation is reminiscent of the reductive C–C coupling of nitriles represented by Equation 4.30c). Reductive C–C coupling can also be carried out with isonitrile complexes such as $[\text{IV}(\text{CO})_2(\text{CNR})_4]$, [Equation (4.40)].^[115c] Here, the two reduction equivalents are delivered by the metal centre.



4.4.2 Vanadium-dependent Nitrate Reductases?

The parallel existence of an Mo- and a V-dependent nitrogenase in particular, and the diagonal relationship between vanadium and molybdenum in general, suggest that vanadium can also be used, in place of molybdenum, in other Mo-based enzymes, viz. the increasingly growing molybdopterine family, containing the molybdopterine cofactor. A prominent member of this family is nitrate reductase (for the cofactor, see **66** in Figure 4.38), an enzyme that catalyses the two-electron reduction of nitrate to nitrite and thus is active at the starting point of denitrification (Figure 4.25). Figure 4.38 also contains a model compound, **67**,^[132] of the presumed vanadium cofactor of such an enzyme, mimicking the dithiolenate coordination.

There are two reports on partially characterised vanadium-containing, molybdenum-free nitrate reductases, isolated from the bacteria *Thioalkalivibrio nitratireducens*^[133] and *Pseudomonas isachenkovii*.^[134] *T. nitratireducens* is a facultative anaerobic, alkali- and halophilic bacterium living in soda lakes. Its nitrate reductase has a molecular mass of

**Figure 4.38**

The molybdenum environment in the oxidised form of the molybdopterin cofactor of *E. coli* nitrate reductase A (**66**), and a model compound (**67**) for the vanadium centre in a putative vanadium-containing nitrate reductase containing an analogous cofactor.

195 kDa. The enzyme, which consists of four subunits, contains vanadium and iron in a 1:3 ratio and a haeme-*c* type cofactor. The molybdopterine cofactor is absent, i.e. vanadium is not coordinated to a dithiolene moiety. The enzyme reduces nitrate (and other substrates such as nitrite, bromate and selenate) under anaerobic or micro-oxic conditions, using thiosulphate as electron donor. Interestingly, it also exhibits peroxidase and haloperoxidase activity in that it oxidises, by H_2O_2 , *o*-dianisidine and halogenates monochlorodimedone.

The periplasmatic vanadium-containing nitrate reductase from *P. isachenkovii* has a molecular mass of 220 kDa (four subunits). The pterin cofactor is again absent. In media supplemented with vanadate and nitrate, vanadate is first reduced by a membrane-bound reductase using NADH as electron donor. This dissimilatory reduction was followed by nitrate consumption.^[134b]

Although the question of whether or not vanadium-dependent nitrate reductases actually exist has still to be settled, the ability of bacteria to use vanadate(V) as a primary electron acceptor is well established by now and will be addressed in the next section.

4.5 Vanadate as Energiser for Bacteria, and Vanadophores

Vanadium is a comparatively rare but ubiquitous element, particularly abundant in sea water, where – as noted previously (chapter 1) – its concentration is ca 30 nm, classifying it as the second-to-most (next to molybdenum) abundant transition metal in the oceans. Vanadium contents in soil can range from 3 to 310 mg kg⁻¹. Despite the fact that vanadate(V) is readily soluble, the mobility of vanadium is low. Furthermore, in river water, close to 90% of the vanadium present is confined to the colloid fraction; only about 10% is present in the form of dissolved vanadium, i.e. vanadate or water-soluble vanadium complexes with siderophoric ligands (see below). The restricted mobility and the low amount of molecularly dispersed vanadium in water may have their origin in bacterial activity, resulting in the transformation of soluble vanadate to insoluble oxovanadium(IV) hydroxides, followed by geogenic conversion into vanadium minerals. Minerals such as simplonite (with V^{IV}) vanoxite and sherwoodite (with V^{IV}/V^V) (Table 1.1) are potential candidates for minerals which can, basically, also have a biogeogenic origin.

Whereas higher animals and plants use oxygen as the electron acceptor in respiration, bacteria and archaea exhibit a broad respiratory flexibility in that they can employ a variety of alternative electron acceptors, including high-valent metal ions such as Fe^{3+} , Mn^{4+} and U^{6+} and oxo-anions such as arsenate(V), selenate(VI), molybdate(VI) and vanadate(V). Despite the well-established ability of beer yeast (*Saccharomyces cerevisiae*) to metabolise vanadium,^[135] and sporadic reports on the use of vanadate by bacteria during the last two decades,^[136] systematic investigations, on the soil bacterium *Shewanella oneidensis*, have only recently been carried out.^[137–139] In Table 4.12, bacteria are listed which can use external vanadate as a substrate for electron delivery. The reduction can be respiratory or dissimilatory. In respiratory redox processes, the electron flow is coupled to proton translocation, allowing for the generation of adenosine triphosphate (ATP) and growth of the organism. *S. oneidensis*, a facultative anaerobic nonfermenting Gram-negative²⁰ bacterium, belongs to this category, correct conditions for growth provided; otherwise, it is dissimilatory. Dissimilatory redox works without the generation of a proton motive force. The vanadate-reducing salt-water bacterium *Vibrio parahaemolyticus*, which causes acute gastroenteritis, is an example. Since vanadate has the potential to exert toxic effects on the cell metabolism by interference with phosphatases, kinases and ribonucleases (Section 5.2.1), prevention of growth can also be an outcome of toxic effects, and the transfer of electrons to vanadate a means of detoxification for the bacteria. Interestingly, the vanadate reducer *Pseudomonas isachenkovi* was isolated from tunicates,^[136b] marine organisms which are able to take up vanadate from sea water and to reduce it to oxovanadium(IV) and further to vanadium(III); (Section 4.1)

Table 4.12 Bacteria which can use vanadate(V) as a primary substrate for electron delivery.

Species	Reduction product(s)	Electron donor	Ref.
<i>Pseudomonas vanadium-reductans</i> ; <i>P. isachenkovi</i>	V^{IV} , V^{III} ; sherwoodite-like mineral	H_2 , CO, sugars, organic acids	136
<i>Shewanella oneidensis</i> ^a strain MR-1	V^{IV} (soluble → granular brown precipitate)	Lactate, formate	137–139
<i>Vibrio parahaemolyticus</i>	V^{IV}	Glycerol, formate	137
<i>Geobacter metallireducens</i>	V^{IV} (soluble → green vanadylphosphate precipitate)	Acetate	140
Bacterial strains isolated from deep-sea hydrothermal vents	V^{IV} and V^{III}	Lactate	141

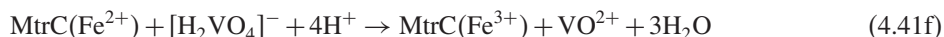
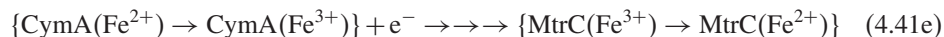
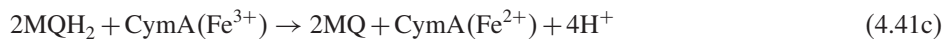
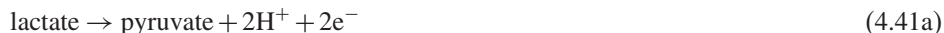
^aThe following strains are able to reduce vanadate: MR-1 (from Lake Oneida, NY),^[137–139] MR-4 and MR-8 (Black Sea),^[139] MR-30 and MR-42 (Lake Michigan).^[139]

S. oneidensis cells pre-grown on fumarate exhibit a pronounced ability to use vanadate as an electron acceptor. Formate and, in particular, lactate are employed as electron sources. Under optimal conditions, ca 16 mM of vanadate is reduced per gram of bacteria per hour, with a biomass doubling time of $10(\pm 1)$ h,^[138] the absolute yield being proportional to the amount of V^{V} available. As noted, electron transport is coupled to proton translocation; 0.62 protons are released per 2 electrons in response to vanadate,

²⁰The outer membrane of Gram-negative bacteria is coated with a lipopolysaccharide, making these bacteria ‘resistant’ against Gram staining – unlike the Gram-positive bacteria.

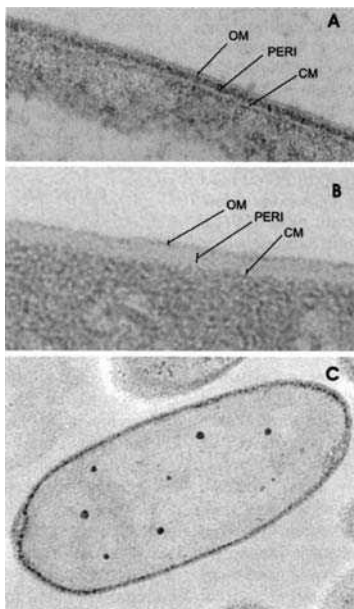
which compares with 0.57 H⁺ for the reduction of ferric ions and 1 H⁺ for the reduction of fumarate.

Vanadate-containing culture media which are inoculated with *S. oneidensis* turn blue due to the formation of vanadyl ions (VO²⁺), momentarily stabilised by constituents of the culture medium or extruded by the bacteria. In the course of time, a granular precipitate (with granule diameters >0.2 μm) forms, mainly consisting of vanadyl hydroxides, and colonised by *S. oneidensis*. These findings point to reduction of extracellular vanadate in contact with the outer cell membrane, and hence by a terminal vanadate reductase associated with the outer membrane. Images taken by transmission electron microscopy (TEM) (Figure 4.39), visualising the presence of vanadium, show that vanadium is also present in the periplasmatic space (Figure 4.39A) and, to a limited extent, even in the cytosol (Figure 4.39C), where it forms vacuole-like inclusions. The intracellular vanadium contents possibly reflect cytosolic detoxification of vanadate(V) by reduction to vanadium(IV). Periplasmatic reduction can occur, as in the case of bacterial reduction of ferric to ferrous ions, by periplasmatic reductases. The main amount of vanadium is, however, present in the extracellular space. A model for the electron transfer pathway, coupled with proton delocation and ATP formation, is depicted in Figure 4.40, and the several steps are additionally represented by the reaction sequence in Equation (4.41). Electrons can be delivered by, e.g., cytosolic lactate [Equation (4.41a)] and picked up by a menaquinone (MQ)²¹ [Equation (4.41b)] associated with the inner (the cytosolic) membrane. The enzyme responsible for the reduction of the substrate delivering the electrons, e.g. lactate dehydrogenase, and the reduction of the menaquinone, contribute to the generation of a proton gradient. The reoxidation of the menahydroquinone is achieved by the tetrahaeme *c*-type cytochrome²² CymA [Equation (4.41c)], which again is located in the cytosolic membrane. ATP is formed as protons are transported back to the cytoplasm [Equation (4.41d)]. The passage of the electrons across the periplasmatic space has not yet been clarified in detail for vanadate. A possibility is a periplasmatic shuttle system [Equation (4.41e)] consisting of cytochromes, or a multihaeme system spanning the periplasmatic space, such as the decahaeme MtrA used in the reduction of Fe³⁺. In any case, the electrons are finally taken up by cytochrome MtrC, which is known to be surface exposed on the external site of the outer membrane, and thus a likely candidate for the terminal vanadate reductase [Equation (4.41f)].^[139] Mutants of *S. oneidensis* lacking this cytochrome do not reduce vanadate. MtrC is another decameric cytochrome-*c* type haeme.

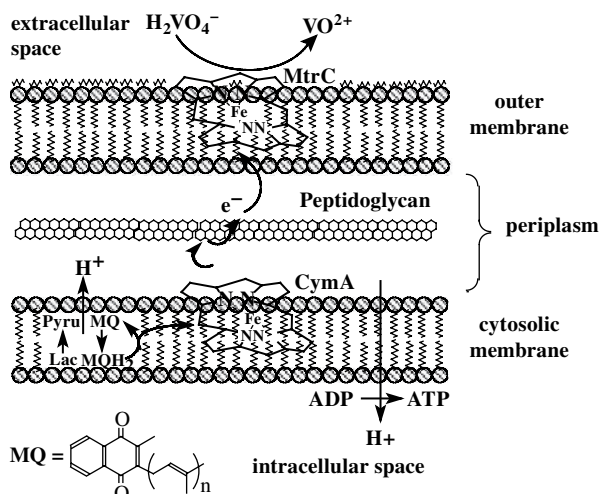


²¹ Menaquinones are 3-methylnaphthoquinones with a polyisoprene chain in position 2.

²² Characteristic features of *c*-type cytochromes include an axial histidine, an axial methionine (both coordinated to the iron centre) and two thioether linkages between the porphyrin and cysteine functions of the protein.

**Figure 4.39**

Transmission electron microscopic images of *Shewanella oneidensis* grown on vanadate(V) (A and C) and fumarate (B), as electron acceptors. Images (A) (magnification 50 000) and (C) (magnification 20 000) show the presence of vanadium in the membrane region [(A) dark zones in the periplasm] and intracellular vanadium [(C) dark spots]. Abbreviations: OM = outer membrane, CM = inner membrane, PERI = periplasmatic space. Courtesy by Wesley Carpentier, University of Gent, Belgium.

**Figure 4.40**

Schematised electron transfer pathway across a Gram-negative bacterial cell membrane (with lactate as the primary electron donor), coupled with H^+ translocation and ATP synthesis, adopted and simplified from ref. 137. MQ and MQH_2 are menaquinone and -hydroquinone, respectively; CymA is a tetrameric and MtrC a decameric cytochrome-*c* type haemoprotein. See also the text and Equation (4.41)). Peptidoglycan (or murein), serving a structural role in the cell membrane, is a block copolymer built up from acetylhexoses and oligopeptides.

A potential application of bacterial vanadate reduction is the detoxification of groundwater, which can contain elevated vanadate concentrations in areas impacted by mining activities. A bacterium capable of reducing metals in high oxidation states is *Geobacter metallireducens*, which is present in various subsurface environments and able, in laboratory experiments, effectively to convert vanadate(V) in concentrations up to 5 mM to vanadyl by respiratory reduction, using acetate as the electron delivery source.^[140] In on-site experiments, with groundwater containing vanadate in concentrations up to 50 µM, injection of acetate stimulated vanadate reduction by *Geobacter* to the extent of complete removal of vanadate within days.

The deposition of mineralised vanadium(IV) oxide/hydroxide by bacterial activity has, in principle, its antipole in bacterial mobilisation of mineralised vanadium. Most aerobic and anaerobic bacteria are well known for their ability to synthesise and excrete low molecular weight ligands capable of mobilising iron(III) from insoluble ferric oxide and hydroxide deposits and thus to secure the iron supply under aerobic conditions and physiological pH. These ligand systems are commonly termed siderophores (Greek for ‘iron carrier’), and the most prestigious ones are the enterobactins, which are based on tris catecholates derived from cyclic tris-serine lactone, and hydroxamate-based systems such as ferrioxamines and ferriochromes. Although it is unknown whether bacteria actively use siderophores to mobilise vanadium from its insoluble deposits, basically the possibility exists, and in any case, mobilisation of vanadium can be a side-effect of iron mobilisation. This is evidenced by the fact that vanadyl can inhibit the growth of bacteria such as *Pseudomonas aeruginosa*, possibly by competing for siderophores and thus causing undersupply of iron.

Enterobactin is a siderophore, produced by, *inter alia*, enteric bacteria such as *Escherichia coli*, belonging – as *Schewanella oneidensis* – to the Gram-negative gamma subgroup of bacteria. Vanadium(IV) forms a stable anionic complex with enterobactin H₆ent, [V(ent)]²⁻ (**68** in Figure 4.41), with structural features very much resembling those of the corresponding Fe³⁺ complex. As in other catecholato complexes (Sections 2.3.2.2 and 4.1.2), vanadium loses its otherwise typical oxo group and coordinates to the six phenolate oxygens. The coordination geometry is intermediate between trigonal prismatic and octahedral, with a twist angle of 28°. The conformation of the tris-serine backbone imposes Δ chirality (cf. Figure 2.25). Another important feature of the complex is a hydrogen bonding network between the amide protons and the catechol oxygens in the *ortho*-position, a feature which, together with the coordination of V⁴⁺ into the catecholate core, provides the necessary rigidity for the pseudo-spherical, hydrophilic outer sphere of the metal-loaded siderophores, allowing for facile transport through water.

The related azotochelin H₄azc is a bis catecholate with a lysine backbone. It is biosynthesised by the nitrogen-fixing soil bacterium *Azotobacter vinelandii* and forms a strong complex with oxovanadium(V), [VO(OH)(azc)]²⁻ (**69** in Figure 4.41).^{23[143]} The stability (apparent stability constant $K = 6.3 \times 10^8 \text{ M}^{-1}$ at pH 6.6) is in-between those for the dioxomolybdenum(VI) and tungsten(VI) complexes. *A. vinelandii* is able to express an alternative, i.e. a vanadium nitrogenase (see the previous section), and azotochelin may thus act as a vanadophore in supplying this nitrogen-fixing organism with vanadium.

²³ A specific formulation for the complex azotocheline – vanadate complex **69** is not provided in ref. 143. The formula shown is based on analogy with the structurally characterised [MoO₂(azc)]²⁻ (counter ions: K⁺).

Vanadium readily forms complexes with hydroxamates, the functional groups in siderophores such as desferrioxamine (**70**). The coordination mode of the hydroxamate group, through the two oxo functions, is revealed by the model complex **71** in Figure 4.41, carrying, along with benzhydroxamate, a Schiff base ligand derived from salicylaldehyde and aminoethylbenzimidazole.^[144] The formation constant for the 1:1 complex between desferrioxamine and vanadium(V) in 0.1 M HClO₄ is 3×10^6 M⁻¹, which is comparable to the stability of the corresponding iron(III) complex in this strongly acidic medium.^[145]

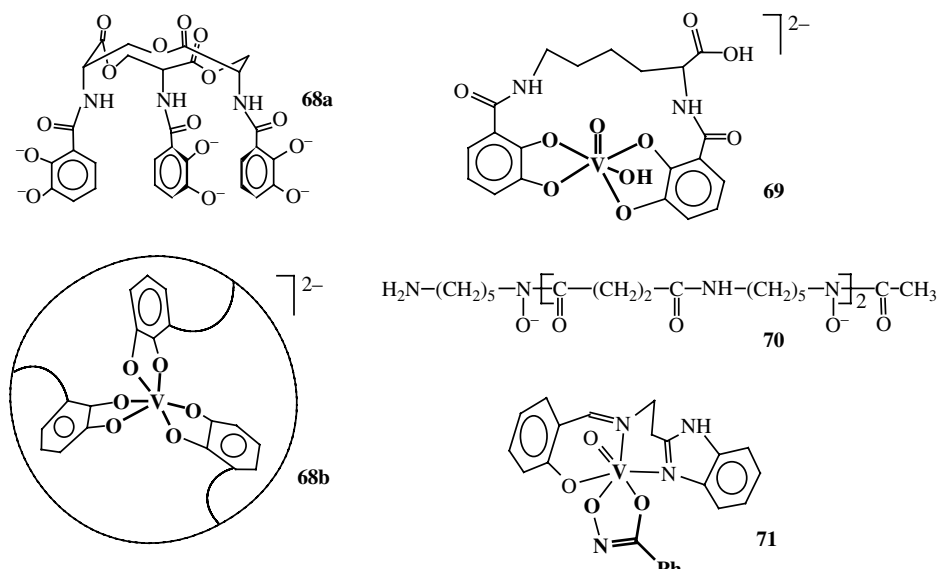


Figure 4.41

'Vanadophores' (vanadium carriers) and (model) complexes: **68a** is the hexaanion of the siderophore enterobactin; **68b** represents the structurally characterised non-oxo vanadium(IV) complex, with the peripheral cyclic tris-serine lactone symbolised by the enclosing circle. The structure of the oxovanadium(V) complex of azotochelin (a siderophore produced by *A. vinelandii*), **69**, has been adapted from the corresponding dioxomolybdenum(VI) complex.^[143] **70** is the siderophore desferrioxamine-B in its trianionic form, and the complex **71**,^[144] carrying benzhydroxamate as a ligand, models the coordination of siderophores based on hydroxamic acids.

References

- [1] M. Henze, *Z. Physiol. Chem.* **1911**, 72, 494–501.
- [2] H. Michibata, N. Yamaguchi, T. Uyama and T. Ueki, *Coord. Chem. Rev.* **2003**, 237, 41–51.
- [3] (a) L. S. Botte, S. Scippa, M. de Vincentiis, *Experientia* **1979**, 35, 1228–1230; (b) S. Scippa, K. Zierold, M. de Vincentiis, *J. Submicrosc. Cytol. Pathol.* **1988**, 20, 719–730.
- [4] (a) I. G. Macara and G. C. McLeod, *Comp. Biochem. Physiol.* **1979**, 62A, 821–826; (b) D. Baldwin, M. McCabe and F. Thomas, *Comp. Biochem. Physiol.* **1984**, 79A, 479–482.
- [5] L. Califano and P. Caselli, *Pubbl. Staz. Zool. Napoli* **1947**, 21, 235–271.
- [6] (a) M. Henze, *Z. Physiol. Chem.* **1932**, 213, 125; (b) L. Califano and E. Boeri, *J. Exp. Biol.* **1950**, 27, 253–256.
- [7] M. J. Smith, *Experientia* **1989**, 45, 452–457.

- [8] D. A. Webb, *J. Exp. Biol.* **1939**, *16*, 499–523.
- [9] (a) E. Bayer, G. Schiefer, D. Waidelich, S. Scippa and M. de Vincentiis, *Angew. Chem. Int. Ed. Engl.* **1992**, *31*, 52–54; (b) D. L. Parry, S. G. Brand and K. Kustin, *Bull. Mar. Sci.* **1992**, *50*, 302–306.
- [10] H.-J. Bielig and E. Bayer, *Liebigs Ann. Chem.* **1953**, *580*, 135–158.
- [11] (a) S. Lee, K. Kustin, W. E. Robinson, R. B. Frankel and K. Spartalian, *J. Inorg. Biochem.* **1988**, *35*, 183–192; (b) R. M. K. Carlson, *Proc. Natl. Acad. Sci. USA* **1975**, *72*, 2217–2221.
- [12] (a) P. Frank and K. O. Hodgson, *Inorg. Chem.* **2000**, *39*, 6018–6027; (b) P. Frank, R. M. K. Carlson, E. J. Carlson and K. O. Hodgson, *Coord. Chem. Rev.* **2003**, *237*, 31–39; (c) P. Frank, E. J. Carlson, R. M. K. Carlson, B. Hedman and K. O. Hodgson, in: *Vanadium the Versatile Metal* (K. Kustin, J. Costa Pessoa and D. C. Crans, Eds), ACS Symposium Series, Vol. 974, American Chemical Society, Washington, DC, **2007**, 281–295. See also: DOI: 10.1016/j.jinorgbio.2007.12.001.
- [13] P. Frank, B. Hedman and K. O. Hodgson, *Inorg. Chem.* **1999**, *38*, 260–270.
- [14] (a) A. L. Dingley, K. Kustin, I. G. Macara, G. C. McLeod, *Biochim. Biophys. Acta* **1981**, *649*, 493–502; (b) H.-J. Bielig, E. Jost, K. Pfleger, W. Rummel and E. Seifen, *Z. Physiol. Chem.* **1961**, *325*, 122–131.
- [15] D. E. Ryan, N. D. Ghatlia, A. E. McDermott, N. J. Turro and K. Nakanishi, *J. Am. Chem. Soc.* **1992**, *114*, 9659–9660.
- [16] N. Yamaguchi, Y. Amakawa, H. Yamada, T. Ueki and H. Michibata, *Zool. Sci.* **2006**, *23*, 909–915.
- [17] T. Hamada, M. Asanuma, T. Ueki, F. Hayashi, N. Kobayashi, S. Yokoyama, H. Michibata and H. Hirota, *J. Am. Chem. Soc.* **2005**, *127*, 4216–4222.
- [18] K. Fukui, T. Ueki, H. Ohya and H. Michibata, *J. Am. Chem. Soc.* **2003**, *125*, 6352–6353.
- [19] M. Yoshinaga, T. Ueki, N. Yamaguchi, K. Kamino and H. Michibata, *Biochim. Biophys. Acta* **2006**, *1760*, 495–503.
- [20] (a) T. Ishii, I. Nakai, C. Numaco and T. Otake, *Naturwissenschaften* **1993**, *80*, 268–270; (b) T. Ishii, T. Otake, K. Okoshi, M. Nakahara and R. Nakamura, *Mar. Biol.* **1994**, *121*, 143–151; (c) T. Ishii, in: *Vanadium in the Environment, Part 1: Chemistry and Biochemistry* (J. O. Nriagu, Ed.), John Wiley & Sons, Inc., New York, **1998**, vol. 23, Ch. 9.
- [21] C. L. Simpson and C. G. Pierpont, *Inorg. Chem.* **1992**, *31*, 4308–4313.
- [22] B. Baruah, S. Das and A. Chakravorty, *Inorg. Chem.* **2002**, *41*, 4502–4508.
- [23] P. Buglyó, A. Dessi, T. Kiss, G. Micera and D. Sanna, *J. Chem. Soc., Dalton Trans.* **1993**, 2057–2063.
- [24] D. C. Crans, J. J. Smee, E. Gaidamauskas and L. Yang, *Chem. Rev.* **2004**, *104*, 849–902.
- [25] R. Meier, M. Boddin, S. Mitzenheim and K. Kanamori, in: *Metal Ions in Biological Systems* (H. Sigel and A. Sigel, Eds), Marcel Dekker, New York, **1995**, Ch. 2.
- [26] S. Ghosh and M. Mukherjee, *Acta Crystallogr., Sect. C* **1994**, *50*, 1204–1207.
- [27] M. R. Maurya, A. Kumar, M. Ebel and D. Rehder, *Inorg. Chem.* **2006**, *45*, 5924–5937.
- [28] R. E. Berry, E. M. Armstrong, R. L. Beddoes, D. Collison, S. N. Ertok, M. Halliwell and C. D. Garner, *Angew. Chem. Int. Ed. Engl.* **1999**, *38*, 795–798.
- [29] H. Ter Meulen, *Rece. Trav. Chim. Pays-Bas* **1931**, *50*, 491–504.
- [30] (a) E. Bayer and H. Kneifel, *Z. Naturforsch., Teil B* **1972**, *27*, 207; (b) H. Kneifel and E. Bayer, *Angew. Chem. Int. Ed. Engl.* **1973**, *12*, 508; (c) P. Krauss, E. Bayer and H. Kneifel, *Z. Naturforsch., Teil B* **1984**, *39b*, 829–832.
- [31] H.-U. Meisch, J. A. Schmitt and W. Reinle, *Z. Naturforsch., Teil C* **1978**, *33*, 1–6.
- [32] E. Bayer, E. Koch, G. Anderegg, *Angew. Chem. Int. Ed. Engl.* **1987**, *26*, 545–547.
- [33] M. A. A. F. de C. T. Carrondo, M. T. N. L. S. Duarte, J. Costa Pessoa, J. A. L. Silva, J. J. R. Fraústo da Silva, M. C. T. A. Vaz and L. F. Vilas-Boas, *J. Chem. Soc., Chem. Commun.* **1988**, 1158.
- [34] (a) E. M. Armstrong, D. Collison, R. J. Deeth and C. D. Garner, *J. Chem. Soc., Dalton Trans.* **1995**, 191–195; (b) E. M. Armstrong, R. L. Beddoes, L. J. Calviou, J. M. Charnock, D. Collison, N. Ertok, J. N. Naismith and C. D. Garner, *J. Am. Chem. Soc.* **1993**, *115*, 807–808.

- [35] M. A. Nawi and T. L. Riechel, *Inorg. Chim. Acta* **1987**, *136*, 33–39.
- [36] J. Lenhardt, B. Baruah, D. C. Crans and M. D. Johnson, *Chem. Commun.* **2006**, 4641–4543.
- [37] (a) T. Hubregtse, E. Neeleman, T. Maschmeyer, R. A. Sheldon, U. Hanefeld and I. W. C. E. Arends, *J. Inorg. Biochem.* **2005**, *99*, 1264–1267; (b) T. Hubregtse, U. Hanefeld and I. W. C. E. Arends, *Eur. J. Org. Chem.* **2007**, 2413–2422.
- [38] (a) J. J. R. Fraústo da Silva, *Chem. Spec. Bioavail.* **1989**, *1*, 139–150; (b) P. M. Reis, J. A. L. Silva, J. J. R. Fraústo da Silva and A. J. L. Pombeiro, *Chem. Commun.* **2000**, 1845–1846.
- [39] (a) P. M. Reis, J. A. L. Silva, A. F. Palavra, J. J. R. Fraústo da Silva, T. Kitamura, Y. Fujiwara and A. J. L. Pombeiro, *Angew. Chem. Int. Ed.* **2003**, *42*, 821–823; (b) P. M. Reis, J. A. L. Silva, A. F. Palavra and J. J. R. Fraústo da Silva, *J. Catal.* **2005**, *235*, 333–340.
- [40] M. F. C. Guedes da Silva, J. A. L. da Sila, J. J. R. Fraústo da Silva, A. J. L. Pombeiro, C. Amatore and J.-N. Verpeaux, *J. Am. Chem. Soc.* **1996**, *118*, 7568–7573.
- [41] (a) K. Kanamori, K. Kusajima, H. Yachi, H. Suzuki, Y. Miyashita and K.-I. Okamoto, *Bull. Chem. Soc. Jpn.* **2007**, *80*, 324–328; (b) E. Ludwig, H. Hefele, E. Uhlemann and F. Weller, *Z. Anorg. Allg. Chem.* **1995**, *621*, 23–28; (c) T. K. Paine, T. Weyhermüller, E. Bill, E. Bothe and P. Chauduri, *Eur. J. Inorg. Chem.* **2003**, 4299–4307.
- [42] S. J. Angus-Dunge, P. C. Paul and A. S. Tracey, *Can. J. Chem.*, **1997**, *75*, 1002–1010.
- [43] L. Saussine, H. Mimoun, A. Mitschler and J. Fisher, *New. J. Chem.* **1980**, *4*, 235–237.
- [44] K. Wieghardt, U. Quilitzsch, B. Nuber and J. Weiss, *Angew. Chem. Int. Ed. Engl.* **1978**, *17*, 351–352
- [45] A. D. Keramidas, S. M. Miller, O. P. Anderson and D. C. Crans, *J. Am. Chem. Soc.* **1997**, *119*, 8901–8915.
- [46] (a) H. Vilter, K.-W. Glombitza and A. Grawe, *Bot. Mar.* **1983**, *26*, 331–340; (b) H. Vilter, *Phytochemistry* **1984**, *23*, 1387–1390; (c) P. Jordan and H. Vilter, *Biochim. Biophys. Acta* **1991**, *1073*, 98–106.
- [47] (a) G. E. Krenn, Academisch Proefschrift (PhD thesis), Free University of Amsterdam, **1989**; (b) D. R. Morris and L. P. Hager, *J. Biol. Chem.* **1966**, *241*, 1763–1768.
- [48] (a) J. W. P. M. Van Schijndel, E. G. M. Vollenbroek and R. Wever, *Biochim. Biophys. Acta* **1993**, *1161*, 249–256; (b) N. Bar-Nun, S. Shcolnick and A. M. Mayer, *FEMS Microbiol. Lett.* **2002**, *217*, 121–124.
- [49] H. Plat, B. E. Krenn and R. Wever, *Biochem. J.* **1987**, *248*, 277–279.
- [50] A. Butler, *Coord. Chem. Rev.* **1999**, *187*, 17–35.
- [51] (a) R. Wever, M. C. M. Tromp, B. E. Krenn, A. Marjani and M. Van Tol, *Environ. Sci. Technol.* **1991**, *25*, 446–449; (b) N. Itoh and M. Shinya, *Mar. Chem.* **1994**, *45*, 95–103.
- [52] J. V. Walker and A. Butler, *Inorg. Chim. Acta* **1996**, *243*, 201–206.
- [53] (a) S. Macedo-Ribeiro, W. Hemrika, R. Renirie, R. Wever and A. Messerschmidt, *J. Biol. Inorg. Chem.* **1999**, *4*, 209–219; (b) Z. Hasan, R. Renirie, R. Kerkman, H. J. Ruijsenaars, A. F. Hartog and R. Wever, *J. Biol. Chem.* **2006**, *281*, 9738–9744.
- [54] M. Weyand, H.-J. Hecht, M. Kiess, M.-F. Liaud, H. Vilter and D. Schomburg, *J. Mol. Biol.* **1999**, *293*, 595–611.
- [55] (a) A. Messerschmidt and R. Wever, *Inorg. Chim. Acta* **1998**, *273*, 160–166; (b) S. Macedo-Ribeiro, W. Hemrika, R. Renirie, R. Wever and A. Messerschmidt, *J. Biol. Inorg. Chem.* **1999**, *4*, 209–219; (c) A. Messerschmidt and R. Wever, *Proc. Natl. Acad. Sci. USA* **1996**, *93*, 392–396; (d) A. Messerschmidt, L. Prade and R. Wever, *Biol. Chem.* **1997**, *378*, 209–315.
- [56] (a) M. N. Isupov, A. R. Dalby, A. A. Brindley, Y. Izumi, T. Tanabe, G. N. Murshudov and J. A. Littlechild, *J. Mol. Biol.* **2000**, *299*, 1035–1049; (b) J. A. Littlechild and E. Garcia-Rodriguez, *Coord. Chem. Rev.* **2003**, *237*, 65–76.
- [57] (a) H. Dau, J. Dittmer, M. Epple, J. Hanss, E. Kiss, D. Rehder, C. Schulzke and H. Vilter, *FEBS Lett.* **1999**, *457*, 237–240. (b) U. Christmann, H. Dau, M. Haumann, E. Kiss, P. Liebisch, D. Rehder, G. Santoni and C. Schulzke, *Dalton Trans.* **2004**, 2534–2540.

- [58] J. M. Arber, E. de Boer, C. D. Garner, S. S. Hasnain and R. Wever, *Biochemistry* **1989**, *28*, 7968–7973.
- [59] (a) E. de Boer, K. Boon and R. Wever, *Biochemistry* **1988**, *27*, 1629–1635; (b) E. de Boer, C. P. Keijzers, A. A. K. Klaaseen, E. J. Reijerse, D. Collison, C. D. Garner and R. Wever, *FEBS Lett.* **1988**, *235*, 93–97; (c) K. Fukui, H. Ohya-Nishiguchi and H. Kamada, *Inorg. Chem.* **1998**, *37*, 2326–2327.
- [60] N. Pooransingh-Margolis, R. Renirie, Z. Hasan, R. Wever, A. J. Vega and T. Polenova, *J. Am. Chem. Soc.* **2006**, *128*, 5190–5208.
- [61] D. Rehder, M. Časný and R. Grosse, *Magn. Reson. Chem.* **2004**, *42*, 745–749.
- [62] G. Zampella, P. Fantucci, V. L. Pecoraro and L. De Gioia, *J. Am. Chem. Soc.* **2005**, *127*, 953–960.
- [63] (a) O. Bortolini, M. Carraro, V. Conte and S. Moro, *Eur. J. Inorg. Chem.* **2003**, *42*–46; (b) V. Conte, F. di Furia and G. M. Licini, *Appl. Catal.* **1997**, *157*, 335–361; (c) V. Conte, F. di Furia and S. Moro, *J. Phys. Org. Chem.* **1996**, *9*, 329–336.
- [64] (a) M. A. Andersson and S. G. Allenmark, *Tetrahedron* **1998**, *54*, 15293–15304; (b) M. A. Andersson, A. Willets and S. Allenmark, *J. Org. Chem.* **1997**, *62*, 8455–8458; (c) H. B. ten Brink, H. E. Schoemaker and R. Wever, *Eur. J. Biochem.* **2001**, *268*, 132–138.
- [65] (a) J. N. Carter-Franklin, J. D. Parrish, R. A. Tschirret-Guth, R. D. Little and A. Butler, *J. Am. Chem. Soc.* **2003**, *125*, 3688–3689; (b) J. S. Martinez, G. L. Carroll, R. A. Tschirret-Guth, G. Altenhoff, R. D. Little and A. Butler, *J. Am. Chem. Soc.* **2001**, *123*, 3289–3294.
- [66] Y. Zhang and R. H. Holm, *Inorg. Chem.* **1990**, *29*, 911–917.
- [67] B. J. Hamstra, G. J. Colpas and V. L. Pecoraro, *Inorg. Chem.* **1998**, *37*, 949–955.
- [68] R. I. de la Rosa, M. J. Clague and A. Butler, *J. Am. Chem. Soc.* **1992**, *114*, 760–761.
- [69] G. B. Schul'pin and E. R. Lachter, *J. Mol. Catal. A*, **2003**, *197*, 65–71.
- [70] (a) M. R. Maurya, A. Kumar, M. Ebel and D. Rehder, *Inorg. Chem.* **2006**, *45*, 5924–5937; (b) G. Santoni and D. Rehder, *J. Inorg. Biochem.* **2004**, *98*, 758–764; (c) C. R. Cornman, J. Kampf, M. Soo Lah and V. L. Pecoraro, *Inorg. Chem.* **1992**, *31*, 2035–2043.
- [71] J. Tatiersky, P. Schwendt, A. Sivák and J. Marek, *Dalton Trans.* **2005**, 2305–2311.
- [72] M. Časný and D. Rehder, *Dalton Trans.* **2004**, 839–846.
- [73] R. E. Drew and E. W. B. Einstein, *Inorg. Chem.* **1973**, *12*, 829–835.
- [74] C. Dordjevic and S. A. Craig, *Inorg. Chem.* **1985**, *24*, 1281–1283.
- [75] H. Mimoun, L. Saussine, E. Daire, M. Postel, J. Fischer and R. Weiss, *J. Am. Chem. Soc.* **1983**, *105*, 3101–3110.
- [76] D. C. Crans, A. D. Keramidas, H. Hoover-Litty, O. P. Anderson, M. M. Miller, L. M. Lemoine, S. Pleasic-Williams, M. Vandenberg, A. J. Rossomando and L. J. Sweet, *J. Am. Chem. Soc.* **1997**, *119*, 5447–5448.
- [77] M. Vennat, J. M. Brégeault and P. Herson, *Dalton Trans.* **2004**, 908–913.
- [78] H. Schmidt, I. Andersson, D. Rehder and L. Pettersson, *Chem. Eur. J.* **2001**, 251–257.
- [79] H. Mimoun, P. Chaumette, M. Mignard, L. Saussine, J. Fischer and R. Weiss, *Nouv. J. Chim.* **1983**, *7*, 467–475.
- [80] C. Wikete, P. Wu, G. Zampella, L. deGioia, G. Licini and D. Rehder, *Inorg. Chem.* **2007**, *46*, 196–207.
- [81] S. Groysman, I. Goldberg, Z. Goldschmidt and M. Kol, *Inorg. Chem.* **2005**, *44*, 5073–5080.
- [82] W. R. Browne, A. G. J. Ligtenbarg, J. W. de Boer, T. A. van den Berg, M. Lutz, A. L. Spek, F. Hartl, R. Hage and B. L. Feringa, *Inorg. Chem.* **2006**, *45*, 2903–2916.
- [83] T. Moriuchi, M. Nishiyama, T. Beppu, T. Hirao and D. Rehder, *Bull. Chem. Soc. Jpn.* **2007**, *80*, 957–959.
- [84] M. Greb, J. Hartung, F. Köhler, K. Špehar, R. Kluge and R. Csuk, *Eur. J. Org. Chem.* **2004**, 3799–3812.
- [85] H. Glas, E. Herdtweck, G. R. J. Artus and W. R. Thiel, *Inorg. Chem.* **1998**, *37*, 3644–3646.
- [86] (a) G. J. Colpas, B. J. Hamstra, J. W. Kampf and V. L. Pecoraro, *J. Am. Chem. Soc.* **1996**, *118*, 3469–3478; (b) T. S. Smith, II, and V. L. Pecoraro, *Inorg. Chem.* **2002**, *41*, 6754–6760.

- [87] K. P. Bryliakov, E. P. Talsi, T. Kühn and C. Bolm, *New. J. Chem.* **2003**, *27*, 609–614.
- [88] P. Wu, G. Santoni, C. Wikete and D. Rehder, in: *Vanadium the Versatile Metal* (K. Kustin, J. Costa Pessoa and D. C. Crans, Eds.), ACS Symposium Series, Vol. 974, American Chemical Society, Washington, DC, **2007**, 61–69.
- [89] C. Ohta, H. Shimizu, A. Kondo and T. Katsuki, *Synlett.* **2002**, 161–163.
- [90] G. Liu, D. A. Cogan and J. A. Ellman, *J. Am. Chem. Soc.* **1997**, *119*, 9913–9914.
- [91] C. Bolm and F. Bienewald, *Angew. Chem. Int. Ed. Engl.* **1995**, *34*, 2883–2885.
- [92] D. Balcells, F. Maseras and A. Lledós, *J. Org. Chem.* **2003**, *68*, 4265–4274.
- [93] X. Zhang, M. Meuwly and W.-D. Woggon, *J. Inorg. Biochem.* **2004**, *98*, 1967–1970.
- [94] (a) V. Vergopoulos, W. Priebisch, M. Fritzsche and D. Rehder, *Inorg. Chem.* **1993**, *32*, 1844–1849; (b) C. Grüning, H. Schmidt and D. Rehder, *Inorg. Chem. Commun.* **1999**, *2*, 57–59.
- [95] M. Časný and D. Rehder, *Chem. Commun.* **2001**, 921–922.
- [96] C. Kimblin, X. Bu and A. Butler, *Inorg. Chem.* **2002**, *41*, 161–163.
- [97] S. Nica, A. Pohlmann and W. Plass, *Eur. J. Inorg. Chem.* **2005**, 2032–2036.
- [98] (a) H. Bortels, *Zentralbl. Bakteriol. Parasitenkd. Infektionskr.* **1933**, *87*, 476–477; (b) H. Bortels, *Zentralbl. Bakteriol. Parasitenkd. Infektionskr.* **1936**, *95*, 193–217.
- [99] C. K. Horner, D. Burk, F. E. Allison and M. S. Sherman, *J. Agric. Res.* **1942**, *65*, 173–192.
- [100] H. L. Jensen and D. Spencer, *Proc. Linnean Soc. N.S.W.* **1947**, *72*, 73–87.
- [101] (a) R. L. Robson, R. R. Eady, T. H. Richardson, R. W. Miller, M. Hawkins and J. R. Postgate, *Nature* **1986**, *322*, 388–390; (b) R. Cammack, *Nature* **1986**, *322*, 312.
- [102] (a) R. N. Pau, in: *Biology and Biochemistry of Nitrogen Fixation* (M. J. Dilworth and A. R. Glenn, Eds), Elsevier, Amsterdam, **1991**, Ch. 3; (b) R. R. Eady, *Coord. Chem. Rev.* **2003**, *237*, 23–30.
- [103] R. L. Robson, P. R. Woodley, R. N. Pau and R. R. Eady, *EMBO J.* **1989**, *8*, 1217–1224.
- [104] (a) C. Z. Blanchard and B. J. Hales, *Biochemistry* **1996**, *35*, 472–478; (b) R. C. Tittsworth and B. J. Hales, *Biochemistry* **1996**, *35*, 479–487.
- [105] G. Boison, C. Steingen, L. J. Stal and H. Bothe, *Arch. Microbiol.* **2006**, *186*, 367–376.
- [106] (a) J. M. Arber, B. R. Dobson, R. R. Eady, P. Stevens, S. S. Hasnain, C. D. Garner and B. E. Smith, *Nature* **1987**, *325*, 372–374; (b) J. Chen, J. Christiansen, R. C. Tittsworth, B. J. Hales, S. J. George, D. Coucouvanis and S. P. Cramer, *J. Am. Chem. Soc.* **1993**, *115*, 5509–5515.
- [107] B. J. Hales, A. E. True and B. M. Hoffman, *J. Am. Chem. Soc.* **1989**, *111*, 8519–8520.
- [108] J. E. Morningstar, M. K. Johnson, E. E. Case and B. J. Hales, *Biochemistry* **1987**, *26*, 1795–1800.
- [109] N. Ravi, V. Moore, S. G. Lloyd, B. J. Hales and B. H. Huynh, *J. Biol. Chem.* **1994**, *269*, 20920–20924.
- [110] M. J. Dilworth and R. R. Eady, *Biochem. J.* **1991**, *277*, 465–468.
- [111] K. Fisher, M. J. Dilworth and W. E. Newton, *Biochemistry* **2006**, *45*, 4190–4198.
- [112] W. Plass, *J. Mol. Struct. (Theochem)* **1994**, *121*, 53–62.
- [113] (a) F. Studt, T. Tuczak, *Angew. Chem. Int. Ed.* **2005**, *44*, 5639–5642; (b) F. Neese, *Angew. Chem. Int. Ed.* **2006**, *45*, 196–199.
- [114] D. V. Yandulov and R. R. Schrock, *Inorg. Chem.* **2005**, *44*, 1103–1117.
- [115] Y. Gao and Y. Zhou, *Huaxue Tongbao* **2007**, *70*, 270–276; (b) Z. Janas and P. Sobota, *Coord. Chem. Rev.* **2005**, *249*, 2144–2155; (c) D. Rehder, *J. Inorg. Biochem.* **2000**, *80*, 133–136.
- [116] N. C. Smythe, R. R. Schrock, P. Müller and W. Weare, *Inorg. Chem.* **2006**, *45*, 9197–9205.
- [117] S. C. Davies, D. L. Hughes, Z. Janas, L. B. Jerzykiewicz, R. L. Richards, J. R. Sanders, J. E. Silverston and P. Sobota, *Inorg. Chem.* **2000**, *39*, 3485–3498.
- [118] (a) W.-G. Chu, C.-C. Wu and H.-F. Hsu, *Inorg. Chem.* **2006**, *45*, 3164–3166; (b) H.-F. Hsu, W.-C. Chu, C.-H. Hung and J.-H. Liao, *Inorg. Chem.* **2003**, *42*, 7369–7371.
- [119] Z. Janas and P. Sobota, *Coord. Chem. Rev.* **2005**, *249*, 2144–2155.
- [120] (a) C. Woitha and D. Rehder, *Angew. Chem. Int. Ed. Engl.* **1990**, *29*, 1438–1440; (b) H. Gailus, C. Woitha and D. Rehder, *Dalton Trans.* **1994**, 3471–3477.

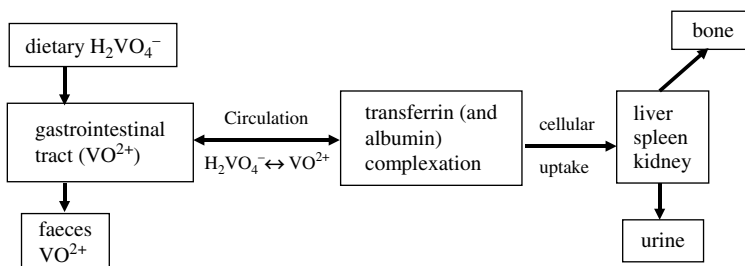
- [121] I. Vidyaratne, S. Gambarotta and I. Korobkov, *Inorg. Chem.* **2005**, *44*, 1187–1189.
- [122] R. Ferguson, E. Solari, C. Floriani, D. Osella, M. Ravera, N. Re, A. Chiesi-Villa and C. Rizzoli, *J. Am. Chem. Soc.* **1997**, *119*, 10104–10115.
- [123] (a) J. J. H. Edema, A. Meetsma and S. Gambarotta, *J. Am. Chem. Soc.* **1989**, *111*, 6878–6880; (b) G. J. Leigh, R. Prieto-Alcón and J. R. Sanders, *Chem. Commun.* **1991**, 921–922.
- [124] B. Hessen, G. Liu, A. Batinas and A. Meetsma, personal communication; see also: Abstracts of Papers, 232nd ACS National Meeting, San Francisco, CA, **2006**.
- [125] S. Hao, P. Berno, R. K. Minhas and S. Gambarotta, *Inorg. Chim. Acta* **1995**, *244*, 37–49.
- [126] (a) A. Shilov, N. Denisov, O. Efimov, N. Shuvalov, N. Shuvalova and A. Shilova, *Nature* **1971**, *231*, 460–461; (b) N. P. Luneva, A. P. Moravskii and A. E. Shilov, *Nouv. J. Chim.* **1982**, *6*, 245–251; (c) N. P. Luneva, S. A. Mironava, A. E. Shilov, M. Yu. Antipin and Y. T. Struchkov, *Angew. Chem. Int. Ed. Engl.* **1993**, *32*, 1178–1179.
- [127] B. Folkesson and R. Larsson, *Acta Chem. Scand. Ser. A* **1979**, *33*, 347–357.
- [128] (a) C. Hauser, E. Bill and R. H. Holm, *Inorg. Chem.* **2002**, *41*, 1615–1624; (b) D. V. Fomitchev, C. C. McLauchlan and R. H. Holm, *Inorg. Chem.* **2002**, *41*, 958–966.
- [129] M. Tsaramyrsi, D. Kavousanaki, C. P. Raptopoulos, A. Terzis and A. Salifoglou, *Inorg. Chim. Acta* **2001**, *320*, 47–59.
- [130] D. W. Wright, R. T. Chang, S. K. Mandal, W. H. Armstrong and W.-H. Orme-Johnson, *J. Bioinorg. Chem.* **1996**, *1*, 143–151.
- [131] V. Vergouopoulos, S. Jantzen, D. Rodewald and D. Rehder, *Chem. Commun.* **1995**, 377–378.
- [132] J. J. A. Cooney, M. D. Carducci, A. E. McElhaney, H. D. Selby and J. H. Enemark, *Inorg. Chem.* **2002**, *41*, 7086–7093.
- [133] A. N. Antipov, D. Y. Sorokin, N. P. L'Vov and J. G. Kuenen, *Biochem. J.* **2003**, *369*, 185–189.
- [134] (a) A. N. Antipov, N. L. Lyalikova, T. V. Khijniak and N. P. L'vov, *FEBS Lett.* **1998**, *441*, 257–260; (b) A. N. Antipov, N. L. Lyalikova, T. V. Khijniak, N. P. L'vov and A. N. Bach, *IUBMB Life* **2000**, *50*, 39–42.
- [135] G. R. Willsky, D. A. White and B. C. McCabe, *J. Biol. Chem.* **1984**, *259*, 13273–13281.
- [136] (a) N. A. Yukova, N. D. Saveljeva and N. N. Lyalikova, *Mikrobiologiya* **1993**, *62*, 597–603; (b) N. N. Lyalikova and N. A. Yukova, *Mikrobiologiya* **1990**, *59*, 968–975; (c) N. N. Lyalikova and N. A. Yukova, *Geomicrobiol. J.* **1992**, *10*, 15–26; (d) A. N. Antipov, N. N. Lyalikova and N. P. L'vov, *IUBMB Life* **2000**, *49*, 137–141.
- [137] W. Carpentier, PhD Thesis, University of Gent, **2005**.
- [138] (a) W. Carpentier, K. Sandra, I. De Smet, A. Brigé, L. De Smet and J. Van Beeumen, *Appl. Environ. Microbiol.* **2003**, *69*, 3636–3639; (b) W. Carpentier, L. De Smet, J. Van Beeumen and A. Brigé, *J. Bacteriol.* **2005**, *187*, 3293–3301.
- [139] J. M. Myers, W. E. Antholine and C. R. Myers, *Appl. Environ. Microbiol.* **2004**, *70*, 1405–1412.
- [140] I. Ortiz-Bernad, R. T. Anderson, H. A. Vrionis and D. R. Lovley, *Appl. Environ. Microbiol.* **2004**, *70*, 3091–3095.
- [141] J. T. Csotonyi, E. Stackebrandt and V. Yurkov, *Appl. Environ. Microbiol.* **2006**, *72*, 4950–4956.
- [142] T. B. Karpishin, T. M. Dewey and K. N. Raymond, *J. Am. Chem. Soc.* **1993**, *115*, 1842–1851.
- [143] J. P. Bellenger, F. Arnaud-Neu, Z. Asfari, S. C. B. Myneni, E. I. Stiefel and A. M. L. Kraepiel, *J. Biol. Inorg. Chem.* **2007**, *12*, 367–376.
- [144] M. R. Maurya, A. Kumar, M. Ebel and D. Rehder, *Inorg. Chem.* **2006**, *45*, 5924–5937.
- [145] I. Batinić, M. Biruš and M. Pribanić, *Croat. Chem. Acta* **1987**, *60*, 279–284.

This page intentionally left blank

5 Influence of Vanadium Compounds on Cellular Functions

In this chapter, medicinal aspects of vanadium compounds acting on the cellular/molecular level (Section 5.1) and the interaction of vanadium with proteins (including, to some extent, interferences with protein substrates and DNA; Section 5.2) will be covered. Since beneficial and adverse effects can go hand and hand, or are dose dependent and/or controlled by a multitude of influential factors, this coverage also considers aspects directed towards absorption, distribution and the toxic implications of vanadium, some of which have already been addressed briefly in the Introduction. A comprehensive treatise on nutritional, environmental and toxicological aspects is beyond the scope of this book. The interested reader is referred to review articles in books and journals mentioned and recommended in the section ‘Further Reading’ at the end of Chapter 1.

The (metabolic) pathways of dietary vanadium, such as vanadate $[H_2VO_4]^-$, can be expressed as illustrated in Scheme 5.1:¹ after oral uptake, vanadate reaches the gastrointestinal tract, where it is partially reduced and precipitated to vanadyl (VO^{2+}) hydroxides, which are excreted with the faeces. Another portion is absorbed and circulated in the blood, where it undergoes redox speciation and complexation by the serum proteins transferrin and albumin. Vanadate and vanadyl are finally incorporated into cells, mainly those of the liver, spleen and kidney. Excretion is achieved via the urine. Part of the vanadium is taken up by bones, where the mean retention time is comparatively long.



Scheme 5.1

¹ Scheme 5.1 has been adapted (and slightly modified) from a presentation by E. J. Baran, Universidad Nacional de La Plata (Argentina), at the 13th International Conference on Bioinorganic Chemistry, 2007, in Vienna.

Certainly, Scheme 5.1 (and the accompanying statements) only roughly represents the overall complex situation, intended to familiarise the reader with the basic course of action. More details will be provided in Sections 5.1 and 5.2. The ‘cellular level’ starts where a vanadium compound is taken up by cell tissues. Prior to and after uptake, speciation at the ‘molecular level’ is implemented; see also Chapter 2. The modified vanadium compound(s) thus generated, or the original compound, influence the cellular function, which can result in toxic and beneficial effects.

5.1 Medicinal Aspects of Vanadium

5.1.1 The Anti-diabetic Potential of Vanadium Compounds

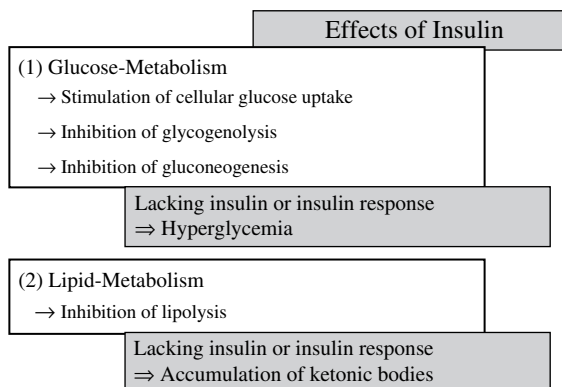
This section will be structured as follows:

1. diabetes mellitus – general aspects;
2. historical development of the potential of vanadium compounds in the treatment of diabetes;
3. ‘modern’ vanadium compounds which are active *in vitro* and *in vivo*;
4. speciation and distribution of vanadium under *in vivo* conditions;
5. molecular mechanism and function at the cellular level.

5.1.1.1 Diabetes Mellitus – General Aspects

For the function and survival of all organs, a continuous supply of the ‘correct’ amounts of glucose is essential. Undersupply (hypoglycaemia) leads to apoptosis (cell death), and hyperglycaemia to various organ damages. It is therefore necessary to maintain the physiological blood concentration regulated at the optimal level of around 5 mM. After uptake of food and absorption of sugar present in food or mobilised by degradation of starch and the like in the gastrointestinal tract, the glucose level has to be lowered. For this purpose, insulin, produced by the β -cells in the Langerhans’ islets of the pancreas and stored in its hexameric, Zn^{2+} -connected form, is mobilised, i.e. released into the bloodstream, from where it stimulates cellular uptake of glucose by skeletal muscle (ca 75%) and adipose tissues. On the other hand, in-between meals and during fasting, glucose, set free from glycogen in the liver (glycogenolysis), is distributed. Mobilisation of insulin is balanced/repressed by its antagonist glucagon, produced in the α -cells of the pancreas. Glucose may also be synthesised from lactate or alanine (gluconeogenesis), and excess glucose be stored after conversion to glycerol and further to triglycerides (lipogenesis). In all of these processes, insulin plays a central role, and its lack, insufficient supply or insufficient recognition by cell receptors causes the chronic disease diabetes mellitus. Insulin is also an important inhibitor of lipolysis. The lack of insulin causes uncontrolled degradation of fat and thus production of acetyl-coenzyme-A in amounts which can no longer be tackled with by the citric acid cycle. As a consequence, ketonic bodies such as acetoacetic acid form, the main factor responsible for severe damage of the peripheral blood vessels, creating extensive open wounds and necroses mainly at the limbs. Another typical symptom of diabetes mellitus is diabetic retinopathy, severe damage of the eye (blurred vision and blind spots) caused by destruction of the small blood vessels in the retina, finally leading to blindness. Other complications associated with diabetes are kidney failure, heart disease and neuropathy.

The main actions of insulin and the dysfunctions caused in the case of diabetes are sketched in Scheme 5.2.



Scheme 5.2

The two principle forms of diabetes mellitus are:

- Type 1 diabetes,² in which the pancreas fails to produce insulin. This failure may go back to an (inherited or virus-induced) auto-immune reaction, or to damage to the pancreas in, e.g., an accident. This form develops most frequently in children and adolescents. About 10% of diabetics belong to this type.
- Type 2 diabetes, which results from the body's inability to respond properly to insulin still produced in the pancreas. On a cellular basis, this type of 'insulin tolerance' or 'insulin resistance' can be traced back to a lack of response of the membrane-bound insulin receptor and/or a decrease in receptor density. About 90% of the diabetes cases worldwide fall into this category, which most frequently occurs in elderly adults, but is being noticed increasingly in obese adolescents. Little is known about why insulin resistance occurs. One suggestion is that increased levels of reactive oxygen species (ROS) are an important trigger.^[1] The biochemical aspects of type 2 diabetes have been reviewed.^[2]

Worldwide, 150 million people suffer from diabetes, and this number will double by 2025, according to estimates by the World Health Organization. Diabetes is thus one of the main epidemic challenges of the future. Treatment of type I diabetes is commonly carried out by external supply of insulin, applied by subcutaneous injection. Type II diabetes can, to a certain extent, be coped with and the symptoms even suppressed by physical exercise and a reasonable diet (both of which are certainly not on the agenda of obese adolescents). In later stages, insulin injections can help but, since type II diabetes goes along with an increasing lack of response to insulin, this medication ultimately becomes ineffective. Alternative methods of treatment have been advanced. Since insulin is a peptide hormone (Figure 5.1), oral application is not feasible. Respirable insulin preparations, containing additives to increase the permeability of the lung aveoles have been developed, but

² Type I diabetes is also known as IDMM (insulin-dependent diabetes mellitus) and type II as NIDDM (noninsulin-dependent diabetes mellitus).

discontinued due to serious side-effects. A few groups of drugs for oral application are on the market that keep, at least for a period, glucose levels under control, but they are all associated with unpleasant side-effects. These drugs (for examples see Figure 5.1) are derived from sulfonylurea (**1**), which stimulate insulin production by the β -cells, and from thiazolidinediones (**2**), so-called glitazones,³ which stimulate uptake of glucose by fat cells. A side-effect of the former is hypoglycaemia, and a side-effect of the latter is increasing production of fatty tissue, i.e. substantial weight gain, and gastrointestinal problems. A novel development for treating type II diabetes is glucagon-like peptides.

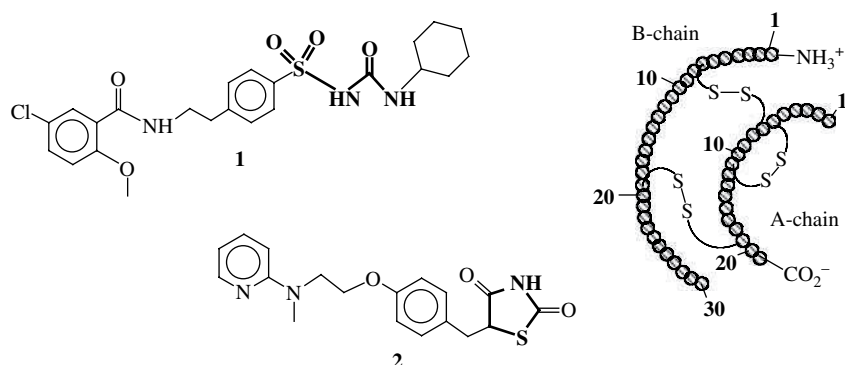


Figure 5.1

Left: two representatives of two groups of orally applied anti-diabetic drugs. Compound **1** derives from sulfonylurea and **2** from thiazolidinedione. Right: schematic drawing of the hormone insulin. The active form, a monomer (shown), consists of two peptide chains which are linked by two disulfide bridges. Chain A contains an additional disulfide link.

5.1.1.2 Historical Development of the Potential of Vanadium Compounds in the Treatment of Diabetes

In 1897–98, aqueous solutions of sodium vanadate were tested in the L'Hôtel-Dieu hospital in Lyon with respect to vanadium's possible benefits in the treatment of 44 test subjects with various health problems, including anaemia, tuberculosis, rheumatism, arnyotrophia, hysteria, neurasthenia – and diabetes (three individuals).^[3] The test subjects were treated orally over 24 h, and three times per week, with 4–5 mg of Na[VO₃] dissolved in water prior to meals. All of the patients showed an increase in appetite, a gain in weight, and an improvement of their physical status. For the three diabetics, a slight decrease in blood sugar [*'le sucre peut diminuer un peu chez les diabétiques'*] was observed for two individuals. This appears to be the first report on the possible benefits of vanadate in the treatment of diabetes mellitus. The medication of humans with vanadate has been resumed only sporadically, probably due to the toxicity of vanadate in nonphysiological doses: 17 mg kg⁻¹ sufficed to kill a hare and 75 mg kg⁻¹ a dog.^[3] For humans, the lethal dose appears to be somewhat higher (see Table 1.2). The second report on human subjects, the treatment of five type I and five type II diabetics with sodium vanadate, appeared in 1995.^[4] Daily intake of 125 mg of Na[VO₃] over a period of 2 weeks improved

³ For the possible hazards of this drug family see, e.g., *Chem. Eng. News*, **2007**, 85 (22), 8.

insulin sensitivity in type II and some of the type I patients, accompanied by a significant decrease in cholesterol levels. The most common adverse effect was mild gastrointestinal intolerance.

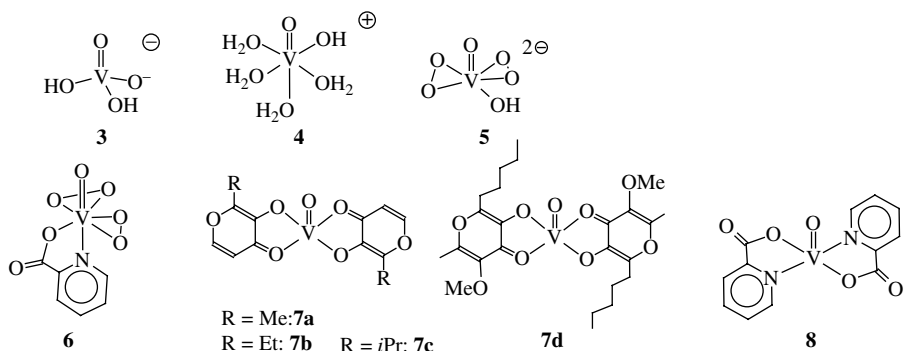
Eighty years after the first account, an *in vitro* study on the insulin-mimetic⁴ action of vanadate was published, revealing the vanadate-stimulated uptake and degradation of glucose by adipocytes (fat cells), the stimulation of glycogenesis in the liver and the inhibition of hepatic gluconeogenesis.^[5] The effects of vanadate on glucose oxidation in adipocytes was shortly thereafter related to the reduction of vanadate(V) to vanadyl (VO^{2+}), and the action of vanadyl proposed to root in the inhibition of a cellular phosphatase,^[6] well in accord with ‘modern’ views of the mode of operation of vanadium(IV) and -(V) compounds. The *in vivo* effects of vanadate in streptozotocin (STZ)-induced diabetic rats was first reported by Heyliger *et al.*^[7a] and Meyerovitch *et al.*^[7b] Streptozotocin is an antibiotic that is produced by *Streptomyces achromogenes*; intravenously applied, it destroys the insulin-producing β -cells in the pancreas and thus induces type I diabetes. STZ rats are thus animal models of human type I diabetes. Oral gavage of vanadate to STZ rats reduces blood glucose levels to normal, and also prevents myocardial dysfunction that otherwise accompanies diabetes. Vanadate also lowers glucose levels in *ob/ob* homozygote mice (*ob* stands for the obesity gene),^[8] which are animal models for human type II diabetes.⁵ In these *in vivo* assays, vanadate is dissolved in the drinking water of the animals, where it is present (at millimolar concentrations) as a mixture of $[\text{H}_2\text{VO}_4]^-$ (3 in Figure 5.2), $[\text{H}_2\text{V}_2\text{O}_7]^{2-}$ and $[\text{V}_4\text{O}_{12}]^{4-}$.

Later, vanadyl sulfate was shown to have comparable effects in STZ rats.^[9] Vanadyl sulfate is advantageous over vanadate because it is sufficiently less toxic. A disadvantage is its low rate of absorption in the gut, estimated to be 1% or less (see also Chapter 1). The unsatisfactory absorption is due to the formation of insoluble vanadyl hydroxides under the slightly alkaline conditions in the small intestine. In aqueous solution, vanadyl sulfate can only exist in the somewhat acidic region [Equations (2.3) and (2.4) in Section 2.1.1], where it is present as $[\text{VO}(\text{H}_2\text{O})_4\text{OH}]^+$ (4 in Figure 5.2). In the assays used *in vitro*, stabilisation towards neutral pH can occur by complex formation with, e.g., buffer components. Another potential vanadium drug is peroxovanadate (‘pervanadate’) (5 Figure 5.2), first noted in the form of a synergistic effect when incubating adipocytes with a combination of vanadate and hydrogen peroxide, an effect which was abolished in the presence of catalase.^[10] Among the effects noted were the stimulation of the insulin receptor tyrosine kinase/inhibition of phosphotyrosine phosphatase (for details see Section 5.1.1.4), coupled with the stimulation of lipogenesis/inhibition of lipolysis (cf. Scheme 5.2) and the stimulation of protein synthesis. In skeletal muscle cells isolated from animal models, peroxovanadate stimulated glucose oxidation and glycogen synthesis.^[11]

Despite the particularly high efficacy of peroxovanadate, exceeding that of vanadate by two orders of magnitude, its *in vivo* applicability is questionable, since, when applied

⁴ For the actions of insulin mimicked by vanadium compounds, the terms ‘insulin-like’, ‘insulin-mimetic’ and ‘insulin-enhancing’ are in use. The question of which of these terms is the most appropriate one essentially is a semantic one. ‘Insulin-enhancing’ presupposes that vanadium compounds are only effective in case of residual insulin production.

⁵ Another common animal model for type II diabetes is the Zucker *fa/fa* rat. These animals are homozygous for the *fa* allele (*fa* for fat).

**Figure 5.2**

Inorganic (top row) and organic (bottom row) vanadium compounds which are of (historical) interest as insulin mimics: (sodium) vanadate (**3**); vanadyl (sulfate) (**4**); peroxovanadate (mixtures of vanadate and H₂O₂) (**5**); a peroxy–picolinate complex (**6**); bis(maltolato) complexes (**7**; R = CH₃: BMOV = [VO(ma)₂] **7a**; R = C₂H₅: BEOV **7b**; R = iPr: **7c**; and the allixinato complex **7d**); and bis(picolinato)oxovanadium(IV) (**8**). The predominant compositions present in aqueous solution under physiological conditions are provided, except for vanadyl sulfate, which forms insoluble hydroxides at pH 7 (see text).

orally, peroxovanadates will hardly survive the passage through the gastrointestinal tract and, if absorbed intact, will readily be decomposed by catalase to form vanadate. The potential toxicity of vanadate and the very low absorption rate for the less toxic vanadyl (sulfate) also exclude these inorganics from potential use as anti-diabetic drugs. As an alternative, starting about 15 years ago, vanadium coordination compounds containing organic ligands have been developed and tested. The advantage of *organic* vanadium compounds is obvious: With the choice of the organic ligand, steering and fine-tuning of the properties of the vanadium drug can be achieved, such as:

- minimising toxicity;
- optimising stability under the conditions pertinent to the stomach (pH ca 2) and the small intestine (pH ca 7.2);
- optimising absorption by the mucosa cells and desorption into the blood;
- controlling stability against redox and ligand exchange during the transport with the bloodstream;
- designing the periphery of the coordination compound to allow its uptake by the cell, which can be achieved by balancing the hydro-/lipophilicity of the complex or by attaching peripheral groups recognisable by cell membrane receptors;
- controlling lability for degradation and re-functionalisation within the cell.

The first organovanadium compounds tested in the context of the treatment of diabetes were bis(peroxo)vanadium complexes with auxiliary *NN*, *ON* and *OO* ligands such as **6** in Figure 5.2,^[12] and bis(maltolato)oxovanadium(IV) (BMOV)^[13] (**7a** in Figure 5.2). Extensive information on BMOV and its ethyl analogue BEOV (**7b**), introduced by McNeill and Orvig's group^[13], and further developed by Thompson and Orvig, is now available, and it is no exaggeration to state that BMOV and its congeners have become the most intriguing developments in this field. These developments include clinical trials

phase 1 of BEVO,^[14] which are about to go into phase 2.⁶ Another recent advance in the field of maltol-derived complexes is the allixinato complex **7d**, which has a particularly long residence time in the blood of rats, probably a consequence of the lipophilic residues.^[15a] Allixin is a component in garlic, *Allium sativum*. A second family of oxovanadium(IV) complexes, containing picolinate (**8** in Figure 5.2) and derivatives thereof, was introduced by Sakurai's group^[15b] and is further being developed by Sakurai's and other groups, including my group in Hamburg. (see the next section).

The theme 'vanadium and diabetes' has been reviewed many times, focusing on various topics. Of particular value, from my personal point of view, are the following (in chronological order):

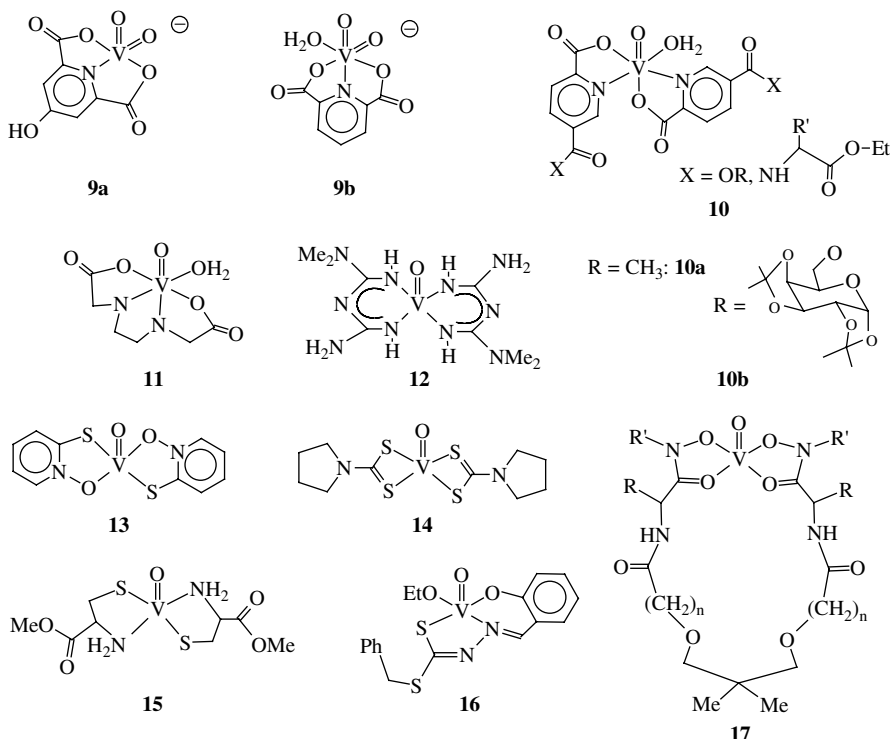
- 'Mechanism of actions of vanadium in mediating the biological effects of insulin' (1998),^[16] describing the mechanisms by which vanadate enables its insulin-like effect at the molecular level.
- 'Vanadium compounds as insulin mimics' (1999)^[17a] and 'Design of vanadium compounds as insulin enhancing agents' (2000),^[17b] providing a well-classified overview of the various types of insulin-mimetic/enhancing vanadium compounds.
- 'Insulin-like actions of vanadium: potential as a therapeutic agent' (2003),^[18] in which the molecular mechanisms underlying the metabolic effects of vanadium *in vivo* are highlighted.
- 'Chemistry and biochemistry of insulin-mimetic vanadium and zinc complexes. Trial for treatment of diabetes mellitus' (2006),^[19] focusing on the current state of insulin-mimetic metal ions (VO^{2+} and Zn^{2+}), including speciation and mechanistic aspects.

5.1.1.3 'Modern' Vanadium Compounds Which are Active *In Vivo* and *In Vitro*

A selection of vanadium-organic compounds (**9–17**) which have been shown to exhibit insulin-mimetic activity *in vitro* and/or *in vivo* are presented in Figure 5.3; the corresponding findings are given in Table 5.1 together with those for complexes **6–8** (Figure 5.2). The selection of sample complexes was made so as to demonstrate the large variety in coordination modes, encompassing ligand functions exclusively furnished by oxygen (**7, 17**), nitrogen (**12**) or sulfur (**14**), and mixed-functional ligands such as *ON* (**6, 8, 9, 10, 11**), *OS* (**13**), *NS* (**15**) and *ONS* (**16**). Most of the complexes that have been tested contain vanadium in the oxidation state +IV; vanadium(V) complexes (**6, 9, 16**) can, however, be equally active, as can vanadium(III) complexes such as $\text{V}(\text{maltolate})_3$. The lack of a clear correlation between activity and oxidation state on the one hand, and the nature of the ligating functions on the other, suggests that the active species formed under intracellular conditions is not identical with the originally applied compound (see below).

An essential factor for differentiation in activity appears to be (i) stability, allowing the compound to reach its target cell, and (ii) a balanced hydro-/lipophilicity provided by the ligand periphery, or the presence of a peripheral function which is recognised by a membrane receptor, allowing the compound to be transferred into the cytosol. This is demonstrated in Figures 5.4 and 5.5. In the left part of Figure 5.4, the plasma glucose levels as a function of time are indicated after intraperitoneal application, to STZ rats, of vanadyl sulfate(VS) and the maltolato complexes **7a** (with a methyl substituent on the

⁶ Personal communication from C. Orvig, University of British Columbia, Vancouver. See also the website of Akesis Pharmaceuticals (San Diego), www.akesis.com.

**Figure 5.3**

Selection of vanadium complexes with organic ligands, for which *in vitro* and/or *in vivo* insulin-mimetic (or insulin-enhancing) activity has been reported. See Table 5.1 for specification and references.

Table 5.1 Insulin-like effects of selected vanadium complexes with organic ligands.

Complex No. (Figures 5.2 and 5.3)	Cell type or test animal mode of application ^a	Effect	Ref.
6	(1) Hepatoma cells; (2) adipocytes; (3) rat liver endosomes	(1) Activation of insulin receptor kinase; (2) stimulation of lipogenesis; (3) inhibition of tyrosine phosphatase	12
7a	STZ rats/oral or i.p.	Restoring normal plasma glucose and lipid levels	13
7d	Wistar rats	Hypoglycaemic effect	15a
8	STZ rats/oral or i.p.	Lowering of plasma glucose	20
9a	STZ rats/oral	Lowering of blood glucose; normalising triglyceride and cholesterol levels	21
9b	Naturally diabetic cats/oral	Improvement in glycaemic control, increase in body weight	b
10	(1) SV-3T3 mice fibroblasts ^c ; (2) rat adipocytes	(1) Stimulation of glucose uptake and degradation; (2) inhibition of FFA ^d release	22

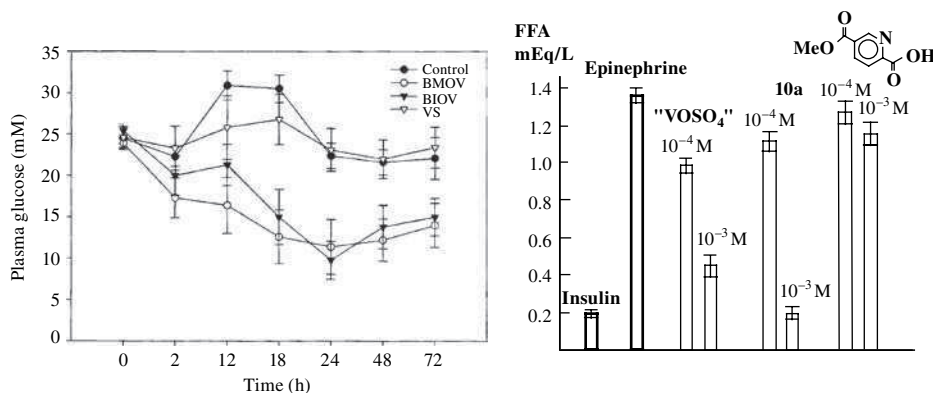
11	Rat adipocytes	Inhibition of FFA ^d release	23
12	STZ rats/oral or i.p.	Lowering of plasma glucose	24
13, 14	(1) Rat adipocytes; (2) STZ rats/oral	(1) Inhibition of FFA ^d release; (2) normalisation of serum glucose and improvement of serum FFA ^d and BUN ^e	25a, 25b
13^f	3T3-L1 mouse fibroblasts differentiated into adipocytes	Increase of protein tyrosine phosphorylation	26
15	STZ rats	Normoglycaemic effect	25c
16	SV-3T3 mice fibroblasts ^c	Stimulation of glucose uptake and degradation	27
17	Rat adipocytes	Stimulation of glucose metabolism	28a
VO ²⁺ trehalose	Mouse calvaria osteoblasts MC3T3E1	Mitogenic, enhancement of glucose consumption, stimulation of cell proliferation ^g	28b

^a i.p. = intraperitoneal.^b Personal communication from Debbie C. Crans, Colorado State University, Fort Collins, Co, USA.^c Simian virus transformed fibroblasts (cells from the connecting tissues; transformation towards the metabolism of adipocytes).^d FFA = free fatty acids.^e Blood urea nitrogen.^f Synergistically with insulin.^g At low doses (5–25 µM).

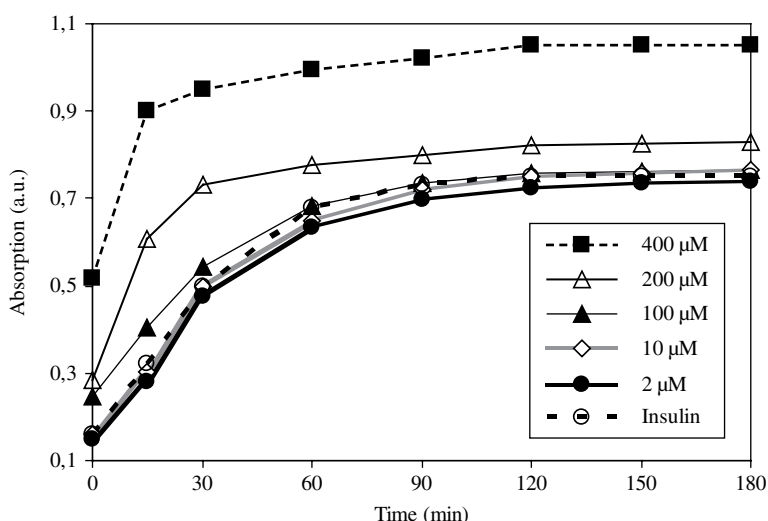
maltol ring) and **7c** (with an isopropyl substituent). Both maltolato complexes are clearly more effective than vanadyl sulfate in lowering the plasma glucose level. Vanadyl sulfate, hardly distinguishable from a control group (treated with 0.9% NaCl), readily forms stable complexes with transferrin (Tf), which may hamper its availability. For the stability of maltolato complexes against ligand exchange (including Tf), see below. The right part of Figure 5.4 illustrates the situation for the release of free fatty acids (FFA) on treating isolated rat adipocytes with hydrophilic vanadyl sulfate and the picolinato complex **10a**. Complex **10a** is an example for a picolinatovanadium complex with a particularly well-balanced hydro-/lipophilicity.^[22a] The picolinato complex, at a concentration of 1 mM, is as effective as insulin. No effect is observed with the ligand alone; within the error range, the release of FFA is comparable to that of a control group treated with epinephrine (also known as adrenaline), an antagonist of insulin. Figure 5.5 shows the dependence of glucose uptake and degradation by modified fibroblasts, stimulated by the galactosyl derivative **10b** in Figure 5.3, as a function of time and concentration.^[22b] At low concentrations, i.e. in the concentration range 2–100 µM, **10b** behaves similarly to insulin; the maximum level of activity is reached after ca 90 min. At higher concentrations, 200–400 µM, **10b** is more efficient than insulin and saturation is achieved after about 30 min. At concentrations approaching 1 mM, apoptosis (cell death) begins to occur.

5.1.1.4 Speciation of Insulin-mimetic Vanadium Compounds and Distribution of Vanadium Under *In Vivo* Conditions

An important factor in assessing the mechanism of action of an insulin-mimetic vanadium compound is its interaction with serum components present under physiological

**Figure 5.4**

Left: time dependence of the glucose-lowering effect of insulin-mimetic vanadium compounds after intraperitoneal administration to STZ rats, compared with a control group (0.9% NaCl).^[13b] BMOV and BIOV are the maltolato complexes **7a** and **7c** in Figure 5.2; VS is vanadyl sulfate. Doses are 0.1 mmol kg⁻¹ body weight. Reproduced from K. H. Thompson *et al.*, *J. Biol. Inorg. Chem.* 8, 66–74. Copyright (2003), with permission from Springer Science and Business Media. Right: demonstration of the inhibition of lipolysis by vanadium compounds;^[22a] insulin effectively inhibits the release of free fatty acids (FFA), and thus counteracts the insulin antagonist epinephrine. Vanadyl sulfate and the picolinato complex **10a** (Figure 5.3) also suppress FFA release, in particular so **10a** at higher concentrations (1 mM). The ligand as such does not have an effect.

**Figure 5.5**

Time and concentration dependence of glucose uptake and degradation by Simian virus modified (i.e. adipocyte-like) mice fibroblasts, stimulated by the galactosylicpicolinato complex **10b** (Figure 5.3).^[22b] The ordinate indicates the absorption (in arbitrary units) in an MTT assay as a measure of the amount of glucose degraded in the cells after uptake.

conditions. These include (i) water, which can act as a ligand *and* promote hydrolysis, accompanied, should the situation arise, by protonation or deprotonation, (ii) O₂ and other reactive oxygen species capable of oxidising V^{IV} to V^V, (iii) reducing systems such as NAD(P)H, FADH₂, ascorbate, glutathione and catecholamines, which may convert V^V to V^{IV} (and eventually further to V^{III}), commonly accompanied by ligand exchange, and (iv) ligand exchange by interaction with redox-innocent low and high molecular weight constituents in the body fluids and tissues (cf. Table 2.5). In Section 2.2, the speciation of vanadate and vanadyl in the presence of organic ligands was described in detail. Here, the speciation of vanadium–organic complexes in aqueous media in the absence and the presence of additional, competitive components will be addressed.

Simple vanadyl complexes such as bis(methylacetylacetonato)oxovanadium(IV), [VO(Meacac)₂] (**18** in Figure 5.3),^[29] and bis(maltolato)oxovanadium(IV), [VO(ma)₂] (or BMOV; **7a**), when dissolved in water, take up water as a sixth ligand *trans* or *cis* to the oxo group, with the *cis* arrangement being predominant. Depending on the pH and the ligand:VO²⁺ ratio, monoligand complexes, produced by partial hydrolysis, are in equilibrium with the original complex. The species present in an aqueous solution of VO(Meacac)₂ or [VO(ma)₂], as identified by EPR on the basis of the additivity relationship for the parallel hyperfine coupling constant ($A_{||}$, Section 3.3.2), are shown in Figure 5.6. Oxidation of **7a** ($pK_a = 7.2$) is preceded by deprotonation; the oxidation product, [VO₂(ma)₂]⁻ (Figure 5.6), has been identified by its chemical shift $\delta(^{51}\text{V}) = -496\text{ ppm}$.^[30] The proposed reaction cascade for the oxidation, [Equation (5.1)], includes a superoxo intermediate, a dinuclear peroxy-bridged vanadium species and a hydroxo(oxo)vanadium(V) complex, and thus resembles the reaction path, as far as vanadium is concerned, proposed for the oxidation of hydrocarbons catalysed by

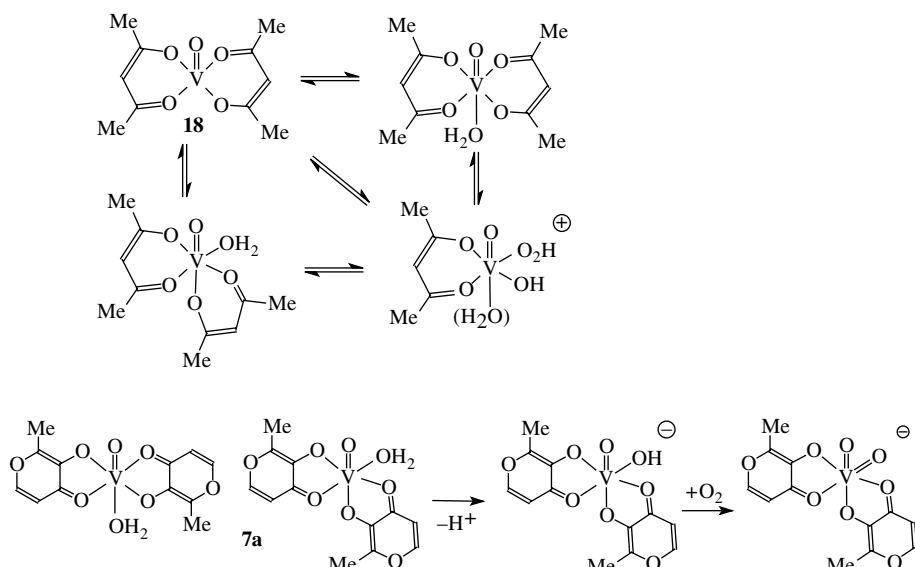
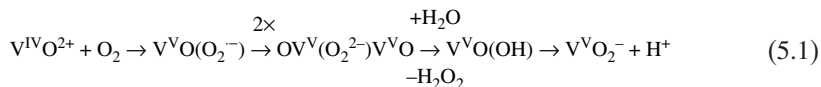


Figure 5.6

Top: Speciation of [VO(Meacac)₂] (**18**) in water. Bottom: The maltolato complexes **7a** present in aqueous solution are *trans*- and *cis*-[VO(ma)₂(H₂O)]. The *cis* isomer is dominant; its deprotonation product can be oxidised to [VO₂(ma)₂]⁻.

oxovanadium (see Figure 4.19 in Section 4.3.3. The rate-determining step in Equation (5.1) is the formation of oxo-superoxovanadium(V).



On the other hand, the vanadate(V)-maltol system, containing $[\text{VO}_2(\text{ma})_2]^-$ as the main component in the pH range 5–9.5, is susceptible to ‘spontaneous’ reduction to $[\text{VO}(\text{ma})_2]$. The rate at which this reduction occurs is a function of time, concentration and pH; at pH values <5, reduction is particularly effective.^[31]

Speciation studies in the ternary system vanadyl/ligand A/ligand B over a broad pH range have provided insight into the possible nature of oxovanadium(IV) complexes present in biofluids. Ligand A is a chelator such as the anions of picolinic acid, dipicolinic acid, maltol or pyrimidone, forming vanadium complexes of the general composition $[\text{VO}(\text{L}_A)_n]^q$ ($n = 1$ or 2; q is a charge), whereas ligand B corresponds to a low molecular weight constituent in the fluid, the more common ones (see Table 2.5) being oxalate, citrate, phosphate and lactate. As an example, the speciation diagrams for $\text{L}_A = 5\text{-carbomethoxypicolinate}$ (see complex **10a** in Figure 5.3) and $\text{L}_B = \text{lactate}$ or phosphate are displayed in Figure 5.7, top left and right.^[22a] The diagram at the bottom

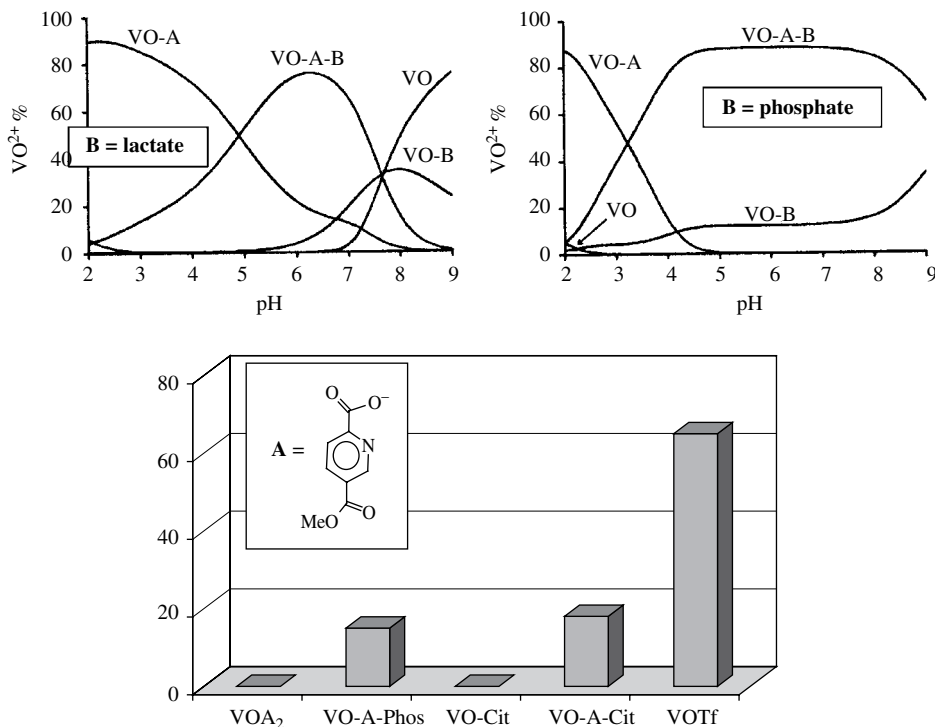


Figure 5.7

Speciation in the ternary systems $\text{VO}^{2+}-\mathbf{A}-\mathbf{B}$ (top) and the quaternary system, additionally containing transferrin [Tf (bottom); from results kindly provided by T. Kiss, University of Szeged, Hungary]. **A** is the picolinato ligand shown in the inset; **B** as indicated.

in Fig. 5.7 reflects the situation in the quaternary system vanadyl-L_A-L_B-Tf. Transferrin (Tf) is, along with albumin, the main high molecular weight blood constituent (see below). In its presence, most of the vanadyl is released from its original ligands and the VO²⁺ ion bound tightly to Tf. Only the ternary complexes containing phosphate or citrate along with the picolinato ligand can survive to a certain extent.

Vanadyl complexes containing picolinato ligands (**8** in Figure 5.2) appear to be stable against oxidation in the blood, as has been shown by EPR investigations. The residence times and elimination rates for picolinato complexes have been obtained through *in vivo* EPR of healthy, anaesthetised rats.^[32] In these studies, polyethylene tubes are connected to the left femoral artery and vein, and the free ends joined with a silicone rubber tube, thus making available an external blood circuit which is directly connected to a quartz capillary tube serving as the EPR cell. The circulation is maintained by the rat's own heart beat and blood pressure. The half-lives of the complexes, obtained from the decay of the intensity of the EPR signals with time, reflect the distribution from the 'inner compartment' (heart, lung, liver, kidney) towards the 'peripheral compartment' (brain, muscle, fatty tissue). The half-lives for intravenous injection of saline solutions of the vanadium compounds (final V concentration 0.5 mg kg⁻¹ body weight) vary from 3 min for vanadyl sulfate to 30 min for the 5-iodopicolinato complex, with methylpicolinato complexes in-between, and there appears to be a direct correlation between the normoglycaemic effect of the vanadium compounds and its retention in blood.

In general, these results are in agreement with distribution studies, using ⁴⁸V-labelled BMOV (**7a** in Figure 5.2) and vanadyl sulfate.^[33] The isotope ⁴⁸V is a β⁺ and γ emitter, and decays with $t_{1/2} = 16$ days to ⁴⁸Ti. In particular, these studies showed that BMOV is more effectively distributed towards the tissues (and less effectively secreted) than vanadyl sulfate over a period of 24 h, both when applied orally and intraperitoneally to rats. The highest concentrations were found in bone, followed by kidney and liver. The residence time⁷ in bone is 11 days for vanadium delivered in the form of vanadyl sulfate, and 31 days for BMOV. The amount of ⁴⁸V excreted in the faeces 24 h after oral gavage were estimated to be 75% for vanadyl sulfate and 62% for BMOV. On the basis of other studies, absorption of *orally* administered vanadium is much lower and comes close to 1% in the case of vanadyl sulfate.

'The interaction of pharmaceuticals with serum proteins (e.g. transferrin and serum albumin) is an important aspect in drug metabolism, capable of strongly affecting the distribution, biotransformation, and ultimately the mechanism of action. [. . .] The true active form of vanadium pharmaceuticals is the subject of much debate. Thus, delineation of transport and biotransformation functions is important to provide insight into the chemical form of the vanadium species that ultimately leads to its anti-diabetic effect.'^[34] The two main high molecular weight blood serum constituents are the iron transport protein transferrin and albumin. Vanadyl ions bind specifically into the two iron binding sites of transferrin (see below) and to a histidine of the N-terminal end of albumin. In addition, there are several unspecific and weak binding sites. Recent studies of the interaction of the maltolato complex [VO(ma)₂] with Tf have been interpreted in terms of Tf completely removing the maltolato ligand, firmly coordinating VO²⁺.^[34] Since the iron binding sites are generally only 30% occupied by Fe³⁺, there is a significant reservoir of binding sites available for VO²⁺. Consequently, [VO(ma)₂], according to these studies, is

⁷ The residence time t_R is defined by $t_R = \frac{1}{2} \exp(t_{1/2})$, where $t_{1/2}$ is the half-life (the decline of C(V) by 50%).

not likely to reach the target tissue intact in any appreciable amounts,⁸ and other vanadium complexes should suffer the same fate. In contrast, human serum albumin (HSA), the complex formation of which with vanadyl ions is less favoured thermodynamically, forms a ternary complex of composition $[VO(\text{ma})_2\text{HSA}]$. The protein probably binds into the sixth position (otherwise occupied by water; see **7a** in Figure 5.6) through an imidazolyl moiety. Although serum albumin can thus, in principle, transport $[\text{VO}(\text{ma})_2]$ intact, it is unclear whether this protects the complex from degradation by Tf. In any case, the interaction of vanadium chelates (and/or VO^{2+} formed by their degradation) with albumin, and also the complexation of VO^{2+} by transferrin, may help to slow plasma clearance of vanadium, thus augmenting the insulin-like effects. *In vitro* investigations with adipocytes have shown that albumin (but not Tf) enhances the insulin-like activity of $[\text{VO}(\text{ma})_2]$.^[26]

As outlined above, bones incorporate vanadium particularly efficiently. The residence time for vanadium (delivered by $[\text{VO}(\text{ma})_2]$) in bone is 1 month, corresponding to a half-life of ca 4 days. Bones may therefore be a significant *in vivo* storage and source for the long-term delivery of vanadium and thus for prolonged insulin-mimetic and insulin-enhancing effects. Insight into the putative environment of the vanadyl ion in the hydroxyapatite matrix forming the inorganic part of the bone structure has been obtained by ESEEM studies (Section 3.4) of the complex formed between VO^{2+} and triphosphate in an aqueous solution containing vanadyl and triphosphate in a ratio of 1:3. The two-pulse ESEEM spectrum together with the proposed structure of the vanadyl-triphosphate complex is shown in Figure 5.8 (left).^[35] Alternatively, vanadyl may be

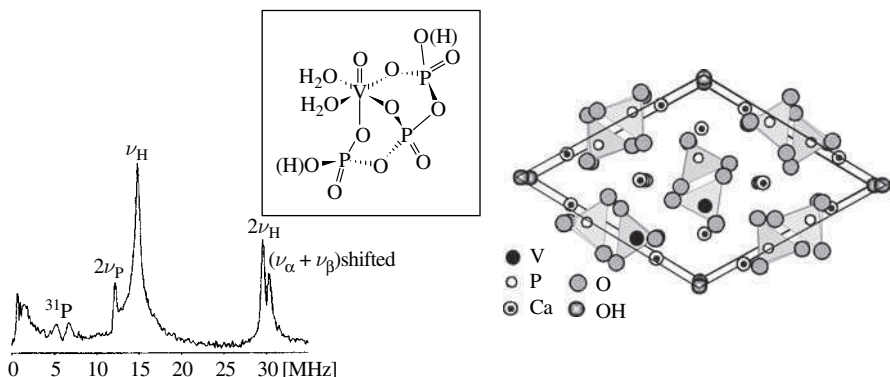


Figure 5.8

Left: ESEEM spectrum of a solution containing triphosphate and vanadyl ions in the ratio 3:1, $\text{pH} = 5$, $c(\text{VO}^{2+}) = 0.7 \text{ mM}$, recorded at the $m_I = -1/2$ EPR transition; ν_{P} and ν_{H} are the Zeeman frequencies for ^{31}P and ^1H , respectively. The doublets at 5.3 and 6.7 MHz (superhyperfine coupling constants 1–1.5 MHz) are indicative of direct bonding of phosphate to VO^{2+} , as represented by the proposed structure (inset).^[35] The presence of water/hydroxide in the coordination sphere of vanadium is inferred from the respective HYSCORE spectrum. Reproduced from S. A. Dikanov *et al.*, *J. Am. Chem. Soc.* 124, 2969–2978. Copyright (2002), with permission from the American Chemical Society. Right: section of the structure of hydroxyapatite, with two phosphorus sites arbitrarily replaced by vanadium (full circles). The drawing of the apatite structure was provided by Barbara Albert, Technical University of Darmstadt, Germany.

⁸ See, however, the *Interjection* further down.

oxidised to vanadate prior to incorporation, and built into phosphate sites of the hydroxyapatite structure (Figure 5.8, right). Note that vanadinite, a lead vanadate (Table 1.1), is isomorphous with apatite.

Another interesting case of speciation has been reported for the insulin-mimetic pyridinone complex **19** in Figure 5.9. In human blood, **19** is readily oxidised to the dioxovanadium complexes **20** and **21**, along with the formation of some vanadate, i.e. oxidation is accompanied by partial hydrolysis, leading to **21**, and complete hydrolysis, resulting in the formation of vanadate. This speciation of the vanadium(V) compounds is clearly revealed by ^{51}V NMR spectroscopy.^[36a] Vanadate $[\text{H}_2\text{VO}_4]^-$ (but not the condensed vanadate species) can enter blood cells via phosphate channels; specific phosphate channel blockers prevent its uptake. Complex **21** is present in its neutral aqua form (**21a**) and the deprotonated, anionic hydroxo form (**21b**), and the two forms are in exchange equilibrium. Kinetic investigations have shown that only the neutral complex **21a** can pass the cell membrane of the blood cells, presumably by diffusion. In the intracellular space, reduction and degradation to VO^{2+} occur. Although transformation of **19** by low molecular weight constituents in biofluids, such as oxalate, lactate, citrate and phosphate, is negligible,^[36b] **19** is not stable in the presence of transferrin, which, as in the case of $[\text{VO}(\text{ma})_2]$, takes up the vanadyl ion.^[36c]

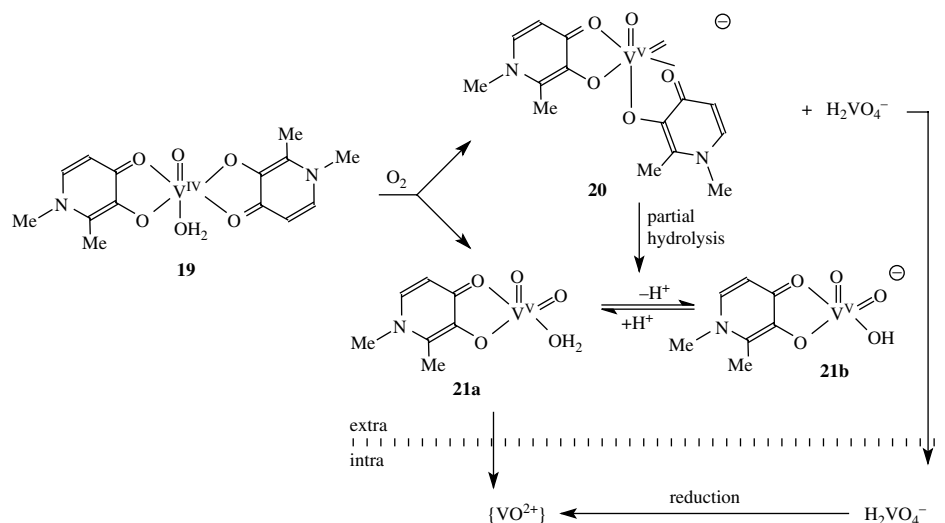


Figure 5.9

Speciation of the pyrimidone complex **19** in blood as revealed by EPR and ^{51}V NMR, based on ref. 36a. ‘Extra’ refers to blood serum, ‘intra’ to the intracellular medium of red blood cells. **21a** enters the cells by diffusion and vanadate through phosphate channels. $\{\text{VO}^{2+}\}$ stands for any vanadyl complex formed with cytosolic constituents after intracellular reductive degradation of **21a** or reduction of vanadate.

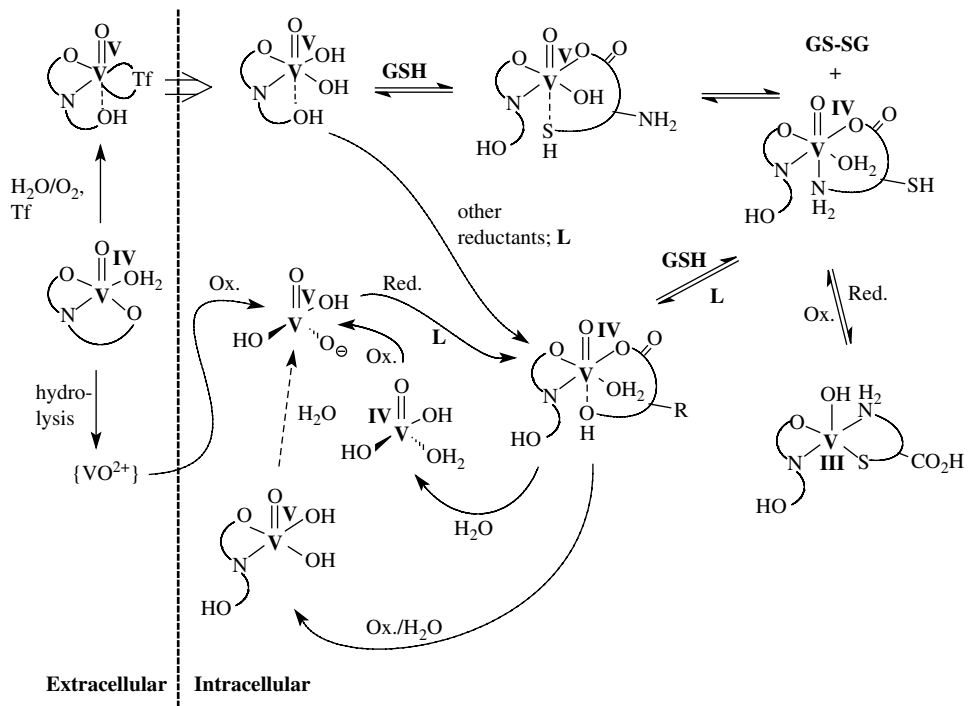
Interjection: In the light of the lability of $[\text{VO}(\text{ma})_2]$ under physiological conditions in the presence of transferrin discussed above (ref. [34]), the bulk of the complex should not reach the target cells intact after absorption or injection. According to previous reports (see, e.g., ref. 36d), $[\text{VO}(\text{ma})_2]$ also forms a ternary complex with transferrin (Tf), viz. $\text{VO}^{2+}-\text{ma}-\text{Tf}$. Further, as shown in Figure 5.7 (bottom), ternary

vanadyl–picolinate–phosphate/citrate complexes can exist in the presence of transferrin. Thermodynamic considerations (i.e. the high stability of the VO^{2+} –Tf complex; $pK = 14.6$) favour the findings reported in ref. 34. It should be noted, however, that thermodynamic models relate to equilibrium conditions which cannot unambiguously be applied to living systems. In addition, there may be kinetic restrictions when it comes to the removal of chelating ligands in the original vanadium compound, or a secondary compounds formed by additional coordination of albumin or replacement of the original chelating ligand, by, e.g., citrate and phosphate. The findings on the pyrimidone complex **19** in whole human blood (Figure 5.9^[36a]) support such a view. As a result, the establishment of the thermodynamic equilibrium may be delayed to the extent where a sizable amount of the complex carrying the original ‘information’ (i. e. the original ligand) is still intact when in contact with and eventually taken up by the target cell. Finally, retardation of ligand displacement by outer-sphere interaction (notably through hydrogen bonding) between the original complex and the protein has to be taken into account. Such a kind of interaction is suggested by spin-lattice relaxation rates of ^1H NMR resonances, implemented by paramagnetic VO^{2+} .

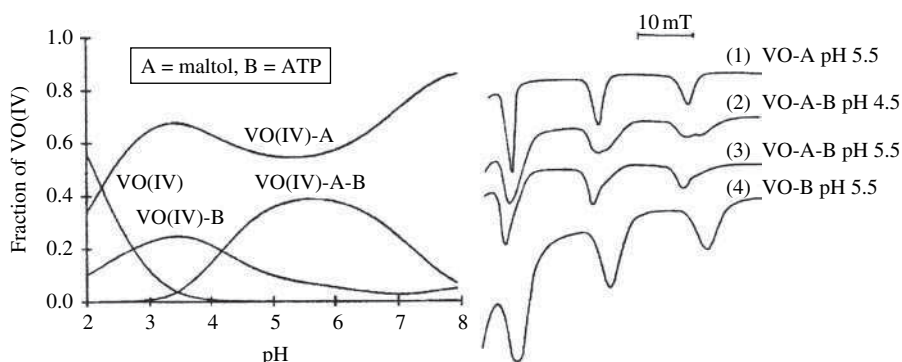
Let us consider the possible reaction paths of vanadium complexes which enter the target cells directly or through the Tf membrane receptor, encountering competitive ligands present in the cytosol. Among others, these are glutathione (GSH) and adenosine triphosphate (ATP), both of which are present in millimolar concentrations. GSH, although not a particularly potent reductant for V^{V} , can act both by reducing V^{V} to V^{IV} and by stabilising V^{V} and V^{IV} through complexation (see also Section 2.2.1). The overall situation is depicted in Figure 5.10 for a complex containing a tridentate *ONO* ligand [such as provided by 2,6-dipicolinate(2–), dipic] and includes the possible reoxidation of V^{IV} to V^{V} in cell compartments where reactive oxygen species [H_2O_2 , O_2^- , O_2^- , OH^- ; see also Equation (5.1)] are formed. The interconnections between the various (hypothetical) species formed in the intracellular medium also take into consideration the possibility of further reduction of V^{IV} to V^{III} ; potential reducing agents are NAD(P)H and ascorbate. Kiss and co-workers investigated the speciation of $\text{VO}(\text{dipic})$ in the presence of GSH and found that a stable ternary complex, $[\text{VO}(\text{dipic})\text{GSH}]^-$, is present only in the pH range 2–7, dominating between pH 4 and 6. A stable complex $[\text{VO}(\text{ma})_2\text{GSH}]^-$ exists in the system VO^{2+} –maltol–GSH in the pH range 4–8.^[37a] Maltol forms stable ternary complexes with ATP of composition $[\text{VO}(\text{ma})\text{ATP}]^{n-}$ around pH 7.^[37b] For the VO^{2+} –maltol–ATP system, the predominance diagram and characteristic EPR features are shown in Figure 5.11.

5.1.1.5 Molecular Mechanism and Function on the Cellular Level

In this section, the present view will be outlined of the action of insulin in stimulating the cellular uptake of glucose, and the interference of vanadate in the absence of insulin (diabetes I), insulin tolerance (diabetes II) or as a synergistically insulin-enhancing agent. This will be done on a somewhat simplified basis, amenable to those (including the author) who are less familiar with biochemical depths. For a more detailed discussion, see, e.g., refs 2 and 38a (on the mechanism of the action of insulin) and refs 15, 17 and 18 (include the targeting points of vanadium compounds). Many of the details of

**Figure 5.10**

Possible speciation pathways for a vanadium(IV) complex with an *ONO* ligand (such as dipicolinate) approaching a target cell and being incorporated by the target cell. The pathways encompass oxidation (by O_2 and other reactive oxygen species), hydrolysis, reduction and stabilisation of the reduction product (exemplified by glutathione, GSH), ligand exchange and re-coordination (by a cytosolic ligand such as lactate). Tf = transferrin. Drawn on the basis of ref. 27 and speciation results detailed in the text.

**Figure 5.11**

Left: the predominance diagram for the system VO^{2+} -maltol-ATP (1:2:2), $c(VO^{2+}) = 2 \text{ mM}$, as determined by potentiometry, clearly shows the presence of the ternary complex (along with the binary maltolato complex $VO\text{-A}$) in the physiological pH range. Right: high-field region ($m_I = +3/2, +5/2$ and $+7/2$ parallel transitions) of EPR spectra ($T = 140 \text{ K}$) in the VO^{2+} -maltol-ATP system. (1): VO^{2+} -maltol; (4) VO^{2+} -ATP; (2) and (3) represent overlaps of binary and ternary complexes.^[37b] Reproduced from T. Kiss *et al.*, *Inorg. Chim. Acta* 283, 202–210. Copyright (1998), with permission from Elsevier.

the action of vanadate (or other vanadium species) have still to be clarified, and some are controversial. A few focal points, enjoying a comparatively broad consensus, have, however, emerged during the last few years, and these are summarised on the basis of the diagrammatic presentation provided in Figure 5.12.

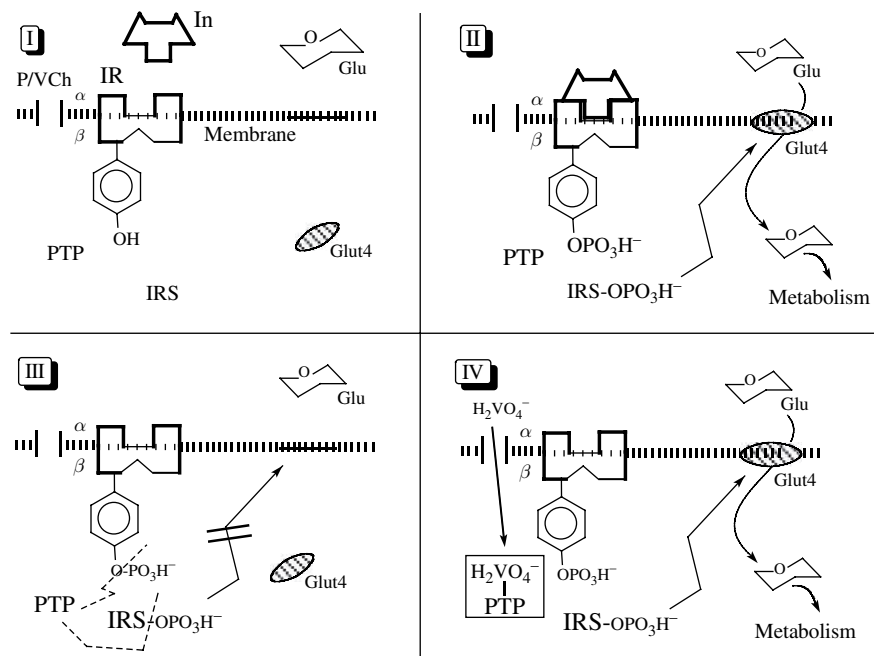


Figure 5.12

Mechanism of the stimulation of glucose uptake by insulin or vanadate. Scenario **I** describes the situation prior to docking of insulin (In) to its receptor (IR). Other abbreviations: P/VCh = anion channel for phosphate and vanadate; Glu = glucose; Glut4 = glucose transporter 4; PTP = protein tyrosine phosphatase; IRS = insulin receptor substrates. Scenario **II**: docking of insulin to the outside (α subunit) of its receptor leads to phosphorylation of tyrosine at the inside (β subunit) of the receptor, which initiates the phosphorylation of IRS. Phosphorylation of IRS in turn induces a signal transduction (zigzag arrow), by which Glut4 is translocated to the membrane, internalising glucose (curved arrow). Scenario **III**: in the absence of insulin, PTP catalyses the hydrolysis of the phospho-ester bonds (formed by auto-phosphorylation) of the IR and IRS (broken lines), and thus blocks off the signal transduction. Scenario **IV**: vanadate enters the cell, inhibiting the phosphatase and thus re-establishing signal transduction.

The cellular insulin receptor (IR) is a tetrameric trans-membrane protein consisting of two α and two β subunits. In a first step, insulin docks to the α subunits at the extracellular surface, initiating autophosphorylation of tyrosines on the β subunits at the intracellular surface (scenarios **I** and **II** in Figure 5.12). Subsequently, various endogenous substrates are phosphorylated. These substrates can be subsumed, in part, as insulin receptor substrates (IRS). In other words: insulin stimulates the tyrosine kinase⁹ activity

⁹ A kinase is a protein (enzyme) which catalyses phosphorylation reactions, resulting in the formation of an ester of hydrogenphosphate (phospho-ester). Tyrosine and serine are typical phosphorylation sites. Phosphorylation goes along with an *activation* of the phosphorylated substrate; hence the term *kinase*.

of subunit β of the IR and thus the phosphorylation of IRS.^[28b] As shown in scenario **II**, phosphorylation of IRS gives rise to a signal transduction cascade downstream the insulin receptor, finally activating the vesicle containing glucose carrier Glut4, which is translocated to the membrane and transports glucose into the cell. Glucose is either oxidised, metabolised to triglycerides or used up in glycogen synthesis. Crucial in this mediation of signalling in response to insulin, leading to the activation of Glut4, is a phosphatidylinositol-3'-kinase (PI3K; not shown). In the absence of insulin, or in the case of a lack of insulin response, autophosphorylation of the β subunit is counteracted by a protein tyrosine phosphatase¹⁰ (PTP), annulling the phosphorylation of IRS and thus the signal transduction (broken lines in scenario **III**). Scenario **IV** describes the situation in the presence of a vanadium compound, entering the cell by diffusion, endocytosis or via ion channels, such as phosphate channels (P/VCh) in the case of vanadate (shown). Vanadate, either entering the cell directly or generated by speciation within the cell (Figure 5.10) is a very efficient inhibitor of phosphatases. Vanadate(V), and possibly also vanadate(IV), bind tightly into the active site of phosphatases (more details on this are given in Section 5.2.1), forming covalent bonds with OH⁻, SH⁻ or N-functional amino acid side-chains, and thus prevent phosphatases from dephosphorylating substrates. In the specific case depicted in scenario **IV**, PTP is inhibited. Consequently, the signal transduction pathways remain intact and glucose is transported into the cell. It has been shown that wortmannin,¹¹ a classical suppressor of insulin-signalling activities, does not suppress IR and IRS phosphorylation stimulated by vanadium (or vanadium + insulin), providing evidence that vanadium compounds exert their activity at an early stage, i.e. by enabling signal transduction through the inhibition of PTP.^[12,26] Activation of nonreceptor kinases by vanadate may come in as a side-effect.

Since insulin-mimetic effects of vanadium compounds include glucose homeostasis based in the liver, normalisation of the serum glucose concentration (normoglycaemia) may also be achieved by vanadate-mediated restoration of hepatic glycogenesis/inhibition of hepatic glycogenolysis, and by inhibiting gluconeogenesis, a possible key step being the inhibition, by vanadate, of glucose-6-phosphatase.

The promotion of the synthesis of lipids (lipogenesis) and the inhibition of the release of free fatty acids (lipolysis) by insulin also requires a complex network of signalling pathways, partially coupled to those for the Glut4 activation. In adipocytes, insulin inhibits lipolysis primarily through inhibition of a hormone-sensitive lipase via reduction of the amount of cyclic adenosine monophosphate (cAMP) present in the cells. In this specific action, a phosphodiesterase is involved,^[38a] a level where again the phosphate antagonist vanadate can interfere.

5.1.2 Other Potential Medicinal Applications

Proposed medicinal applications of vanadium compounds encompass beneficial effects in the treatment of, *inter alia*, tuberculosis, amoebiasis, HIV, herpes and, in particular,

¹⁰ Phosphatases are ‘antagonists’ to kinases in the sense that they catalyse the dephosphorylation (often by hydrolysis) of a substrate.

¹¹ Wortmannin, a metabolite of the fungus *Penicillium wortmanni* (or *funiculosum*), is a steroid furanoid, which reacts at its furan moiety in a ring-opening reaction with lysine side-chains. Wortmannin is particularly effective in inhibiting PI3K. See ref. 38b.

cancer. I will deal in some detail with the cancer preventive and anti-cancer potential first, and then briefly address other medicinal effects.

5.1.2.1 Vanadium in Cancer and Pre-cancer Therapy

Cancer types against which vanadium compounds have been found to be effective include several variants of leukaemia, Ehrlich ascites tumours, carcinomas of the lung, breast, gastrointestinal tract, prostate, testes, ovaria and liver, nasopharyngeal carcinoma and malignant myeloma cells. Usually, simple preparations, such as vanadyl (sulfate), vanadate or peroxovanadate are employed in low (micromolar) and hence subtoxic doses. Among the oxovanadium(IV) coordination compounds evaluated for their anti-cancer activity, the *o*-phenanthroline complex ‘metvan’ (**22** in Figure 5.13) was identified as a promising multitargeting anti-cancer agent with apoptosis-inducing activity towards human leukaemia cells, multiple myeloma cells and various solid tumour cells, working in the nanomolar to low micromolar concentration range.^[39] In the light of what has been worked out in the context of the speciation of vanadium complexes with chelating ligands when using vanadium compounds in the treatment of diabetes, ‘metvan’ is not likely to survive *in vivo* conditions, and the active species will again be a simple vanadium compound. This does not apply to the ‘classical’ anti-cancer agent vanadocene dichloride $[(\eta^5 - C_5H_5)_2 VCl_2]$,^[40] Cp₂VCl₂ for short, **23** in Figure 5.13], the active fragment of which, the cyclopentadienylvanadium moiety, survives in biofluids (see below). Also stable under *in vitro* conditions is the vanadyl complex **24**, containing the ligand system present in chlorophyll. As has been shown for [⁴⁸V]**24**, this agent is taken up by certain tumour cells more readily than inorganic vanadium, thus demonstrating its survivability.^[41]

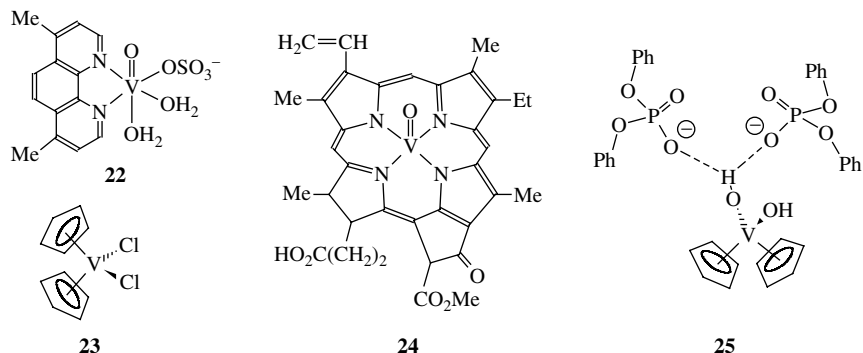


Figure 5.13

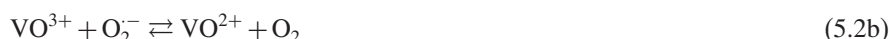
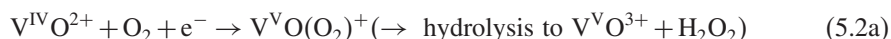
The complexes **22** (‘metvan’), **23** and **24** have been employed in chemo-preventive and anti-cancer treatment. Complexes **23** and **24** are particularly stable under physiological conditions. The outer-sphere complex **25** models the possible mode of interaction between Cp₂VX₂ and phosphate linkers in DNA.

The inhibition of cellular tyrosine phosphatases discussed in the previous section as the primary mode of action of vanadate underlying its anti-diabetic potential may also be an effective mechanism explaining the chemo-preventive potential of vanadium compounds in cancer genesis.^[42] Inhibition of tyrosine phosphatase, and thus increased

phosphorylation of tyrosine residues in proteins, activates signal transduction pathways leading to apoptosis or activation of tumour suppressor genes. Other regulatory functions of vanadate on phosphate-metabolising enzymes can be involved.^[42]

Additional qualities of action of vanadium compounds are feasible and include intervention with or generation of reactive oxygen species, and detoxification of alkylating agents. Carcinogen-induced DNA damage has been implicated as one of the early steps in chemically induced carcinogenesis due to alkylation and/or oxidative damage. DNA alkylation occurs at nucleophilic sites, e.g. guanine-N⁷ and thymine-O⁴, resulting in the disability to base-pair properly, and consequently yielding genomic mutations after replication, and carcinogenesis.

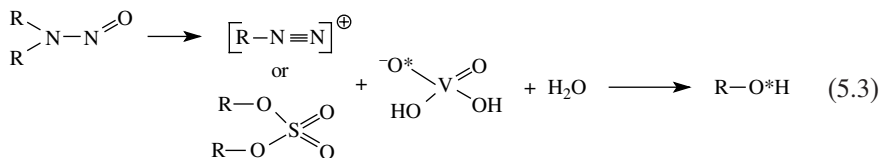
The most sensitive marker for *oxidative* damage of DNA is an increased concentration of 8-hydroxy-2'-deoxyguanosine (8-OHdG). Additional markers are increased levels of DNA single strand breaks, DNA–protein cross-links and chromosomal aberrations. In addition, proliferation of tumour cells is associated with increased thioneine expression in the liver. All of these aberrations from normal, detected in experimental rats with diethylnitrosamine-induced hepatocarcinogenesis, have been suppressed by treating the animals with vanadate at a concentration of ca 4 µM in the drinking water, demonstrating the chemo-preventive potential of vanadate.^[43] Oxovanadium(IV) and -(V) can act both as scavengers and as generators^[42b] of ROS (peroxide, superoxide, hydroxyl radicals, singlet oxygen), very much depending on the conditions such as pH and auxiliary ligands temporarily binding to vanadium and thus shifting redox potentials. Equations (5.2a–e) are exemplary for either action. Reactions (5.2a) and (5.2b) have been modelled by the complexes **6a** and **6c** in Figure 3.15 in Section 3.3.2; Reaction (5.2d) is a Fenton-type reaction. The formation of singlet oxygen from H₂O₂, mediated by vanadate [Equation (5.2e)], is reminiscent of the generation of singlet oxygen by vanadate-dependent haloperoxidases in the absence of a substrate [Equation 4.10 in Section 4.3.1].¹² Whether or not the chemo-preventive effect – or ‘carcinogen interception mechanism’^[44] – of vanadium is an outcome of the removal of DNA-hurtful ROS, or of limited generation of ROS which competitively eliminates other carcinogenic factors, does not seem to have been clarified. The abatement of the formation of 8-OHdG^[43] on supplementing vanadate^[43] appears to point towards an antioxidant effect.



Alkylating agents such as dialkylnitrosamines present in tobacco-borne smoke and various (in particularly fried) foods, but also formed intrinsically by biosynthesis, and also

¹² *In vitro* studies have shown that vanadyl very effectively cleaves DNA in the presence of peroxide. Apart from the possible beneficial effect of this process in anti-neoplastic activity, toxic effects pertinent to vanadium – damage of DNA of healthy cells – has to be taken into account.

1-methyl-1-nitrosourea are well-established candidates for chemical carcinogenesis due to their ability to alkylate DNA. Alkylating agents can be detoxified by transfer of the electrophilic alkyl to a nucleophile such as vanadate $[H_2VO_4]^-$. The toxin is thus consumed and DNA damage prevented, a reaction which has been modelled, using diethyl sulfate as the alkylating agent, acetonitrile with residual water as the solvent and trivanadate $[V_3O_9]^{3-}$ as the nucleophile.^[44] One might argue that these model conditions do not properly reflect the *in vivo* situation, where water is the solvent and oligovanadates can hardly be present at micromolar concentrations. On the one hand, the dielectric properties of acetonitrile come closer to those of the intracellular aqueous medium than water itself. On the other hand, oligovanadates may form in specific cell compartments where vanadate accumulates, particularly so under the slightly acidic conditions pertinent to cancer cells. The dealkylating action of vanadate is represented by Equation (5.3): from the alkylating agent, the alkyl group R, formally positive, is transferred to an oxo anion of vanadate and converted, by protons stemming from water, to an alcohol. In the case of dialkylnitrosamines, the active alkylation agent is the intermittently generated alkyl diazonium cation.



For the action of vanadocenes such as **23** in Figure 5.13, the hypothesis had been advanced that they might function in a manner comparable to that of the well-established anti-cancer drug cisplatin [*cis*-diamminedichloroplatinum(II)]. Cisplatin is converted to diammine-aqua/hydroxo species *in vivo*, and the $\{cis-Pt(NH_3)_2\}$ moiety firmly coordinates to two adjacent guanine-N⁷ of the DNA of cancer cells, forming an intrastrand cross-link,¹³ leading to a ‘kink’ in the DNA and preventing its duplication. Given the fact that Cp_2VCl_2 undergoes hydrolytic reactions similar to cisplatin, it is tempting to assume a comparable mode of action. The bite angle $\angle(X-M-X)$ ($X = OH$ or H_2O) and the distance $d(X \cdots X)$ are almost identical, despite the differing steric conditions: whereas the geometry in a four-coordinated Pt^{II} complex is square planar, the arrangement in Cp_2VX_2 is tetrahedral. Comparison of the *in vitro* action of cisplatin and Cp_2VCl_2 indicated mechanistically dissimilar cytotoxic action of the two compounds.^[45] On the other hand, morphological phenomena within Ehrlich ascites tumour cells treated with Cp_2VCl_2 (or Cp_2TiCl_2) can be interpreted in terms of a molecular attack of the metallocene dihalide upon intracellular DNA (cf. Figure 5.14).^[40] Among the metallocene complexes tested ($M = Ti, V, Zr, Hf, Mo$), vanadocenes are most effective in anti-proliferation of cultured tumour cells (Ehrlich ascites tumour or HeLa cells¹⁴); cell proliferation is reduced at concentrations as low as $5 \mu M$. Cp_2VCl_2 has also been shown to reduce tumour weights of solid Ehrlich tumours when applied intraperitoneally to mice carrying this tumour.

¹³ Other intercalations are possible and have been observed.

¹⁴ Ehrlich tumours are poorly differentiated malignant tumours (originally a breast carcinoma in a mouse), which grow in solid and ascetic forms. HeLa cells are a cell line developed from cervical cancer of a woman (Henriette Lacks), who died from that cancer in 1951.

Interestingly, Cp_2VCl_2 interacts with the phosphate moiety of desoxyadenosyl phosphate in aqueous solution at physiological pH to form outer-sphere complexes with a half-life of $0.49(8)\text{ ms}$, and a distance $d(\text{V}\cdots\text{P})$ of ca 5.5 \AA (interaction with two phosphate moieties).^[46a] This structural result, obtained from an analysis of the influence of the paramagnetic vanadium centre on the ^{31}P nuclear relaxation times, is in good agreement with the structurally characterised model compound $\text{Cp}_2\text{V}(\text{OH})_2\cdot 2\text{PO}_2(\text{OPh})_2^-$ (**25** in Figure 5.13). The damage to DNA by CpVCl_2 or its hydrolysis products may therefore also be due to a comparable mode of action.

DNA cleavage as the mechanism by which tumour growth is inhibited is also been suggested for the action of bis(peroxo)vanadium(V) complexes of the general composition $[\text{VO}(\text{O}_2\text{L})_2]^-$ ($\text{L} = o\text{-phenanthroline or bipyridyl}$) and traced back to the formation of hydroxyl radicals.^[46b]

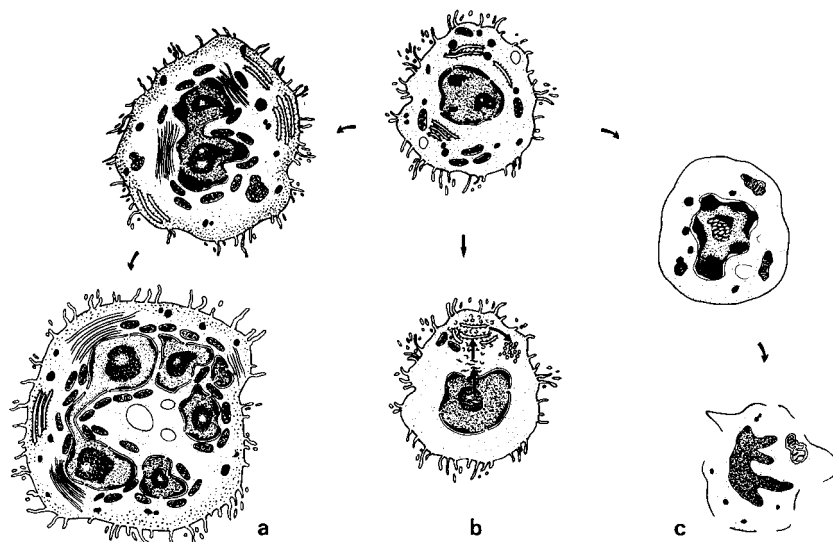


Figure 5.14

Morphological changes within Ehrlich ascites tumour cells caused by CpVCl_2 (and CpTiCl_2). **a:** Formation of giant cells with degenerated features of the cytoplasm. **c:** Cellular degeneration and necrosis. *In vitro*, giant and necrotic cells disintegrate; *in vivo*, these cells are eliminated by macrophages. **b:** Formation of endogenous viruses. Reproduced, from P. Köpf-Maier and H. Köpf, *Drugs Future*, 11, 297–319. Copyright (1986), with permission from Prous Science Journals.

5.1.2.2 Other Medicinal Effects of Vanadium

Vanadium compounds containing thiosemicarbazide- and hydrazide-derived ligands, such as **26** and **27** in Figure 5.15, exhibit antimoebic activity against *Entamoeba histolytica*.^[47] This water-borne amoebic protozoan parasitises the human intestines and in some cases other visceral organs, especially the liver. It is the aetiological agent of amoebiasis (also known as amoebic dysentery) and thus responsible for amoebic colitis and intestinal and liver abscesses. Symptomatic patients typically suffer from abdominal pain, diarrhoea

and bloody stool. The disease has epidemic dimensions, affecting millions of people worldwide, in particular in tropical developing countries. *E. histolytica* is considered the third largest killer after malaria and schistosomiasis.^[48] The mainstay of therapy for invasive amoebiasis are nitroimidazoles such as metronidazole, (**28** in Figure 5.15), to which 90% of patients having mild to moderate amoebic dysentery respond. Side-effects are common, however, and include nausea, neurological alterations and impairment of the cardiac rhythm. Metronidazole is further classified by the Agency for Research on Cancer in group 2B, i.e. potentially carcinogenic to humans. The complexes **26** and **27** and related compounds efficiently inhibit the growth of *E. histolytica* *in vitro*. These vanadium compounds are about as efficient as or even ‘better’ in this respect than metronidazole, as shown in Figure 5.15. The ligands alone do not have a substantial effect, nor does the benchmark compound *bis*(acetylacetone)oxovanadium(IV), [VO(acac)₂].

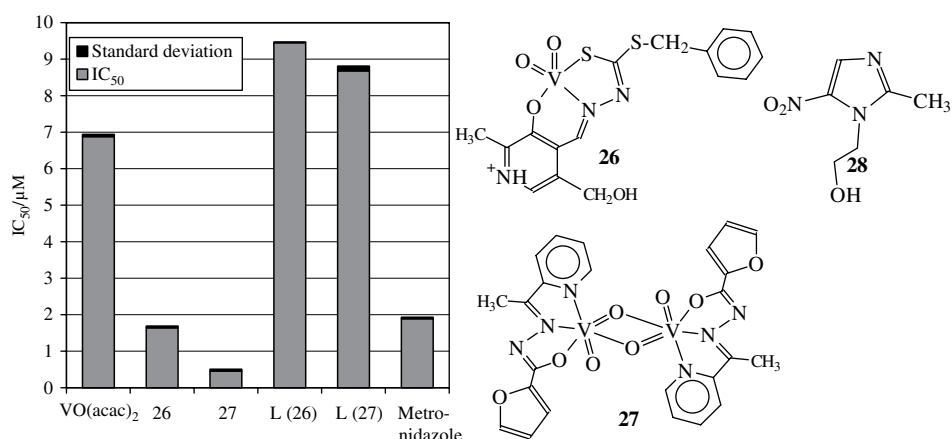


Figure 5.15

Biocidal compounds against *Entamoeba histolytica*, a parasite causing amoebiasis. The Schiff base-related complexes **26** and **27** are active *in vitro*, metronidazole, (**28**) is commonly used in the medication of amoebiasis. In the diagram on the left, the activities of metronidazole, the complexes **26**, **27** and VO(acac)₂ and the free ligands (L) of **26** and **27** are compared. The IC₅₀ values indicate the concentrations at which growth of 50% of the amoebae is inhibited.

Cyclopentadienylvanadium complexes have also been shown to be spermicidal.^[49] Spermicidal plus anti-HIV activity is pertinent to certain oxovanadium(V) complexes with specific thioureas (Htu) as ligands such as **29** in Figure 5.16.^[50] Thioureas are currently used to treat HIV infections through inhibition of the virus’s replication by blocking HIV-1 reverse transcriptase (an RNA-dependent DNA polymerase found in retroviruses including the HIV virus), and which are effective at nanomolar concentrations. The oxovanadium(V)-thiourea complexes [VO(OMe)(tu)₂]¹⁵ exhibit anti-HIV activity with

¹⁵ The structural formulae provided for the thiourea (Htu) complexes [VO(OMe)(tu)₂] in ref. 50, with the coordination number 4 for vanadium, are not likely to represent the correct composition.

inhibitory concentrations IC₅₀ around 1 μM combined with fast sperm immobilisation in human semen and lacking toxicity to human female genital tract epithelial cells. Anti-HIV-1 activity has also been reported for the water-soluble oxovanadium(IV)-porphyrin complex **30** in Figure 5.16, which showed 97% *in vitro* inhibition at a concentration of 5 μM. The presence of both vanadyl and the porphinogenic ligand is essential for activity: the ligand alone, and the corresponding zinc complex or vanadyl sulfate, are markedly less active.^[51]

Like many other polyoxometalates (POMs), vanadium-containing POM systems can also be potent anti-viral drugs. A vanadium-substituted polyoxotungstate has anti-viral *in vitro* activity against viruses causing influenza, parainfluenza, Dengue fever, HIV-1 and SARS¹⁶.^[52] A possible mechanism of action is the (inhibitory) interference with phosphate-metabolising enzymes and/or inositol-induced Ca²⁺ release, a level of action which has been elucidated for decavanadate (see also the next section). The polyanionic POMs may survive by protection through (cationic) macroligands present in the extra-/intracellular media (cf. Figure 2.7 in Section 2.1.1). Without such protection, they are thermodynamically unstable at physiological pH and concentrations, and break down to form mono- and oligonuclear oxometalates as outlined for vanadates in Section 2.1. The kinetics for this degradation are, however, slow, with half-lives up to several hours around pH 7.

The treatment with vanadate of humans suffering from tuberculosis mentioned at the beginning of this chapter^[3] does not seem to have been pursued further for many decades. In the early 1970s, a Russian group re-started experiments with test animals, looking at the effect of vanadyl sulfate against tuberculosis mycobacteria.^[53] More recent developments include the vanadyl complex of a macrocyclic tetraaza ligand, (**31** in Figure 5.16)^[54a] and

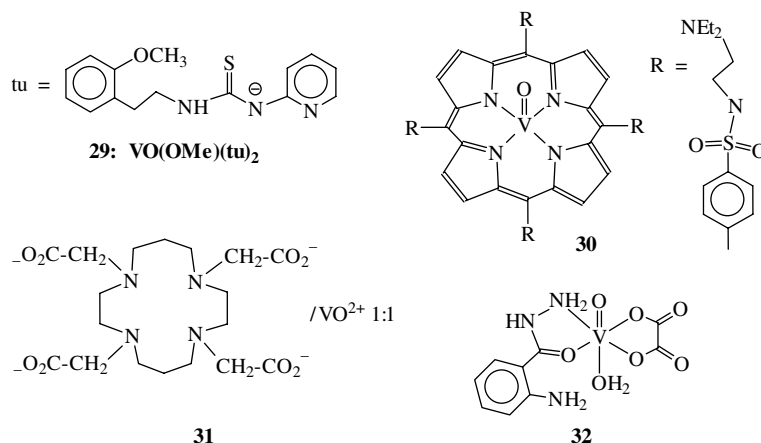


Figure 5.16

Complexes formed between thiourea (Htu) and vanadyl with the putative formulation [VO(OMe)(tu)₂] (**29**) and the porphyrin complex **30** exhibit activity against HIV-1. **29** additionally is a spermicide. Preparations containing the macrocycle **31** and vanadyl in a 1:1 ratio and the hydrazide complex **32** are examples of *in vitro* inhibitory effects against tuberculosis mycobacteria.

¹⁶ SARS (severe acute respiratory syndrome) is an atypical pneumonia caused by a coronavirus.

hydrazide complexes such as **32**.^[54b] Both systems are effective against *Mycobacterium tuberculosis*.

5.2 Interaction of Vanadium with Proteins and Protein Substrates

Indigenous functional proteins containing vanadium are scarce. Those which are known and have been characterised to date have been addressed in previous chapters:

1. Vanadate(V)-dependent haloperoxidases, catalysing the two-electron oxidation of halides X^- to $\{X^+\}$, contain vanadate $H_2VO_4^-$ covalently bonded to the $N\epsilon$ of a protein-histidine (Section 4.3 and Figure 4.16).
2. Vanadium nitrogenases with vanadium(II–IV) as a constituent of the Fe_7VS_9 cluster (FeV -cofactor), coordinated to three bridging sulfides, the vicinal hydroxide and carboxylate of homocitrate and a histidine (Section 4.4 and Figure 4.26).
3. Vanabins, storage proteins for the vanadyl cation found in ascidians, and containing up to 20 VO^{2+} attached to amine terminals of lysines (section 4.1.2 and Figure 4.4). A vanadium(IV)-binding protein was also isolated from the bacterium *Pseudomonas isachenkovii* (Section 4.5) which utilises vanadate as terminal electron acceptor in anaerobic respiration, and appears as well to be present in the hydrogen bacterium *Xanthobacter autotrophicus*.^[55]

In addition, vanadyl, vanadate(IV) and, first and foremost, vanadate(V) play a prominent role as phosphate analogues: Vanadate and vanadate analogues of phosphatised substrates can serve as an alternative ligand or substrate in proteins for which phosphate is the natural ligand/substrate. Alternatively, vanadate can be a very efficient inhibitor or, less commonly, stimulator of phosphate-metabolising enzymes. The inhibitory effect against the sodium–potassium pump (Na^+, K^+ -ATPase), discovered and confirmed three decades ago,^[56] was a milestone in bioinorganic vanadium chemistry, which has enormously stimulated investigations into phosphate–vanadate antagonism. The inhibition of intracellular protein tyrosine phosphatases by vanadate had been addressed in the context of the insulin-mimetic potential of vanadate (Section 5.1.1.5). Vanadium species as antagonists of phosphate will be treated on a more general basis in Section 5.2.1. Section 5.2.2 is concerned with the inhibition of lactamases.

Vanadyl, V^{III} and, less pronounced, vanadate also bind to various proteins, in many cases in an unspecific manner, i.e. without imposing a vanadium-specific function on the protein. Noteworthy is the strong binding to the metal ion binding sites in the two lobes of transferrin, which can be considered a transport protein for the physiologically relevant forms of vanadium, VO^{2+} and $H_2VO_4^-$. The essentially unspecific binding of vanadyl (and vanadate) to proteins, and the competitive incorporation of vanadium into metal cofactor sites of enzymes depending on other metal ions, are increasingly employed for the characterisation of unspecific and specific binding sites for metal ions such as Mg^{2+} and Ca^{2+} , exploiting the versatile properties of vanadium as a probe in spectroscopic detection modes, such as ^{51}V NMR (for vanadate) and EPR, ESEEM and ENDOR (for VO^{2+}). Selected examples were introduced in Chapter 3 (on methods); additional examples are dealt with in Section 5.2.4.

Finally, in Section 5.2.5, some insight is provided into modifications of proteins by the action of vanadate and vanadyl.

5.2.1 Vanadium- and Phosphate-metabolising Enzymes

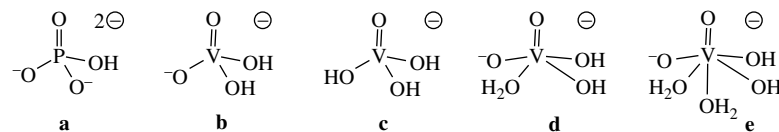
This section will be divided as follows:

1. general;
2. interference with phosphatases and ribonucleases;
3. haloperoxidase activity of vanadate-inhibited phosphatases; phosphatase activity of apo-haloperoxidases;
4. stimulation of phospho-transfer enzymes;
5. structural vanadium analogues of phosphate esters and anhydrides.

5.2.1.1 General

The inhibition^[57a] and stimulation^[57b] of phosphate-metabolising enzymes are commonly, and convincingly, traced back to what is termed ‘the vanadate–phosphate antagonism’, largely reflected in a similarity of the physiological actions of the two anions.^[58] The intriguing similarity between phosphatases and apo-haloperoxidases on the one hand, and vanadate-inhibited phosphatases and genuine haloperoxidases on the other, both in active site and tertiary structure of the protein and in function (see below), has led to speculation with regard to a common evolutionary origin or, alternatively, convergent evolution of the two enzyme classes.

In most of the investigations directed towards the exploitation of the similarity between phosphate and vanadate (**a** and **b** in Scheme 5.3), vanadate(V) is considered. It is worth noting, however, that vanadate(IV) is also present in solution under physiological conditions (Section 2.1.1; **c** in Scheme 5.3). At first sight, vanadate and phosphate are indeed very much alike: the manifestation is tetrahedral and the outer-sphere charge distribution thus essentially spherical. The net ionic charge of the main species present at pH 7 is, however, different, –2 in the case of phosphate and –1 for the vanadate, and this can result in differing means of transport and interactions with electrophiles. There are other distinct differences, which are, at least in part, responsible for the inhibitory effect of vanadates towards phosphate-metabolising enzymes. The main differences lie in the susceptibility of vanadate to (one-electron) reduction and in the ability to stabilise, as a consequence of the presence of energetically low-lying d-orbitals, coordination numbers >4 (usually 5 and 6). This implies the presence of the five- to six-coordinated aqua anions **d** and **e** (in equilibrium with the tetrahedral species) in Scheme 5.3 and, in many but not all instances, fixation of vanadate by covalent and thus firm coordination to functional groups provided by amino acid side-chains of the enzyme itself, or by constituents of enzyme substrates/cofactors, such as uridine in ribonucleases.



Scheme 5.3

5.2.1.2 Interference with Phosphatases and Ribonucleases

The two main groups of phosphate-metabolising enzymes inhibited by vanadate are the phosphatases and the ribonucleases. Phosphatases catalyse the hydrolysis of phospho-ester bonds in a variety of substrates. The net reaction path is shown in the upper part of Figure 5.17 for a phosphatase having a histidine in its active site, common in acid phosphatases. Ribonucleases (RNases) split one of the two phosphoester bonds in ribonucleic acids and thus fragment RNA. The generally accepted mechanism of action of RNases is the two-step catalytic reaction depicted in the lower part of Figure 5.17. The first step is a ‘trans-phosphorylation’, i.e. the cleavage of one of the ester bonds by protonation with concomitant formation of a cyclic ribosephosphate. In the second step, the acyclic monoester is formed by hydrolysis. In both phosphatase mechanisms shown in Figure 5.17, an intermediate plays a central role, in which phosphorus is pentacoordinated (‘phosphorane intermediate’) in a trigonal bipyramidal array. These intermediates are labile in phosphorus chemistry, but can be stable in vanadium chemistry, and the inhibitory effect of vanadate is commonly traced back to the formation of such a ‘frozen-in’ intermediate with vanadate in the active site of the enzyme. In simpler terms: vanadate is picked up by the phosphatase because ‘it looks like’ phosphate. However, in contrast to phosphate, it forms a stable covalent bond to an active site function, thus blocking off the genuine phospho-ester substrate.

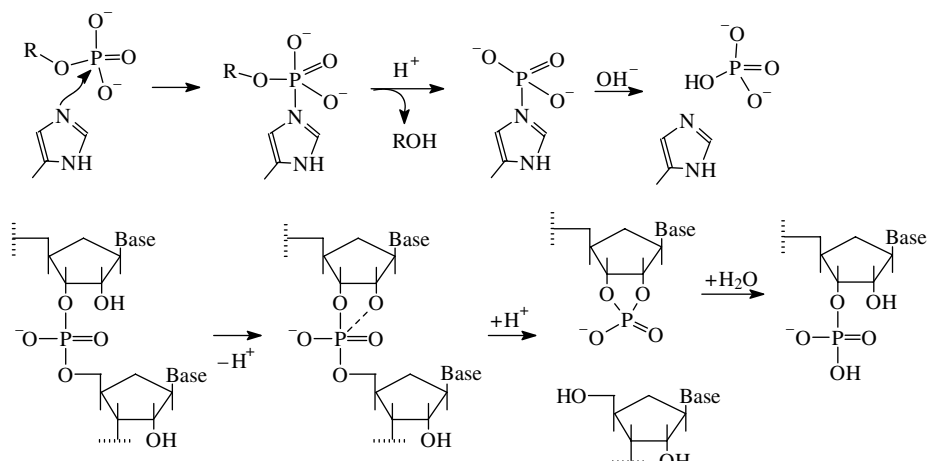


Figure 5.17

Top row: schematic representation of the hydrolysis of the phospho-ester bond as catalysed by a phosphatase with a histidine in the active site, including the pentacoordinated intermediate state. Bottom row: the two-step mechanism for the cleavage of the phospho-diester bond by ribonucleases, showing the transphosphorylation to cyclic ribose phosphate (step 1) and hydrolysis (step 2).

Vanadate-inhibited forms of RNases have been structurally characterised,¹⁷ and in Figure 5.18 two examples, bovine pancreatic RNase-A (**I**)^[59b] and RNase-T₁ (**II**) from the fungus *Aspergillus oryzae*,^[60a] are shown, which exemplify two possible modes

¹⁷ For an overview of ‘The power of vanadate in crystallographic investigations of phosphoryl transfer enzymes’, see: ref. 59a.

of binding of vanadate. In **I**, vanadate is covalently bonded to the ribose-2' and -3' oxo groups of the substrate uridine, and additionally fixed to the enzyme through a hydrogen bonding network. Bovine pancreatic RNase-A, a single-chain protein composed of 124 amino acids, catalyses the hydrolysis of phosphate ester linkages in single-stranded RNA. RNase-T₁ specifically cleaves RNA at guanosine to yield oligonucleotides with terminal guanosine-3'-phosphate. In the substrate-free vanadate complex **II**, there are no covalent bonds connecting vanadate to the protein. Rather, vanadate ($[H_2VO_4]^-$) is firmly embedded into the catalytic site through hydrogen bonding interactions. The incorporation of vanadate is confirmed by ^{51}NMR in Tris buffer,¹⁸ showing a considerably broadened resonance signal, shifted somewhat downfield with respect to free monovanadate. ^{51}V NMR studies also revealed a drastic increase in stability in the ternary system containing the substrate analogue inosine. Here, binding of vanadate is revealed by a signal, $\delta(^{51}\text{V}) = -523$ ppm, typical of pentacoordinated, trigonal bipyramidal vanadium, suggesting a coordination comparable to that in **I**. For the power of ^{51}V NMR as a probe in studying vanadate–protein interaction, see also Figure 5.20. The structure motif represented by **I** has also been found for the vanadate–uridine complex formed with the RNase-related cyclic nucleotide phosphodiesterase (*cNPDase*) from *Arabidopsis thaliana* (**III** in Figure 5.18).^[61] *A. thaliana* is a cruciferous plant (a close relative of the cauliflower), the first plant of which the genome has been completely sequenced, and which is therefore often used as a model organism. The enzyme *cNPDase* catalyses the hydrolytic cleavage of cyclic adenosine phosphate (cf. the second, hydrolytic step of phosphoester cleavage in Figure 5.17, bottom). Human tyrosyl-DNA phosphodiesterase, **IV**, catalyses the hydrolysis of a phosphodiester bond between a tyrosine side-chain and a DNA 3'-phosphate.^[62] Its vanadate-inhibited form

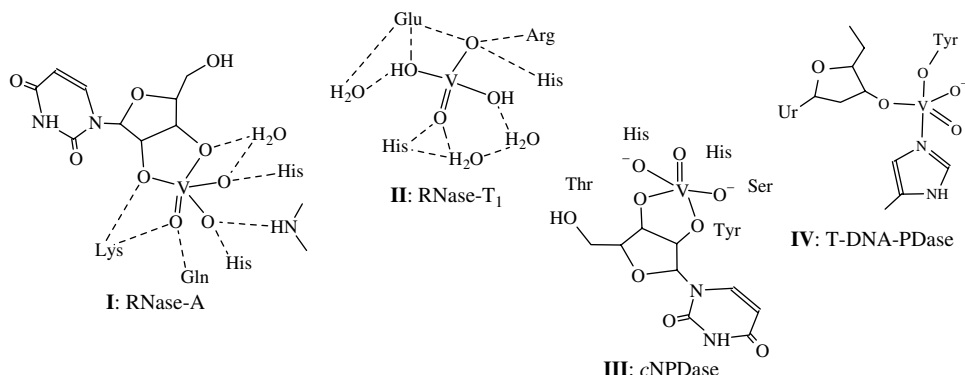


Figure 5.18

Four examples of structurally characterised, vanadate-inhibited phosphorylation enzymes working on the hydrolysis of phospho-ester bonds in nucleotides: **I**, the vanadate–uridine complex of bovine pancreatic ribonuclease-A; **II**, the vanadate complex of ribonuclease-T₁ from the fungus *Aspergillus oryzae*; **III**, the vanadate–uridine complex of cyclic nucleotide phosphodiesterase from the cruciferous plant *Arabidopsis thaliana*; **IV**, human tyrosyl-DNA phosphodiesterase (Ur = uridine).

¹⁸ Tris buffer is a buffer used in the pH range ca 7–9, containing variable ratios of tris(hydroxymethyl) aminoethane and HCl. This buffer also forms weak complexes with vanadate.

contains ester bonds to desoxyribose (equatorial) and tyrosine (axial). The second axial position is occupied by the $\text{N}\varepsilon$ of a histidine, giving rise to an overall appearance very much resembling the active centre in vanadate-dependent haloperoxidases.

The structural features of the phosphodiesterase **IV** in Figure 5.18 link up to the structural characteristics of vanadate-inhibited phosphatases. The amino acids of phosphatases involved in phosphate binding/abstraction and the amino acids in the active centre of vanadate-dependent haloperoxidases (VHPOs) are largely conserved, leading to a striking structural similarity between vanadate-inhibited phosphatases and the haloperoxidases. This is illustrated by the examples depicted in Figure 5.19. As in VHPO (**V**), vanadate in rat prostate acid phosphatase (**VI**) is firmly coordinated to histidine, while the distal histidine in the VHPOs is replaced by aspartate.^[63] The same general motif as in the VHPOs is also realised in bovine heart protein-tyrosine phosphatase (PTP, **VII**),^[64a] where the covalent linkage is formed to an active site cysteinate.¹⁹ Remarkably, there is no redox interaction with cysteine, as otherwise commonly observed in vanadium(V)-thiol systems (Section 2.3.2.4), but in accord with the nonreductive interaction of vanadates with glycerol-6-phosphate dehydrogenase, which also contains a cysteine at the active site. Apparently, this stabilisation of the vanadate-cysteinate system against redox interaction is a consequence of a shift in redox potential imparted by close-by amino acid residues of the active site pocket in electrostatic contact with vanadate. Peroxovanadate, which is a sufficiently more powerful oxidising agent than vanadate, has been shown to oxidise thiols present in mitochondrial calcium ion release pathways, possibly to sulfonates, thus inhibiting Ca^{2+} release from mitochondria.^[64b] In the Cys215Ser mutant of protein-tyrosine phosphatase PTP-1B **VIII**,^[65] and in the *E. coli* alkaline phosphatase **IX**,^[66] cysteinate is replaced by serinate, another remarkable feature, since in model complexes with small serine-containing peptides serine tends to avoid direct coordination to vanadium (Figure 2.15 in Ch. 2.2.1). The active centre of **IX** also contains two zinc ions which are in contact with vanadate and additionally coordinated to histidine and aspartate.

Apart from His, Cys and Ser, the hydroxyamino acid threonine can also be a residue in the active site of phosphatases: the Thr214Ala mutant of Na^+K^+ -ATPase exhibits a drastically reduced vanadate affinity for inhibition of ATPase activity,^[67] suggesting that Thr is essential in vanadate binding. In the light of what has been said above, threonine very probably coordinates to vanadium into one of the axial positions in much the same manner as the other amino acid residues.

The inhibition of PTPs by vanadate is of particular interest since this mode of action is supposed to be the primary effect exerted by vanadium applied as an insulin-mimetic agent (see 5.1.1.5). The vanadate-inhibited PTP-1B **VIII** in Figure 5.19, the structure of which was revealed both by single-crystal X-ray diffraction and two-dimensional $^1\text{H}-^{15}\text{N}$ NMR spectroscopy, was prepared by treating the phosphatase with either vanadyl sulfate or bis(maltolato)oxovanadium(IV) (BMOV) (**7a** in Figure 5.2). Irrespective of the nature of the intrinsically applied vanadium species, the same compound with incorporated vanadate(V) was obtained, nicely demonstrating that the active species is vanadate(V), formed by elimination of the ligands and oxidation of V^{IV} to V^{V} . *In vivo* studies further showed that intracellular PTP-1B from rat heart tissue was actively inhibited, and autophosphorylation of the insulin receptor concomitantly enhanced.

¹⁹ Interestingly, molybdate, which is alternatively taken up into the active site of the phosphatase, does not form covalent bonds to protein residues.

While reaction between VO^{2+} and the complete PTP-1B apparently is accompanied by oxidation of vanadyl to vanadate, the PTP-1B active site peptide Val-His-Cys-Ser-Ala-Gly-NH₂ coordinates the vanadyl ion without coupled redox interaction. The preferred coordination site depends on the pH. At pH 6, the preferential binding site is the histidine (**Xa** in Figure 5.19), whereas coordination to cysteinate is dominant at pH 9 (**Xb**). The proposed structures **Xa** and **Xb** are consistent (Table 3.3) with the EPR spectroscopic hyperfine coupling constants $A_{||} = 161 \times 10^{-4} \text{ cm}^{-1}$ (**Xa**) and $144 \times 10^{-4} \text{ cm}^{-1}$ (**Xb**).^[68]

Apart from their role in steering the signal transmission in hormonal response to insulin, protein phosphorylation/dephosphorylation is one of the major signal transduction mechanisms for controlling and regulating intracellular processes, where – at least in principle – vanadate can thus interfere. An example is mammalian glucose-6-phosphatase (G-6Pase), another member in the family of acid phosphatases containing a histidine as an indispensable phosphate acceptor in the active site. G-6Pase is a key enzyme in glucose homeostasis. Its effective interaction with vanadate may have implications for the treatment of Von Gierke disease, an inherited disease in which gluconeogenesis is prevented and glycogen ineffectively broken down to glucose, leading to severe hypoglycaemia during fasting periods.

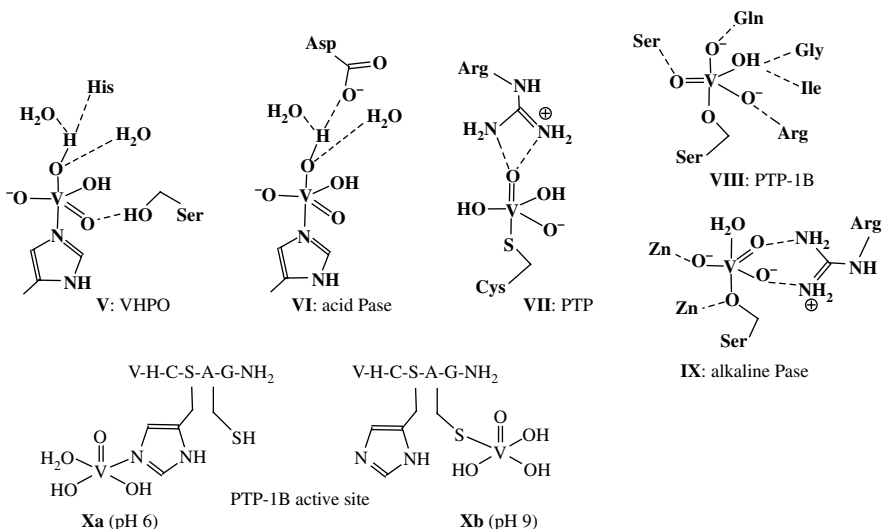


Figure 5.19

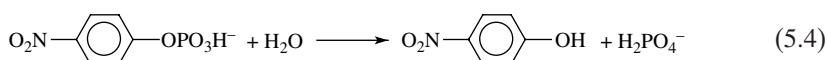
VI–IX are structurally characterised, vanadate-inhibited phosphatases. **VI**, Rat prostat acid phosphatase; **VII**, bovine phosphotyrosyl phosphatase; **VIII**, mammalian protein tyrosine phosphatase PTP-1B (mutant Cys215Ser); **IX**, *E. coli* alkaline phosphatase. For comparison, the active centre of vanadate-dependent haloperoxidases (VHPO) (**V**), is also shown. The structures **Xa** and **Xb** have been proposed, based on EPR, for the vanadyl complexes formed with the PTP-1B active site peptide Val-His-Cys-Ser-Ala-Gly.

5.2.1.3 Haloperoxidase Activity of Vanadate-inhibited Phosphatases; Phosphatase Activity of Apo-haloperoxidases

The similarity of the active sites of VHPOs and (acid) phosphatases with respect to (i) the amino acid homology and (ii) the structure of the vanadate/phosphate centres has

intriguing implications for the potential of vanadate-inhibited phosphatases in peroxidase reactions, and for the potential of apo-VHOPs in phosphatase reactions. Both phenomena have been observed and investigated.

Apo-VCIPO in fact does show phosphatase activity in the usual assay, where *p*-nitrophenyl phosphate is hydrolysed to *p*-nitrophenol and phosphate, [Equation (5.4)]. The presence of His496 (cf. **b** in Figure 4.16) is essential; the mutant His496Ala consequently is inactive. Hydrolysis of a phosphohistidine intermediate (see Figure 5.17, top row) is the rate-determining step.^[69] Two arginines and a lysine are needed to stabilise the pentacoordinate transition state. Phosphatase activity also affords a protonation step, and the distal His404 is the most likely candidate for mediating protonation.



On the other hand, vanadate-substituted acid phosphatases from the pathogenic bacteria *Shigella flexneri* and *Salmonella enterica* catalyse the oxidative bromination of phenol red to bromophenol blue (Scheme 4.3, left), using hydrogen peroxide as oxidant. The turnovers are, however, an order of magnitude lower than with native VBrPO. Thioanisole (methyl phenyl sulfide), a substrate for VHPOs, is equally oxidised to form the sulfoxide with medium chiral induction.^[70] Similarly, incorporation of vanadium into phytase affords a peroxidase capable of catalysing the oxidation of thioanisole and derivatives thereof.^[71] Phytases are plant phosphatases belonging to the family of histidine acid phosphatases. They catalyse the hydrolysis of the phosphoester bond in phytic acid (inositol hexaphosphate) (Figure 5.20) in the 3-position (3-phytases) or in the 6-position (6-phytases). The formation of the vanadate–enzyme complexes is demonstrated by the appearance of a comparatively broad resonance signal in the ^{51}V NMR spectrum (Figure 5.20) at a chemical shift typical of vanadium in an environment dominated by oxo-functional ligands in a (distorted) trigonal bipyramidal environment.

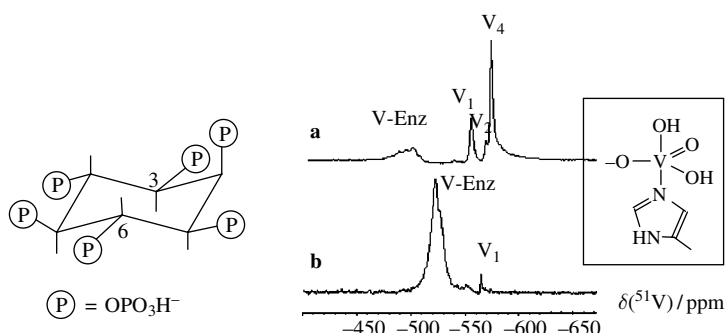


Figure 5.20

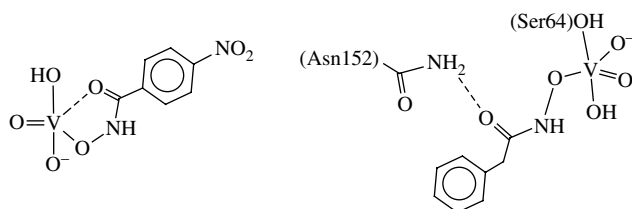
Left: phytic acid (inositol hexaphosphate), the substrate of phytases. Right: ^{51}V NMR spectra of solutions (pH 7.6) containing 5 mM vanadate and 3-phytase (a) or 6-phytase (b). The signals labelled ‘V-Enz’ correspond to vanadate incorporated into the active site of the enzyme, with the probable structure shown in the inset; the sharp signals at high field indicate mono-, di- and tetravanadate. Courtesy of Isabel Correia, Centro Química Estrutural, TU Lisbon, Portugal; see also DOI: 10.1016/j.jinorgbio.2007.09.005.

5.2.1.4 Stimulation of Phospho-transfer Enzymes

In contrast to phosphohydrolases, the phosphatase activity of enzymes which *non-hydrolytically* catalyse the transfer of phosphate groups can be *stimulated* by vanadate. Vanadate can spontaneously form esters with unphosphorylated substrates such as sugars. These vanadate esters act as alternative substrates for mutases and isomerases, stimulating their phosphatase activity. Examples are phosphoglucomutase, which catalyses the ‘mutation’ (phosphate shift) between glucose-1-phosphate and glucose-6-phosphate, and phosphoribose isomerase, which catalyses the isomerisation between ribose-5-phosphate and ribulose-5-phosphate.^[57]

5.2.2 Inhibition of Lactamases

Bacteria frequently develop resistance to antibiotics based on β -lactams, a problem that has been present since these antibiotics were introduced into clinical practice more than half a century ago. The resistance comes about by, *inter alia*, bacterial production of β -lactamases, enzymes that catalyse the hydrolysis of lactams. It is of particular interest that hydroxamate complexes of vanadium(V) turned out to inhibit lactamases effectively.^[72] This has been demonstrated for the β -lactamase of *Enterobacter cloacae*. The most effective inhibition, with a K_i value of $0.5\text{ }\mu\text{M}$, was achieved with the 4-nitrobenzohydroxamic acid complex shown in Scheme 5.4. The hydroxamate coordinates to vanadium through the hydroxamic hydroxyl-O, with an additional weak interaction with the acid carbonyl-O. According to spectral features and model calculations, the results of which are also depicted in Scheme 5.4, this weak interaction is abandoned in favour of hydrogen bonding to asparagine (Asn152) and occupation of the ‘abandoned’ vanadium site by a serine residue (Ser64) of the enzyme. We are hence dealing with a coordination environment similar to that in protein tyrosine phosphatase 1B (**VIII** in Figure 5.19), with the exception that the extra ligand, hydroxamate, remains ligated to vanadium. The ternary complex is characterised by a broad ^{51}V NMR signal at -494 ppm , which compares with -497 ppm for the hydroxamate complex not bound to the enzyme.



Scheme 5.4

5.2.3 Structural Vanadium Analogues of Phosphate Esters and Anhydrides

In Section 2.1.3, vanadate esters were addressed in the general context of inorganic aspects of vanadium compounds. Although vanadate esters form readily in aqueous solutions, they are not particularly stable (formation constants are of the order of magnitude of 10^{-1} – 1 M^{-1}) and easily hydrolyse. Equilibria such as represented by Equation (5.5) describe the

situation, and the position of these equilibria depends on concentration, vanadate:alcohol ratio, ionic strength and pH. A kinetic component is also involved, i.e. ester formation and saponification can be slow for sterically hindered alcohols. In physiological systems, vanadate esters are usually not readily distinguished from phosphate esters, and enzymes such as dehydrogenases, isomerases and aldolases respond to vanadate esters in competition with phosphate esters. As noted above for vanadate, a vanadate ester, once taken up as an alternative substrate, can stabilise the ‘transition’ state of the enzyme by expanding the coordination sphere of vanadium. For anhydrides of vanadate (e.g. divanadate) and mixed phosphate–vanadate anhydrides, similar considerations apply (see Sections 2.1.1 and 2.1.2).

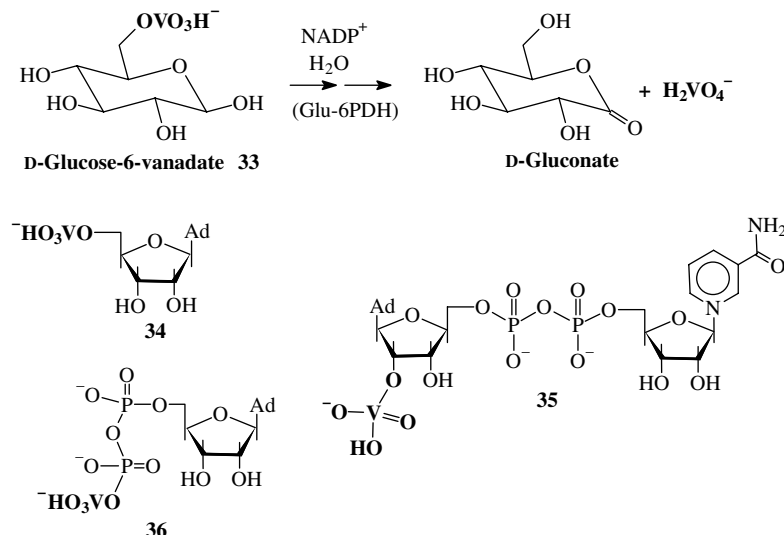


Figure 5.21 shows structures of biologically relevant vanadate esters and anhydrides. One example is glucose-6-vanadate (**33**, see also Ch. 2.2.1), which is recognised by glycose-6-phosphate dehydrogenase (Glu-6PDH) and rapidly oxidised and hydrolysed to gluconate.^[73a] Other examples of vanadate esters formed with sugar-OH groups are adenosyl vanadate (**34**),^[73b] an analogue of AMP, and nicotine adenine dinucleotide vanadate (NADV) (**35**), an analogue of NADP. NADV can be a potent cofactor in reductases otherwise dependent on NADP.^[73b] Compound **36**, adenosine diphosphate vanadate (ADPV),^[74] an analogue of ATP, exemplifies mixed anhydride formation under physiological conditions. Its potent role in photo-induced protein cleavage, imparted by vanadate, will be addressed in Section 5.2.5. The vanadium analogue of free linear triphosphate, linear $\text{V}_3\text{O}_9^{5-}$ exists only at pH values around 9 (where it is a minor constituent along with other vanadate species) and hence is physiologically irrelevant. The ability of the vanadate analogues of adenosine phosphates such as ADPV and AMPV to respond to the corresponding phosphatases is limited to non-existent. A likely explanation is the thermodynamically less potent vanadate–phosphate bond, viz. ca 10 kJ mol⁻¹, vs ca 30 kJ mol⁻¹ for the phosphate–phosphate bond. Further, the vanadate–phosphate analogues do not bind Mg²⁺ effectively (as do diphosphate residues in, e.g., ATP and ADP), a precondition for efficient turnover in physiological kinetics and energetics.

On the other hand, *vanadyl* ions can coordinate to ATP in a chelating manner, via the phosphate oxo groups in the α , β and γ positions, forming $[\text{VO}(\text{ATP})\text{H}_x]^{(x-2)}$ ($x = 0, 1, 2$) and $[\text{VO}(\text{ATP})_2]^{6-}$ in the weakly acidic to neutral pH range. With increasing pH, the ribose moiety becomes the preferential binding site, and in a slightly alkaline medium, a complex of composition $[\text{VO}(\text{ATP})_2]^{8-}$ with a mixed binding mode is observed.^[75a] The mechanism by which vanadyl inhibits protein kinase (PKA), dependent on cyclic adenosine monophosphate at low micromolar concentrations, is based on vanadyl binding to ATP.^[75b] VO²⁺ is a more efficient binder to diphosphate and triphosphate than Mg²⁺, and therefore increasingly employed as a paramagnetic probe in the structure elucidation, by ENDOR and ESEEM, of ATP-protein complexes.^[75c]

5.2.4 Nonfunctional Binding of Vanadate and Vanadyl to Proteins

The main proteins present in blood plasma are albumin (Alb, $M \approx 70$ kDa, $c \approx 600 \mu\text{M}$) and transferrin (Tf, $M \approx 80$ kDa, $c \approx 35 \mu\text{M}$). Apo-Tf is a bilobal single-chain protein and efficient transporter for Fe³⁺ and other tri- and divalent cations, including V³⁺ and VO²⁺. Anions, e.g. [H₂VO₄]⁻, are also taken up, but possibly ‘reconstructed’ and bound in the form of VO₂⁺. A maximum of two metal ions can be coordinated, one in each binding site

**Figure 5.21**

Biologically relevant vanadate esters (**33–35**) and a mixed vanadate–phosphate anhydride (**36**); Ad = adenosyl. For **33**, the oxidation of activated glucose to gluconic acid (the lactone form is shown), as catalysed by glucose-6-phosphate dehydrogenase (Glu-6PDH), is also depicted.

at the C- and N-terminal lobe, requiring a synergistic anion, usually hydrogencarbonate. Tf loading with iron commonly amounts to one-third of its overall capacity, leaving a binding reservoir for other metal ions of ca 50 μM. The ligands available at the metal binding sites are two tyrosines, one aspartate and one histidine. Serum albumin is a globular protein with various physiological roles: it serves as a transporter for fatty acids, for Zn²⁺ and Cu²⁺, and helps in maintaining the osmotic pressure. Vanadate is only weakly bound by albumin; in contrast, vanadyl binds comparatively strongly to the N-terminus through histidine in the position 3 ('strong site'). In addition, there are up to 20 weak, nonspecific interactions with carboxylate side-chains of surface amino acids.^[76]

As has been noted earlier, the strong binding of vanadyl to transferrin can lead to extensive ligand stripping as oxovanadium complexes enter the bloodstream. The presence of both reducing agents (ascorbate, cysteine, catecholamines) and oxygen can interconvert oxovanadium(IV) and vanadate(V). The half-lives for redox interconversion of Alb- and Tf-bound V^{IV} and V^V at pH 5 are 5–30 min.^[77] The extent to which vanadyl is distributed between Alb and Tf does not seem to have been settled. Based on earlier EPR investigations, the Alb-VO²⁺:Tf-VO²⁺ ratio is 2.3 [*c*(V) = 25 μM] and 6.4 [*c*(V) = 50 μM].^[77] More recent investigations appear to indicate that, in the presence of Tf, vanadyl does not interact with albumin to an appreciable extent.^[34,78] The log *K* value (*K* = binding constant) for VO²⁺ binding to the two proteins is 10.0(1) for the complex formed with albumin, and log *K*₁ = 14.3(6) for the complexation of the first VO²⁺ to transferrin. The log *K*₂ for the second vanadyl is 13.7(5), and hence does not significantly deviate from log *K*₁.^[78] The corresponding log *K* for Fe³⁺ is ca 20, i.e. iron(III) is sufficiently more effectively coordinated than vanadyl.

The nature of the binding sites for vanadyl and vanadate in Tf has been inferred from EPR and ⁵¹V NMR spectroscopy, respectively. Figure 5.22 provides selected spectral

results. Both spectroscopic methods indicate that there are slight – although distinct – differences between the N- and C-terminal binding sites. Due to the slow tumbling of the VO^{2+} -Tf molecules, the EPR spectra are anisotropic (axial) already at room temperature. Clear differentiation of the sites is visible: at liquid nitrogen temperature, a square pyramidal conformer **A** (corresponding to the C-terminal site) and two conformers **B** (corresponding to the N-terminal site) are observed, the latter with distortions from axial symmetry. The room temperature EPR parameters for the two isomers are as follows:

$$\text{Signal A (C-terminal site)} : A_{\parallel} = 166.8 \times 10^{-4}, A_{\perp} = 60.1 \times 10^{-4} \text{ cm}^{-1},$$

$$g_{\parallel} = 1.940, g_{\perp} = 1.947$$

$$\text{Signal B (N-terminal site)} : A_{\parallel} = 170 \times 10^{-4}, A_{\perp} = 56 \times 10^{-4} \text{ cm}^{-1},$$

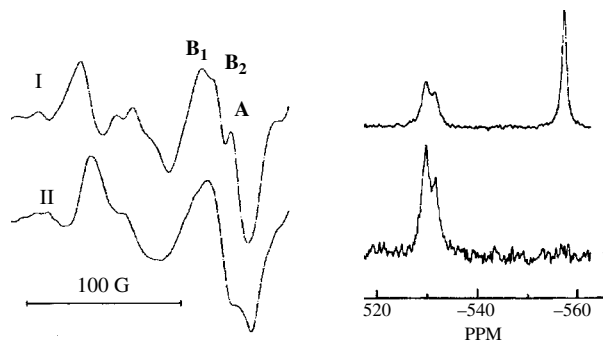
$$g_{\parallel} = 1.934, g_{\perp} = 1.969$$

Based on the size of the parallel hyperfine coupling constant and the additivity relationship (Section 3.3.2), only one tyrosinate binds in the equatorial plane (the second one thus is in the axial position), together with a histidine and aspartate. The fourth equatorial ligand is either the synergistic carbonate/hydrogencarbonate, giving rise to the overall arrangement shown in Figure 5.22 (bottom centre), or an – exchangeable – aqua/hydroxo ligand. The possible presence of water or hydroxide has been inferred, based on ESEEM studies, from the observation of a proton with dipolar coupling to the V^{IV} centre, at a distance of ca 2.6 Å.^[79] Alternatively, a proton might be delivered, e.g. to carbonate or aspartate, via the hydrogen bonding network.

Slow tumbling of Tf also has consequences for the ^{51}V NMR of its vanadate adduct: Restricted translational and rotational motion places the system outside the extreme narrowing (but within the motional narrowing) limit, allowing for the observation of the central quadrupole transition ($m_I = +\frac{1}{2} \rightarrow -\frac{1}{2}$) only, the chemical shift and linewidth of which become a function of the strength of the applied field, as noted for human apotransferrin loaded with vanadate in Section 3.1.4. The spectra in Figure 5.22 (right) clearly indicate that the binding sites in the C and N lobes are distinct. The assignment of the signal at lower field, $\delta = -529.5$ ppm, to the C-terminal site is based on exchange experiments carried out with Fe^{3+} -Tf. The high-field signal corresponding to the N-terminal site appears at -531.5 ppm.^[80] The chemical shift is typical for vanadium in a coordination sphere dominated by oxo functions.

UV difference spectroscopy and EPR spectroscopy have been employed to investigate the binding of vanadium in its oxidation states +III, +IV and +V to lactoferrin, a close analogue of Tf. The two proteins have identical metal binding sites. Lactoferrin is present in milk and many mucosal secretions such as tears and saliva, acting (due to its high affinity to ferric iron) as a mild antimicrobial agent. It binds V^{3+} in a metal:protein 2:1 stoichiometry. Oxygen readily oxidises V^{3+} to VO^{2+} and further to VO_2^+ .^[81] Based on the structurally characterised Fe^{3+} and Cu^{2+} forms of lactoferrin, the structures shown in Figure 5.22 (bottom) have been proposed for the binding sites of vanadium in its three oxidation states, containing bidentate carbonate (V^{III}), monodentate carbonate (V^{IV}) and no carbonate (V^{V}) in the coordination sphere of vanadium.

The binding of vanadate and vanadyl to the two main serum proteins (Alb and Tf) as studied by EPR and NMR spectroscopy exemplifies the analytical value of these spectroscopic probes when it comes to an evaluation of the coordination environment of a metal ion at a specific protein site, and the strength of the interaction. A large number of

**Figure 5.22**

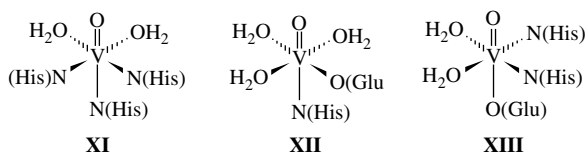
Top left: cut-out of the EPR spectra of VO^{2+} -transferrin at 77 K (I) and room temperature (II), showing the three components A, B₁ and B₂ of the perpendicular $-3/2$ line, corresponding to the C-site (A) and the N-site (B) of Tf, respectively. Reproduced from T. Kiss *et al.*, *Eur.J. Inorg. Chem.* 3607–3613. Copyright (2006), with permission from Wiley-VCH Verlag GmbH & Co. KGaA Top right: 131.5 MHz ⁵¹V NMR spectrum of vanadate:Tf solutions (pH 7.4) at ratios of 2.3:1 (a) and 1:1 (b). The two overlapping low-field signal correspond to the C-terminal site (-529.5 ppm) and N-terminal site (-531.5 ppm); the signal at high field is hydrogenvanadate. Reproduced from A. Butler and H. Eckert, *J. Am. Chem. Soc.* 111, 2802–2809. Copyright (1989), with permission from the American Chemical Society. Bottom row: computer-assisted representations of the coordination environment of vanadium in lactoferrin for V³⁺, VO²⁺ and VO₂⁺ (from left to right) (redrawn from ref. 81).

comparable studies with proteins not (directly) involved in the biochemical functions of vanadium are available, detailed treatment of which would be beyond the scope of this book. A few selected and illustrative examples will, however, be addressed briefly below.

The analogy between vanadate and phosphate initiated a couple of studies designed to find out the extent to which this analogy is reflected in competitive vanadate/phosphate binding to the protein. The phosphatases (Section 5.2.1.2) are examples of proteins where vanadate indeed occupies the site otherwise reserved for phosphate. Copper zinc superoxide dismutase (CuZn-SOD) exemplifies a situation where vanadate is not bound to the site preferentially chosen by phosphate. CuZn-SOD contains a catalytic copper and a structural zinc centre, linked through a bridging histidine(1–). The Cu²⁺ ion is at the bottom of a solvent channel allowing access of the substrate O₂[–] and, should the situation arise, other anions. To facilitate anion transport, two positively charged lysines and the guanidinium functionality of arginine align the funnel-like opening of the channel. The latter, Arg141, is the one that binds phosphate. The binding of vanadate to CuZn-SOD is indicated by signal broadening rather than by a shift of the ⁵¹V NMR signals,^[82] indicative

of noncovalent interaction and thus binding through electrostatic and/or hydrogen bonding interplay. Signal broadening is particularly distinct for cyclic tetravanadate $[V_4O_{12}]^{4-}$, V_4 , which forms two specific complexes of composition $V_4 \cdot SOD$ and $(V_4)_2SOD$, with affinity constants of $2 \times 10^7 \text{ M}^{-1}$ for the first and $5 \times 10^6 \text{ M}^{-1}$ for the second V_4 . In contrast to phosphate, and possibly as a consequence of its larger size and charge, V_4 binds to the two lysines (Lys120 and Lys134) in the funnel. The binding of oligovanadates such as tetravanadate, of course, precludes the overall vanadate concentration being sufficiently high ($>10 \mu\text{M}$), which is usually not the case under physiological conditions. If eventually the concentration of vanadate is high enough, even decavanadate can tightly interact with a protein, as has been demonstrated for the binding of decavanadate to the ‘back door’ of actin-stimulated myosine ATPase at concentrations $>0.9 \text{ mM}$.^[83] Myosin is a major protein of muscles, involved in the process of muscle contraction, coupled with activation by another muscle protein, actin, and powered by the hydrolysis of ATP. Actin and ATP bind to the so-called myosin subfragment 1, and this head segment is also the target for mono-, di- and tetravanadate, again documented by signal broadening as myosin or its subfragment 1 are added to solutions containing the various vanadates.^[84] For the vanadate-induced photo-fragmentation of myosin see the following section.

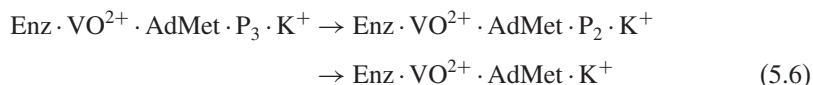
The value of VO^{2+} as a physico-chemical marker of metal binding sites in proteins can hardly be overestimated. EPR patterns of the vanadyl ions have been employed since the early 1970s by Chasteen *et al.* to extract specific information on metal-binding site(s) of peptides and proteins such as insulin and carboxypeptidase-A.^[85] In the hexameric ‘resting’ form of insulin, the subunits are tied together by Zn^{2+} ions in an octahedral environment with three facially arranged histidines and water molecules. In insulin treated with vanadyl sulfate, the VO^{2+} ions go into two binding sites, distinguishable by their EPR patterns. One of the binding sites corresponds to that of zinc, i.e. vanadium is bound to three imidazolyl moieties of histidine residues in a facial configuration and hence with two His in equatorial positions (structure **XI** in Scheme 5.5). The two remaining equatorial positions are occupied by water. In the second binding mode, the carboxylate of glutamate-24 is in an equatorial position (cf. **XII**). In bovine carboxypeptidase-A, where the active centre contains Zn^{2+} coordinated to two His and one Glu plus a water (resting state) or OH (active state), reconstitution of the apoenzyme with VO^{2+} results in the incorporation of the vanadyl ion into the active site, restoring its peptidase and esterase activity. The structural arrangement, again proposed on the basis of EPR characteristics, is such that the equatorial plane is occupied by two His and two water ligands (**XIII** in Scheme 5.5).



Scheme 5.5

One of the major methylating agents in biological systems is *S*-adenosylmethionine. Its biosynthesis, from methionine and ATP, is catalysed by *S*-adenosyl synthase. In the first

step, adenosyl (Ad) is transferred to the sulfur of methionine, and an adenosylmethionine-triphosphate adduct, AdMet-P₃, forms. In a second step, triphosphate is hydrolysed, and next diphosphate is released. This enzyme is stimulated by K⁺ and further requires two magnesium (or other divalent) ions for catalytic activity. To one of the sites, Mg²⁺ binds substrate independently, and this is the site where VO²⁺ can also bind. The overall reaction sequence for the vanadyl variant can be represented by Equation (5.6).



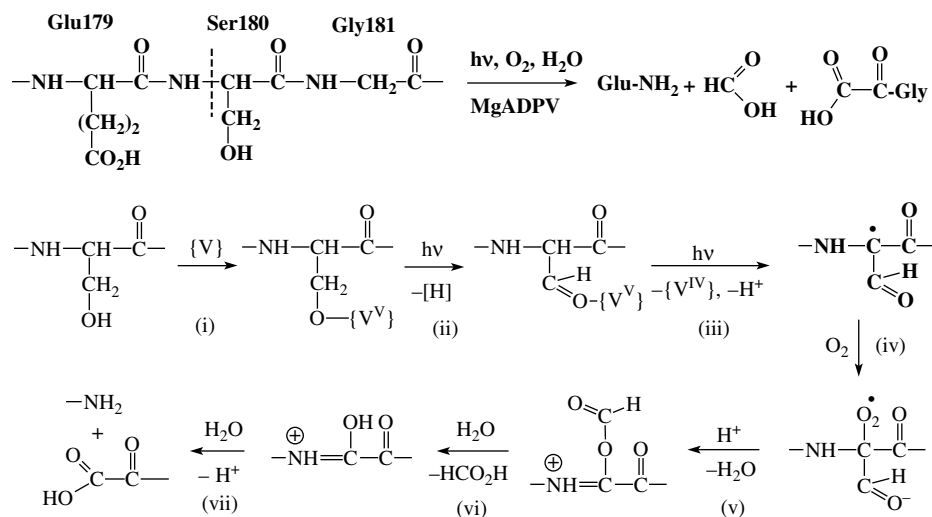
ESEEM spectroscopy (Section 3.4) provides spin echos due to coupling of the vanadyl electron to adjacent ¹⁴N nuclei with superhyperfine coupling constants A^N = 4.8 MHz in the first and second species in Equation (5.6), and 5.3 MHz in the final product (formed upon release of diphosphate), which can be associated to coordinated lysine-NH₂ and the amine nitrogen of the methionine.^[87] A coupling constant A^N = 5.7 MHz, associated with histidine coordination, was also found in ESEEM investigations of vanadyl coordinated into the high-affinity metal-binding site of D-xylose isomerase.^[88] Xylose isomerase catalyses the isomerisation of α-D-xylose to α-D-xylulose and of α-D-glucose to α-D-fructose. It depends on Mg²⁺, which can occupy a high- and a low-affinity binding site per protein subunit. The low-affinity binding site is accessible for VO²⁺ after blocking the high-affinity site with Cd²⁺. ENDOR reveals that, at the low-affinity site, the divalent metal ion is exclusively in an oxygen-functional coordination sphere.

5.2.5 Modification of Proteins by Vanadate

⁵¹V NMR spectroscopy has revealed that the subfragment 1 of the muscle protein myosin interacts with the various vanadates present at sufficiently high concentrations, preferentially so with tetravanadate^[84a] and decavanadate^[84b] (see the previous section). If the myosin subfragment 1 is irradiated with UV light in the presence of vanadates, cleavage occurs and vanadate is reduced to vanadyl, which is not active as an energy transmitter in photo-cleavage.^[89]

The overall reaction and the various reaction steps^[90] are depicted in Scheme 5.6. Photo-cleavage occurs at serine-180 (dashed line in the top part of Scheme 5.6), which is flanked by glutamate-179 and glycine-181. The intricate species is MgADPV, compound **36** in Figure 5.21, which may act as such or deliver vanadate to the active site. The products of cleavage, which takes place in two successive irradiation steps consuming oxygen, are a glutamine-terminated fragment of molecular mass 21 kDa and an oxalylglycyl-terminated fragment of 74 kDa. The serine-Cβ ends up as formic acid. The mode of interaction of vanadate with the serine-180 has not been revealed. Three options can be imagined: (i) vanadate forms an ester HVO₃OSer⁻; (ii) vanadate coordinates to serinate, forming an inner-sphere pentacoordinate complex similar to the inhibitory complex with PTP-1B (**VIII** in Figure 5.19); (iii) vanadate (free or in the form of MgADPV) forms an outer-sphere complex through hydrogen bonding. The last option is particularly attractive in the light of findings for vanadium complexes containing the serine moiety not directly bonded to vanadium but in hydrogen bonding contact with other groups such as interstitial water,

viz. $\{V\}SerOH \cdots OH_2 \cdots O_2H\{V\}$.^[91] In any case, the role of vanadate as an oxidation catalyst is in accord with its common use in oxidation processes not related to biochemical events. The several reaction steps for the cleavage (bottom row in Scheme 5.6) are: (i) activation of serine by MgADPV or vanadate, $\{V^V\}$; (ii) UV-induced oxidation of serine to glycylaldehyde, catalysed by $\{V^V\}$; (iii) second irradiation, resulting in the formation of a free radical on $C\alpha$ by electron transfer to vanadium and formation of $\{V^{IV}\}$; (iv) formation of a superoxo intermediate by attack of O_2 on $C\alpha$; (v) Criegee rearrangement, i.e. acid-assisted migration of the formyl group to the superoxo oxygen directly bonded to carbon, accompanied by release of water; (vi) hydrolytic release of formic acid; and (vii) hydrolytic cleavage of the oxalyl intermediate at the iminium site.



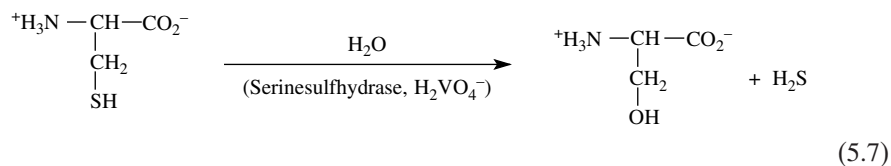
Scheme 5.6

Vanadate-induced photo-oxidation of serine and subsequent cleavage of the protein were also observed for ribulose-1,5-diphosphate carboxylase/oxygenase from spinach leaves.²⁰ Activity could be restored by treatment with sodium boronate, which reduces formylglycine back to serine.^[92a] Similarly, vanadate-induced UV oxidation of threonine (Thr353, at the phosphorylation site) in the sarcoplasmatic reticulum (SR) Ca^{2+} -ATPase can be restored by reduction with $Na[BH_4]$. For monovanadate to become catalytically active it is essential that Mg^{2+} and ADP bind to the phosphorylation site of the enzyme in its Ca^{2+} -receptive conformation, suggesting the formation of an active MgADPV as proposed for the myosin fragmentation. In contrast, decavanadate catalyses the photo-oxidation of a serine (Ser186) residue in the SR ATPase in the absence of ADP.^[92b]

Another group of enzymes modified by vanadate are the sulfhydrases (such as serine sulfhydrase) and sulfatases (e.g. aryl sulfatases). Serine sulfhydrase catalyses the conversion of cysteine to serine with liberation of H_2S [Equation (5.7)]. Vanadate at a

²⁰ Carboxylation of ribulose-1,5-diphosphate is the initiating step in carbon fixation.

concentration of $10\text{ }\mu\text{M}$ stimulates the activity, whereas concentrations higher than $15\text{ }\mu\text{M}$ have an inhibitory effect.^[93]



Aryl sulfatases catalyse the hydrolysis of sulfate ester bonds in, e.g., sugar sulfates, and also in synthetic aryl sulfonates. Aryl sulfatase B (AS-B) in particular attacks *N*-acetylgalactosamine-6-sulfate in chondroitin sulfates and thus initiates the degradation of mucopolysaccharides. A deficiency of this enzyme leads to specific forms of lysosomal²¹ storage diseases. Nascent sulfatases contain an active site cysteine. For the action of sulfatases, enzymatic transformation is required shortly after translocation into the endoplasmatic reticulum. This transformation comes about by enzymatic oxidation of cysteine to formylglycine, followed by hydration to formylglycinehydrate [Equation (5.8a)]. Sulfatase mutants in which an active site cysteine has been replaced by a serine residue are expressed at levels comparable to those of the native enzyme. This specific mutant, AS-B(Cys 91Ser), can be converted into a catalytically active AS-B by irradiation with UV light in the presence of vanadate.^[94] The activation step is the oxidation of serine to formylglycine; the electron acceptor is vanadate [Equation (5.8b)], which is known to have a high affinity to the sulfate binding site of the active formylglycine variant of AS-B^[95] (Figure 5.23). The mechanism of sulfate ester hydrolysis (Figure 5.23) involves a nucleophilic attack of an OH group of the formylglycine to

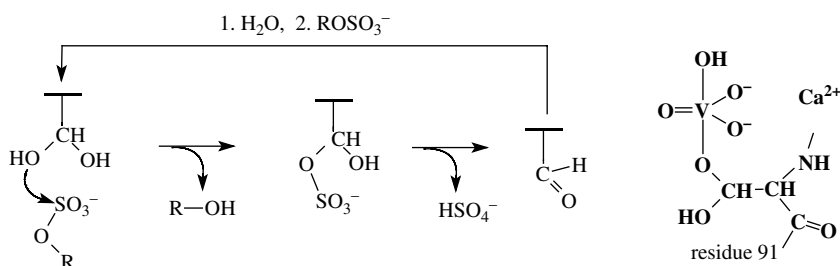
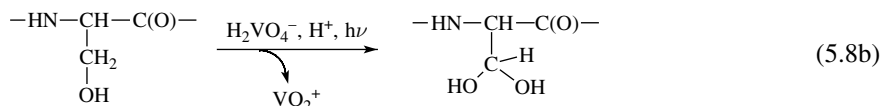
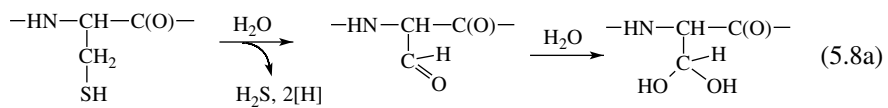


Figure 5.23

Proposed mechanism for the catalytic hydrolysis of the sulfate ester bond by the active form of aryl sulfatase-B (AS-B), and the structure (right) of the active centre of the vanadate AS-B complex, otherwise containing the substrate sulfate. The active centre also accommodates a seven-coordinated calcium ion, ligated to three aspartates (one of which is in the η^2 -mode), an asparagine and two oxo anions of the sulfate/vanadate. Structure modified from that provided in ref. 95.

²¹ Lysosomes are cytoplasmatic organelles responsible for the breakdown, at pH values of 4.5–5.5, of macromolecules such as polysaccharides.

sulfur, followed by elimination of the alcohol, hydrolysis of the resulting sulfonate to sulfuric acid, and re-hydration of the formyl group.



References

- [1] N. Houstis, E. D. Rosen and E. S. Lander, *Nature* **2006**, *440*, 944–948.
- [2] S. A. Ross, E. A. Gulve and M. Wang, *Chem. Rev.* **2004**, *104*, 1255–1282.
- [3] B. Lyonnet, X. Martz and E. Martin, *La Presse Medicale* **1899**, *32*, 191–192.
- [4] A. B. Goldfine, D. C. Simonson, F. Folli, M.-E. Patti and R. Kahn, *J. Clin. Endocrinol. Metab.* **1995**, *80*, 3311–3320.
- [5] E. L. Tolman, E. Barris, M. Burns, A. Pansini and R. Partridge, *Life Sci.* **1979**, *25*, 1159–1164.
- [6] Y. Shechter and S. J. D. Karlish, *Nature* **1980**, *284*, 556–558.
- [7] (a) C. E. Heyliger, A. G. Tahiliani and J. M. McNeill, *Science* **1985**, *237*, 1474–1477; (b) J. Meyerovitch, Z. Farfel, J. Sack and Y. Shechter, *J. Biol. Chem.* **1987**, *262*, 6658–6662.
- [8] S. M. Brichard, C. J. Baily and J. C. Henquin, *Diabetes* **1990**, *39*, 1326–1332.
- [9] S. Ramanadham, J. J. Mongold, R. W. Brownsey, G. H. Cros and J. H. McNeill, *Am. J. Physiol. Heart Circ. Physiol.* **1989**, *257*, 904–911.
- [10] (a) S. Kadota, I. G. Fantus, G. Deragon, H. J. Guyda, B. Hersh and B. I. Posner, *Biochem. Biophys. Res. Commun.* **1987**, *147*, 259–266; (b) I. G. Fantus, S. Kadota, G. Deragon, B. Foster and B. I. Posner, *Biochemistry* **1989**, *28*, 8864–8871.
- [11] B. Leighton, G. J. S. Cooper, C. DaCosta and E. A. Foot, *Biochem. J.* **1991**, *276*, 289–292.
- [12] B. I. Posner, R. Faure, J. W. Burgess, A. P. Bevan, D. Lachance, G. Zhang-Sun, I. G. Fantus, J. B. Ng, D. A. Hall, B. Soo Lum and A. Shaver, *J. Biol. Chem.* **1994**, *269*, 4596–4604.
- [13] (a) J. H. McNeill, V. G. Yuen, S. Dai and C. Orvig, *Mol. Cell. Biochem.* **1995**, *153*, 175–180; (b) K. H. Thompson, B. D. Liboiron, Y. Sun, K. D. D. Bellman, V. Karunaratne, G. Rawji, J. Wheeler, K. Sutton, S. Bhanot, S. B. C. Cassidy, J. H. McNeill, V. G. Yuen and C. Orvig, *J. Biol. Inorg. Chem.* **2003**, *8*, 66–74.
- [14] K. H. Thompson and C. Orvig, *J. Inorg. Biochem.* **2006**, *100*, 1925–1935.
- [15] (a) H. Yasui, Y. Adachi, A. Katoh and H. Sakurai, *J. Biol. Inorg. Chem.* **2007**, *12*, 843–853; (b) H. Sakurai, K. Fujii, H. Watanabe and H. Tamura, *Biochem. Biophys. Res. Commun.* **1995**, *214*, 1095–1101.
- [16] G. Elberg, J. Li and Y. Shechter, in: *Vanadium in the Environment, Part 2: Health Effects* (J. O. Nriagu, Ed.), John Wiley & Sons, Inc., New York, **1998**, Ch. 14.
- [17] (a) K. H. Thompson, J. H. McNeill and C. Orvig, *Chem. Rev.* **1999**, *99*, 2561–2571; (b) K. H. Thompson and C. Orvig, *Dalton Trans.* **2000**, 2885–2892.
- [18] L. Marzban and J. H. McNeill, *J. Trace Elem. Exp. Med.* **2003**, *16*, 253–267.
- [19] H. Sakurai, A. Katoh and Y. Yoshikawa, *Bull. Chem. Soc. Jpn.* **2006**, *79*, 1645–1646.
- [20] M. Melchior, K. H. Thompson, J. M. Jong, S. J. Rettig, E. Shuter, V. G. Yuen, Y. Zhou, J. H. McNeill and C. Orvig, *Inorg. Chem.* **1999**, *38*, 2288–2293.

- [21] D. C. Crans, M. Mahroof-Tahir, M. D. Johnson, P. C. Wilkins, L. Yang, K. Robbins, A. Johnson, J. A. Alfano, M. E. Godzala, III, L. T. Austin and G. R. Willsky, *Inorg. Chim. Acta* **2003**, *356*, 365–378.
- [22] (a) J. Gätjens, B. Meier, T. Kiss, E. M. Nagy, P. Buglyó, H. Sakurai, K. Kawabe and D. Rehder, *Chem. Eur. J.* **2003**, *9*, 4924–4935; (b) J. Gätjens, B. Meier, Y. Adachi, H. Sakurai and D. Rehder, *Eur. J. Inorg. Chem.* **2006**, 3575–3585.
- [23] K. Kawabe, M. Tadokoro, Y. Kojima, Y. Fujisawa and H. Sakurai, *Chem. Lett.* **1998**, 9–10.
- [24] L. C. Y. Woo, V. G. Yuen, K. H. Thompson, J. H. McNeill and C. Orvig, *J. Inorg. Biochem.* **1999**, *76*, 251–257.
- [25] (a) H. Sakurai, H. Sano, T. Takino and H. Yasui, *Chem. Lett.* **1999**, 913–914; (b) H. Watanabe, M. Nakai, K. Komazawa and H. Sakurai, *J. Med. Chem.* **1994**, *37*, 876–877; (c) H. Sakurai, K. Tsuchiya, M. Nakatsuka, J. Kawada, S. Ishikawa, H. Yoshida and M. Komatsu, *J. Clin. Biochem. Nutr.* **1990**, *8*, 193–200.
- [26] H. Ou, L. Yan, D. Mustafi, M. W. Makinen and M. J. Brady, *J. Biol. Inorg. Chem.* **2005**, *10*, 874–886.
- [27] D. Rehder, J. Costa Pessoa, C. F. G. C. Geraldes, M. M. C. A. Castro, T. Kabanos, T. Kiss, B. Meier, G. Micera, L. Pettersson, M. Ranger, A. Salifoglou, I. Turel and D. Wang, *J. Biol. Inorg. Chem.* **2001**, *7*, 384–396.
- [28] (a) Y. Shechter, A. Shisheva, R. Lazar, J. Libman and A. Shanzer, *Biochemistry* **1992**, *31*, 2063–2068; (b) D. A. Barrio, P. A. M. Williams, A. M. Cortizo and S. B. Etcheverry, *J. Biol. Inorg. Chem.* **2003**, *8*, 459–468.
- [29] S. S. Amin, K. Cryer, B. Zhang, S. K. Dutta, S. S. Eaton, O. P. Anderson, S. M. Miller, B. A. Reul, S. M. Brichard and D. C. Crans, *Inorg. Chem.* **2000**, *39*, 406–416.
- [30] (a) G. R. Hanson, Y. Sun and C. Orvig, *Inorg. Chem.* **1996**, *35*, 6507–6512; (b) Y. San, B. R. James, S. J. Rettig and C. Orvig, *Inorg. Chem.* **1996**, *35*, 1667–1673.
- [31] K. Elvingson, A. G. Baró and L. Pettersson, *Inorg. Chem.* **1996**, *35*, 3388–3393.
- [32] H. Yasui, A. Tamura, T. Takino and H. Sakurai, *J. Inorg. Biochem.* **2002**, *91*, 327–338.
- [33] I. A. Setyawati, K. H. Thompson, V. G. Yuen, Y. Sun, M. Battel, D. M. Lyster, C. Vo, T. J. Ruth, S. Zeisler, J. H. McNeill and C. Orvig, *J. Appl. Physiol.* **1998**, *84*, 569–575.
- [34] B. D. Liboiron, K. H. Thompson, G. R. Hanson, E. Lam, N. Aebischer and C. Orvig, *J. Am. Chem. Soc.* **2005**, *127*, 5104–5115.
- [35] S. A. Dikanov, B. D. Liboiron and C. Orvig, *J. Am. Chem. Soc.* **2002**, *124*, 2969–2978.
- [36] (a) T. C. Delgado, A. I. Tomaz, I. Corriera, J. Costa Pessoa, J. G. Jones, C. F. G. C. Geraldes and M. M. C. A. Castro, *J. Inorg. Biochem.* **2005**, *99*, 2328; (b) P. Buglyó, T. Kiss, E. Kiss, D. Sanna, E. Garribba and G. Micera, *Dalton Trans.* **2002**, 2275–2282; (c) T. Kiss, T. Jakusch, S. Bouhsina, H. Sakurai and E. A. Enyedy, *Eur. J. Inorg. Chem.* **2006**, 3607–3613; (d) G. R. Willsky, A. B. Goldfine, P. J. Kostyniak, J. H. McNeill, L. Q. Yang, H. R. Khan and D. C. Crans, *J. Inorg. Biochem.* **2001**, *85*, 33–42.
- [37] (a) A. Dörnyei, S. Marcão, J. Costa Pessoa, T. Jakusch and T. Kiss, *Eur. J. Inorg. Chem.* **2006**, 3614–3621; (b) T. Kiss, E. Kiss, G. Micera and D. Sanna, *Inorg. Chim. Acta* **1998**, *283*, 202–210.
- [38] (a) A. R. Saltiel and C. R. Kahn, *Nature* **2001**, *44*, 799–860; (b) P. Wipf and R. J. Halter, *Org. Biomol. Chem.* **2005**, *3*, 2053–2061.
- [39] R. K. Narla, C.-L. Chen, Y. Dong and F. M. Uckun, *Clin. Cancer Res.* **2001**, *7*, 2124–2133; see also O. J. D'Cruz and F. M. Uckun, *Exp. Opin. Investig. Drugs* **2002**, *11*, 1829.
- [40] P. Köpf-Maier and H. Köpf, *Drugs Future* **1986**, *11*, 297–319.
- [41] K. Iwai, T. Ido, R. Iwata, M. Kawamura and S. Rimura, *Nucl. Med. Biol.* **1989**, *16*, 783–789.
- [42] (a) M. Jelicić-Stankov, S. Uskoković-Marković, I. Holclajtner-Antunović, M. Todorović and P. Djurdjević, *Biochemistry* **2007**, *21*, 8–16; (b) A. M. Evangelou, *Crit. Rev. Oncol./Hematol.* **2002**, *42*, 249–265.
- [43] (a) T. Chakraborty, A. H. M. V. Swamy, A. Chatterjee, B. Rana, A. Shyamsundar and M. Chatterjee, *J. Cell. Biochem.* **2007**, *101*, 244–258; (b) T. Chakraborty, A. Chatterjee, M. G. Saralaya and M. Chatterjee, *J. Biol. Inorg. Chem.* **2006**, *11*, 855–866.

- [44] (a) E. E. Hamilton, P. E. Fanwick and J. J. Wilker, *J. Am. Chem. Soc.* **2006**, *128*, 3388–3395; (b) E. E. Hamilton and J. J. Wilker, *Angew. Chem. Int. Ed.* **2004**, *43*, 3290–3292.
- [45] J. Aubrecht, R. K. Narla, P. Ghosh, J. Stanek and F. M. Uckun, *Toxicol. Appl. Pharmacol.* **1999**, *154*, 228–235.
- [46] (a) J. H. Toney, C. P. Brock and T. J. Marks, *J. Am. Chem. Soc.* **1986**, *108*, 7263–7274; (b) J. H. Hwang, R. K. Larson and M. M. Abu-Omar, *Inorg. Chem.* **2003**, *42*, 7967–7977.
- [47] (a) M. R. Maurya, A. Kumar, A. R. Bhat, C. Bader and D. Rehder, *Inorg. Chem.* **2006**, *45*, 1260–1269; (b) M. R. Maurya, S. Agarwala, M. Abid, A. Azam, C. Bader, M. Ebel and D. Rehder, *Dalton Trans.* **2006**, 937–947.
- [48] H. Schuster and P. L. Chiodini, *Curr. Opin. Infect. Dis.* **2001**, *14*, 587–591.
- [49] (a) P. Ghosh, O. J. D'Cruz, D. D. DuMez, J. Peitersen and F. M. Uckun, *J. Inorg. Biochem.* **1999**, *75*, 135–143; (b) O. J. D'Cruz, B. Waurzyniak and F. M. Uckun, *Toxicology* **2002**, *170*, 31–43.
- [50] O. J. D'Cruz, Y. Dong and F. M. Uckun, *Biochem. Biophys. Res. Commun.* **2003**, *302*, 253–264.
- [51] S. Y. Wong, R. W.-Y. Sun, N. P.-Y. Chung, C.-L. Lin and C.-M. Che, *Chem. Commun.* **2005**, 3544–3546.
- [52] S. Shigeta, S. Mon, T. Yamase, N. Yamamoto and N. Yamamoto, *Biomed. Pharmacother.* **2006**, *60*, 211–219.
- [53] Yu. M. Bala and L. M. Kopylova, *Problemy Tuberkuleza* **1971**, *49*, 63–67.
- [54] (a) S. David, V. Barros, C. Cruz and R. Delgado, *FEMS Microbiol. Lett.* **2005**, *251*, 119–124; (b) A. Maiti and S. Ghosh, *J. Inorg. Biochem.* **1989**, *36*, 131–139.
- [55] A. Müller, K. Schneider, J. Erfkamp, V. Wittneben and E. Diemann, *Naturwissenschaften* **1988**, *75*, 625–627.
- [56] L. C. Cantley, Jr., L. Josephson, R. Warner, M. Yanagisawa, C. Lechene and G. Guidotti, *J. Biol. Chem.* **1977**, *252*, 7421–7423.
- [57] (a) M. J. Gresser and A. S. Tracey, in: *Vanadium in Biological Systems* (N. D. Chasteen, Ed.), Kluwer, Dordrecht, **1990**, Ch. IV; (b) G. L. Mendz, *Arch. Biochem. Biophys.* **1991**, *291*, 201–211.
- [58] W. Plass, *Angew. Chem. Int. Ed.* **1999**, *38*, 909–912.
- [59] (a) D. R. Davies and W. G. J. Hol, *FEBS Lett.* **2004**, *577*, 315–321; (b) B. D. Wladowski, L. A. Svensson, L. Sjolin, J. E. Ladner and G. L. Gilliland, *J. Am. Chem. Soc.* **1998**, *120*, 5488–5498.
- [60] (a) D. Kostrewa, H.-W. Choe, U. Heinemann and W. Saenger, *Biochemistry* **1989**, *28*, 7592–7600; (b) D. Rehder, H. Holst, R. Quaas, W. Hinrichs, U. Hahn and W. Saenger, *J. Inorg. Biochem.* **1989**, *37*, 141–150.
- [61] A. Hofmann, M. Grella, I. Botos, W. Filipowicz and A. Wlodawer, *J. Biol. Chem.* **2002**, *277*, 1419–1425.
- [62] D. R. Davies, H. Interthal, J. C. Champoux and W. G. J. Hol, *Chem. Biol.* **2003**, *10*, 139–147.
- [63] Y. Lindquist, G. Schneider and P. Viiko, *Eur. J. Biochem.* **1994**, *221*, 139–142.
- [64] (a) M. Zhang, M. Zhou, R. L. Van Etten and C. V. Stauffacher, *Biochemistry* **1997**, *36*, 15–23; (b) M. Salvi, A. Toninello, M. Schweizer, S. D. Friess and C. Richter, *Cell. Mol. Life Sci.* **2002**, *59*, 1190–1197.
- [65] (a) K. G. Peters, M. G. Davis, B. W. Howard, M. Pokross, V. Rastogi, C. Diven, K. D. Greis, E. Eby-Wilkens, M. Maier, A. Evdokimov, S. Soper and F. Genbauffe, *J. Inorg. Biochem.* **2003**, *96*, 321–330; (b) M. Z. Mehdi and A. K. Srivastava, *Arch. Biochem. Biophys.* **2005**, *440*, 158–164.
- [66] K. M. Holtz, B. Stec and R. Kantrowitz, *J. Biol. Chem.* **1999**, *274*, 8351–8354.
- [67] M. Toustrup-Jensen and B. Vilse, *J. Biol. Chem.* **2003**, *278*, 11402–11410.
- [68] C. R. Cornman, E. P. Zovinka and M. H. Meixner, *Inorg. Chem.* **1995**, *34*, 6099–5100.
- [69] R. Renirie, W. Hemrika and R. Wever, *J. Biol. Chem.* **2000**, *275*, 11650–11657.

- [70] N. Tanaka, V. Dumay, Q. Liao, A. L. Lange and R. Wever, *Eur. J. Biochem.* **2002**, *269*, 2162–2167.
- [71] F. van de Velde, I. W. C. E. Arends and R. A. Sheldon, *J. Inorg. Biochem.* **2000**, *80*, 81–89.
- [72] 58. (a) J. H. Bell and R. F. Pratt, *Inorg. Chem.* **2002**, *41*, 2747–2753; (b) J. H. Bell and R. F. Pratt, *Biochemistry* **2002**, *41*, 4329–4338.
- [73] (a) A. F. Nour-Eldeen, M. M. Craig and M. J. Gresser, *J. Biol. Chem.* **1985**, *260*, 6836–6842; (b) K. Elvingson, D. C. Crans and L. Pettersson, *J. Am. Chem. Soc.* **1997**, *119*, 7005–70012.
- [74] D. C. Crans, R. W. Marshman, R. Nielsen and I. Felty, *J. Org. Chem.* **1993**, *58*, 2244–2252.
- [75] (a) E. Alberico, D. Dewaele, T. Kiss and G. Micera, *J. Chem. Soc., Dalton Trans.* **1995**, 425–430; (b) K. A. Jelveh, R. Zhande and R. W. Brownsey, *J. Biol. Inorg. Chem.* **2006**, *11*, 379–388; (c) J. Petersen, K. Fisher, C. J. Mitchell and D. J. Lowe, *Biochemistry* **2002**, *41*, 13253–13263.
- [76] M. Purcell, J. F. Neault, H. Malonga, H. Arakawa and H. A. Tajmir-Riahi, *Can. J. Chem.* **2001**, *79*, 1415–1421.
- [77] N. D. Chasteen, J. K. Grady and C. E. Holloway, *Inorg. Chem.* **1986**, *25*, 2754–2760.
- [78] T. Kiss, T. Jakusch, S. Bouhsina, H. Sakurai and E. A. Enyedy, *Eur. J. Inorg. Chem.* **2006**, 3607–3613.
- [79] G. J. Gerfen, P. M. Hanna, N. D. Chasteen and D. J. Singel, *J. Am. Chem. Soc.* **1991**, *113*, 9513–9519.
- [80] A. Butler and H. Eckert, *J. Am. Chem. Soc.* **1989**, *111*, 2802–2809.
- [81] C. A. Smith, E. W. Ainscough and A. M. Brodie, *J. Chem. Soc., Dalton Trans.* **1995**, 1121–1126.
- [82] L. Wittenkeller, A. Abraha, R. Ramasamy, D. Mota de Freitas, L. A. Theisen and D. C. Crans, *J. Am. Chem. Soc.* **1991**, *113*, 7872–7881.
- [83] T. Tiago, P. Martel, C. Gutiérrez-Merino and M. Aureliano, *Biochim. Biophys. Acta* **2007**, *1774*, 474–480.
- [84] (a) I. Ringel, Y. M. Geyser and A. Muhlrad, *Biochemistry* **1990**, *29*, 9091–9096; (b) T. Tiago, M. Aureliano and J. J. G. Moura, *J. Inorg. Biochem.* **2004**, *98*, 1902–1910.
- [85] N. D. Chasteen, R. J. DeKoch, B. L. Rogers and M. W. Hanna, *J. Am. Chem. Soc.* **1973**, *95*, 1301–1309.
- [86] R. J. DeKoch, D. J. West, J. C. Cannon and N. D. Chasteen, *Biochemistry* **1974**, *13*, 4347–4354.
- [87] C. Zhang, G. D. Markham and R. LoBrutto, *Biochemistry* **1993**, *32*, 9866–9873.
- [88] S. A. Dikanov, A. M. Tyryshkin, J. Hüttermann, R. Bogumil and H. Witzel, *J. Am. Chem. Soc.* **1995**, *117*, 4976–4986.
- [89] C. R. Cremo, G. T. Long and J. C. Grammer, *Biochemistry* **1990**, *29*, 7982–7990.
- [90] J. C. Grammer, J. A. Loo, C. G. Edmonds, C. R. Cremo and R. G. Yount, *Biochemistry* **1996**, *35*, 15582–15592.
- [91] M. Ebel and D. Rehder, *Inorg. Chem.* **2006**, *45*, 7083–7090.
- [92] (a) S. N. Mogel and B. A. McFadden, *Biochemistry* **1989**, *28*, 5428–5431; S. Hua, G. Inesi, C. Toyoshima, *J. Biol. Chem.* **2000**, *275*, 30546–30550.
- [93] H.-U. Meisch and S. Kappesser, *Biochim. Biophys. Acta* **1987**, *925*, 234–237.
- [94] T. M. Christianson, C. M. Starr and T. C. Zankel, *Biochem. J.* **2004**, *382*, 581–587.
- [95] C. S. Bond, P. R. Clements, S. J. Ashby, C. A. Collyer, S. J. Harrop, J. J. Hopwood and J. M. Guss, *Structure* **1997**, *5*, 277–289.

This page intentionally left blank

6 Epilogue

When I started writing this book, I was not aware of the fact that the isotope ^{50}V , present as a minor component (0.25%) in the natural isotopic mix of vanadium, is radioactive – no panic intended: the half-life amounts to 17 billion years! The main decay route for ^{50}V is electron capture/positron emission (Chapter 1), and that reminds me of Isaac Asimov. Asimov (who died in 1992) was a biochemist and a particularly inspired science fiction writer, and the inventor of robots with positronic brains (not based on vanadium; this is too cheap a metal; rather, Asimov's robotic brains were made of an iridium–platinum alloy). Asimov also created the Three Laws of Robotics, established in 1941–42.^[1] The First Law reads, ‘A robot shall not injure a human being or through inaction allow a human being to come to harm’. This law was later prioritised by the zeroth law, where ‘human being’ is replaced by ‘humanity’. To some extent, this law might remind us of the obligations of (modern) chemistry. The community of human beings certainly expects not to be harmed by chemistry, and is more and more becoming aware of the fact that severe problems, such as medicinal, environmental, but also technical problems, can effectively be tackled by chemists: chemists therefore can contribute, by action, to prevent humanity from coming to harm. Certainly, this sounds rather preposterous, given the fact that there appears still to be a majority in our society who have not (yet) consciously accepted that chemistry can help out when it comes to hazardous situations. This should not discourage us, and the Third Law of Robotics actually is an encouragement: ‘A robot must protect its own existence as long as such protection does not conflict with the First Law’. And in fact, chemists should keep this Third Law well in mind: never let chemistry become corrupted by the intervention of those who try to abuse chemistry.

And what if it does not help to appeal to common sense? We may resort to alchemy or, to be more precise, to the fifth element, the *quinta essentia*, the quintessence. Why? Because here, vanadium again comes in. The *quinta essentia* goes back to Aristotle, who added to the four classical elements (Fire, Earth, Air and Water) a fifth element, the Aether. In the Middle Ages, this *quinta essentia*, or Philosophers's stone was supposed to aid the fabrication of gold from less noble materials. One of the alchemical symbols for the *quinta essentia* contains *V* (the Roman number 5, which is also, although of course unknowingly to the alchemists, the symbol for vanadium as introduced by its discoverer, Sefström, in 1831), fused with an *E* (for element)^[2] (Figure 6.1, top left). This symbol also became an integral part of the logo for the vanadium symposia which have accompanied vanadium chemists for the last decade. In this logo (Figure 6.1, right), the alchemist symbol is combined with an illustration of Vanadis, the goddess of beauty, symbolising all of the perceivable merits of vanadium chemistry.

**Figure 6.1**

Top left: the alchemists' symbol for the *quinta essentia*, the 'fifth essence' (fifth element), a *V* (Roman 5) fused with an *E* (*essentia*). This symbol is also used for emetic wine. Centre and bottom left: alchemical symbols for red wine (*vinum rubrum*) and medicated wine (*vinum medicatum*), respectively. Right: the logo of the 'Symposia on the Chemistry and Biological Chemistry of Vanadium', showing Vanadis on her combat car drawn by cats, and the alga *Ascophyllum nodosum* (from which the first vanadium-dependent enzyme, a bromoperoxidase, was isolated) winding around the *V* and thus making the scenario less menacing (design: Nadja Rehder).

The *V* is also integral constituent of the alchemical symbol for several varieties of wine (*vinum*), two of which are shown in Figure 6.1 (left). French and Californian red wines in fact can contain up to 90 µg of vanadium per litre,^[3] i.e. about twice the amount present in the Vanadium Water from the Fuji region (Chapter 1, Figure 1.5). Whether or not drinking red wine has any implications as to the creativity of vanadium chemists remains to be disclosed.

The reader is not supposed to take what I have delineated above too seriously. It is a play on words and symbols but, like any harmless play, should contain a kernel of truth. And this brings me to another, more realistic tale. In 1988, a new PhD student joined my group, and his task was to synthesise dinitrogenvanadium(–I) complexes as functional models for the newly discovered vanadium nitrogenase, in analogy with the respective molybdenum(0) complexes introduced by Hidai's group and systematically developed by Chatt and co-workers. We soon realised that vanadium(–I) is not molybdenum(0), and after a year of effort, the results were zero. So I told the student to quit this project and to make diazadiene complexes of vanadium instead. And because I was angry, I added that, if I had been him, I would have used lithium as a reducing agent (for VCl_3 as the starting material) instead of sodium or potassium. I didn't know why this thought came to me. In any case, it was not the outcome of systematic thinking, evidencing that 'the final thought, the real inspiration comes when thinking is under involuntary control' (another statement of Asimov). In any case, I forgot about it and was quite satisfied with my student being successful with the diazadiene story. When another year had elapsed, I found (it was my birthday), on the desk in my office, several ^{51}V and ^7Li NMR spectra (for a vanadium NMR see Figure 4.33), clearly indicating that the student had secretly pursued the dinitrogen issue and actually succeeded with lithium as reducing agent. The reason for this success immediately became obvious: Li^+ has a higher charge density than Na^+ and thus stabilises the dinitrogenvanadates through $\text{Li}\cdots\text{N}$ contacts. A structure (of a sodium complex, crystallised at dry-ice temperature) followed, nicely rounding off the results,

and to date, these vanadium complexes have remained the only completely characterised functional models of vanadium nitrogenase with end-on coordinated dinitrogen.

I am sometimes asked by young researchers interested in the biological aspects of vanadium chemistry what I would consider an innovative and promising topic to be dealt with in upcoming research. And I am still referring to what I commented on in the Conclusions of my review article in *Angewandte Chemie* in 1991: Vanadium is used as an essential element in vanadate-dependent haloperoxidases in a variety of comparatively simple organisms such as algae, fungi and lichens (it does not appear to have a cofactor function in more developed organisms). In addition, there is some evidence that amavadin, the molecular non-oxo vanadium(IV) compound present in the fly agaric and other *Amanita* mushrooms, is a relic of an evolutionary overcome oxygenase cofactor. It is also of interest in this context that peroxidases can rely on iron or vanadium (although in completely different coordination environments). All this hints towards a more widely distributed role of vanadium in the early stages of evolution. Of the two branches of prokaryotes, Archaea and Bacteria, bacteria such as *Azotobacter* and *Shewanella* have been shown to resort to vanadium, while archaea, which are phylogenetically somewhat younger than bacteria, appear not to have been studied in this context and may thus represent promising objects for new findings in the biochemistry of vanadium.^[4] I should remind you that vanadium is the second-to-most abundant transition metal in the oceans, i.e. its availability was guaranteed – if our primordial oceans actually have been the cradle of life. But even if the seeds of life had been carried to Earth from extra-terrestrial sources,^[5,6] the supply of the cosmic ubiquitous element vanadium would not have been a problem. And the versatility of vanadium, such as the ease of changing between the oxidation states +V and +IV, its ability to form oxo and non-oxo complexes in the oxidation state +IV and its amphoteric character, i.e. its readiness to be present in cationic and anionic form, can hardly have been neglected by Nature.

And this brings me back to Asimov, and his Second Law (of Robotics): ‘A robot must obey the orders given it by human beings [. . .].’ It is certainly not as simple as that when it comes to (vanadium) chemistry. A couple of days ago, I ran into Bart Hessen (University of Groningen) at a meeting in Boston, MA. We talked about the ups and the (more frequent) pitfalls of vanadium chemistry, or, as he put it, ‘I love vanadium because it is such a nasty element’. I am pretty convinced, certainly also by my own experiences, that, if you are sufficiently decided, even this element will ‘obey’.

References

- [1] I. Asimov, *The Rest of the Robots*, Panther Books, St Albans, **1968**.
- [2] G. W. Gessmann, *Die Geheimsymbole der Alchymie, Arzneikunde und Astrologie des Mittelalters*, Arkana-Verlag, Ulm, **1959**.
- [3] P. L. Teissedre, M. Krosniak, K. Portet, F. Gasc, A. L. Waterhouse, J. J. Serrano, J. C. Cabanis and G. Cros, *Food Addit. Contam.* **1998**, *15*, 585–591.
- [4] D. Rehder, *Org. Biomol. Chem.* **2008**, DOI: 10.1039/B717565P.
- [5] F. Hoyle, *The Black Cloud*, Signet, New York, **1959**.
- [6] K. W. Plaxco and M. Gross, *Astrobiology*, Johns Hopkins University Press, Baltimore, **2006**.

This page intentionally left blank

Index

- Actin 194
S-adenosylmethionine 194–5
Adenosine triphosphate (ATP) 172, 190, 194
Alanylhistidine 29, 30
Alanylserine 28, 29
Albumin 34, 169–70, 190, 191
Alcohols/alcoholates 25, 40, 41
Aldaric acids 33
Alkoxides 64, 65
Alkylation and alkylating agents 177–8
Amanita muscaria 100
Amanita spp. 37, 81, 100, 205
 X-ray studies 84
Amavadin 21, 37, 39, 81, 100–5, 205
 in *Amanita muscaria* 102–3
 in *Amanita* spp. 100
 catalytic actions 103
 characteristics 100–1
 hydroxamido complexes 104–5
 ligands
 noninnocent 59, 60
 stabilising 103–4
 non-oxo complexes 103–4
 structure 100–2
 X-ray studies 84
Amoebiasis (amoebic dysentery) 179–80
Anhydrides 189–90
Aqueous vanadium systems 13–26
 aqua-sulfato complexes 15
 and pH 15, 16, 19
 predominance diagrams 17
 protonation/deprotonation 18, 19
 speciation/speciation diagrams 16–17
 vanadate structures 17–18
Archaea 146, 205
Aryl sulfatases 197
Ascidians 9–10, 15, 67, 74, 87–96
 anatomy 87
 blood 88–9, 90
 glutathione transferases (GST) 96
 habitat and life style 88
 K-edge X-ray absorption spectroscopy 92, 93
 and oxygen 88–9
 signet ring cells (vanadocytes) 67, 89, 90–1
 sulfur compounds 92, 94
 tunichromes 91
 vanabins 93, 94–6
 vanadium
 in blood 90
 composition 91, 92
 concentration 88
 discovered 87
 entry into organism 93
 redox chemistry 93–4
 and water ligands 91–2
 XAS studies 84
Ascophyllum nodosum 84, 107, 109–10, 111, 113, 114
Asimov, Isaac 203, 204, 205
Azotobacter spp. 84, 128, 129, 131, 149–50
Bacterial action 5–6, 128, 129–30, 145–50
Baes–Mesmer diagram 13, 14
Berzelius, J. J. 1, 2, 4, 8
Binary vanadium(IV and V) systems 20–4
Biological importance of vanadium 9–10, 205
 in bones 170–1
 and cellular functions 157–98
 metabolic pathways 157–8
 reaction paths 172, 173

- Biological importance of vanadium
(Continued)
- effect on animals 8, 9
 - in human body 5, 9, 157
 - spectroscopic investigations 83–4
 - spermicidal activity 180–1
 - Blood 26–8, 190–1
 - see also* Plasma; Serum components
 - BMOV 169
 - Bones 20, 170–1
 - Bortels, Hans 128
 - Bromoform 108
 - Bromoperoxidases 107–8, 109, 111
 - Cancer therapy 176–9
 - cancer types 176
 - and DNA 177, 179
 - tyrosine phosphatase inhibition 176–7
 - Carboxylates/carboxylato 27, 42, 43, 142
 - Catalytic action
 - by amavadin 103
 - in haloperoxidases 116–17
 - by peroxovanadium complexes 121
 - of vanadium oxides 7, 8
 - of vanadium-phosphate salts 21
 - Catechols/catecholates/catecholato 41, 42, 91, 97–8, 142
 - Cellular functions 157–98
 - Chemistry, contribution to humanity 203
 - Chloroperoxidases 107–8, 111
 - Chromium 1, 2, 4
 - Circular dichroism (CD) 79–80
 - applications 79, 80
 - magnetic circular dichroism 79
 - Cisplatin 178
 - Citric acid and derivatives 26, 27, 28, 33–4, 73, 143, 168
 - Clostridium butyricum* 129
 - Coordination compounds of vanadium 34–47
 - Copper zinc superoxide dismutase (CuZn-SOD) 193–4
 - Corallina spp.* 107, 110, 111, 113
 - Curvularia inaequalis* 107, 109–10, 111, 113
 - Cyclopentadienylvanadium complexes 47, 180
 - Cysteine 32, 45, 94, 103, 186, 196–7
 - Decavanadate 18, 19, 34, 194, 195, 196
 - Del Rio, Andres Manuel 3–4
 - Diabetes mellitus 158–63
 - control 159
 - and glucose metabolism/uptake 158, 166
 - and insulin 158, 159, 160, 172–5
 - insulin receptor substrates (IRS) 174–5
 - treatment 159–60
 - Type 1 and Type 2 159
 - vanadium compound treatment 160–5
 - chronology 162–3
 - insulin-mimetic action 161, 164–5, 166, 175, 186
 - organovanadium compounds 162–5
 - activity levels 163–5
 - advantages 162
 - ligands 163
 - oxidation state 163
 - peroxovanadate 161–2
 - serum interaction 165–7
 - vanadium absorption 169
 - vanadyl sulfate 161
 - Dithiobene 44, 45
 - Dithiothreitol 30, 31
 - Divanadate 19
 - DNA cleavage 179
 - DNA damage
 - alkylation 177–9
 - agents 177–8
 - dealkylation 178
 - oxidative 177
 - Ehrlich tumours 178, 179
 - Electron absorption spectroscopy 21–2
 - Electron nuclear double resonance spectroscopy, *see* ENDOR spectroscopy
 - Electron paramagnetic resonance (EPR) spectroscopy 21–2, 31–2, 53, 67–75
 - anisotropic axial spectra 68–9
 - applications 69–74
 - complex distortions 71–2
 - dinuclear complexes 73, 74
 - equatorial ligand set
 - assignment 69–70
 - size 70–1
 - superoxo complex formation 74–5
 - valence localisation 73
 - vanadium complex parameters 71–3
 - compared with NMR 67
 - haloperoxidases 113
 - hyperfine coupling constants 69–70
 - resonance conditions 68
 - spin criteria 67–8
 - on vanadium nitrogenases 134
 - Electron spin-echo envelope modulation spectroscopy, *see* ESEEM spectroscopy

- ENDOR spectroscopy 75, 76–7
electron spin echo ENDOR (ESE-ENDOR)
 77
 procedure 76
Entamoeba histolytica 179–80
Enterobactin 149
Enzymes 121–5
ESEEM spectroscopy 75–6, 113, 170
 procedure 75–6
Esters 26, 36, 189–90, 191
 MAS spectra 64, 65
 of orthovanadic acid 25, 26, 41, 59
 sulfate ester hydrolysis 197–8

Ferrovanadium 8
Fly agaric 100
Fossil ‘fuels’ 6–7
 crude oil 6, 7

Geobacter metallireducens 149
Glucose-6-phosphatase 187
Glutathione (GSH) 30–1, 172, 173
Glutathione transferases (GST) 96
Glycyl-L-cysteine 32
Glycyl-L-histidine 32
Groundwater 149

Haber–Bosch process 130
Haemovanadin 89–90
Halides
 of orthovanadic acid 24–5
 in sea water 107–8
Haloperoxidases, *see* Vanadate-dependent haloperoxidases (VHPOs)
Apo-haloperoxidases (apo-VCIPO) 109,
 187–8
Health risks 7–8
 concentration levels 8
Henze, M. 9–10, 87, 88, 89, 90
Histidine
 complexes 29, 30, 32, 121–2
 in phosphatases 186, 187
HIV 180–1
Homocitrate 131–3, 143
Humboldt, Baron von 1
Hydrazine 134, 138, 141–2
Hydrogen bonding 195–6
Hydrogencarbonate 20
Hydrogenphosphate 20
Hydroxamido groups/ligands 59, 104–5
Hydroxycarboxylates 27
Hydroxylamine 21, 23–4
Imidazole 30, 32, 70–1
Insulin 158, 159, 160
 binding modes 194
 and maltolatovanadium 22
 stimulates glucose uptake 172–5
 vanadium as mimetic agent 161, 164–5,
 166, 175, 186
Insulin receptor substrates (IRS) 174–5
Iodoperoxidases 107–8
Iron mobilisation 149

Johnston, J. F. W. 2, 4

Keggin structure 19–20, 22
Kinases 146, 175

Lactamases 189
Lactic acid and lactate 26–7, 33
Lactoferrin 192, 193
Laws of Robotics 203, 205
Ligands
 sulfate 15, 27, 90–93, 98–100
 thiofunctional 30, 43–5
 vanadate/vanadyl interactions 26–34
Lipolysis 175
Lippmann, E. O. von 9
Lyosomal storage diseases 197

Magnetic circular dichroism (MCD) 79
Maltol 162, 167, 172, 173
Maltolatovanadium 22
Medicinal aspects of vanadium 9,
 158–82
Metabolic pathways 157–8
Metavanadates 20
Metronidazole 180
‘Metvan’ 176
Molybdenum, in nitrogen cycle 128–9
Molybdenum nitrogenase 131, 134
Molybdopterines 144, 145
Monovanadate 19
Myosin 194

Nitrate reductases 144–5
Nitrogen cycle 128–45
 bacterial action 128, 129–30
 chemical steps 129–30
 historical aspects 128–30
 molybdenum (role of) 128–9
 tungsten (role of) 128, 129
 vanadium (role of) 128–9, 130
 vanadium nitrogenase 131–44

- Non-oxo vanadium complexes 35, 41, 45
 Nuclear magnetic resonance (NMR) 66–7
 coordination-induced shift (CIS) 66
 paramagnetic vanadium(III) 67
 see also Vanadium-51 NMR spectroscopy
- Optical spectroscopies 77–80
- Organovanadium compounds (organic vanadium compounds) 47–8
 diabetes treatment 162–5
 see also Vanadium–carbon bond
- Orthovanadates 20
- Orthovanadic acid
 esters 25
 structure 25, 26
 halides and other salts 24–5
- Oxidation reactions
 haloperoxidase reactions 116–18, 121, 124, 125
 of sulfides 114
 superoxo intermediates 167–8
- Oxidation states 13–15, 48, 163
- Oxovanadium complexes 31, 35, 167–8
 ROS scavengers/generators 177
- Pentavanadate 19
- Peroxidases
 classification 105
 historical background 105–6
 isolation 106
 see also Vanadate-dependent haloperoxidases (VHPOs)
- Peroxides 20–1, 22, 27, 30
- Peroxo ligands 37, 38, 59
- Peroxovanadates 20–1, 24, 186
- Peroxovanadium complexes 116–17, 119–21
 catalytic action 121
 coordination numbers 120
 oxidation reactions 121
 speciation 120–1
 structure 119–20
- Phallusia mamillata*, *see* Ascidians
- Phosphatases 30, 109, 175, 183–4, 187–8
 structure 186
- Phosphate-metabolising enzymes 183–9
 inhibited by vanadate 184–8
 phosphatases 184, 186–8
 ribonucleases 184–6
 stimulated by vanadate 189
- Phosphate–vanadate antagonism/competition 20, 25, 182, 183, 193–4
- Phosphates 20, 21, 26, 27
- Phosphovanadates 24, 190–1
- Phytic acid and phytases 188
- Picolinate ligand 169
- Plants 9
- Plasma 5, 20, 190–1
 see also Blood; Serum components
- Pollution 7
- Polychaeta fan worms 96–7
 vanadium
 accumulation 96–7
 function 97
- Polyoxometalates (POMs) 181
- Porphinogens 7
- Priestley, John 9
- Protein tyrosine phosphate (PTP) 174–5, 182, 186–7
- Proteins 182–98
 bind to vanadate 182, 190–5
 bind to vanadyl 94–5, 182, 190–5
 in blood plasma 190–1
 modified by vanadate 195–8
 nonfunctional binding of vanadate and vanadyl 190–5
 occurrence 182
 in vanadium nitrogenase 131–3
- Pseudopotamilla occelata*, *see* Polychaeta fan worms
- Pyridinone complex 171
- Quinta essentia* 203–4
- Radioactivity 5
- Redox potentials 13, 14, 15
- Respiration 146
 electron acceptors 146
 vanadate as substrate 146
- Ribonucleases (RNases) 184–6
 vanadate incorporation 184–6
- Roscoe, Henry Enfield (Sir) 4
- Schiff base complexes 45, 46–7
- Sea squirts, *see* Ascidians
- Sea water 5, 107–8, 145
- Sefström, Nils Gabriel 2
- Serine 28–30, 126–7, 149, 195–6
 photocleavage 195–6
 reaction steps 196
- Serum components 165–7
 albumin 169–70, 190, 191
 proteins 190
 transferrin (Tf) 34, 168, 169–70, 171–2, 190–1, 193

- water 167
as ligand 167
see also Blood; Plasma
- Sherwoodite 5–6, 146
- Shewanella oneidensis* 146–7
- Siderophores 149, 150
- Signet ring cells 20, 25, 182, 183, 193–4
- Speciation analysis, notation 31
- Spectroscopic methods 53–84
- Spermicidal properties 180–1
- Sulfatases 196, 197
- Sulfate ester hydrolysis 197–8
- Sulfatovanadium complexes 98–9
- Sulphydrases 196–7
- Sulfides 43, 109
oxygenation 124, 125
peroxidation 124–5
- Ternary vanadium(IV and V) systems 20–4
- Tetravanadate 19, 194, 195
- Thioacetals 124, 125
- Thiocyanates 108–9
- Thiofunctional ligands 30, 43–5
- Thiol (mercapto) groups 30–1
- Thiovianadates 20
- Transferrin (Tf) 34, 168, 169–70, 171–2, 190–1, 193
- Tridecavanadate 19–20
- Tuberculosis 181–2
- Tunicata/tunicates 87, 88, 146
- Tunicromes 41, 74, 91, 97–8
- Two-dimensional exchange spectroscopy (2D-EXSY) 60–1
- Ultra-violet spectroscopy, *see* UV-Vis spectroscopy
- Uranium 2
- UV-Vis spectroscopy 77–9
conditions 77
vanadium(III) complexes 79
vanadium(IV) complexes 78
vanadium(V) complexes 77–8
- Vanabins 93, 94–6, 182
amino acid sequences 95
binding functions 96
structure 95
- Vanadate
dealkylating action 178
deavanadate 18, 19, 34, 194, 195, 196
divanadate 19
- electron acceptor 145–50
in groundwater 149
inhibitory effect 184–5
monovanadate 19
pentavanadate 19
phosphate compared 182, 183
protein binding 182, 190–5
competes with phosphate 20, 193–4
nonfunctional 190–5
site nature 191–3
spectroscopic analysis 192–4
- proteins, modification 195–8
in *Shewanella oneidensis* 146–7
electron transfer pathway 147, 148
location 147, 148
TEM images 147, 148
- as stimulant
of glucose uptake 172–5
and lipolysis 175
phosphorylation 174–5
of phosphatase activity 189
- structures 17–18
- system speciation 26–31
- tetravanadate 19, 194, 195
- Vanadate–alanylhistidine system 30, 121–2
- Vanadate–alanylhistidine–peroxide system 30, 121–2
- Vanadate–alanylserine system 28–30
- Vanadate-dependent haloperoxidases (VHPOs) 105–28, 182, 183, 186
activity data 109–10
bonding
carbon–hydrogen bonds 128
hydrogen bonding 126–7
bond lengths 127
and water 127–8
of vanadate centre 125–6
- distribution 105, 107
- halides
converted to hypohalous acid 107–8, 114–15
oxidation (active species) 113
- inhibition 109
- isolation 106
- model chemistry 116–28
enzymes 121–5
functional models 118, 123
halogenation 123
hydroxylation reactions 117–18
monobromination catalysis 117
organic syntheses 123

- Vanadate-dependent haloperoxidases (VHPOs)
(Continued)
- oxidation reactions 117–18
 - sulfides/thioacetals reactions 124
 - oxo transfer reactions 116
 - peroxovanadium complexes 116–17
 - structural models 118, 119–21
 - peroxovanadium complexes 119–21
 - reduced haloperoxidases 119
 - peroxo/hydroperoxo intermediates 115, 117
 - protonation 114–15
 - structure 110–16, 186
 - active sites 111, 112
 - bonding and bond lengths 111–12
 - EPR linewidths 113
 - helices 110, 111
 - MAS spectra 114
 - reduced form 112–13
 - X-ray diffraction data 112, 113–14
 - substrates 107–9
 - sulfides 115–16
 - uses 109
 - and vanadate-inhibited phosphatases 186, 187–8
- Vanadate-dependent peroxidases, *see*
- Vanadate-dependent haloperoxidases (VHPOs)
- Vanadate-inhibited phosphatases 187–8
- Vanadate–hydroxylamine system 23–4
- Vanadate–peroxide system 22, 23
- Vanadate–phosphate antagonism/competition 20, 25, 182, 183, 190–1, 193–4
- Vanadate–phosphate–peroxide system 22–3
- Vanadate–phosphate system 21–2
- Vanadinite 2, 3
- Vanadium
- discovery 1–5
 - inorganic compounds 13–48
 - isolation 4
 - minerals 5–6
 - naming 2
 - occurrence 5–6, 145
 - radioactivity 5
 - redox chemistry 93–4
 - synthesis 4–5
- Vanadium-51 NMR spectroscopy 16, 53–66
- criteria 53
 - linewidths 61–2
 - influential factors 62
 - molecular correlation time 62
- quadrupole coupling constant 62
 - relaxation process 61–2
 - nuclear spin–spin coupling 62–3
 - Fermi contact term 62–3
 - relaxation effects 63
 - parameters under ‘confined’ conditions 64–6
 - magic angle spinning (MAS) 64, 65
 - magnetic field strength 66
 - quadrupolar interactions 64
 - Zeeman transitions 64
 - quadrupolar nuclei 53, 54
 - reference standard 54
 - scalar coupling 62–3
 - shielding ranges 57–60
 - coordination geometry 58–9
 - coordination number 58–9
 - electronegativity dependence 57–8
 - noninnocent ligands 59–60
 - peroxo and hydroxamido ligands 59
 - shift limits 57
 - steric effects 59
 - theory 55–7
 - LCAO coefficient 56
 - molecular orbital scheme 56–7
 - paramagnetic term 56
 - shielding 54, 55–6
 - vanadium nucleus parameters 53–4
- Vanadium–carbon bond 47–8
- bonding interaction 48
 - occurrence 47
 - oxidation states of vanadium 48
- Vanadium coordination compounds 34–47
- and biogenic ligands 40–7
 - alcohols and alcoholates 40, 41
 - carboxylates/carboxylato 42, 43
 - catecholates/catecholato 41, 42
 - enolates/enolato 41, 42
 - mixed ligand spheres 46–7
 - multifunctional ligands 45–6
 - phenolates/phenolato 41, 42
 - thiofunctional ligands 43–5
 - structural features 34–9
 - bond lengths and bond orders 36–7
 - bridging ligands 37–8
 - chelating ligands 39
 - chirality 39
 - coordination geometries 37
 - octahedral arrangement 36, 37
 - oxo- and dioxovanadium complexes 35
 - peroxo ligands 37, 38
 - substitution variations 38

- trans* influence 36
vanadium–carbon bond 47–8
vanadium–oxygen bond 36–7
Vanadium lead ore 2
Vanadium-metabolising enzymes 183–8
Vanadium nitrogenase 131–44, 182, 204–5
cluster structure 131–2
 M clusters (iron–vanadium cofactor, FeVco) 131, 132, 134, 143
 P clusters 131, 132, 134
constituents 131
model chemistry 135–44
 alkyne coordination 143–4
 catecholato complexes 142
 citrate coordination 143
 cubane clusters 142–3
 dicarboxylates 142
 dinitrogen activation/reduction site 135–6
 dinitrogen-bridged complexes 139–41
 dinitrogen vanadium complexes 138–9
 hydrazine reactions 138
 metal centre 135–6
 nitrogen–nitrogen bond 139–41
 phosphine 138–9
 vanadium–nitrogen bond 140–1
Yandulov–Schrock cycle 136, 137
molybdenum nitrogenase compared 131, 134
protein components 131–3
reduction reactions 131, 134–5
 in alkaline solutions 141–2
 of azide 135
 hydrocarbon substrates 134–5, 143–4
 of methyl isocyanide 135
structure information
 from EPR spectra 134
 from XAS investigations 133–4
VFe-protein 131–3
 biosynthesis 132–3
Vanadium oxides 7, 8
 catalytic action 7, 8
physiological importance 13–15
reduction 13–15
Vanadocene dichloride 176, 178–9
Vanadocenes 178
Vanadocytes 67, 89, 90–1
'Vanadophores' 149, 150
Vanadyl 16
 complexes 167–8
 coordinates with ATP 190
 as phosphate analogue 182
 protein binding 182, 190–5
 nonfunctional 190–5
 physico-chemical marker 194
 site nature 191–3
 spectroscopic analysis 192–4
system speciation 31–4
Vanadyl–ligand A–ligand B system 168–9
Vanadyl–phosphate complexes 21–2
Vanadyl–picolinate–phosphate/citrate complexes 171–2
Vilter, Hans 106
Westinghouse Lamp Co. 4–5
Wine 204
Wöhler, F. 1, 2, 8
X-ray absorption spectroscopy (XAS) 80–4
 biological applications 83–4, 92–3, 107, 112, 133
 extended X-ray absorption spectroscopy (EXAFS) 80, 81, 82, 133–4
K-edge 80–2, 92, 93
L-edge 83
near-edge X-ray absorption fine structure (NEXAFS) 80
pre-edge 81–2
on vanadium nitrogenase 133–4
X-ray absorption near-edge structure (XANES) 80–3
Xylose isomerase 195
Yandulov–Schrock cycle 136, 137